Characterization of Dry Etching Processes of III-V Semiconductors in Silicon Tetrachloride Plasmas

thesis by

Saad Kheder Murad

Submitted for the degree of Doctor of Philosophy

to the Faculty of Engineering of Glasgow University

July 1994

ProQuest LLC.
789 East Eisenhower Parkway
P.O. Box 1346
Ann Arbor, MI 48106 – 1346

To my family
in Shinjar mountains

Acknowledgements

The work done in this thesis would have not been possible without the help and support of many people.

First, I would like to sincerely thank my supervisor Professor Chris Wilkinson for invaluable advice and support he gave me throughout this work, without his constant encouragement this work would have not been possible. I would like also to thank Professor Peter Laybourn, the head of the department for allowing me to continue my study on deferred payment of fees. I am indebted to Professor Steve Beaumont for many useful discussions and also for supporting me to attend ME 93 conference.

Special thanks go the dry etch technicians Ray Darkin, Gillian Hopkins and Dave Clifton, with whom I shared very heated but enjoyable discussions! Without their technical support this work would have not been possible.

Special thanks also to my fellow research students and RAs in the dry etch group, Simon Hicks, Andy Bunting, Bill Parks and Yiping Song, with whom I enjoyed very useful discussions and shared many outdoor activities (in the pubs?).

The technical support of the Electronics and Electrical Engineering Department is greatly appreciated, in particular H. McLelland, S. Ferguson, D. Gourlay, D. MacIntyre in the UltraSmall Laboratory, L. Hobbs and J. Carson in the clean room, Peter the photographer for printing my SEM pictures many times.

Thanks also to Professor Colin Stanley and all people in the MBE for the supply and growth of high quality materials. I am grateful also to Dr. S. Thoms for his advice on nanolithography, N. Cameron, P. D. Wang and N. Johnson for their collaboration in this work.

I would like also to express my personal gratitude to my supervisor Chris and his wife Judy for their help and understanding of my problems.

Finally my deepest appreciation goes to my friend Theresa, for her love and support, which kept me going during my long studying years.

Abstract of Thesis

This thesis is concerned with the development of Reactive Ion Etching (RIE) processes for GaAs/AlGaAs material system in Silicon Tetrachloride ($SiCl_4$) and mixed Silicon Tetrachloride and Silicon Tetrafluoride ($SiCl_4/SiF_4$) plasmas. Etch processes which etch GaAs and not AlGaAs (selective) and ones etch both (non selective) have been developed. Particular attention has been paid to achieving a damage free etch. The chemistry and mechanisms behind the etching process in these plasmas have been thoroughly studied using Optical Emission Spectroscopy (OES) as a tool for plasma diagnosis.

Optical Emission Spectroscopic analysis of the $SiCl_4$ plasma showed that the chemistry and the etching mechanism are strongly dependent on the applied rf power. Two chemical regimes and hence two mechanisms of etching were identified including: "the low power regime" in the rf power range of 5-20 W and "the high power regime" in the range of 25-150 W. In the low power regime, $SiCl_4$ molecules breakdown gradually by multiple electron impact excitations into $SiCl_2$ and SiCl radicals, Si and Cl atoms and molecular ions of Cl_2^+. In the high power regime, the breakdown of $SiCl_4$ molecules is mostly through one electron impact excitation into $SiCl_2$ and SiCl radicals, Cl and Si atoms, and atomic Cl ion Cl^+. This gives rise to two etching mechanisms, the first is in the low power regime where the etching depends on the concentration of mainly Cl_2^+ ions and chlorosilicon radicals. The second is in the high power regime where the etching depends on the concentration of Cl^+ ions and chlorosilicon radicals.

A very low damage, anisotropic selective or nonselective RIE has been developed in $SiCl_4$ plasma for etching GaAs/AlGaAs which stops on an extremely thin AlGaAs layer (1.13 nm thick). Using a very low rf power of 10-15 W and a low dc bias $\leq$ 60 V, this process can be selective or nonselective over the AlGaAs depending on the $SiCl_4$ flow rate and pressure; selectivities of the order of 10000:1 are readily obtained whilst maintaining excellent verticality. Nanostructures 50-60 nm wide in GaAs have successfully been etched to a depth of 1.5 μm under very low damage conditions. Selective RIE for gate recessing for MESFET fabrication has been successfully implemented, where T- shaped gates with vertical gate profiles with little gate off-set have been obtained. The mechanism of the selectivity depends on the formation of some form of Al_xO_y or Al_xN_y from the residual O_2, air or water in the chamber. Both the surface and sidewall damage were measured and the results were confirmed by the evaluation of the performance of Metal Semiconductor Field Effect Transistors (MESFET) whose gate recess etching was performed using this process. The results of sidewall damage made on quantum wires showed that this process is virtually damage free in the first two minutes of etching. Results from Raman scattering

and MESFET characteristics confirmed that no significant degradation of carrier mobility or free carrier concentration in the channel occurs even after 3600% of overetching.

A "damage free" and selective RIE process for etching GaAs/AlGaAs has been developed in a mixture of $SiCl_4/SiF_4$ plasma using very low rf power and high pressure.

The selectivity results showed that very high selectivities of the order of > 5000:1 can be achieved by the addition of large amounts (70-85 %) of SiF_4 to $SiCl_4$ at high pressures and reduced dc biases. On the other hand the results of the OES on $SiCl_4/SiF_4$ plasma showed that no free atomic F exists in the plasma and that the dominant species are the silicon chlorides and silicon fluorides. Dry etch damage assessment carried out by Raman scattering on heavily doped GaAs showed that "damage free" etching is possible. The above results were confirmed by Hall measurements on pseudomorphic High Electron Mobility Transistor (HEMT) structures which showed that no detectable change in the free carrier concentration of the channel nor in the electron mobility can be observed even after 5000% of overetching. This SRIE process was applied to T-gate recessing and the results showed a controllable gate off-set can be readily obtained.

Table of Contents

Chapter 1

Introduction

1.1 General introduction

Over the past ten years or so the creation of structures in semiconducting material on a nanometric scale has opened up new possibilities for electronic, optoelectronic and molecular electronic devices. In the electronic area, improvements in the speed of field effect transistors such as MESFET and HEMTs are possible only by reduction in the time spent by the electrons under the gate region. In these devices the electric field in the gate region is so high that the electrons travel at their saturation velocity, the only way of reducing the transit time is by reducing the gate length. Devices with gate lengths of less than 100 nm operating at frequencies as high as 200 GHz have been reported [1-4]. The behaviour of electrons when confined to travel in essentially straight line is of great physical interest, the understanding of such behaviour is potentially important for the development of new electronic devices. The study of electron or phonon transport requires the fabrication of very fine structures; and as the electrons are laterally confined to a region only a few atoms in cross-section, quantum mechanical effects become very important. A good example is the appearance of wavelike nature of electrons confined in quantum wires and dots [5-6]. In the bioelectronics area, the possibilities of direct control of biological moieties are opened up, for example the control of the orientation of biological cells by very fine gratings have been reported [7]. These achievements would have not come about without the remarkable advances in other areas of research such as the ultra thin epitaxial growth techniques. For example Molecular Beam Epitaxy (MBE) began the era of reduced dimensionality physics [8], where heterojunction interfaces with large energy band discontinuities such as GaAs/AlGaAs are produced routinely with precision control of the composition, periodicity and any other desirable variables.

The formation of the nanostructures which are used in understanding of the physics of electronic transport requires a pattern definition stage and then a means of transferring this pattern into the semiconductors.

State-of-the-art pattern definition implies the use of a focused beam of electrons, photons or ions. At present, electron beam lithography is the most widely used method for pattern definition at a nanometric scale. The transfer of the defined patterns into the semiconductor requires wet or dry etching. In the formation of nanostructures the isotropic nature of wet etching makes it unsuitable, so dry etching is used as it can be highly anisotropic. Dry

etching has the advantages of high uniformity of etching across the wafer, reproducibility, and can be made to be selective so that it etches one material and stops on the other; for example selective RIE of GaAs over AlGaAs used in the fabrication of MESFETs. In such devices the gate recess depth and the gate off-set have to be accurately controlled to within few monolayers. Conventionally wet etching techniques have been used for gate recess etching. However wet etching techniques have been shown [3] to be increasingly problematical at nanometre gate lengths due to isotropic and poor repeatability of wet etching techniques. For these reasons dry etching techniques have received great attention [9,10] in gate recess etching as they allow accurate recess depth control with enhanced uniformity and repeatability over conventional wet etching techniques.

However the action of energetic ions in the plasma bombarding the surface and sidewalls of etched structures (e.g. the walls of gate recesses) can cause degradation of the electronic and optical properties (dry etch damage) of these structures. The dry etch damage is especially significant when the scale of the etched structures is nanometric as the extent of dry etch damage can be far more than the dimensions of nanostructures and so such a structure can be completely destroyed. The extent of damage in RIE depends largely on the energies of ions bombarding the etched surfaces and sidewalls [11-13]. Therefore, the mechanism of reducing the damage must involve reducing the ion energies in the discharge. In RIE processes the ion energies primarily depend on the sheath potential with respect to the ground (the dc bias) which in turn depends on the applied rf power and to some extent on the pressure. Therefore to reduce the ion energies one has to reduce the applied rf power provided that the integrity of etching can be maintained. However it is often difficult to reduce the rf power while maintaining reasonable etch rates or anisotropy for various reasons, basically, because of the difficulty of maintaining the discharge at low levels of power. This in turn is due to the presence of impurities and contaminants in the discharge. The sources of impurities and contaminants in RIE processes include; the feed gas, atmospheric air leaks, desorption from chamber surfaces, backstreaming of gases from the pumping system and deposition of nonvolatile species. In a low power discharge, the presence of impurities has marked effect on etching because of low density of etchants at such low levels of power.

Insight into the fundamental chemical and physical processes occurring during plasma etching processes allow the development of reliable RIE processes at reduced rf power. Various plasma diagnostic techniques have been reported [15-17], such as Optical Emission Spectroscopy (OES) or Mass Spectroscopy (MS). These techniques can provide real-time information on process stability, repeatability, and can also be used to determine the etch initiation and end point monitoring. The availability of one or more of these techniques is vital for the development of any reliable etching processes.

The approach adopted in this work was first to understand the chemical nature of the discharge by the use of OES, then identify the etching parameters that are directly related to

the desired etching characteristics such high selectivity and anisotropy whilst maintaining the goal of damage-free dry etching.

The first part of this thesis is concerned with Optical Emission spectroscopy of $SiCl_4$ and CH_4/H_2 plasmas. The chemical species involved and the excitation pathways have been clearly identified. Optical Emission Spectroscopic analysis of $SiCl_4$ plasma have shown that the etching mechanism of GaAs is strongly dependent on the chemistry and the type of prevailing ions in the discharge.

A crucial step was the development of a cleaning technique for the etching chamber. After a discharge in H_2 followed by O_2, the chamber is so clean that a plasma of $SiCl_4$ or $SiCl_4/SiF_4$ can be sustained at rf powers as low as 10 W (0.05 W/cm^2) with corresponding dc biases of 20-60 V. Reactive ion etching processes (RIE) for etching GaAs/AlGaAs in $SiCl_4$ and $SiCl_4/SiF_4$ plasmas have been developed using these low power conditions whilst maintaining high resolution, anisotropic profiles, smooth surfaces and reasonable etch rates. These processes can provide extremely high selectivity ($\geq$10000:1) of etching GaAs/AlGaAs which relies on a new mechanism of etch stop on AlGaAs. Nonselective etching of GaAs/AlGaAs is also possible. Moreover these processes are virtually "damage free".

In the work to be reported in this thesis GaAs/AlGaAs based MESFETs have fabricated with vertical gate profiles with very little gate off-set and thus a very precise control of the effective gate length.

1.2 Thesis outline

In chapter 2 of this thesis the principles of Optical Emission Spectroscopy OES are given. The employment of OES and Actinometry as a tool for plasma diagnostic in reactive ion etching processes is reported. Emission spectra of CH_4/H_2 based plasmas are given and the use of OES as a mean to monitor the etch products from etching InP in a CH_4/H_2 plasma is reported in this chapter too.

In chapter 3 a comprehensive analysis of the OES observation in $SiCl_4$ plasma is given. The effects of various discharge parameters such as rf power, pressure and gas flow rate on the dissociation mechanism and their implication on the discharge chemistry are identified. In this chapter the emission spectra of etch products of a number of III-V materials etched in $SiCl_4$ plasma are given. OES as an end point or etching initiation determination for GaAs, AlGaAs and AlAs etching in $SiCl_4$ plasma, its limitation and application are discussed. Chapter 3 also presents a comparison of $SiCl_4$ microwave generated plasma and rf generated one.

Chapter 4 reports on a comprehensive analysis of GaAs etching in $SiCl_4$ plasma. Two mechanisms of etching have been realised; one at low power and the other at high powers. The correlation of these mechanisms with emission from the plasma is discussed. An

anisotropic RIE of GaAs in $SiCl_4$ plasma using very low powers and dc biases has been developed, the problems associated with chamber contamination, chamber cleaning, low power etching and the possible cures are also given in this chapter.

In chapter 5 of this thesis the characteristics of $Al_xGa_{1-x}As$ etching in $SiCl_4$ plasma are given with special emphasis on the selective and nonselective etching of GaAs/AlGaAs and the etching parameters that control the degree of selectivity. Moreover, a new selective and anisotropic RIE for etching GaAs/AlGaAs in $SiCl_4$ and $SiCl_4/N_2$ is reported in this chapter in which new mechanisms of selective etching of GaAs/AlGaAs has been developed.

Selective etching of GaAs/AlGaAs in a mixture of $SiCl_4/SiF_4$ plasmas is also reported in this chapter and Optical Emission Spectroscopy of these plasmas has been carried out to investigate the relative concentration of the various reactive species in the discharge and their effect on selectivity at various etching parameters.

Chapter 5 also presents T- gate recesses in MESFET and HEMTs material using the selective processes in pure $SiCl_4$ and $SiCl_4/SiF_4$ plasmas, the resulting gate profiles from these processes are compared and the advantages of having more controllable gate profile are discussed.

Chapter 6 of this thesis gives a comprehensive analysis of the damage in n^+-GaAs, MESFET or HEMT material structures caused by RIE in $SiCl_4$ and $SiCl_4/SiF_4$ plasmas. The damage have been measured using a variety of techniques which include: conductivity measurements of n^+-GaAs wires for the measurement of sidewall damage, Raman scattering measurements for surface damage assessment, a combined electrical characterization using Schottky diodes, Transmission Line Model (TLM), Van der Pauw, and characterization of MESFET performance after gate recess etching.

Finally, chapter 7 presents an overall picture of the findings established from this work and presents a few suggestions to extend the kind of analysis and processes developed in this work to other material systems such as InGaAs/AlInAs/InP.

1.3 References

1.1. W. Patrick, W. S. Mackie, S. P.Beaumont, C.D.W. Wilkinson, and C. H. Oxley, IEEE Elect. Dev. Lett., **EDL - 6**, 471, (1985).

1.2. J. A. Adams, IEEE Trans. Electron Devices, **ED - 36**, 2612, (1989).

1.3. I. Thayne, Ph.D. thesis , Glasgow University, (1993).

1.4. B. E. Maile, J. Vac. Sci. Technol., B **11**, 2502, (1993).

1.5. J. N. Randall, M. A. Reed and G. A. Frazier, J. Vac. Sci. Technol., B **7**, 1398, (1989).

1.6. C. D. W. Wilkinson, Superlattices and Microstructures, **7**, 381, (1990) and references therein.

1.7. C. D. W. Wilkinson, Microelectronic Engineering, **6**, 155, (1987) and references therein.

1.8. M. J. Kelly, Semicon. Sci. Technol., **5**, 1209, (1990).

1.9. N. I. Cameron, S. Ferguson, M. R. S. Taylor, S. P. Beaummot, M. Holland, C. Tronche, M. Soulard, and P. H. Ladbrooke, J. Vac. Sci. Technol., B **11**, 2244, (1993).

1.10. A. A. Ketterson, E. Andideh, I. Adesida, T. L. Brock, J. Baillargeon, J. Laskar, K.Y. Cheng and J. Kolodzey, J. Vac. Sci. Technol., B **7**, 1493, (1989).

1.11. C. M. Knoedler, L. Osterling, and M. Heibum, J. Appl. Phys. **65**, 1800, (1989).

1.12. P. Rabinzohn, G. Gautherin, B. Agius, and C. Cohen, J. Electrochem. Soc., **131**, 905, (1984).

1.13. E.M. Clausen, Jr., H. G. Craighead, J. P. Harbison, A. Scherer, L. M. Schiavone, B. Van der Gaag, and L. T. Florez, J. Vac. Sci. Technol. B **7**, 2011, (1989).

1.14. R. Cheung, S. Thoms, M. Watt, M. A. Foad, C. M. Sotomayor-torres, C. D. W. Wilkinson, U. J. Cox, R. A. Cowley, C. Dunscombe, and R. H. Williams, Semicond. Sci. Technol., **7**, 1189, (1992).

1.15. G. Bruno, P. Capezzuto, and G. Cicala, J. Appl. Phys., **69**, 7256, (1991).

1.16. P. Collot, T. Diallo, and J. Canteloup, J. Vac. Sci. Technol., B **9**, 2497, (1991).

1.17. V. M. Donnelly, and D. L. Flamm, J. Appl. Phys., **58**, 2135, (1985).

Chapter 2

Optical Emission Spectroscopy (OES) of Reactive Ion Etching (RIE) Plasmas

2.1 Introduction

The work of this thesis is partly based on using OES in the understanding the chemistry of Reactive Ion Etching plasmas, so in this chapter the basic idea of the Optical Emission Spectroscopy (OES), with commonly used terms are defined. The practical limitations of optical instruments used in this work are discussed. The background theory of Optical Emission Actinometry is given.

As the work of this thesis is primarily based on developing Reactive Ion etching processes, the employment of OES and Actinometry as a tool for plasma diagnostic in Reactive Ion Etching processes is reported. The advantages of using the OES as a diagnostic tool in plasmas are explained.

To acquire knowledge of the emission spectra of CH_4/H_2 plasmas and in particular the effect of the addition of small percentages of O_2 or N_2 to the discharge, optical Emission Spectra of H_2, CH_4/H_2, $CH_4/H_2/O_2$ and $CH_4/H_2/N_2$ are given. As an example of the usefulness of OES as a diagnostic tool in plasmas for the understanding of gas phase chemistry, the origin of the emitting species in CH_4/H_2 plasmas are examined in detail. Finally, the use of OES to monitor etch products from etching InP in a CH_4/H_2 plasma is presented.

2.2 Definition

A spectrum may be defined as an ordering of electromagnetic radiation according to the frequency and amplitude. The complete spectrum of any given source comprises all the frequencies that the source emits. Since no single universal wavelength-resolving instrument exists, the various regions of the electromagnetic spectrum must be investigated by different methods. The so called "Optical" region of the spectrum extends over a wide range, from the far infrared on the one end to the far ultraviolet on the other. It includes the visible region as a relatively small portion. The light emitted by excited atoms or molecules consist of various discrete and unique wavelengths which are the characteristics of the emitting atoms or the molecules. The sources of the optical emission spectrum include arcs, sparks, lamps and electrical discharges or plasmas, the subject of

our study in this chapter. Atoms, molecules or their ions and radicals, all can emit light when they are excited.

Modern spectroscopic notation indicates the spectrum of a given stage of excitation or ionization by a Roman numeral after the element symbol: I for neutral atom, II for single ionization and VI for an atom that have lost five electrons. Therefore Cl I denotes the spectrum of neutral atomic chlorine and Cl III denotes the spectrum of doubly ionized atomic chlorine.

2.2.1 Commonly used terms in OES

Emission spectra have a few general characteristics and terms associated with them. These characteristics, the terms and their definitions are given below;

Spectral line; emission or absorption line: Originally, an image of the entrance slit in monochromatic light, emitted as seen through the spectrometer. Generally, it is defined as very narrow band of frequencies or range of wavelengths of electromagnetic radiation from a transition between two energy levels in an atom or molecule.

Spectral Band; Emission Band: A crowded group of adjacent spectral lines emitted due to radiative transitions in a free molecule, diatomic or polyatomic radical. The intensity of the emission can be degraded either towards longer wavelengths or shorter ones

Band line: One of the many emission lines constituting the emission band.

Band head: The sharp edge of the spectral band lying on either the long-wavelength or the short-wavelength side of the band.

Continuum: Radiation emitted or absorbed throughout an extensive continuous wavelength range.

Multiplet; (singlet, doublet and triplet): A collection of closely spaced single spectral lines belonging to the same transition between two spectroscopic terms, or a collection of closely spaced energy levels belonging to the same term. It is called a singlet, doublet or triplet when the collection comprises 1, 2 or 3 members respectively.

Spectroscopic term: A group of one or more energy levels belonging to the same multiplet.

Resolving power; Resolution: A measure of the difference between the wavelengths of two components of radiation that can barely be separated by a spectral instrument. It is given by $\lambda/\Delta\lambda$ where $\Delta\lambda$ is the half intensity width of a very narrow spectral line imaged by the spectral instrument.

2.3 Optical Instruments used in OES

The demands on instruments for the observation of the Reactive Ion Etching (RIE) plasmas can be quite different from those encountered in the other application of spectroscopy. Depending on the special requirements in a given experiment, the

spectrometer must have sufficient resolution and supply as much light as possible into the detectors.

The resolution R is given by

$R = \lambda/\Delta\lambda$

On the other hand, $\lambda/\Delta\lambda = mN$ where m is the order number and N is the total number of the illuminated grooves, that is the groove density times the width of the grating. Therefore the resolution is a function of the total number of the illuminated grooves.

In many instances the practical limit on the wavelength resolution is governed by a compromise among conflicting parameters such as signal to noise ratio, spectrum acquisition time, the spectral range and the amount of light available or the detection limit. However, the resolution may be much poorer than the theoretical resolving power of the spectrometer under ideal conditions. In any spectroscopic experimental set-up, windows, lenses, mirrors and optical fibres are used to collect and guide the light from the source to the detector. For these components, the most important limit in the present application is probably the short-wavelength limit of their transmission. For windows, lithium and calcium fluorides can be used down to about 135 nm in the vacuum, but they have poor mechanical strength and they lose their transmission early because of surface damage due to UV radiation. A very enduring window material is Sapphire, transmitting down to 155 nm, the best fused Silica is down to 175 nm, Pyrex is 320 nm, Crown glass is 350 nm. The long wavelength limit of windows is not a problem since all these materials can transmit up to 2.5 μm. In practice a range of 200-1000 nm is usually used in RIE plasma observations. Similar considerations apply for lenses and optical fibres. For acquiring a wide spectrum from 200-900 nm say, a resolution of about 0.1-0.5 nm is sufficient. However for the detailed spectrum observation a higher resolution is required, because most of the plasmas can emit lines belong to various species and these can be superimposed on each other. A resolution of about 0.01-0.1 nm is very desirable.

The detectors used in OES include photomultipliers and charged-coupled devices (CCDs) such as diode arrays. Photomultipliers have excellent time response which usually is of order of 0.1 μsec. Another important characteristic is the wavelength sensitivity which depends on photocathode and window materials. In low density plasmas used for RIE processes the emitted light is of low intensity, therefore the signal to noise ratio of the detectors becomes particularly important. In photomultipliers the signal to noise can be improved by cooling the tube. In spectrometers that use diode array detectors the whole spectrum range is obtained at once, however the signal to noise ratio is poor unless long exposure times were used. In RIE processes, for in-situ end point monitoring short sampling times are required. Unlike the diode array detectors, photomultipliers have a good signal to noise ratio even when very short sampling times are used, therefore can be used efficiently for in-situ end point monitoring.

2.4 Experimental

Optical emission spectra were recorded using two spectrometric systems. System 1, consisted of a Silicon diode array (OMA III from EG&G Applied Research) attached to a Jarrell-Ash monochromator with a choice of three gratings. The gratings are supplied with different groove densities, grating 1 with 1200 gr/mm and a fixed spectral range of 60-70 nm blazed at wavelength of 400 nm , grating 2 with 600 gr/mm and spectral range of 120-140 nm, blazed at 500 nm and grating 3 with 150 gr/mm and spectral range of 600 nm, blazed at 500 nm. Since there is no exit slit, the resolution here depends on the width of the entrance slit which was fixed at 25 μm, and the groove density of the grating. The resolutions were 1 nm, 1.5 nm and 3 nm for gratings 1, 2 and 3 respectively. The diode array detector is 50 μm long, comprises 1024 diodes and water cooled to minimize the dark current. The signal to noise ratio is strongly dependent on the exposure time. Since the light emitted from the plasma is of low intensity, an exposure time of 1 minute is required for a practical signal to noise ratio. The accessible spectral range is between 180-1100 nm. The second system is a MultiSEM 440 (Sofie Instruments) with a monochromator equipped with a 2400 gr/mm grating and an adjustable slit width between (50-500)μm, which has a resolution down to 0.1 nm. The light is detected by Hamamtsu photomultiplier R928 equipped with cooling system, the total accessible spectral range is between 200-680 nm. The first system has an advantage of wider accessible spectral range and the whole spectrum in any given range is obtained at once, however it lacks the sensitivity and the high resolution which makes it difficult to be used in end point detection in RIE processes. In both systems the light is collected by quartz optical fibre with large acceptance angle through a quartz window mounted on the top electrode of the discharge machine.

All spectra in this chapter were recorded from discharges in the Oxford Plasma Technology machines which will be described in chapter 4.

2.5 OES as a diagnostic tool in Reactive Ion Etching (RIE) plasmas

A plasma is a complex system: It is therefore helpful to be able to use many different diagnostic techniques to monitor its states. Possible diagnostic techniques include OES, Mass Spectrometry (MS) and Electrostatic probes. The MS data is very useful, but lacks accuracy in the investigations of plasma densities such as ion densities. The Electrostatic probes tend to disturb the plasma under investigation and they are not easy to use routinely. OES has the advantage that it requires no physical contact with the plasma.

The emission intensities are proportional to the densities of the electronically excited states. However these excited states are related to their densities in the ground state which cannot be measured accurately with OES data alone. Nonetheless the OES can be used for many purposes and these include,

1. Monitoring particular lines in the discharge which are emitted by the desired reactive species or neutral atoms, or by impurity gases in the discharge.
2. Investigating the chemistry of the discharge by establishing the probable excitation channels.
3. Detecting an end point. OES can be used to determine when the etching has reached the interface between two different layers by monitoring the etch product of the layer being etched or the product from the layer at which the etching is to stop or from both layers.

The earliest investigations of RIE processes employing OES were made of Si etching in CF_4/O_2 plasma by Harshbarger et.al. (1977)[1] who found that the etch rate of Si was correlated with the intensity of optical emission from excited fluorine atoms when O_2 was added to the discharge. Later more through investigations was made by Mogab, Adams and Flamm et.al (1978)[2] using OES with Mass Spectrometry, Infrared Spectroscopy and gas phase titration. They found a marked increase in atomic fluorine emission (F line at 703.7 nm) as O_2 was added to CF_4 plasma. The enhanced emission approximately correlated with fluorine atoms concentration as determined by gas phase titration. However the concentration of the emitting species in the ground state remained difficult to determine by OES methods, until Coburn and Chan et.al (1980)[3] discovered a method of correlating the emission of plasma species to their densities in the ground state by adding a small quantity of a nobel gas to the discharge, a technique which was later called Optical Emission Actinometry (OEA).

2.5.1 Identification of emission lines in RIE plasmas

Most of the plasmas which are used in reactive ion etching use either mixtures of gases such as $CH_4/H_2/O_2$ or gases that are polyatomic molecules such as $SiCl_4$. This makes the spectrum complex and identifying all emission lines in these plasmas accurately can be, at times, very difficult. Some of these difficulties are caused by a; the plasma having very weak intensity of emission, b; the presence of continuums, headless bands or other structures lacking any outstanding features in the spectrum, c; the presence of impurities in the discharge which can give unexpected emission lines. An example of the latter is the presence of AlCl lines in discharges containing chlorine species when using aluminium chamber or aluminium electrodes. Again, OH lines often show up in a CH_4/H_2 plasma due to presence of moisture in the chamber.

Where the resolution is sufficient to allow reasonably accurate measurement on well-defined bands to be made, identification by means of wavelength tables is usually practical and error free. In using the wavelength tables from the literature, the following procedure is suggested as a guide:

1. Consider the most likely candidates to be present in the given discharge (molecules, atoms and their corresponding ions).

2. Such consideration often helps to eliminate erroneous identification and limits the number of elements (candidates) for which suspected emission lines belong.
3. Select two or more of the strongest emission lines of the spectrum to be identified and compare their wavelength with the list of persistent bands. If entries are found in close agreement with these wavelengths, and if the bands are degraded in the appropriate directions, refer to the detailed list for the corresponding systems.
4. Repeat step 3 for all the candidates considered as established in step 1.
5. If the bands given in the detailed list are found to be present in the spectrum and the details are found to agree, then identification may be considered fully established.
5. If bands or emission lines remain unaccounted for in the spectrum they may be an extension of the identified systems or other emission bands corresponding to the same identified molecule or atom.
If bands or emission lines are still outstanding, then other candidates which are less likely to occur in the discharge have to be considered including the most likely impurities, then step 1-4 should be repeated even with greater care.
It should be mentioned that use of spectrometers with high resolution and as wide an accessible range as possible makes identification a great deal easier.

2.6 Optical Emission Actinometry (OEA)

In RIE processes the excitation and subsequent emission of light by various species in the plasma is mainly by electron impact excitation processes which can take several channels. If the process is direct electron impact excitation from the ground state, then

$$e + X \rightarrow X^* + e \qquad \text{..... (2.6.1)}$$

Here X is species in the ground state and X^* is the species in any excited state above the ground state.
On the other hand, dissociative excitation of the parent molecule to its constituent fragments leads to

$$e + XM \rightarrow X^* + M + e \qquad \text{..... (2.6.2)}$$

where XM is parent molecule dissociated into X^* in the emitting state and M in the ground state. Other electron impact processes that may occur in the discharge include dissociative attachment through electron capture, ionization, dissociative ionization and ionization excitation, i.e.

$$e + XM \rightarrow X^- + M \qquad \text{..... (2.6.3)}$$

$$e + X \rightarrow X^+ + 2e \qquad \text{..... (2.6.4)}$$

$$e + XM \rightarrow X^+ + M + 2e \qquad \text{..... (2.6.5)}$$

$e + X \rightarrow [X^+]^* + 2e$ ..... (2.6.6)

However processes (2.6.4 - 6) require a higher energy than 2.6.1-3.

Free radical concentrations in the low pressure plasmas used in RIE processes may be measured by several techniques, including laser induced fluorescence,[4-9] atomic titration,[10,11] absorption spectroscopy,[12-14] and optical emission spectroscopy.[14,15] Free radical concentration measurements made by direct measurement of the plasma emission intensity using OES can give misleading results because changes in emission intensity can result from changes in electron concentration or electron energy distribution, as well as from changes in gas composition due to dissociation processes that occur in the discharge. For example, in CH_4 plasma, CH_4 can dissociate into CH, H_2 and H fragments, all of which can be a source for the emission of H_α. Therefore changes in the emission intensity of H_α can result from changes in electron concentration or from changes in the concentration of fragments. To correct for these effects the technique of optical emission actinometry (OEA) was developed by Coburn et.al (1980)[3] as mentioned earlier. In OAE a small amount of an inert gas with an excitation cross section similar to that of species of interest (e.g., Ar for Cl detection) is added to the plasma, and the emission of the species of interest is measured relative to the emission from the inert gas. For actinometry to be valid, a number of assumption must hold. First, the excitation of species of interest X must be by the ground state electron-impact process as in (2.6.1) above, and a constant fraction of the excited species X^* must relax by photoemission. Assuming all the excited states relax by photoemission, then at steady state the emission intensity is proportional to the rate of excitation or the excitation efficiency, i.e.

$$I_x \propto C\, k_x\, n_e\, [X] \qquad \text{..... (2.6.7)}$$

Where I_x is the intensity of emission from species x, n_e is the electron density, [X] is the concentration of species x, k_x is the excitation constant or the excitation efficiency of species x and C is generally a constant depending on the apparatus. The electron density n_e is a function of discharge parameters such as power, pressure, electric field, gas composition, and the electrode geometry in a very complicated way which cannot be calculated in general, therefore it has to be eliminated from equation 2.6.7. The excitation efficiency is a function of the electron energy distribution, and may be expressed as [17]

$$k_x = \int_0^\infty v(\varepsilon)\sigma_x(\varepsilon)f(\varepsilon)d\varepsilon \qquad \text{..... (2.6.8)}$$

Where ε is the electron energy, $v(\varepsilon)$ is the electron velocity, $f(\varepsilon)$ is the electron energy distribution function, and $\sigma_x(\varepsilon)$ is the collision cross section for excitation of x. Equation (2.6.7) may not be valid if there are additional pathways for loss of X*. For instance if the collision deactivation is important de-excitation process, Eq. (2.6.7) is only valid when the

rate of collisional de-excitation is constant (e.g. at constant pressure or at constant power).[17]

The emission intensity of species x is proportional to [X], n_e and k_x. Therefore changes in I_x may not be indicative of changes in [X]. OAE is designed to correct for the variations in the electron density by normalizing the emission from X with the emission from the inert actinometric gas of known concentration. Using Eq.(2.6.7), the emission intensity of the actinometre is proportional to its rate of excitation, i.e.

$$I_{ACT} \propto C\, k_{ACT}\, n_e\, [ACT] \qquad \text{..... (2.6.9)}$$

where I_{ACT} is the emission intensity of the actinometric species at a chosen wavelength, k_{ACT} is the excitation efficiency of the actinometre and [ACT] is the concentration of the actinometric gas. The ratio of the emission intensity from species X to that from the actinometric gas is

$$\frac{I_x}{I_{ACT}} \propto \frac{k_x}{k_{ACT}}\left(\frac{[X]}{[ACT]}\right) \qquad \text{..... (2.6.10)}$$

If the actinometric gas is chosen such that excitation cross sections $\sigma_x(\varepsilon)$and $\sigma_{ACT}(\varepsilon)$ are similar functions of electron energy, the excitation efficiencies k_x and k_{ACT} will be similar functions of electron energy. As a result, the ratio k_x/k_{ACT} may be considered constant. Assuming that the mole fraction of the inert gas is fixed, the concentration of the inert gas is proportional to the discharge pressure P, and Eq.2.6.10 may be written as

$$(PI_x)/I_{ACT} \propto [X] \qquad \text{..... (2.6.11)}$$

Therefore, measurements of the actinometric ratio $(PI_x)/I_{ACT}$, are indicative of the concentration of species [X].

2.7 OES of Hydrogen based plasmas

2.7.1 OES of H_2

The hydrogen molecule H_2 is one of the simplest structures nature has provided. In spite of this simplicity of structure, it has an extraordinarily complicated spectrum in which some thousands of lines have been observed. The spectrum of molecular hydrogen has few characteristic features as the rotational structure is so open that there are no heads or close groups of lines to form anything resembling the usual band structure. The spectrum is strongest in the orange but extends throughout the visible region. In fig.2.1 the spectrum of H_2 is given in the range 200-680 nm from a discharge at a rf power of 100 W, a flow rate of 25 sccm and a pressure of 20 mtorr. Emission lines from atomic and molecular hydrogen can be seen but the dominant feature of the spectrum is the emissions from atomic hydrogen, the Balmer series, H_α at 656.27 nm, H_β at 486.13 and H_γ at 434.04 nm. Fig.2.2 shows the spectrum of H_2 in detail in the visible region. Fig.2.3 show the spectrum in the infrared region 680-900 nm. In this region the spectrum

is dominated by emission from the rotational transitions of H_2 where singlet and triplet transitions can occur but not doubled transitions. All the prominent emission lines and their transition systems and excitation energies are given in table 2.1.

The emissions from H atoms mainly result from direct electron impact excitation of the ground state H_2, i.e.

$$e + H_2(X) \rightarrow H_{(n=1)} + H^*_{(n=4)} + e \qquad E_{th}= 17.23 \text{ eV} \quad .... \quad (2.7.1)$$

Similarly the emissions from H_2 molecules result from direct electron impact excitation of the ground state [30], i.e.

$$e + H_2(X) \rightarrow H_2^*(G\,^1\Sigma_g^+) + e \qquad E_{th}= 14.17 \text{ eV} \quad .... \quad (2.7.2)$$

In Eq.2.7.1, the minimum excitation energies (E_{th}) have been calculated by summing up the energy of dissociation of H_2 into the fragments H and H in their ground state and the relevant excitation energy of one or more of these fragments. The dissociation energy of H_2 is 4.48 eV, given by ref.[18].

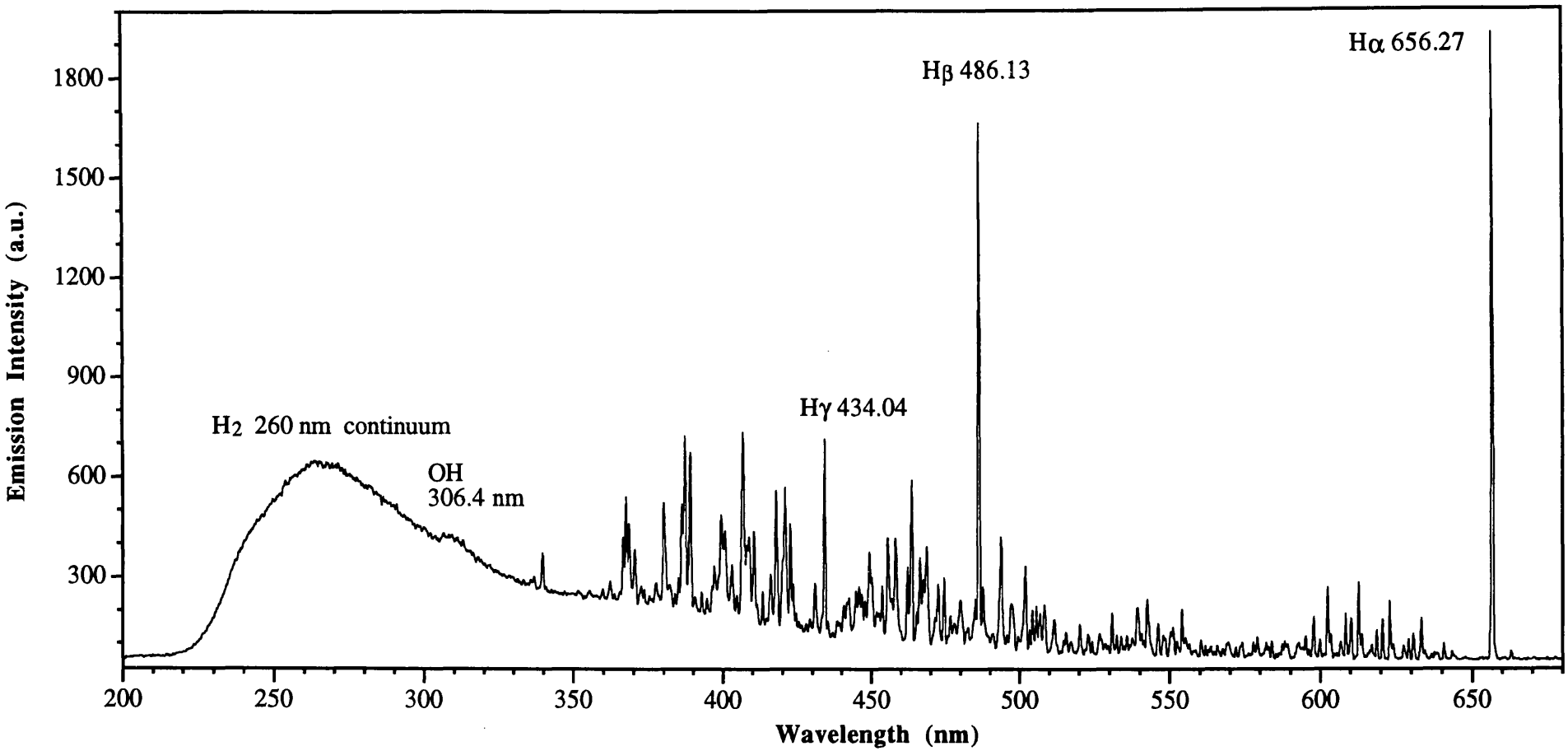

Fig.2.1: Spectrum of Hydrogen plasma in the range 200-680 nm, shows the prominent atomic Hydrogen lines of Balmer series, Hα, Hβ and Hγ, the emissions from molecular hydrogen, and the emission from H_2 Continuum at 260 nm the triplet transition $^3\Sigma_g - ^3\Sigma_u$. The emission from OH appears due to the presence of moisture in the chamber.

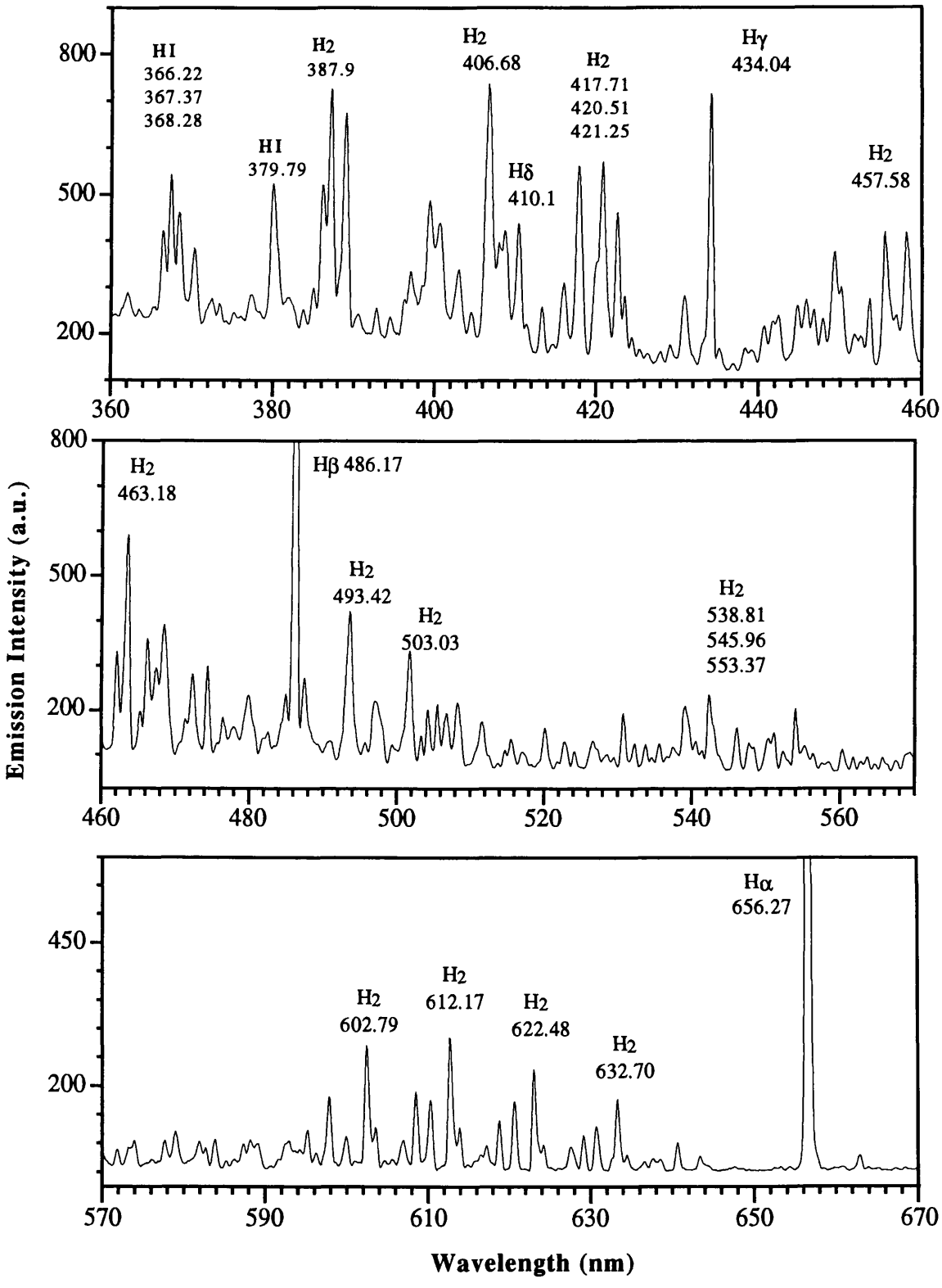

Fig.2.2: Spectrum of Hydrogen in detail, which shows the rotational structure of H_2 lines as well as the atomic lines.

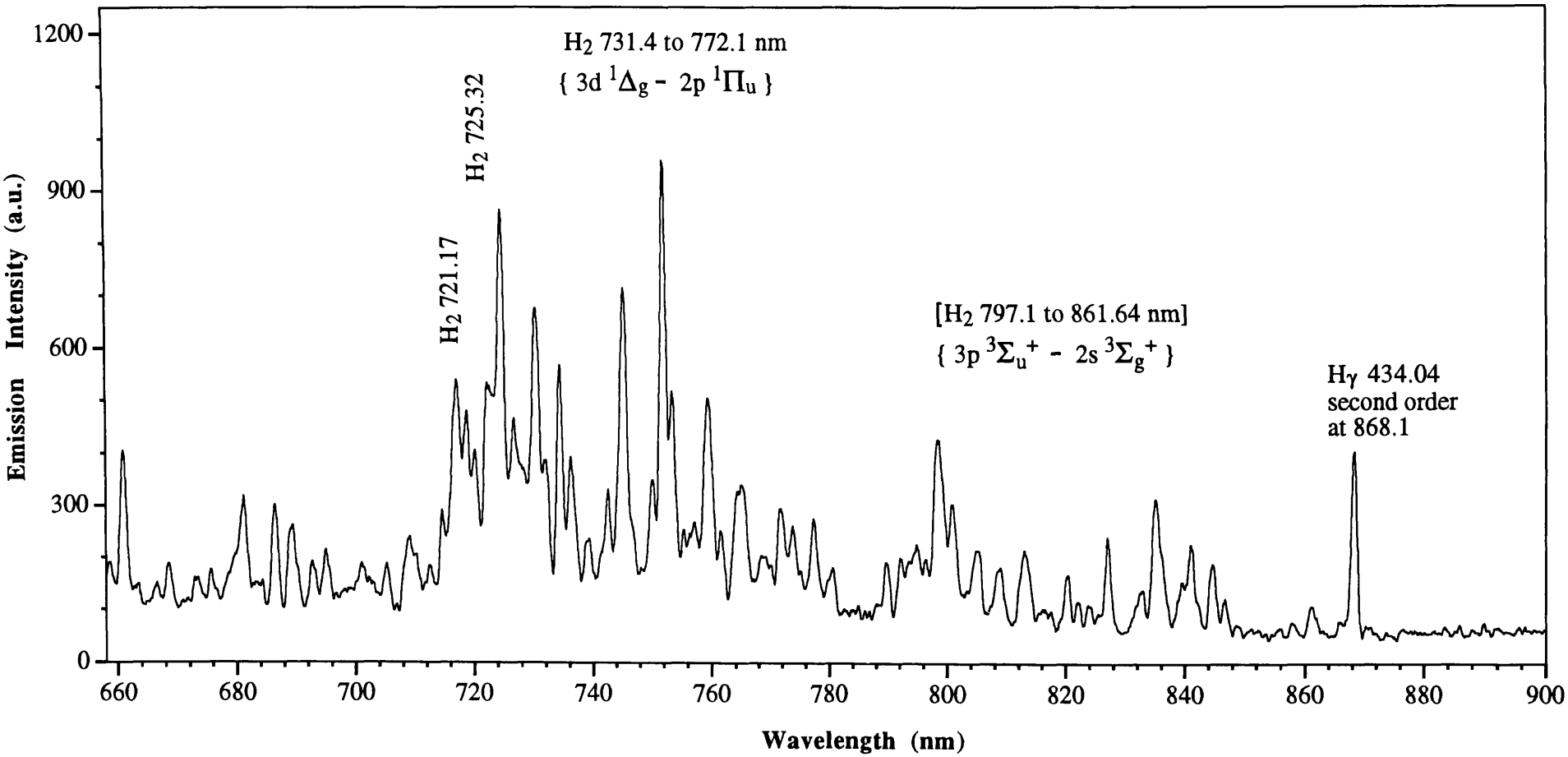

Fig.2.3: Spectrum of H_2 plasma in the infrared region (660-900) nm, shows the rotational-vibrational transitions, also the second order of H_γ at 868.1 nm.

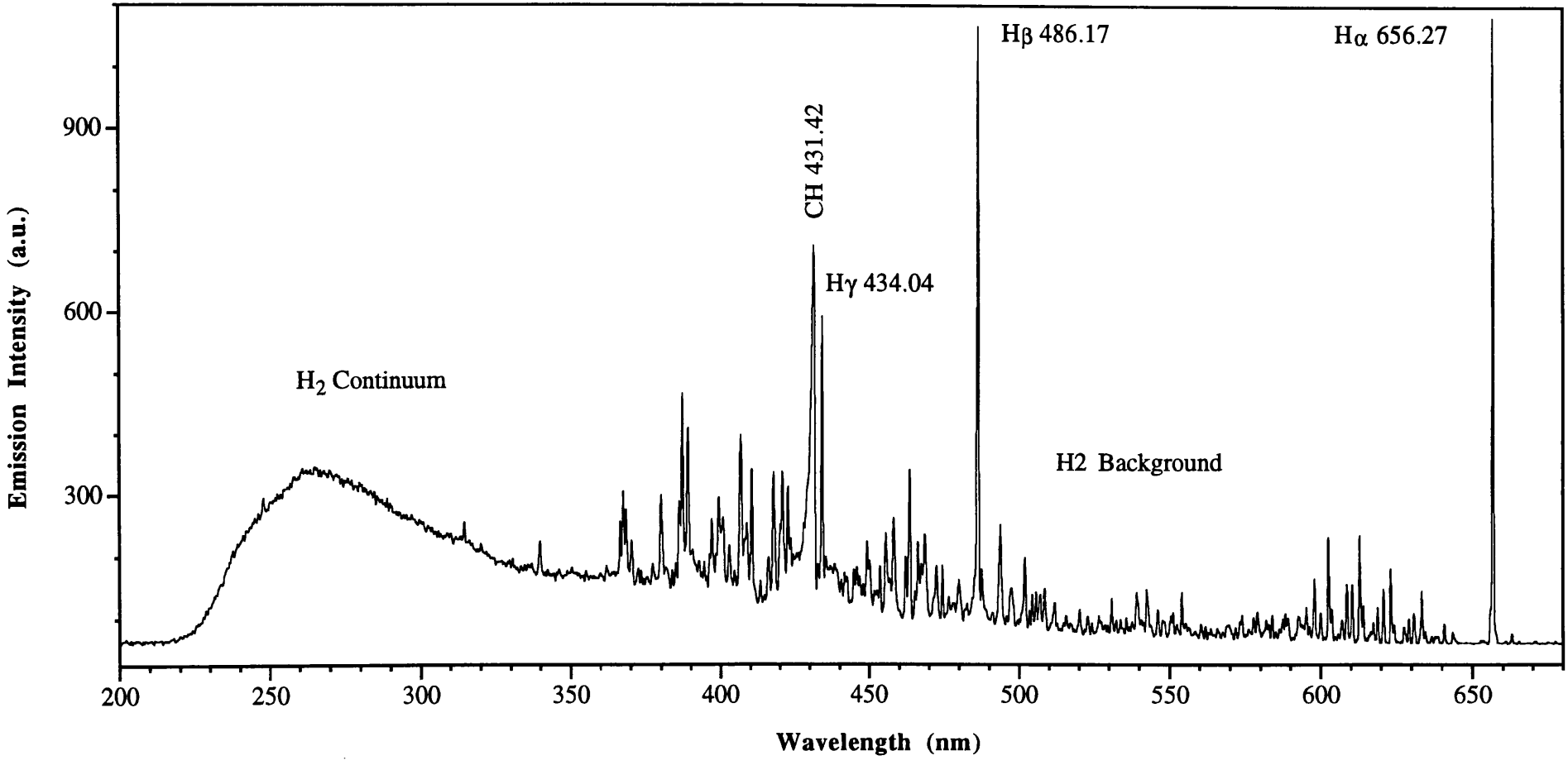

Fig.2.4: Spectrum of CH_4/H_2 plasma in the range of 200-680 nm, shows the prominent atomic H lines and the only indication of the presence of CH_4 is the emission from CH at 431.42 nm.

2.7.2 OES of CH_4/H_2 plasma

The discharges of a mixture of CH_4/H_2 were performed in Electrotech SRS 340 etching machine. In fig.2.4 the spectrum of a mixture of CH_4/H_2 is given in the range of 200-680 nm, the discharge was performed at a power of 100 W, CH_4/H_2 ratio of 5/25 sccm and at pressure of 25 mtorr. The spectrum in this range as in the case of pure H_2 discharge is dominated by the emissions from atomic hydrogen (H_α, H_β, and H_γ) and molecular hydrogen H_2. No emission from CH_4, CH_3 or CH_2 was detected. CH_4 is known not to show emission spectra. CH_2 and CH_3 radicals are known to have absorption spectra in the deep UV and visible regions[19-20], however no emission spectra of these radicals have been observed. The only indication of the CH_4 presence in the discharge is the emission from CH ($A\ ^2\Delta \rightarrow X\ ^2\Pi$) transition, the band head of which appears at 434.42 nm as shown in fig.2.5.

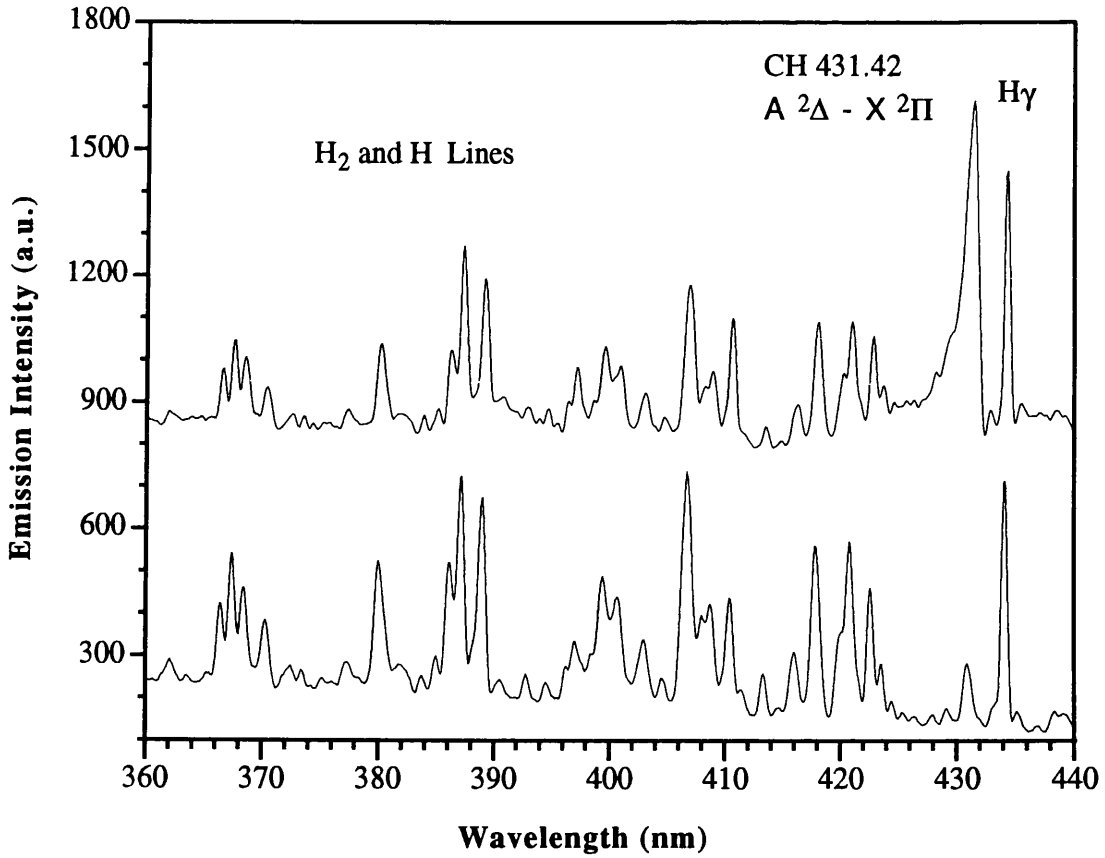

Fig.2.5: The top spectrum is of CH_4/H_2 plasma ratio of (1:5 at 100 W, 700 V dc bias and 20 mtorr pressure) and the bottom spectrum is of H_2 using the same discharge conditions.

2.7.3 OES of $CH_4/H_2/O_2$ plasma

The spectrum of a mixture of $CH_4/H_2/O_2$ together with spectrum of CH_4/H_2 for comparison is given in fig.2.6 in the range of 200-460 nm. The discharge was

performed at 100 W, $CH_4/H_2/O_2$ ratio of 5/25/0.5 sccm, pressure of 25 mtorr and dc bias of 360 V. Emission lines from CO at 283.3, 297.74 nm; the third positive system of CO^+ at 218.98, 229.96, 247.42 nm; the first negative system of CO_2, 288.3, 289.6 nm bands, and emission from OH 306.6 nm bands are detected in the spectrum. No emission from O_2 or O was detected in this region. The appearance of CO, CO_2 and OH in the spectrum is due to the addition of O_2 which reacts with CH_4, H_2 and their fragments in the gas phase and leads to formation of these species in ground or in the excited state. Emission lines and the corresponding transitions of these species are given in detail in table I. In RIE processes utilizing CH_4/H_2 chemistry, the formation of polymer is a well known problem. The addition of O_2 in small percentages can reduces the formation polymer[21], by forming volatile CO, CO_2 and OH which will subsequently be excited in the plasma.

2.7.4 OES of $CH_4/H_2/N_2$

The spectra of $CH_4/H_2/N_2$ and CH_4/H_2 in the range of 280 - 560 nm are compared in fig.2.7. The discharge was performed at a rf power of 100 W, the flow rates of $CH_4/H_2/N_2$ were 5/25/0.3 sccm, at a pressure of 25 mtorr and a dc bias of 380 V. The spectrum is dominated by emission from N_2 lines at 337.13, 315.93, 357.69 and 375.54 nm (the second positive system of N_2) and emission from N_2^+ at 391.44 nm (the first positive system of N_2^+). Emission lines from CN at 387.1 and 388.3 nm were also detected indicating that N_2 reacts with CH_4 fragments in the discharge, however no emission from NH or NH_2 was detected. The addition of N_2 into the CH_4/H_2 plasma can serve two objectives. The first objective is that N_2 can be used as an actinometric gas to measure the relative changes in the emission intensity of the various species in the plasma such as CH and H_α, because the emission from N_2 can only be by direct electron impact excitation from the ground state by the process,

$$e + N_2 \rightarrow N_2^* + e \qquad E_{th} = 11.15 \text{ eV} \qquad \text{.... (2.7.4.1).}$$

The second objective is that N_2 reacts with CH_4 fragments in the discharge to form volatile species of CN, thereby reducing polymer formation during the RIE processes as this will be discussed further in the next two sections.

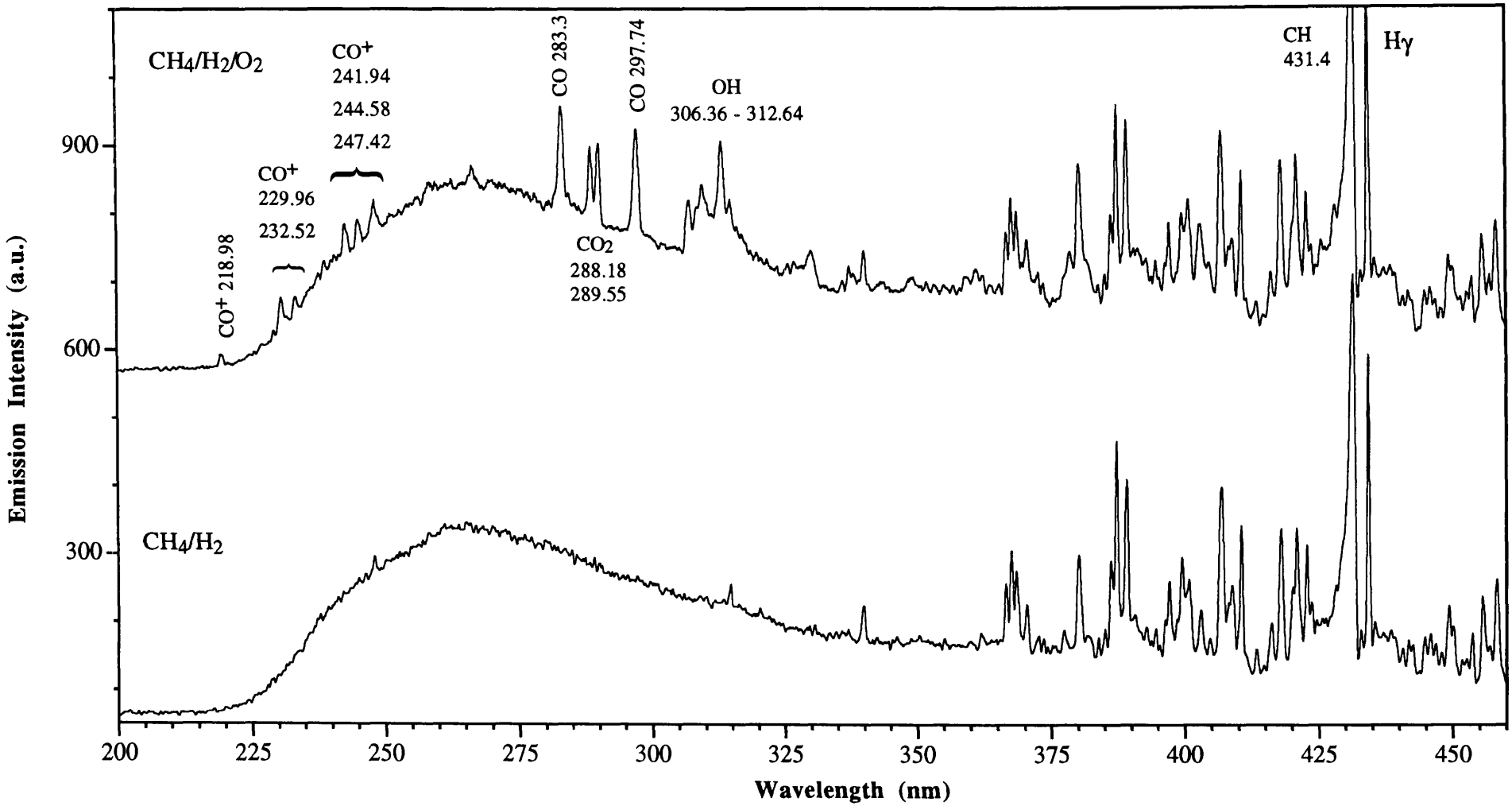

Fig.2.6: Spectrum of $CH_4/H_2/O_2$ and CH_4/H_2 in the range of 200-440 nm which shows the presence of CO, CO^+, CO_2 and OH lines formed due to O_2 addition in small amounts to CH_4/H_2 plasma.

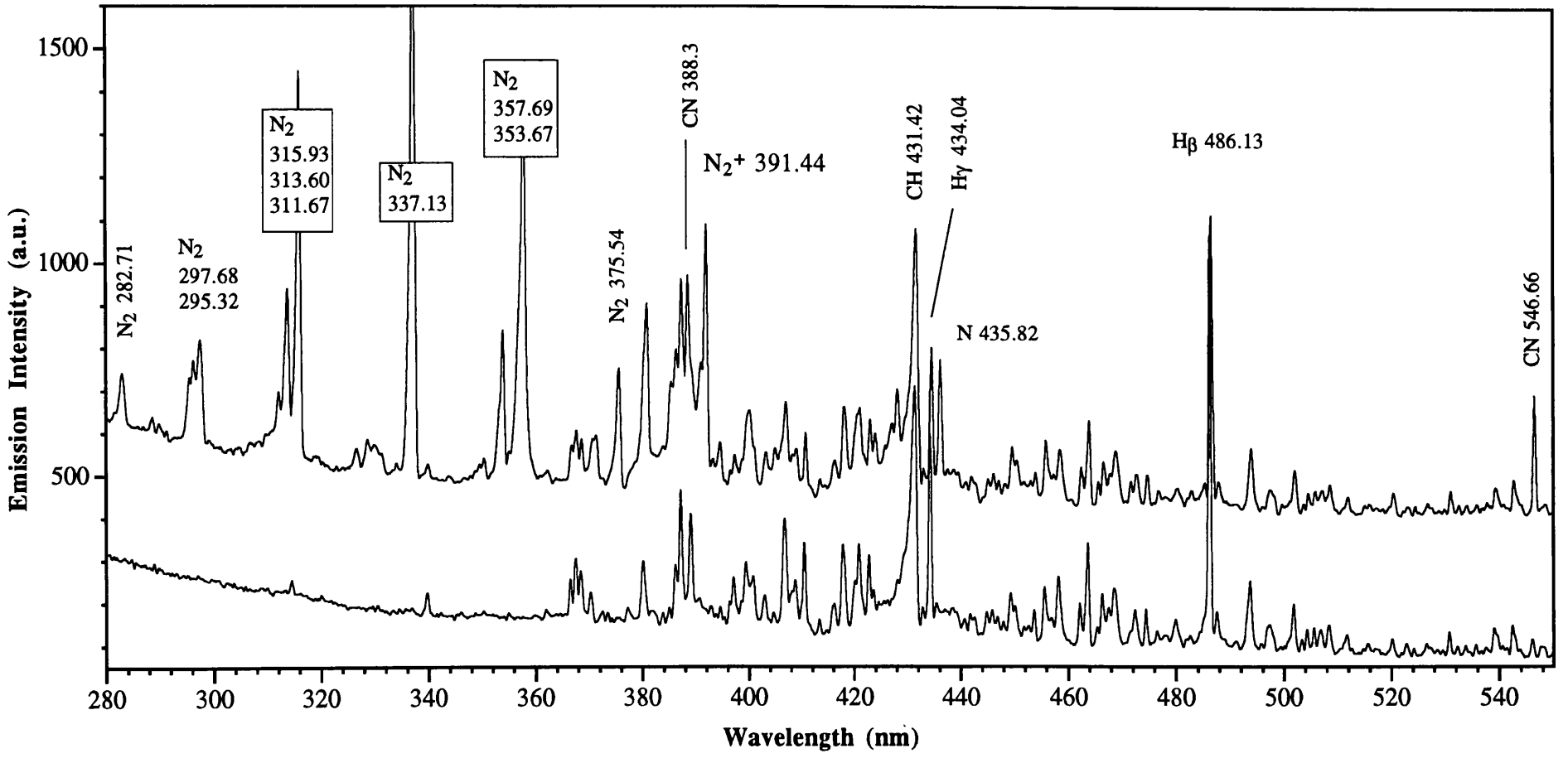

Fig.2.7: Spectrum of $CH_4/H_2/N_2$ ratios of 5/25/0.2 sccm, shows the N_2, N_2^+ and CN lines

2.8. Origin of the emitting species in CH_4/H_2 plasma

All the species in the discharge are decomposition products of CH_4 and H_2. The emitted lines result either from dissociative excitation processes of CH_4 and H_2 molecules or from electron impact excitation of radicals and atoms. The optical emission cross sections of CH line (431.42) nm and the emission cross section of Balmer series of H resulting from the dissociation of CH_4 have been measured by several authors (Aarts et.al.1971, Bonohue et.al. 1977). These have similar energy dependencies, rising steeply from threshold up to values of about 10^{-18} cm^{-2} for an electron energy of ~ 100 eV and then decay slowly. Similar emission cross sections are also observed for the emission of Balmer series from direct electron impact on H_2 molecules (Kayrallah et.al. 1976, Miles et.al. 1969) and H atoms (Kleinpoppen and Kraiss 1968, Walker and St. John 1974). All these excitation processes and their theoretical onset energies are given in table 2.2. The minimum excitation energies have been calculated by adding up the energy of dissociation of the parent molecules into their constituent fragments in the ground state and the relative excitation energies of one or more of those fragments. The excitation energies of all the species are given in table 2.1; the dissociation energies have been taken from[18], and are D(H-H) = 4.48 eV, D(C-H) = 3.47 eV, D(CH-H) = 4.46 eV, $D(CH_2\text{-}H)$ = 4.90 eV and for $D(CH_3\text{-}H)$ = 4.41 eV.

In order to determine which dissociation processes are more likely to occur, a small amount of N_2 (0.5% of the total flow) was added to discharge to monitor the emission intensities of H_α 656.27 nm, CH 434.42 nm and H_2 463.4 nm emission lines as the applied rf power was increased from 10 - 120 W. The emission intensities of these species and the emission from the added N_2 at 337.13 nm as a function of the rf power is shown in fig.2.8. It is clear that the emission intensity of CH, H_2, and N_2 have approximately the same power dependence. However the emission intensity of H_α is more strongly dependent upon power. In fig.2.9, the emission intensities of CH, H_2 and H are plotted as a function of the corresponding emission intensity of N_2 in log-log scale. Since the data fell on good straight lines, power law fits are made. The emission intensities of CH and H_2 are found to vary as the 0.89 and 0.62 power of the emission intensity of N_2, respectively. By contrast, the emission intensity of H_α was found to vary as the 1.85 power of the emission intensity of N_2. This implies that the emission intensities of CH and H_2 are approximately proportional to the emission intensity of N_2, whereas the emission intensity of H_α is proportional to the square of the emission intensity of N_2. Since the formation of an emitting excited state of N_2 requires only one electron impact excitation, because N_2 in the excited state can only be formed form N_2 in the ground state, so will the formation of the emitting excited states of CH and H_2. Therefore the emitting excited states of CH and H_2 (CH^* and H_2^*) are primary products of the dissociative excitation of CH_4 and H_2 parent molecules.

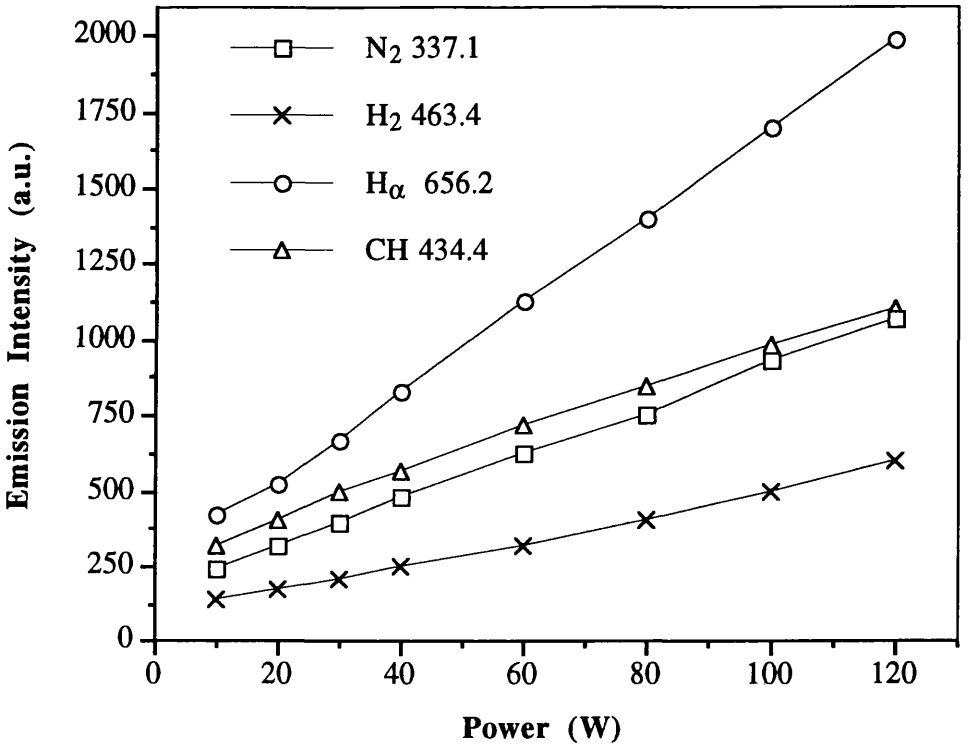

Fig.2.8: Emission intensities of CH, H_2, H_α and N_2 as a function of rf power.

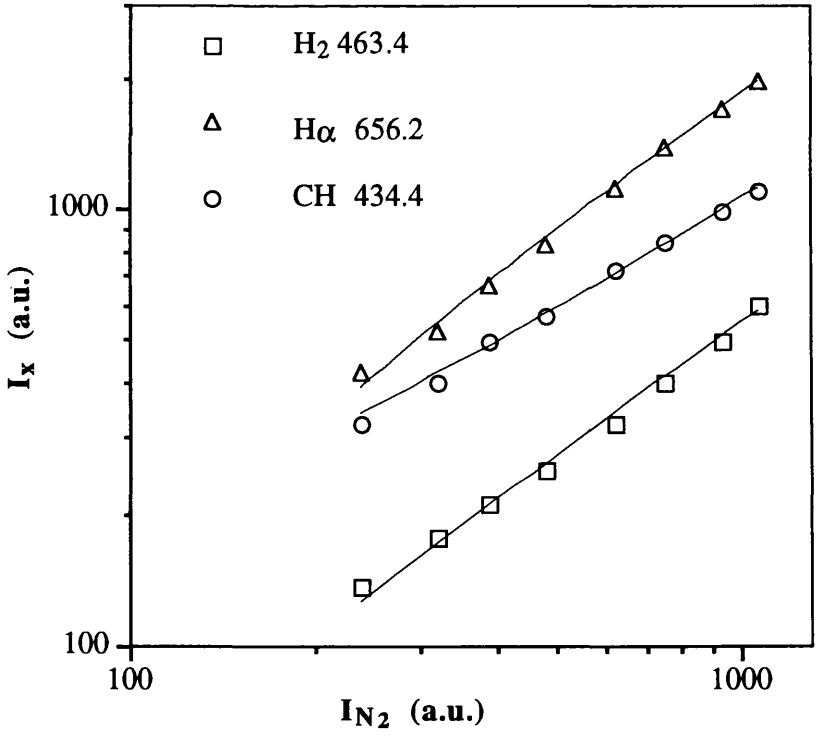

Fig.9: Log-log plots of the emission intensities of CH, H_2, and H_α as a function of the emission intensity of N_2 for the same power.

For H_α, since the emission intensity is approximately proportional to the square of the emission intensity of N_2, two electron impact excitations must be required to form the excited state of H (H_α). The first electron is required to produce H in the ground state mainly through reactions (1, 2, 4, and 8). The second electron then excites H species to the emitting state (H_α) through process 14. Therefore the emitting excited state of H (H_α) is not a primary product of the dissociation of CH_4 or H_2. Now, in order to identify the processes that are more likely to be responsible for the formation of CH* and H_2^*, all the processes that contain CH*, H_2^* or both and do not contain H_α have to be considered. Therefore the formation of CH* from direct dissociative excitation of CH_4 is mainly by process 8 for low energy electrons and process 10 for high energy electrons. H_2^* formation is by two sources, one, by processes (6, 7, and 10) from dissociative excitation of CH_4, and two, by process 15 from electron impact on ground state H_2.

2.9 Reactive Ion Etching in CH_4/H_2 plasmas

In the last few sections we studied the spectra of CH_4/H_2 plasmas, the effect of O_2 or N_2 addition on formation of the reactive species in the discharge and the probable excitation channels. In this section a brief introduction is given on Reactive Ion Etching of III-V semiconductors in CH_4/H_2 based plasmas and the analytical techniques used to study the etching mechanisms and etch depth monitoring in these plasmas.

The use of CH_4/H_2 for the Reactive Ion Etching of semiconductor compound materials was first developed by Niggebrugge et.al.[35] Using CH_4:H_2 ratio of 1:3, power density of 0.5 W/cm^2 and pressure of 20 mtorr, he reported reactive ion etching of InP at an etch rate of 50-70 nm/min with good anisotropy and smooth surfaces. However the etched surfaces were covered with a thick layer of carbonic polymer. On the other hand, when the same mixture was used to etch GaAs, slow etch rates below 10 nm/min and rough surfaces were obtained. Since the pioneering work of Niggrebrugge,[35] RIE of III-V compounds in CH_4/H_2 has become an important technique in the fabrication of InP based devices, since no other reliable chemistries are available yet which produce acceptable etching of InP based materials. However the disadvantage of using CH_4/H_2 chemistry is that it leads to formation of polymers on the masked regions which makes further processing more difficult. On the other hand, the addition of small percentages of O_2 to the discharge reduces the amount of polymer.[21] Because oxygen reacts with the involatile carbonic radicals in the discharge and forms volatile products of CO and CO_2 (see fig.2.6).

Hydrogen passivates the donors or acceptors in the III-V semiconductor materials.[39-41] By forming complexes with the donor or acceptor atoms, hydrogen leads to reduction of the carrier concentration of the active layers of the devices upon etching. In some cases this passivation effect can be reversed by Rapid Thermal Annealing (RTA) at elevated temperatures (≥300 °C). However, such annealing process is not possible in all devices.

Overall, CH_4/H_2 chemistry cannot be regarded as an ideal etching chemistry for III-V semiconductors.

Reactive ion etching of InP and GaAs in CH_4/H_2 chemistry is believed to be the reverse of the MOCVD process, in that the etch products of InP are phosphine (PH_3) and methylated indium compounds such as trimethylindium [$In(CH_3)_3$] or triethylindium [$In(C_2H_5)_3$]. Similarly the formation of methylated gallium compounds such as trimethylgallium [$Ga(CH_3)_3$] or triethylgallium [$Ga(C_2H_5)_3$] and AsH_3 are thought to take place during etching of GaAs [34-36]. The analytical techniques which have been used to study the mechanism of etching process of III-V materials in CH_4/H_2 plasmas include Mass Spectrometry [36,37] and Optical Emission Spectroscopy.[38] Mass Spectrometric analysis of the CH_4/H_2 plasma species during RIE of InP carried out by Schmid et.al.[36] showed that ethane, ethene, ethine, CH_5^+, $C_2H_5^+$, PH_3 and molecules which contain a higher order of carbon chains are present in the discharge. Moreover, a strong signal from PH_4^+ was detected which was later used for etch end point monitoring. However no In containing compounds could be detected which was ascribed to the limited resolution of the Mass spectrometer (the signals from In compounds interfere with those of high molecular hydrocarbons). On the other hand using OES to monitor the etch products during reactive ion of InP, Collot et.al.[38] and co-workers were able to detect several emission lines of In atoms. However no emission from P containing compounds was detected.

2.9.1 OES monitoring of etch products in CH_4/H_2 plasmas

To study the adequacy of OES for monitoring the etch products from etching GaAs and InP in CH_4/H_2 plasma, optical emission spectra were recorded during reactive ion etching of InP in CH_4/H_2 plasma using discharge conditions of; CH_4/H_2 ratio of 1:5, a pressure of 25 mtorr, 100 W rf power and bias of 350 V. An etch rate of 50 nm/min was obtained using these conditions. The spectrum of CH_4/H_2 while etching InP and without etching is given in fig.2.10. While emission from In lines (303.93, 325.62 and 451.13) nm can be detected with good resolution, no emission from P containing compounds was detected, even though some of these compounds are known to have emission spectra in the UV and visible regions (P_2, PH and PH_2 have their strongest bands at 342 nm) [31-33]. No emission from any of methylated Indium compounds mentioned in the last section was detected either. The reasons we have not observed these etch products are a; most of them do not emit or emit very weakly below wavelength of 1 μm, b; the sensitivity of our OES system is inadequate and c; these compounds are highly reactive in the discharge and tend to dissociate into fragments or rapidly incorporate into polymers upon collision with the surfaces. A high reaction rate results in a low steady state concentration in the gas phase and difficulties in detection [37]. Some of these methylated Indium compounds are believed to dissociate to atomic In and free radicals, and then the liberated Indium can be excited and

detected using OES. One of the problems associated with using OES to detect etch products in CH_4/H_2 are the low etch rates of all the materials etched in CH_4/H_2 chemistry which means that the partial pressure of these products is a few orders of magnitude less than the flow rates used in the discharge. In detecting In lines a substrate area of about 200 mm^2 was needed with etch rate of about 50-60 nm/min. For GaAs etching even with a 2-inch wafer no emission was detected from any of the etch products or their fragments such as Ga or As atoms as the etch rate of GaAs is only about 20-25 nm/min. To improve the monitoring ability of the OES for detecting etch products in CH_4/H_2 plasmas higher etch rates are required.

2.10 Chapter summary

In this chapter a brief introduction to the Optical Emission Spectroscopy (OES) and Optical Emission Actinometry was given. OES as a diagnostic tool for RIE plasmas was discussed. Emission spectra of H_2, CH_4/H_2 were studied in detail. In the spectrum from a CH_4/H_2 plasma, the only indication of the presence of CH_4 in the dicharge is the emission from the CH radical at 431.4 nm and the spectrum is dominated by the emission from the (Balmer series) of atomic hydrogen. The effect of adding O_2 to CH_4/H_2 plasma was studied and the results showed that CO and CO_2 and their ions can form in the plasma even for a very small percentage of O_2 in the dicharge. The addition of O_2 was seen to reduce the formation of polymer on the inner walls of the discharge chamber. The addition of N_2 to CH_4/H_2 plasma has a similer role in reducing the amount of polymer on chamber surfaces. In this case CN radicals were detected in the discharge as an indication of the reaction between N_2 molecules and carbonic radicals. Optical Emission Spectroscopic analysis of the origin of the emitting species in CH_4/H_2 plasma showed that the formation of CH and H_2 in the excited state (CH^* and H_2^*) requires only one electron impact dissociative excitation of H_2 and CH_4 parent molecules. On the other hand the formation of atomic hydrogen in the excited state (H_α) requires two electron impact excitations. Theoretically, the formation of methyls CH_3 and CH_2 from a CH_4/H_2 plasma is much easier than CH and H (as would be expected from an energetic point of view). However these radicals were not detected in the plasma as they are not known to emit below 1 μm. Optical emission spectra recorded during reactive ion etching of InP in CH_4/H_2 plasma showed that In lines can be detected with good resolution, whereas no emission from P containing compounds could be detected. On the other hand OES monitoring of GaAs etching in CH_4/H_2 plasma failed to detect any primary etch products or their fragments. This was ascribed to the low etch rate of GaAs in this plasma.

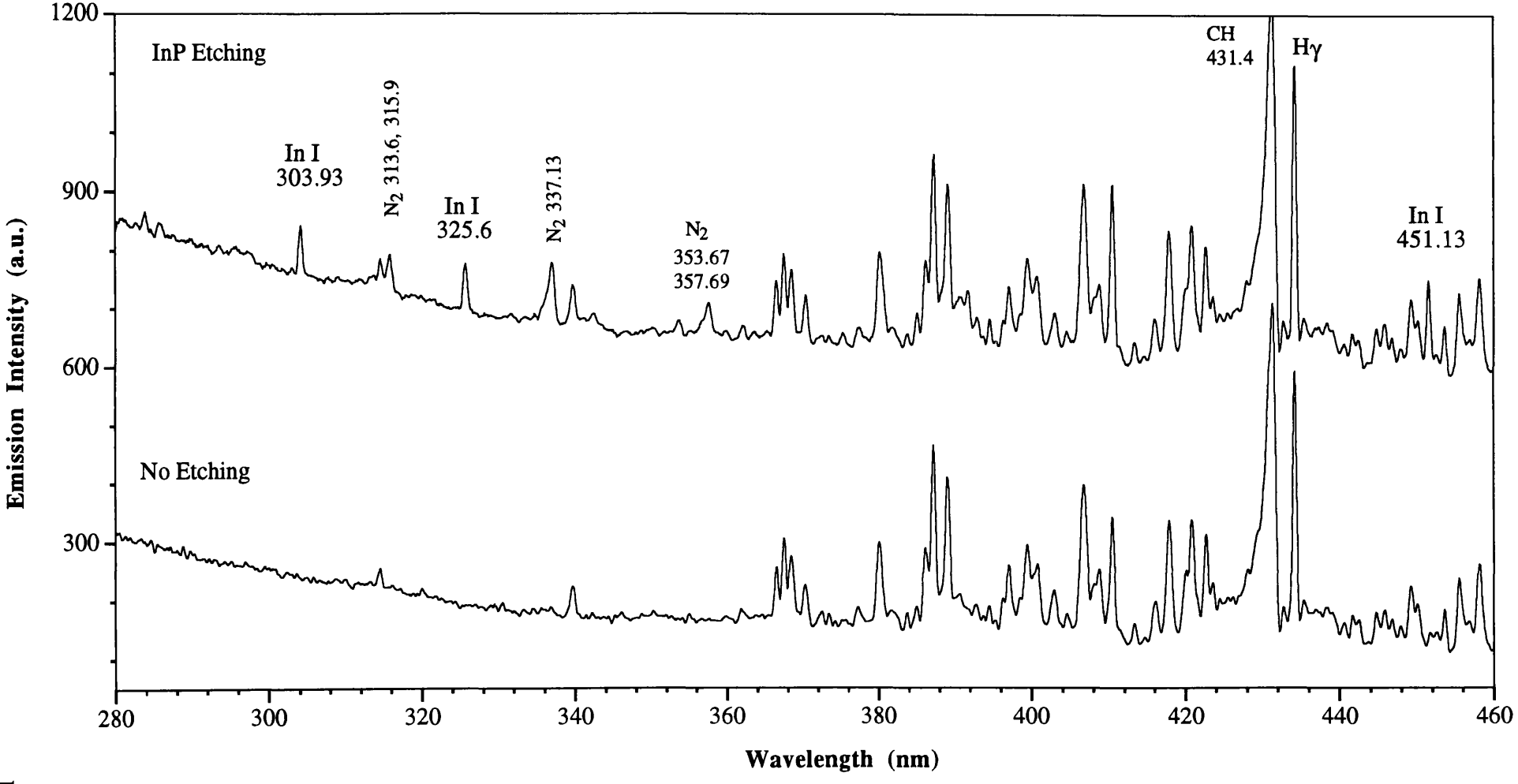

Fig.2.10: Spectrum of CH_4/H_2 while etching InP shows the emission from the etching products, In lines at 303.93, 325.6 and 451.13 nm also emission from N_2 which was detected due to a trace of N_2 in the etching system.

Table 2.1: The prominent emission lines, transitions and their direct excitation energy in the spectra of CH_4/H_2, $CH_4/H_2/N_2$ and $CH_4/H_2/O_2$.

Wavelength Range (nm)	Species	Transition Systems	Upper State Energy (eV)	Ref. no.
220 - 280	H_2	Continuum $1s\sigma\ 2s\sigma\ {}^3\Sigma_g^+ \rightarrow 1s\sigma\ 2p\sigma\ {}^3\Sigma_u^+$	11.89	28
368.35	H_2	$1s\sigma\ 4s\sigma\ {}^1\Sigma_g^+ \rightarrow 1s\sigma\ 2p\sigma\ {}^1\Sigma_u^+$	14.81	28
370.	H_2			19
381.2	H_2	$1s\sigma\ 6p\pi\ {}^3\Pi_g^+ \rightarrow 1s\sigma\ 2s\sigma\ {}^3\Sigma_g^+$	15.31	28
387.9.	H_2			19
389.02	H	$n = 8 \rightarrow n = 2$	13.385	19
397.12	$H\varepsilon$	$n = 7 \rightarrow n = 2$	13.32	19,28
406.68	H_2	$1s\sigma\ 3d\sigma\ {}^1\Sigma_g^+ \rightarrow 1s\sigma\ 2p\sigma\ {}^1\Sigma_u^+$	13.984	19,28
410.1	$H\delta$	$n = 6 \rightarrow n = 2$	13.22	19
417.71	H_2			28
420.51	H_2			28
422.25	H_2			28
434.04	$H\gamma$	$n = 5 \rightarrow n = 2$	13.06	28
461.7	H_2	$1s\sigma\ 4p\pi\ {}^3\Pi_u^+ \rightarrow 1s\sigma\ 2s\sigma\ {}^3\Sigma_g^+$	14.7	28
462.7	H_2	$1s\sigma\ 3d\sigma\ {}^1\Sigma_g \rightarrow 1s\sigma\ 2p\sigma\ {}^1\Sigma_g^+$	13.9	28
463.18	H_2	$1s\sigma\ 3d\sigma\ {}^1\Sigma_g^+ \rightarrow 1s\sigma\ 2p\sigma\ {}^1\Sigma_u^+$	14	28
486.17	$H\beta$	$n = 4 \rightarrow n = 2$	12.75	19
493.42	H_2	${}^1\Sigma_g^+ \rightarrow {}^1\Sigma_u^+$		28,31
602.79	H_2	$1s\sigma\ 3p\pi\ {}^3\Pi_u^+ \rightarrow 1s\sigma\ 2s\sigma\ {}^3\Sigma_g^+$	13.97	28
612.17	H_2			28
622.48	H_2			28
632.70	H_2			28
656.28	$H\alpha$	$n = 3 \rightarrow n = 2$	12.09	19
725.32	H_2	$1s\sigma\ 3s\sigma\ {}^1\Sigma_g^+ \rightarrow 1s\sigma\ 2p\pi\ {}^1\Pi_u$	14.12	28,31
753.92	H_2	$1s\sigma\ 3d\delta\ {}^1\Delta_u^+ \rightarrow 1s\sigma\ 2p\sigma\ {}^1\Sigma_u^+$	14.06	28,31

Table 2.1 continued

431.42	CH	$A\,^2\Delta \rightarrow X\,^2\Pi$	2.85	28,31
218.98 229.96 232.52 241.94 244.58 247.42	CO^+	The first negative system of CO^+ $B\,^2\Sigma^+ \rightarrow X\,^2\Sigma^+$		31
283.3 297.74	CO	The third positive system of CO		31
306.36 to 312.64	OH	The 306.4 band of OH $A\,^2\Sigma^+ \rightarrow X\,^2\Pi$		31
288.18 289.55	CO_2^+	The 288.3 and 289.6 bands		31
387.1 388.3	CN	The 388.3 nm band of CN		29,31
282.71	N_2	Gayden and Henmen singlet systems		31
295.32 to 389.46	N_2	The second positive system		31
391.44 427.81	N_2^+	The first positive system		31

Table 2.2: Calculated minimum energies in eV for the formation of H(n = 3), CH(A) and $H_2(G^1\Sigma_g^+)$ in the electron impact dissociative excitation of CH_4/H_2 plasma.

Process	Dissociation products	E_{th} (eV)	Ref. no.
1	$CH_4 + e \rightarrow CH(X) + H_2(X) + H(n=1) + e$	9.2	calcul.
2	$\rightarrow CH(X) + 3H(n=1) + e$	13.7	calcul.
3	$\rightarrow CH(\tilde{X}) + H_2(X) + e$	4.74	22,23
4	$\rightarrow CH(\tilde{X}) + 2H(n=1) + e$	9.24	22,11
5	$\rightarrow CH(X) + H_2(X) + H_\alpha(n=3) + e$	21.29	22,23
6	$\rightarrow CH_2(\tilde{X}) + H_2(G^1\Sigma_g^+) + e$	18.74	22,23
7	$\rightarrow CH(X) + H_2(G^1\Sigma_g^+) + H(n=1) + e$	23.2	23,23
8	$\rightarrow CH(A) + H_2(X) + H(n=1) + e$	12.2	23,30

Table 2.2 continued

9	$\rightarrow CH(A) + H_2(X) + H_\alpha(n=3) + e$	24.14	23,30
10	$\rightarrow CH(A) + H_2(G^1\Sigma_g^+) + H(n=1) + e$	26.2	11-13
11	$\rightarrow CH_2(\tilde{X}) + H_\alpha(n=3) + H(n=1) + e$	21.33	11-13
12	$\rightarrow CH_3(\tilde{X}) + H_\alpha(n=3) + e$	16.55	11-13
13	$H_2 + e \rightarrow H_\alpha(n=3) + H(n=1) + e$	16.57	28,30
14	$H + e \rightarrow H_\alpha(n=3) + e$	12.09	28,30
15	$H_2 + e \rightarrow H_2(G^1\Sigma_g^+) + e$	14	28,30

2.11 References

2.1. W. R. Harshbarger, R.A. Porter, T. A. Miller, and P. Norton, Appl. Spectro., **31**, 201, (1977).

2.2. C. J. Mogab, A. C. Adam, and D. L. Flamm, J. Appl. Phys., **49**, 3796, (1978).

2.3. J. W. Coburn, and M. Chan, J. Appl. Phys., **51**, 3134, (1980).

2.4. R. A. Gottscho, R. H. Burton, D. L. Flamm, V. M. Donnelly, and G. P. Davis, J. Appl. Phys., **55**, 2707, (1984).

2.5. V. M. Donnelly, D. L. Flamm, and G. Collins, J. Vac. Sci. Technol., **21**, 817, (1982).

2.6. R. A. Gottscho, G. P. Davis, and R. H. Burton, J. Vac. Sci. Technol., A **1**, 622 (1983).

2.7. P. J. Hargis, Jr. and M. J. Kushner, Appl. Phys. Lett., **40**, 779, (1982).

2.8. R. A. Gottscho, and T. A. Miller, Pure & Appl. Chem., **56**, 189, (1984).

2.9. S. G. Hansen, G. Luckman, Appl. Phys. Lett., **53**, 1588, (1988).

2.10. V. M. Donnelly, D. L. Flamm, W. C. Dautremont-Smith, and D. J. Werder, J. Appl. Phys., **55**, 242, (1984).

2.11. D. A. Danner, and D. W. Hess, J. Appl. Phys., **59**, 940, (1986).

2.12. W. W. Clark, and F. C. DeLucia, J. Chem. Phys., **74**, 3139, (1981).

2.13. L. A. Farrow, J. Chem. Phys. 82, 3625 (1985).

2.14. J. C. Knights, J. P. M. Schmitt, J. Perin, and G. Guelachvili, J. Chem. Phys. **76**, 3414, (1982).

2.15. R. d'Agostino, V. Colaprico, and F. Cramarossa, Plasma Chem. Plasma Proc., **1**, 365, (1981).

2.16. R. d'Agostino, F. Cramarossa, S. De Benedictis, F. Fracassi, L. Laska, and K. Masek, Plasma Chem. Plasma Proc. **5**, 239, (1985).
2.17. R. d'Agostino, F. Cramarossa, S. De Benedictis, and G. Ferraro, J. Appl. Phys., **52**, 1259, (1981).
2.18. CRC Handbook of Physical Chemistery, 74th edition 1992.
2.19. G. Herzberg, Proc. Roy. Soc., **262**, 291, (1961).
2.20. G. Herzberg, and J. W. C. Johns, Proc. Roy. Soc., **295**, 107, (1966).
2.21. S. E. Hicks, C. D. W. Wilkinson, and G. Doughty, Proceedings of ECIO, (1993).
2.22. J. M. F. Aarts, C. I. M. Beenaker, and F. J. De Heer, Physica, **53**, 32, (1971).
2.23. D. E. Donohue, J. A. Schiavone, and R. S. Freund, J. Chem. Phys., **67**, 769 (1977).
2.24. G. A. Kayarallah, Phys. Rev. A **13**, 1989, (1976).
2.25. W. T. Miles, R. Thompson, and A. E. S. Green, J. Appl. Phys., **43**, 678 (1972).
2.26. H. Kleinpoppen, and E. Kraiss, Phys. Rev. Lett., **20**, 361 (1968).
2.27. J. D. Walker, and R. M. St. John, J. Chem. Phys., **61**, 2394 (1974).
2.28. G. Herzberg, Spectra of Diatomic Molecules Vol.**I**, (1950).
2.29. G. Herzberg, Electronic Spectra of Polyatomic Molecules, Vol.**III**, (1966).
2.30. K. P. Huber, and G. Herzberg, Constants of Diatomic Molecules, Vol. **IV**, (1979).
2.31. R. W. B. Pearse, and A. G. Gaydon, The Identification of Molecular Spectra, **4th** edition, (1976).
2.32. C. L. Sam, and J. T. Yardley, J. Chem. Phys., **69**, 4621, (1978).
2.33. G. Di Stefano, M. Lenzi, A. Margani, and C. N. Xuan, J. Chem. Phys., **68**, 959, (1978).
2.34. S. J. Pearton, Mat. Res. Soc. Symp. Proce., Vol. **216**, 277, (1991).
2.35. U. Niggebrugge, M. Klug, and G. Grarus, Proc. 12th, Inter. Symp. on GaAs and related compounds, Int. Phys. Confer. Ser.no. **79**, pp 367, (1986).
2.36. H. Schmid, Proc. **6th**, Int. Confer. on Ion and Plasma Assited Techniques (IPAT), pp 98, (1987).
2.37. T. R. Hayes, M. A. Dreisbach, P. M. Thomas, W. C. Dautremont-Smith, and L. A. Heimbrook, J. Vac. Sci. Technol., B **7**, 1130, (1989).
2.38. P. Collot, T. Diallo, and J. Canteloup, J. Vac. Sci. Technol., B **9**, 2497, (1991).
2.39. M. A. Foad, Ph.D. thesis, Glasgow University, (1992).
2.40. R. Cheung, S. Thoms, I. McIntyre, C. D. W. Wilkinson, and S. P. Beaumont, J. Vac. Sci. Technol., B **6**, 1911, (1988).
2.41. S. W. Pang. J. Electrochem. Soc., **133**, 784, (1986).

Chapter 3

Optical Emission Spectroscopy (OES) of $SiCl_4$ Plasmas

3.1 Introduction

The behaviour of Silicon tetrachloride($SiCl_4$) in various plasmas is of interest in a number of applications, including RIE and deposition processes. Depending on the operating conditions, a variety of RIE processes have been established for etching III-V semiconductors in $SiCl_4$ plasmas[1-4]. Optical Emission Spectroscopy (OES) of $SiCl_4$ plasma is essential for understanding the basic mechanisms involved in plasma etching. Few studies [34,37] of emission spectroscopic observations of $SiCl_4$ plasma etching processes have been reported in comparison with the number on deposition systems involving SiH_4, SiF_4 and $SiCl_4$. To gain some insight into the fundamental processes occurring in the gas phase and to acquire knowledge of how $SiCl_4$ is broken down to its fragments, a comprehensive analysis of the OES observations in $SiCl_4$ plasma is given in this chapter. In particular the effect of various discharge parameters such as rf power, pressure and the flow rate on the dissociation mechanisms and their implications on the discharge chemistry. Emissions from excited species of N_2, H_2, HCl, O_2 and AlCl have been observed in $SiCl_4$ plasmas; the origin and the significance of these emissions is discussed. The emission spectra of etch products of a number of III-V materials etched in $SiCl_4$ are given. OES as an end point monitoring tool for GaAs, AlGaAs and AlAs etching in $SiCl_4$, and its limitations and applications are discussed. Finally a comparison of microwave generated $SiCl_4$ plasma and rf generated plasma is given.

3.2 $SiCl_4$ Spectrum

The discharges in $SiCl_4$ were carried out in Plasma Technology RIE80 machine. The spectra were recorded in the range of 200-600 nm using a Sofie spectrometer, and in the 500-970 nm range using the diode array spectrometer described in chapter 2. The overlap of the two ranges in the range of 500-600 nm is meant to show the discrepancies in the grating response between the two spectrometers. In fig.3.1 the spectrum of $SiCl_4$ is given in the range 200-600 nm from a discharge at a rf power of 100 W, a flow rate of 9 sccm and at a pressure of 12 mtorr. Intense emission lines from SiCl radicals at 280.7 and 282.3 nm were observed as well as strong emission from the atomic Si lines at 251.6 and 288.16 nm, whereas weak emissions from atomic Cl lines were observed in this range.

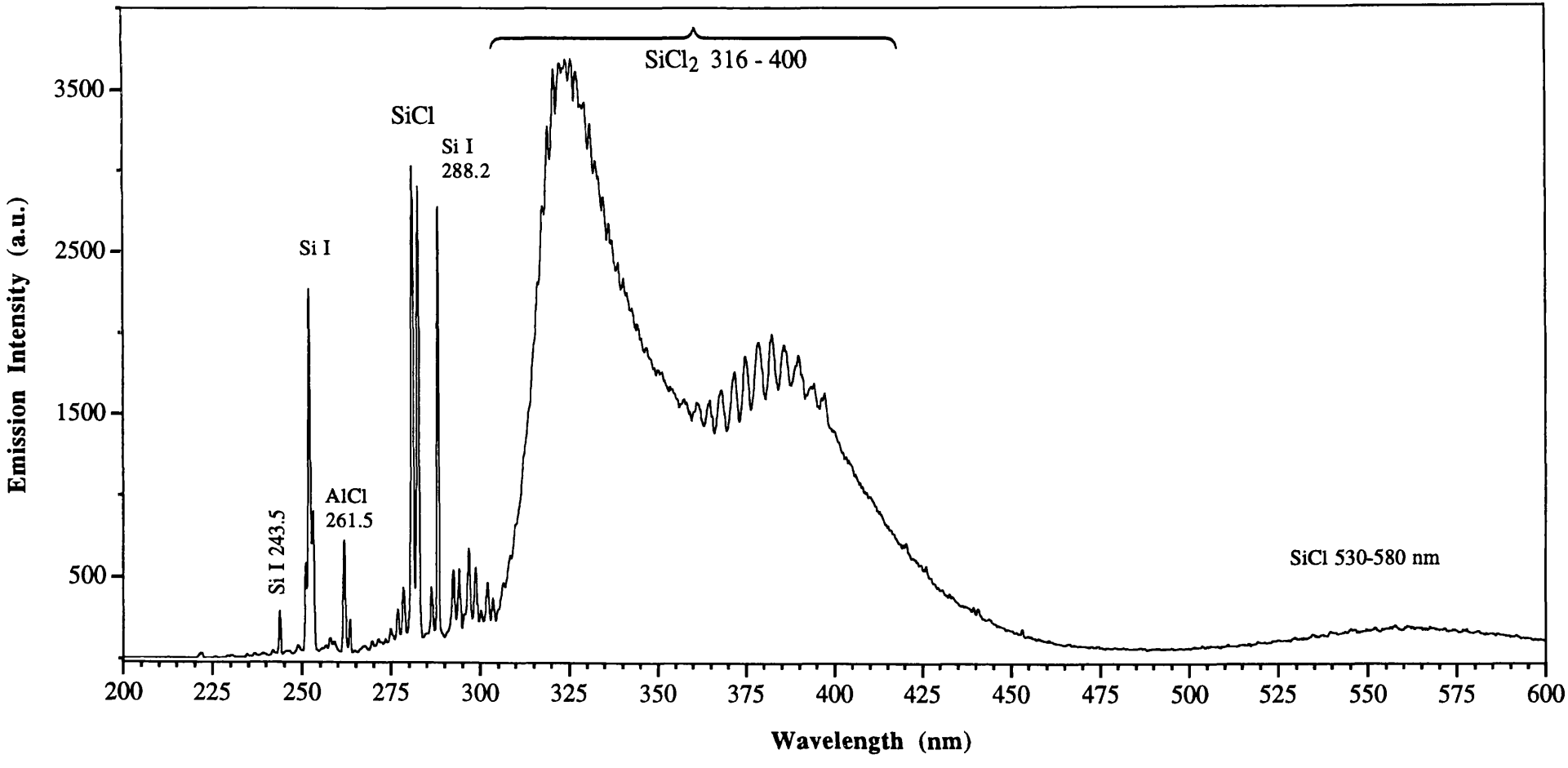

Fig.3.1: Spectrum of $SiCl_4$ plasma in the 200-600 nm range recorded using the Sofie spectrometer. The discharge is at a power of 100 W, a flow rate of 9 sccm and at pressure of 12 mtorr. The main species detected are SiI, SiCl, and $SiCl_2$. AlCl is due to contamination from etching of the electrodes.

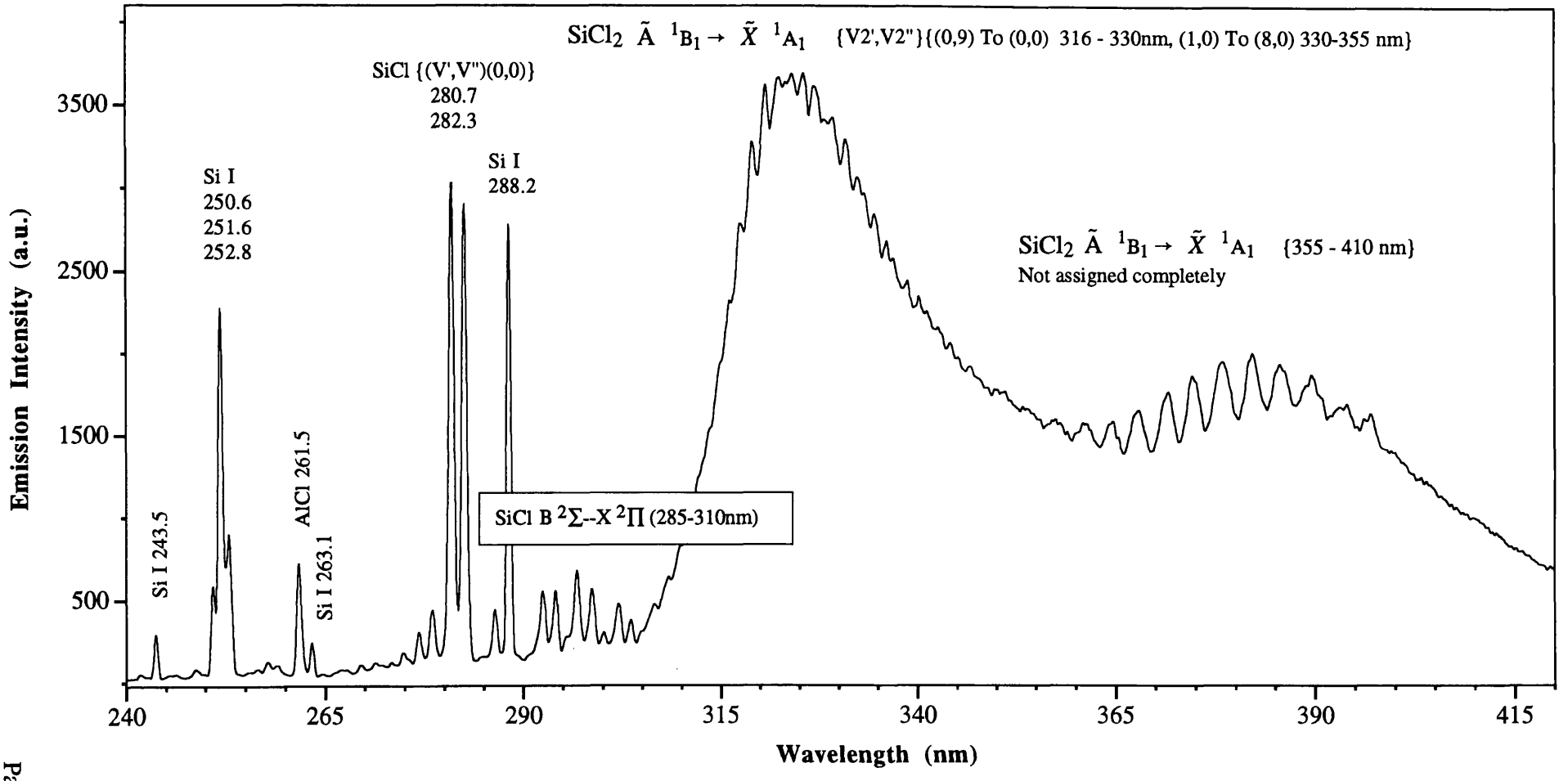

Fig.3.2: Detail of the $SiCl_4$ spectrum in the (240-420) nm range which shows the transitions from atomic Si lines and emission from SiCl molecule and the continuous and intense transitions of $SiCl_2$ molecules. The emission from AlCl is due to the etching of discharge electrodes.

As shown in fig.3.2, the emission spectrum in the wavelength range 300-420 nm is dominated by two continuous and intense emissions with maximum intensity at 330 and 390 nm, respectively. These two continuum bands are believed to belong to $SiCl_2$ radicals, however their assignment and analysis have been the subject of some controversy in the literature.[5-8] The band with the 330 nm emission maximum has recently been assigned by many authors[9-10] to the $SiCl_2$ ($\tilde{A}\ ^1B_1 \rightarrow \tilde{X}\ ^1A_1$) transition. The band with the 390 nm emission maximum is not fully understood yet, However, it has been assigned tentatively by [11] as a "superposition of valence-and deformation vibrations within $\tilde{A}\ ^1B_1 \rightarrow \tilde{X}\ ^1A_1$ transition". No emissions from $SiCl_3$ radical or $SiCl_4$ molecule were observed; these species are known not to show visible emission spectra. Emission lines from the atomic chlorine ion; Cl^+ at (413.24, 481.0, 479.45, 521.79 and 507.82) nm and molecular chlorine ion; Cl_2^+ at 403.3, 419.44 and 432.22 nm were detected, but with some difficulty, because of the weakness of the emission. Moreover, the emissions from these species are strongly dependent on the discharge power. This will be discussed in the next few sections. On the other hand no emission from Cl_2 molecule was observed, which has its strongest emission band at 256 nm. In fig.3.3 the spectrum has been recorded in the range of 500-960 nm using the diode array system. In the range of 500-640 nm the spectrum is dominated by the broad emission from SiCl radical, $A\ ^2\Sigma \rightarrow X\ ^2\Pi$ rotational transitions. In the red and near infrared regions the emissions from atomic Cl dominate the spectrum. All the observed emission lines, bands, their transitions and upper state energies are listed in table 3.1 and they are obtained from references [5-25].

The spectra in the whole range of 240-950 nm from the diode array system and in the range of 240-600 nm using Sofie system are given for comparison in fig.3.4. The spectra were recorded simultaneously from the same $SiCl_4$ discharge. As it can be seen the wavelength response of the grating in both systems has a remarkable effect on the overall picture of the spectrum. For the diode array system the grating effectively cuts-off at about 300 nm missing important parts of the UV region. In contrast, the spectrum obtained from Sofie system has the UV region well obtained, however the red and the infrared are unobtainable. Therefore to have a complete picture of the spectrum the two systems are used simultaneously.

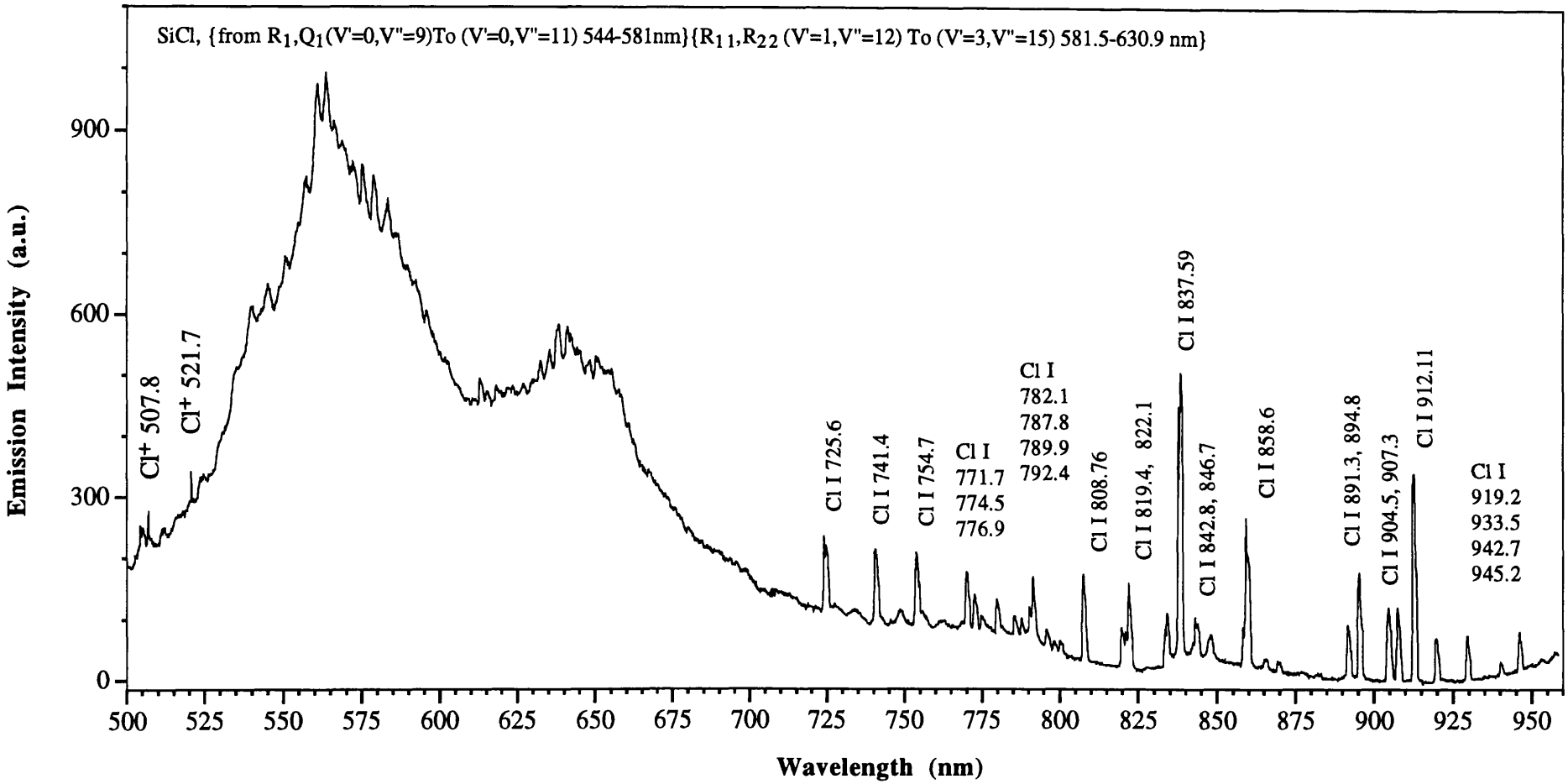

Fig.3.3: Spectrum of $SiCl_4$ plasma in the region of 500-960 nm, recorded using the diode array spectrometer (described in chapter 2). The emission from SiCl continuum and the emission from atomic Cl are dominating the spectrum. The discharge conditions are; rf power of 100 W, flow rate of 9 sccm and at pressure of 12 mtorr.

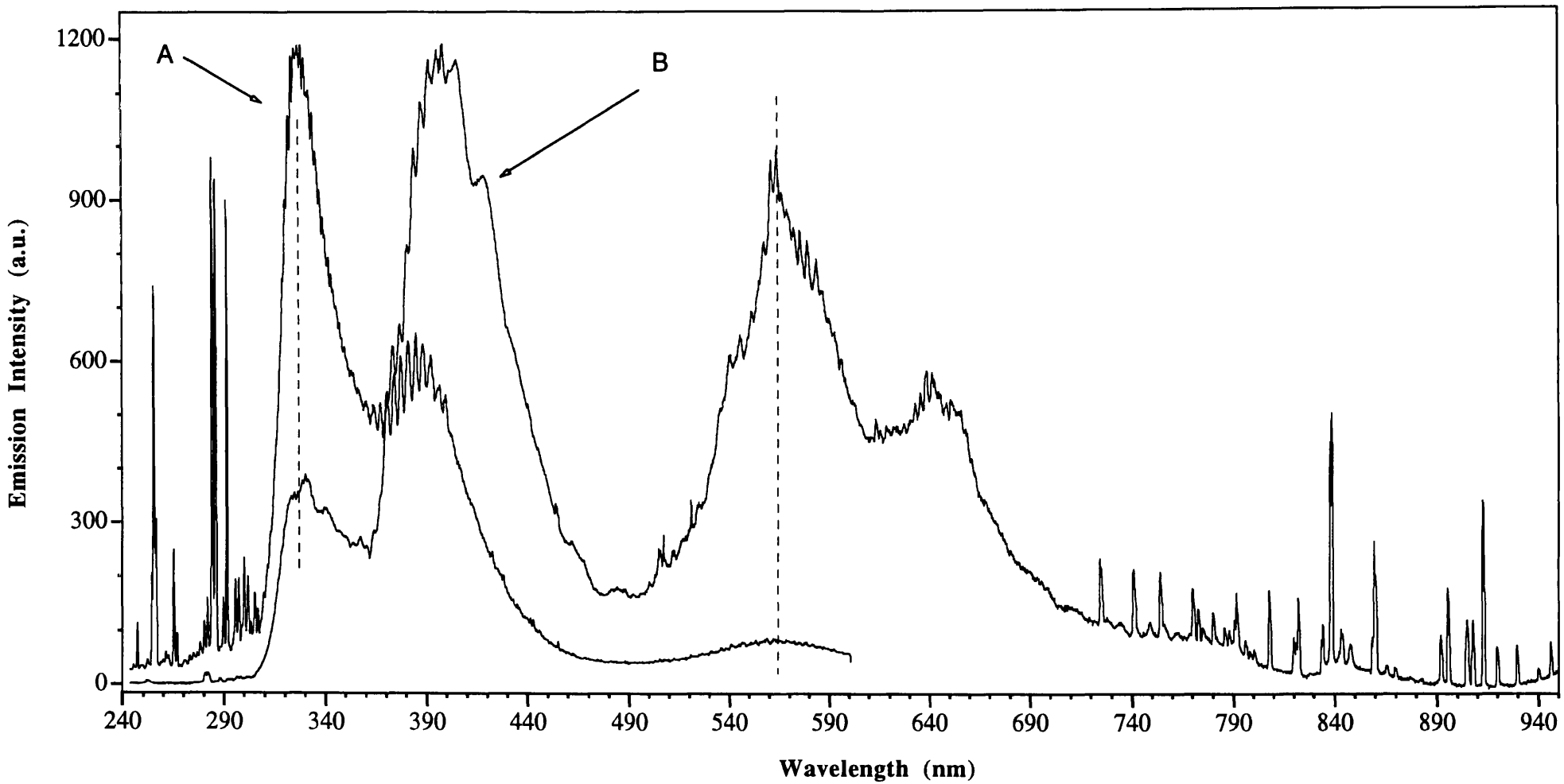

Fig.3.4: Spectra of $SiCl_4$ plasma recorded at the same time, A; recorded using Sofie spectrometer, and B; recorded using the diode array spectrometer, shows that very important parts of the spectrum are missing if only one spectrometer is used.

3.3 The chemistry of $SiCl_4$ plasma

In the spectra reported in the last section, it was shown that a variety of reactive species can be generated in the $SiCl_4$ plasma including neutral silicon chlorides, Si and Cl atoms and also Cl ions. This wealth of reactive species from polyatomic $SiCl_4$ gives rise to a complex plasma chemistry. It is clear that several types of gas phase reactions can occur in the discharge; including electron-impact dissociations, dissociative excitations, dissociative ionizations, electron attachment and recombination processes. The rates at which these processes occur are dependent on plasma conditions, such as electron energy distribution and electron density which in turn depend on the applied rf power. These rates also depend on the total gas pressure and the temperature of the species. To study the possible reaction mechanisms involved in $SiCl_4$ plasma, OES and OEA were used to monitor the changes in the emission intensities of various species in the discharge as a function of rf power at constant gas flow rate and pressure.

3.3.1 Effect of rf power

The spectra of $SiCl_4$ with (1-2)% of Ar added to act as an actinometer, were recorded at rf powers of 5-150 W and at a constant $SiCl_4$ flow rate of 6 sccm and a constant pressure of 9 mtorr.

The emission intensities of the Si I line at 288.2 nm, the SiCl line 280.7 nm, the Ar line at 420.0 nm, the AlCl line 261.5 and the broad emission of $SiCl_2$ at 330 nm were monitored as a function of power using Sofie spectrometer as shown in fig.3.5 and 3.6. The emission intensities of both SiCl and $SiCl_2$ increase in a similar way with increasing power. On the other hand, the emission intensity of Si increases rapidly with power increase, and that of Ar increases systematically with power.

The diode array spectrometer was used to monitor the emission intensities of the Cl I line, at 837.6 nm, nm and the Ar line at 763.7 nm as a function of power as shown in fig.3.6. The emission intensity of the Cl is remarkably different from all other species. First in the power range of 5-15 W it increases sharply with increasing power, then decreases displaying a slight minimum at 25 W, and then increases again with increasing power between 25-150 W.

The emission intensity of AlCl (the presence AlCl is due to the contamination from electrodes by etching) exhibits an interesting phenomenon in that it has a value of zero (the emission is not detected) in the power range of 5-15 W, then increases steadily with increasing power. The presence of AlCl will be discussed further in the next few sections.

On the other hand, because of the weakness of the emissions from Cl^+ and Cl_2^+ lines, they were not plotted as a function of power, nonetheless, as shown in spectra of fig.3.7 and fig.3.8, no emissions from Cl^+ can be detected below 25 W, whereas a few but weak

emission lines from Cl^+ at (386.0, 413.24, 479.45, 507.8, 522.13 and 542.32) nm were detected in the power range 25-150 W.

In contrast, weak emissions from Cl_2^+ lines (403.3, 419.44 and 432.22) nm were detected in the power range 15-20 W while no emissions were detected above power of 20 W. The behaviour of the emissions from Cl, Cl^+, Cl_2^+ and AlCl suggests that their production in the excited state is by two different chemical reactions in the gas phase which are very sensitive to power, one below and one above 15 W. We will call the one below 15 W, the low power regime and the one above 15 W, the high power regime.

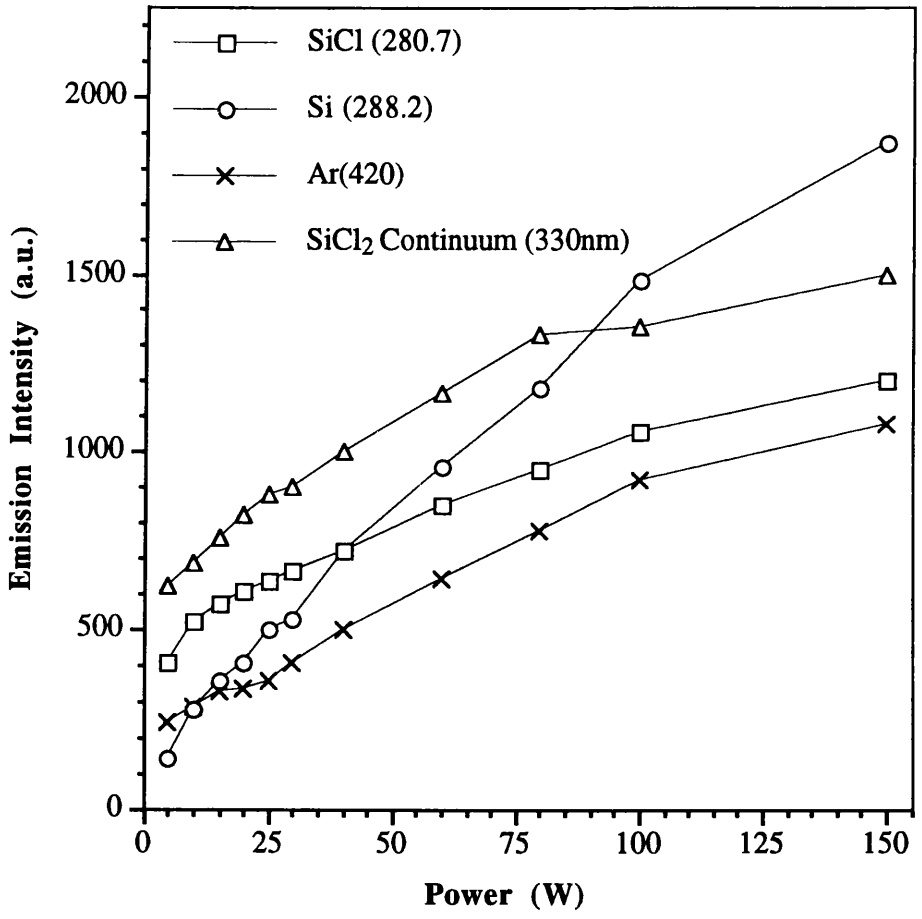

Fig.3.5: Emission intensities of SiCl (282.3) nm, $SiCl_2$ (continuum at 330 nm), Si (288.2) nm and Ar (420) nm as a function of the applied power.

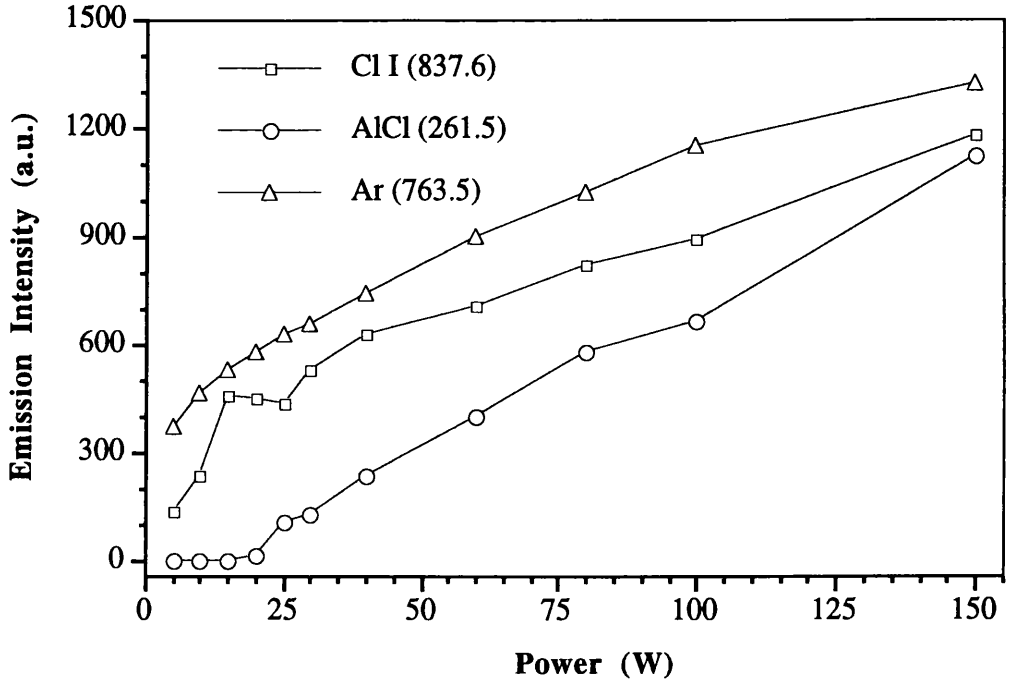

Fig.3.6: Emission intensities of Cl (837.6) nm, AlCl (261.5) nm and Ar (763.5) as a function of the applied power.

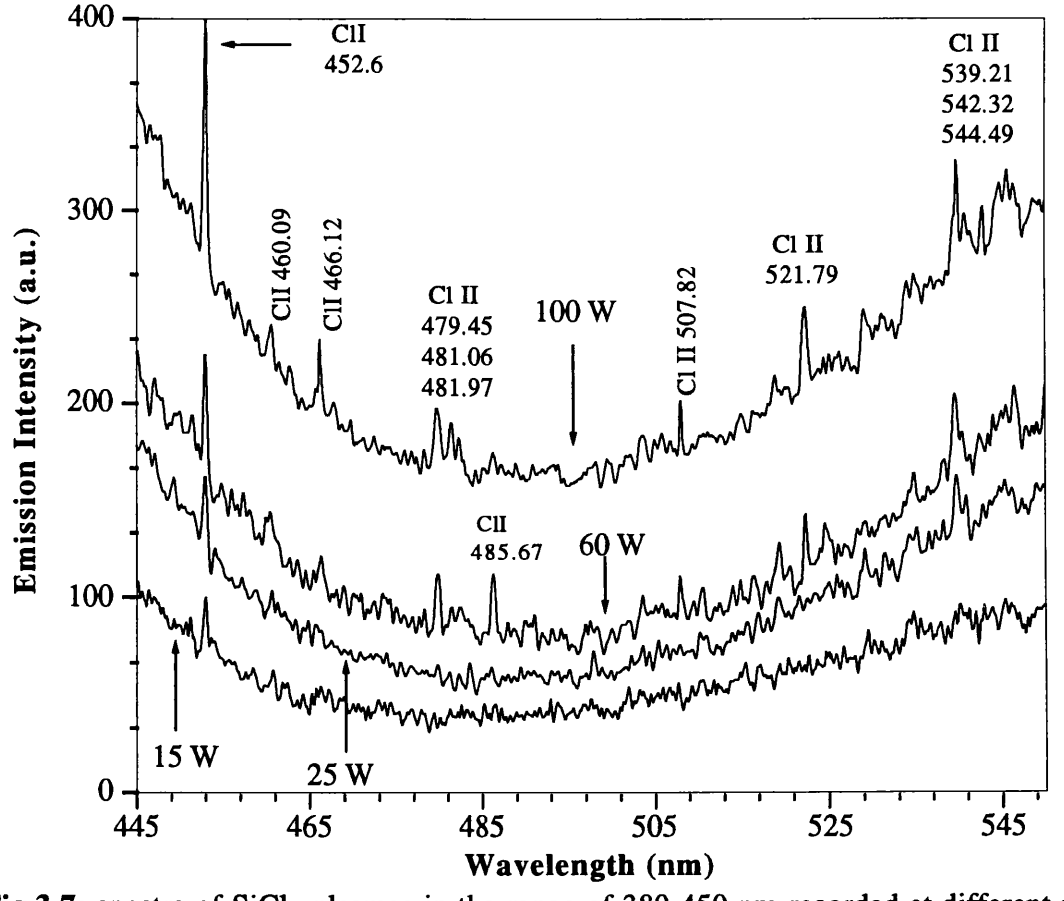

Fig.3.7: spectra of $SiCl_4$ plasmas in the range of 380-450 nm recorded at different rf powers which shows that the emission from Cl^+ is detected at powers higher than 15 W.

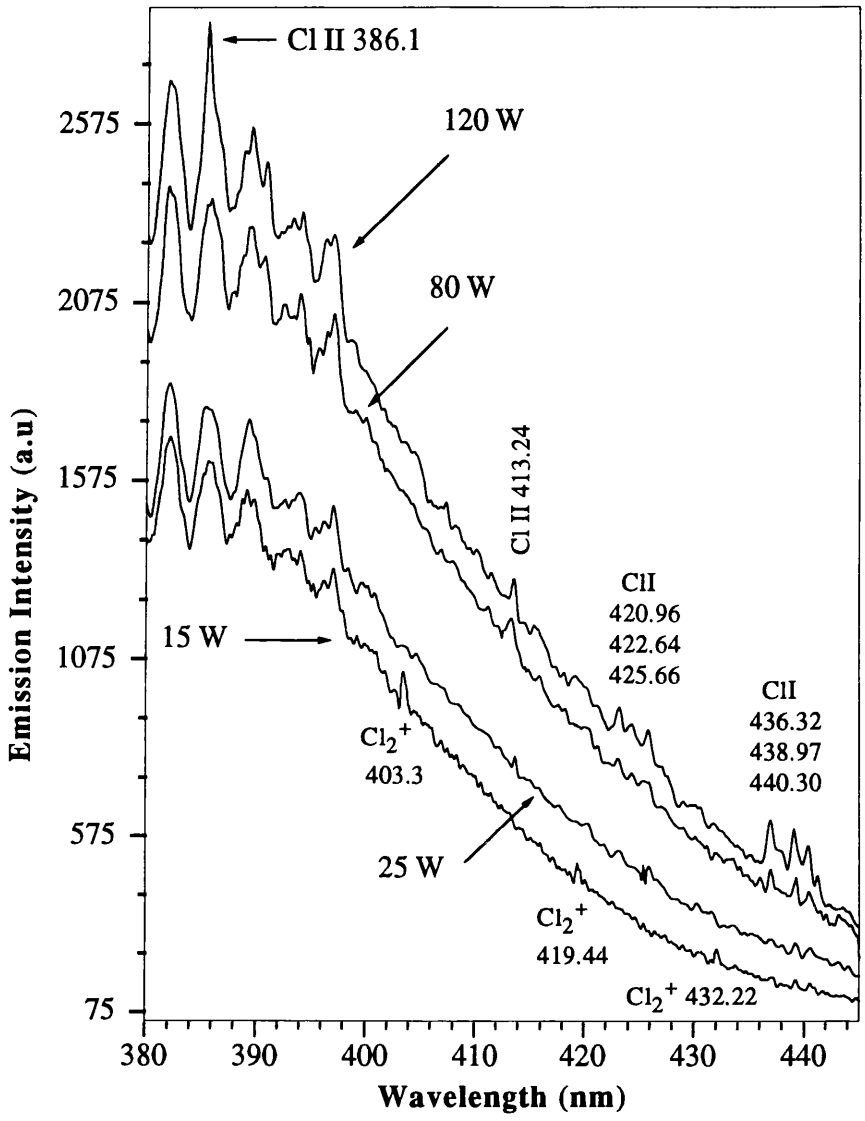

Fig.3.8: spectra of $SiCl_4$ plasmas in the range of 380-450 nm recorded at different rf powers, which shows that the emission from Cl_2^+ is detected only at power of 15 W, whereas the emission from Cl^+ is detected at powers higher than 15 W.

3.3.2 Origin of the emitting species in the two chemical regimes

To validate the argument of the two chemical regimes, one has to examine the origin of the emitting species in each regime. All the species in the plasma are the products of the electron impact dissociative excitation, ionization and attachment processes that occur in the plasma. The minimum energies for the formation of each species have been calculated using the thermochemical data available in the literature [26-31]. These excitation processes and the minimum energies of formation are given in table 3.2. To determine which excitation processes are more likely to occur in each chemical regime, the technique of OAE described in section 2.8 is carried out. Two Ar lines were used for actinometry,

the Ar line 420 nm is used as an actinometer for the Si, SiCl, and $SiCl_2$ emissions, whereas Ar line 763.7 nm was used for Cl actinometry. The reasons for using two Ar lines are that the emission intensities recorded by the two spectrometers differ considerably and the problem of grating response is eliminated by using a control Ar wavelength close to the wavelength of interest.

A. SiCl and $SiCl_2$ radicals.

In fig.3.9 the emission intensities of SiCl and $SiCl_2$ as a function of the Ar (420 nm) emission intensity for the same power are given in a log-log scale. It can be seen from fig.3.9 that for both SiCl and $SiCl_2$ the emission data falls on two straight lines with different slopes which correspond to the two power regimes.

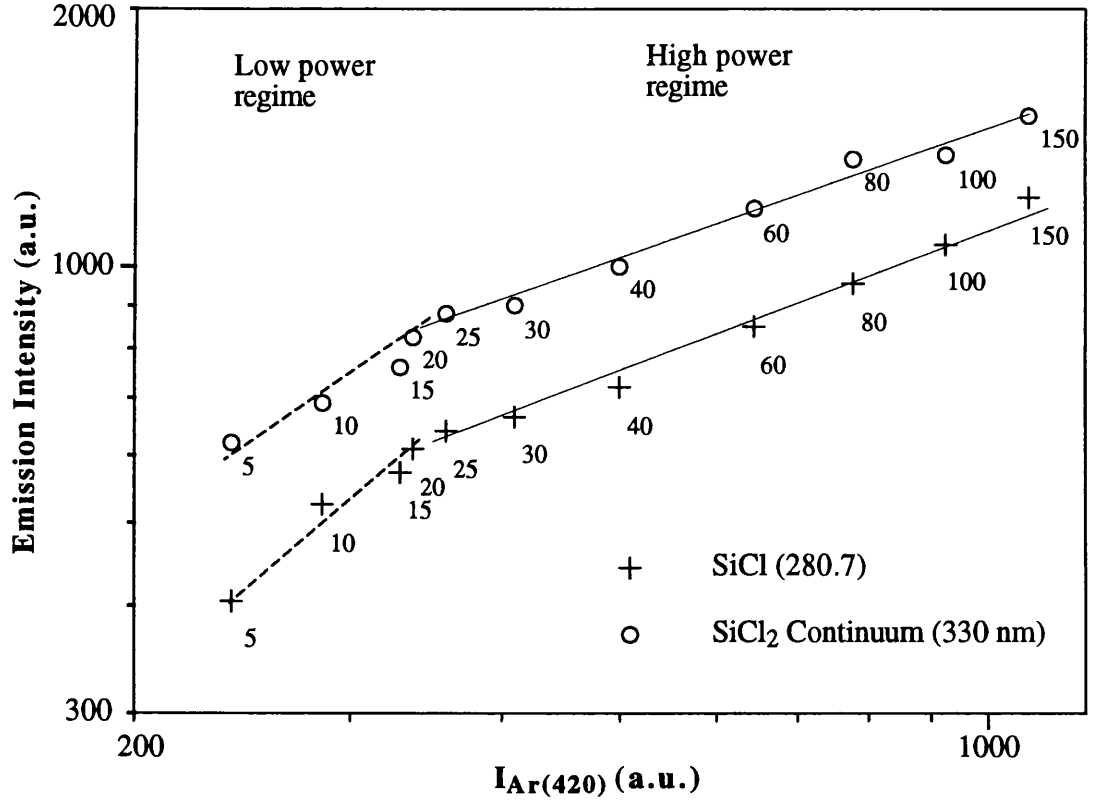

Fig.3.9: Log-Log plots of the emission intensities of SiCl and $SiCl_2$ as a function of the emission intensity of the Ar (420) nm line with the coresponding values of power plotted.

The emission intensity of SiCl in the low power regime varies as the 1.93 power of the Ar emission, which implies that the formation of SiCl in the excited state in this regime is by two electrons, the first electron producing SiCl in the ground state by processes (2,3) of table 3.2 and the second electron then exciting the SiCl to the emitting state by process (1). In the high power regime ≥ 25 W, the emission intensity of SiCl varies as the 0.8 power of

the emission intensity of Ar, this implies that it is proportional to the emission intensity of Ar and that the formation of $SiCl^*$ in this regime requires only one electron and therefore is produced directly from $SiCl_4$ parent molecules by dissociative excitation processes (4) and (5). The emission intensity of $SiCl_2$ has similar power dependence as SiCl, and it varies as the 1.85 power of the Ar emission in the low power regime and as 0.83 power in the high power regime. Therefore the formation of $SiCl_2^*$ in the low power regime requires two electrons and its produced by processes (7,8) and then (6). In the high power regime the formation of $SiCl_2^*$ requires one electron and it is produced directly from $SiCl_4$ molecules by processes (9) and (10).

B. Si and Cl atoms

The assignment of the origin of the emission from Si and Cl atoms is more complicated than SiCl or $SiCl_2$ radicals because the formation of free Si and Cl atoms could have several precursors including $SiCl_4$, SiCl, $SiCl_2$ and Cl_2. The emission intensity of Si (288.2) nm as a function of the emission intensity of Ar (420)nm for the same power is given in fig.3.10 in a log-log scale.

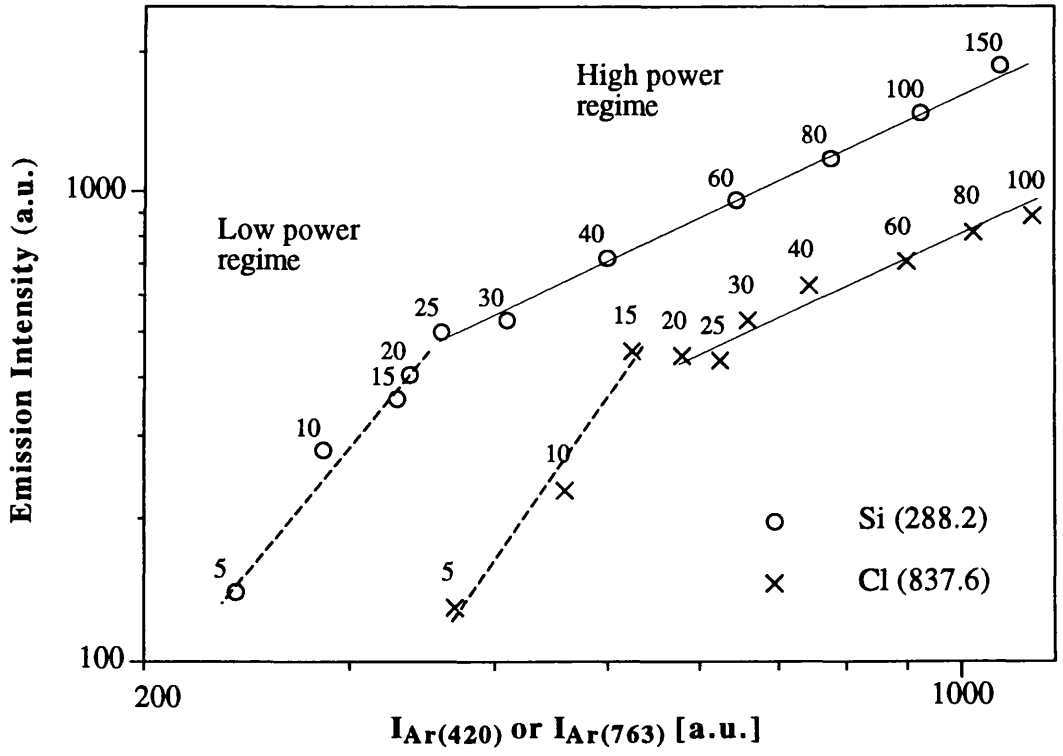

Fig.3.10: Log-log plot of the emission intensity of Si (288.2) nm as a function of the Ar (420) nm emission intensity and log-log plot of the Cl (837.6) nm as a function of the emission intensity Ar (763.5) nm with the coresponding values of power plotted.

It can be seen from Fig.3.10, that the emission data of both Si and Cl have a large difference in the slopes in the two power regimes. For Si atoms in the low power regime, the emission intensity varies as the 2.78 power of the emission intensity of Ar which suggests that up to three electrons are needed to produce Si^* (the * denotes the species in the excited state) from $SiCl_4$. Therefore the formation of Si^* in this regime is derived from Si in the ground state by process (20), which in turn is being produced from either SiCl through process (17) or $SiCl_2$ through processes (18,19) which means that in the low power regime, free Si "even in the ground state" cannot be produced directly from $SiCl_4$. In the high power regime, the emission intensity of Si varies as the 1.88 power of the emission intensity of Ar, therefore two electrons are needed to produce Si^*. This implies that in this power regime, there are two equally important routes for the production of Si^*. The first is from free Si in the ground state which in turn is being produced directly (by the first electron) from $SiCl_4$ through processes (11, 12 and 13). The second route is by dissociative excitation of either SiCl by process (14) or $SiCl_2$ through processes (15) and (16). The processes (21-23) appear not be important for the production of Si^*, since they involve one electron excitation directly from $SiCl_4$ even though they may be energetically accessible in the high power regime. Therefore the difference between the low and high power regimes concerning the production of Si^* is that the Si^* is only produced from Si in the ground state which itself is not produced from $SiCl_4$ directly but from SiCl and $SiCl_2$. In the high power regime the Si^* is produced from both Si in the ground state, SiCl and $SiCl_2$, meanwhile the production of Si in the ground state is produced directly from $SiCl_4$.

The emission intensity of Cl (837.6) nm as a function of the emission intensity of Ar (763.5) nm for the same power is given in fig.3.10 on a log-log scale. In the low power regime the emission intensity of Cl atoms varies as the 1.67 power as the emission intensity of Ar. Therefore two electrons are needed to produce free Cl atoms in the excited state (Cl^*). The first electron is required to produce Cl in the ground state from $SiCl_4$, $SiCl_2$ and SiCl, the second electron then excites Cl into the excited state by process (24). However there is a possibility of another channel for the production of Cl^* which also involves two electrons and that is by the dissociative excitation of SiCl through process (25) or dissociative excitation of $SiCl_2$ through processes (26) and (27). However, as it can be seen in table 3.2, to produce Cl^* from SiCl directly (process 25) an energy of 14.24 eV is required and to produce it from $SiCl_2$ even higher energies are required (15.24 and 19.19 eV process 26 and 27 respectively), as these energies are not easily accessible in the low power regime these processes will not be a significant source for excited-state Cl. To produce Cl^* from Cl in the ground-state an energy of 10.28 eV (process 24) is required. Therefore it seems likely the production of Cl^* from Cl in the ground-state is the dominant mechanism for the production of Cl^* in the low power regime.

In the high power regime the emission intensity of Cl varies as the 0.93 power of the emission intensity of Ar, hence only one electron is needed for the production of Cl^* by direct dissociative excitation of the parent $SiCl_4$ molecules through processes (28-32). Therefore Cl^* is a primary product of the $SiCl_4$ dissociative excitation in the high power regime, whereas in the low power regime it is not a primary product of $SiCl_4$ dissociation and it is derived from Cl in the ground state.

We have seen so far that the mechanisms for the production of the species in the two regimes do differ, therefore there will be some overall dominant reactions in each regime. However we have ignored the fact that there may be some sort of a transitional period between the two power regimes and specifically in the power range of 15-25 W. The emission behaviours of Si, SiCl and $SiCl_2$ with power do not suggest such a period, however the dependence of emission from Cl with power displays a slight minimum in the power range of 15-25 W as it was shown in fig.3.6, which suggest that there is a transitional period. On the other hand if we look at the emission from AlCl on the same fig.3.7 again, we can see that when the emission from Cl starts to fall at about 20 W, as the power is being increased, we start detecting the emission from AlCl. So the temporal fall in the Cl emission could be caused by the formation of AlCl by etching the electrodes, as some of the free Cl will be consumed in the process of forming AlCl.

C. Cl_2^+ and Cl^+

As the emission from Cl_2^+ is weak a log-log plot was not possible. As discussed earlier, emission from these species occurs only in the low power regime. Therefore we can assume that the formation of Cl_2^+ in the excited state is through the least energetic route. The formation of Cl_2^+ in the ground state which cannot be detected using emission spectroscopy, is likely to originate from Cl_2 molecules in the ground state which will require the energy of the ionization potential of Cl_2 (11.48 eV). The first excited state of Cl_2^+ has an energy level of 2.48 eV, so if we calculate the minimum energy required for the formation of Cl_2^+ in the excited-state from Cl_2 directly we will need 13.96 eV (process 42). However if the emission from $[Cl_2^+]^*$ originates from Cl_2^+ in the ground state then electrons with energies of only 2.48 eV are required (process 43). Thus process 43 is the favourable route for the production of Cl_2^+ in the excited state.

For Cl^+, emission was seen only in the high power regime. The ionization potential of Cl is 13 eV and the lowest excited state of Cl^+ has an energy level of 15.95 eV. Therefore if the formation of Cl^+ in the excited state was originating from Cl, electrons with energies of at least 29 eV will be needed (process 34). As a result, process (34) is probably not a significant source for excited-state Cl^+. However if Cl^+ in the excited-state was formed from Cl^+ in ground-state then electrons with energies of 15.95 eV will be needed. In which case two electrons are required to produce Cl^+ in the excited-state, the first electron is

required to produce Cl^+ in the ground state from $SiCl_4$ through excitation processes (35-38), the second electron then excites the Cl^+ to the excited state through process (33).
The mechanisms we have postulated for the production of the excited species in both power regimes are based on energetic arguments and on the number of electrons required to produce them. However, production of these excited states require electrons with various energies. The distribution of electron energies in the discharge will depend on power as both the total electron concentration and the average electron energy depend upon power. Generally one would expect that both the total electron concentration and the average electron energy increase with power. As a result, the concentration of higher-energy electrons should increase more rapidly with power than dose the concentration of lower-energy electrons. Consequently, this leads to a higher concentration of lower-energy electrons in the low power regime and to a higher concentration of higher-energy electrons in the high power regime. Therefore, excitation processes that require lower-energy electrons (electrons with energies of ~ $\leq$10 eV) will not occur or at least will not be significant in the high power regime even if they are energetically accessible. In the low power regime, excitation processes that require higher-energy electrons (electrons with energies of ~ $\geq$15 eV) will not be significant because they are energetically inaccessible. To summarise, the main differences in the production mechanisms of the excited species between the two power regimes are that in the low power regime the excitation of the species involves multiple steps and that the $SiCl_4$ parent molecules only dissociate in the beginning into radicals, molecules and atoms in their ground state with no excitation involved. In the high power regime the $SiCl_4$ parent molecules will undergo dissociative excitation into radicals and atoms in their excited state and can dissociate into radicals in their excited-state and atomic ions in their ground-state in a parallel but single excitation process.

3.3.3 Effect of the pressure on the emission intensities in the low power regime

The effect of the total pressure on the emission intensities of the various species has been studied in the low power regime since we are interested here in the low power regime for reasons will be clear in chapter 4. The total pressure was varied between 9 and 50 mtorr while keeping the $SiCl_4$ flow rate constant for two values of the flow, 6 and 12 sccm. The pressure rise was achieved by using the throttling valve between the vacuum pump and the etching chamber. The machine used was the Oxford Plasma Technology RIE80. In fig.3.11, the emission intensities of Si (288.2) nm, Cl (837.6) nm, AlCl (261.5) nm, SiCl (282.3) nm and $SiCl_2$ (continuum at 330 nm) are given as a function of the pressure using constant power of 15 W and constant flow rate of 6 sccm. The increase in the pressure at

constant flow rate implies an increase in the residence time, therefore fig.3.11 represents the emission intensities as a function of the residence time (as well as the pressure). As it can be seen from the fig.3.11 the emission intensities of both Si and Cl increase in a similar manner in the pressure range of 9 to 20 mtorr, being about 50% higher at pressure of 20 mtorr, and then decrease between 20 to 50 mtorr. The emission intensity of SiCl increases very sharply: about two and half times between 9 and 20 mtorr and then decreases between 20 and 50 mtorr. The emission intensity of $SiCl_2$ increases even faster than SiCl from 9 to 20 mtorr and unlike the rest of the species it continues to increase with pressure between 20-50 mtorr but with a lesser degree. The emission intensity of AlCl has an initial value of zero (emission not detected at 9 mtorr), then it increases dramatically between 12-20 mtorr and finally decreases, following a similar trend to that of Si and Cl. Similar results were obtained when a flow rate of 12 sccm and the same power of 15 W was used except for the emission from AlCl where the emission did not have an initial value of zero.

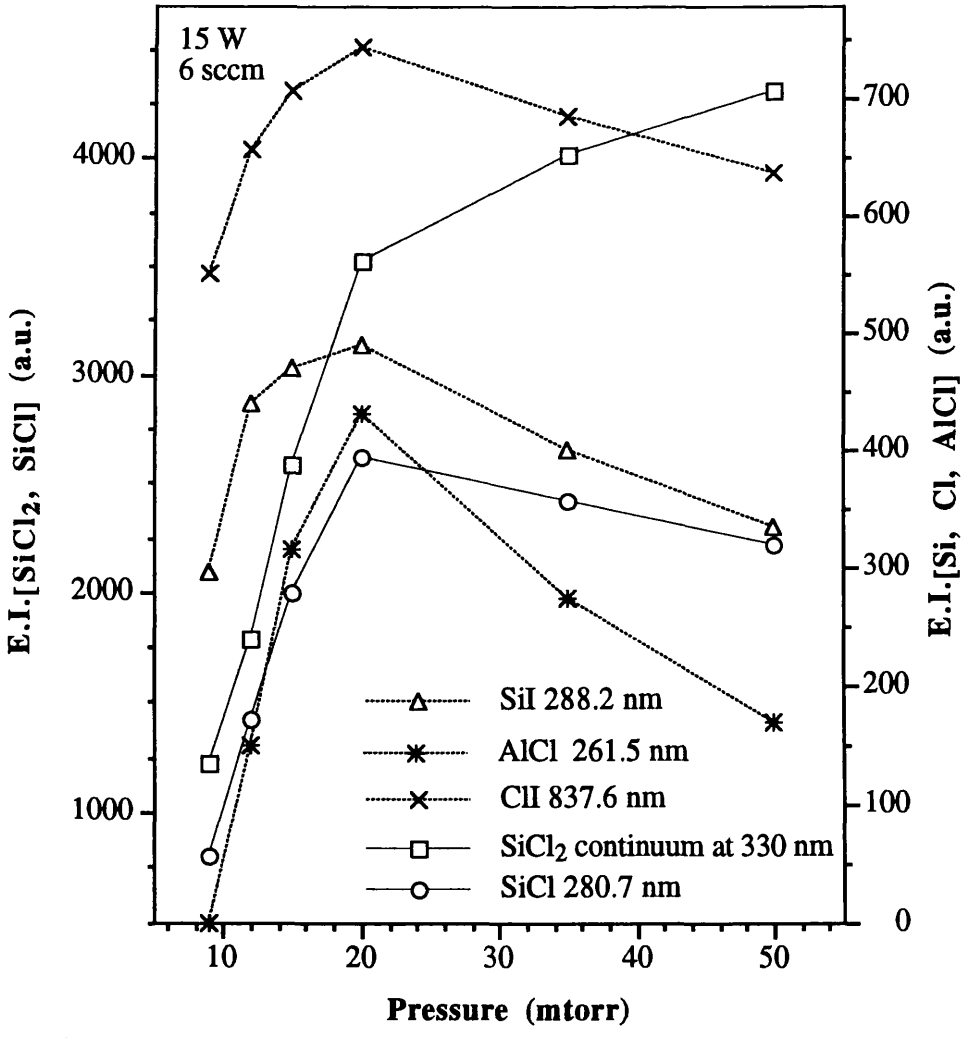

Fig.3.11: Emission intensities of the various species in the $SiCl_4$ plasma as a function of the pressure or (residence time) at constant flow rate of 6 sccm and constant power of 15 W.

The reasons for the increase in the emission intensities of Si, Cl, SiCl, and AlCl in the pressure range of 9-20 mtorr may be attributed to the increase in the collisions leading to higher number of $SiCl_4$ molecules being dissociated. The decrease in the emission of Si, Cl and SiCl in the pressure range of 20-50 mtorr may attributed to the recombination processes involving three body collisions to form $SiCl_2$, that is to say,

$$Si + Cl + M \rightarrow SiCl \quad \text{..... (3.3.3.1)}$$

$$SiCl + Cl + M \rightarrow SiCl_2 \quad \text{..... (3.3.3.2)}$$

where M is the third body which could be the electrode surface or the chamber walls. These collisions are expected to increase with pressure, meanwhile the recombination loss rate of Cl, Si and SiCl is expected to be higher than the formation rate from $SiCl_4$ by dissociation processes. It is seems logical to say that the continued increase in the emission from $SiCl_2$ with pressure is caused by these recombination processes. This is in accord with other researchers in systems containing chlorinated species. Richards and coworkers,[33,34] found that the major mechanism for Cl loss in Cl_2 plasmas at high pressures is through recombination on electrode surfaces. The increase in the formation of $SiCl_2$ at high pressures is associated with the increase of undesirable "deposits" on the chamber surfaces which further enhances the loss of reactive species.

3.3.4 Types of Polymeric deposits in pure $SiCl_4$ plasmas

The deposition of various types of polymers and thin films from plasmas containing hydrocarbons or chloroflorocarbons is well known. In pure $SiCl_4$ plasmas it is clear that there are some deposits in agreement with other reports in the literature [36-37], these deposits can be of yellow or white colour and they can be in a powdery form or a "polymer-like" form. Moreover, these deposits can usually be formed more readily at relatively high pressures $\geq$ 50 mtorr. As it was discussed in last section, the emission intensities of all the species are decreased at high pressure except for $SiCl_2$ which continued to increase with pressure. Therefore it is reasonable to suggest that the increase in the emission from $SiCl_2$ is correlated with the apparent formation of these deposits. However, the chemical nature of these deposits is not very clear. Some workers,[36,37] have referred to these deposits as "polymeric" deposits of the form Si_nCl_{2n+2}, material of composition $SiCl_{2.6}$, "polymeric $SiCl_2$" and Si doped with various amounts of chlorine. Avni, and co-workers [38-42] have gone even further in studying the nature of the deposition from $SiCl_4$, $SiCl_4$-Ar and $SiCl_4$-Ar-H_2 plasmas. They found that in plasmas without hydrogen the $SiCl_4$ is partly dissociated to silicon and chlorine through electron-impact dissociations and through polmerizations of chlorosilicon species containing Si_2, Si_3, Si_4, Si_5, and Si_6. The same authors have listed a number of polymerized species that are formed in $SiCl_4$ plasmas at pressures of about 1 Torr, these include: $SiCl_2$, Si_2Cl_4, Si_2Cl_3, Si_2Cl_2, Si_2Cl, Si_3Cl_6, Si_3Cl_5, Si_4Cl_4, Si_5Cl_3, Si_5Cl_2, Si_5Cl and Si_6Cl_3.

3.3.5 Effect of the flow rate on the emission intensities in the low power regime

The effect of the flow rate on the emission intensities of the various species in the $SiCl_4$ plasma has been studied as a function of the flow rate at constant rf power and constant pressures. The emission intensities of Si (288.2) nm, Cl (837.6) nm, SiCl (282.3) nm and $SiCl_2$ (continuum at 330 nm) as a function of the flow rate at constant pressure of 9 mtorr and power of 15 W are given in fig.3.12. The emission intensities of both Si and Cl areremarkably constant over the whole range of flow rate studied, 2-20 sccm. The emission intensity of AlCl has a peculiar behaviour in the flow rate range 2-6 sccm, the emission was zero or not detected, as the flow rate increased from 6 to 9 sccm, whereas in flow rate range of 9-20 mtorr the emission was detected and it nearly constant.

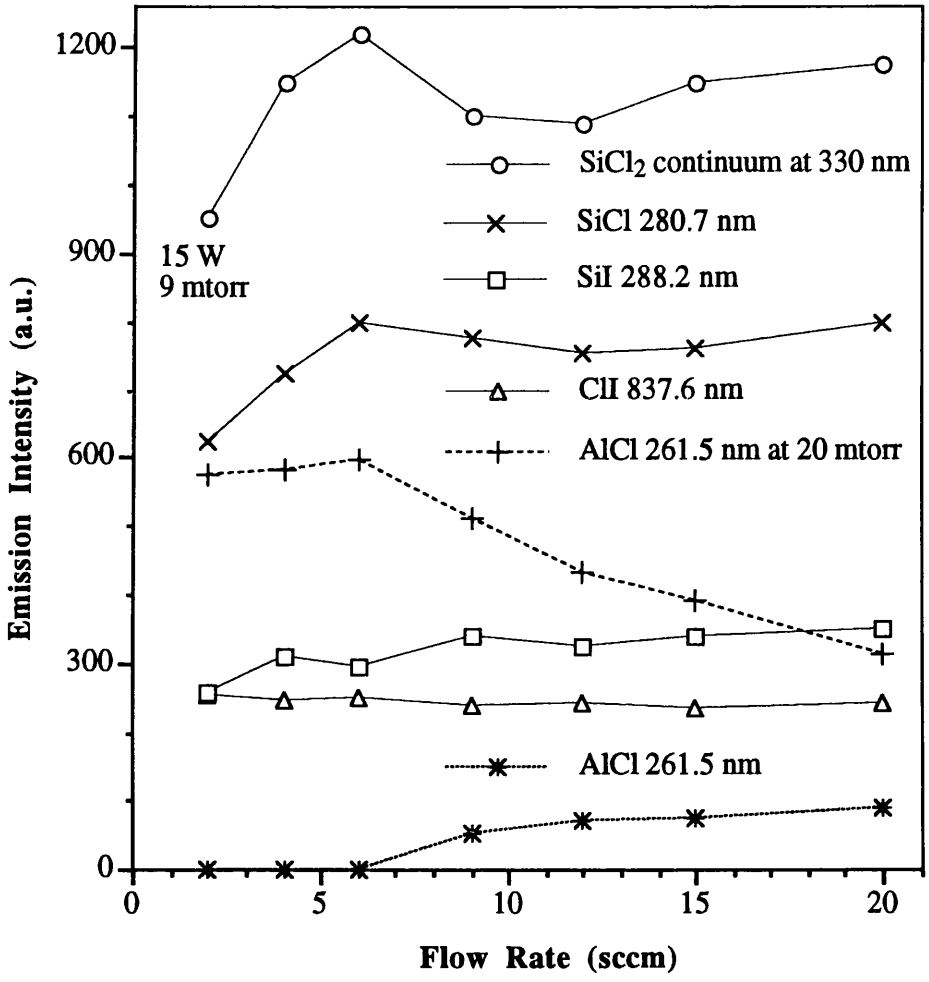

Fig.3.12: Emission intensity of Si, Cl, SiCl, $SiCl_2$ and AlCl in the $SiCl_4$ plasma as a function of the gas flow rate at constant pressure of 9 mtorr and constant power of 15 W.

The emission intensities of both SiCl and $SiCl_2$ show some increase with flow rate in the range of 2-6 sccm exhibiting a slight maximum at flow rate of 6 sccm then they are nearly

constant over the flow rate range of 6-20 sccm. The behaviours of the emissions from Si, Cl, SiCl, and $SiCl_2$ were similar when a pressure of 20 mtorr instead of 9 mtorr was used. However, the emission from AlCl behaves completely in a different way at 20 mtorr as shown in fig.3.12, unlike the emission at 9 mtorr it is detected when very low flow rates are used and it increases slightly between 2-6 sccm and then it decreases for further increases in the flow rate.

These behaviours may be attributed to a large quantity of the species which can lead to formation of the species in the excited state (i.e. $SiCl_4$, $SiCl_2$, SiCl .. etc), and have not undergone dissociation and excitation because of the low power nature of the discharge. In other word we are too far from depleting the gas feedstock even with the least flow rate used. As a result, the additional gas feed will not affect the formation rate of the species in the excited state unless the pressure is changed. "However this may not be necessarily true for the formation of species in their ground state".

3.4 OES detection of impurities and their effect on the discharge chemistry

In this chapter the effect of impurities on the $SiCl_4$ discharge chemistry has been studied using OES, ignoring for the time being the implication this will have on the etching characteristics. Impurities which affect plasma etching processes or affect the discharge chemistry can come from various sources: the feed gas, atmospheric air leaks, desorption from chamber surfaces, backstreaming of gases from the pumping system, etc. The presence of an impurity gas in a glow discharge can affect it in several ways. One way, it can significantly effect the electron energy distribution if the impurity has larger electronic excitation cross-section at lower energies than the dominant cross-sections of the species in the pure gas. For example, impurities in helium discharges significantly affect the electron energy distribution because the lowest electronically excited state of helium is at relatively high energy [35]. Helium addition to other discharges, thus, does not appreciably affect the distribution. Again, a small amount of impurity can form nonvolatile products, through reacting with various species in the discharge, thus altering the species concentration. One of the impurities that can occur very easily is atmospheric air or water vapour. To simulate the effect of an air or water vapour on $SiCl_4$ discharge, N_2, O_2 and H_2 were added separately and the optical emission spectra were recorded.

3.4.1 Spectra of $SiCl_4/N_2$ plasma

To study the effect of an air leak on $SiCl_4$ plasma a small amount of N_2 was added to $SiCl_4$ discharge. The spectra of $SiCl_4/N_2$ plasma for a flow rate ratio of 9/0.3 sccm at various rf powers together with spectrum of a pure $SiCl_4$ plasma using a pressure of 25 mtorris, flow rate of 9 sccm and rf power of 15 W are given in fig.3.13. Besides the

typical emission lines from $SiCl_4$ species, emission lines from N_2 at (297.68, 313.6, 315.93, 337.13, 353.67, 375.54 and 380.49) were detected, however no emission from N_2^+ was detected. N_2^+ is known to emit very strongly when excited, see the spectrum of $CH_4/H_2/N_2$ in section 2.7.4. The reason for not detecting emission from N_2^+ in this case is that the energy threshold required for the formation of N_2^+ (Ionization Potential of N_2) is 15.58 eV and its subsequent excitation require a few more eVs which make such levels inaccessible in the low power regime. In contrast, a weak emission from N_2^+ was detected when a rf power of 25 W was used and a much stonger emission was detected when the power was increased to 40 W, this is again shown in fig.3.13. This can be considered as a further evidence that in the low power regime the density of electrons with energies ≥ 15 eV is not significant, whereas in the high power regime electrons with energies of > 15 eV are easily accessible. No emission from atomic N was detected which is also significant because the bond dissociation energy of N_2 ($N \equiv N$) is 9.97 eV whereas that of Cl_2 (Cl–Cl) for example, is equal to 2.51 eV therefore, higher energies will be needed for N_2 dissociation. Emission lines from SiN at (391.19, 394.98, 401.68 and 405.07) nm were detected while emission form Si was decreased to about 55% of its value with no N_2 added. This suggests that N_2 reacts with Si in the gas phase and forms involatile products of SiN_x species which will have a serious impact on the etching (causing micro-masking). Also notably the emission from AlCl was not detected with the presence of a small amount of N_2 in the discharge which suggest that the etching of electrodes has been stopped. From this discussion we would expect a large effect on the discharge characteristics in case of a small air leak.

3.4.2 Spectrum of $SiCl_4/O_2$ plasma

The spectrum of $SiCl_4/O_2$ plasma for a flow rate ratio of 9/0.3 sccm together with spectrum of a pure $SiCl_4$ plasma for comparison is given in fig.3.14. The discharges were performed using a pressure of 25 mtorr and rf power of 15 W giving a dc bias of 40-50 V. The spectrum of $SiCl_4/O_2$ plasma is considerably different from the spectrum of pure $SiCl_4$ plasma. Firstly, a strong emission from Cl_2 continuum at 256 nm is detected which was not detectable in pure $SiCl_4$ spectrum. Secondly a strong emission from a number of Cl_2^+ lines at (403.3, 417.78, 432.2 and multiplet at 420.16) nm was detected. Moreover strong emissions from a large number of Cl lines were detected. Although strong emissions from Cl and Cl_2^+ lines were detected, no emission from Cl^+ was detected which again emphasises the low energy nature of electrons in the low power regime. Meanwhile the emission from $SiCl_2$ has been decreased to less than 40% of its value in pure $SiCl_4$. As shown in the spectrum, emissions from a number of SiO lines at (225.59-248.68)nm were detected which suggest that the O_2 reacts with $SiCl_4$ molecules and forms involatile species of SiO_x.

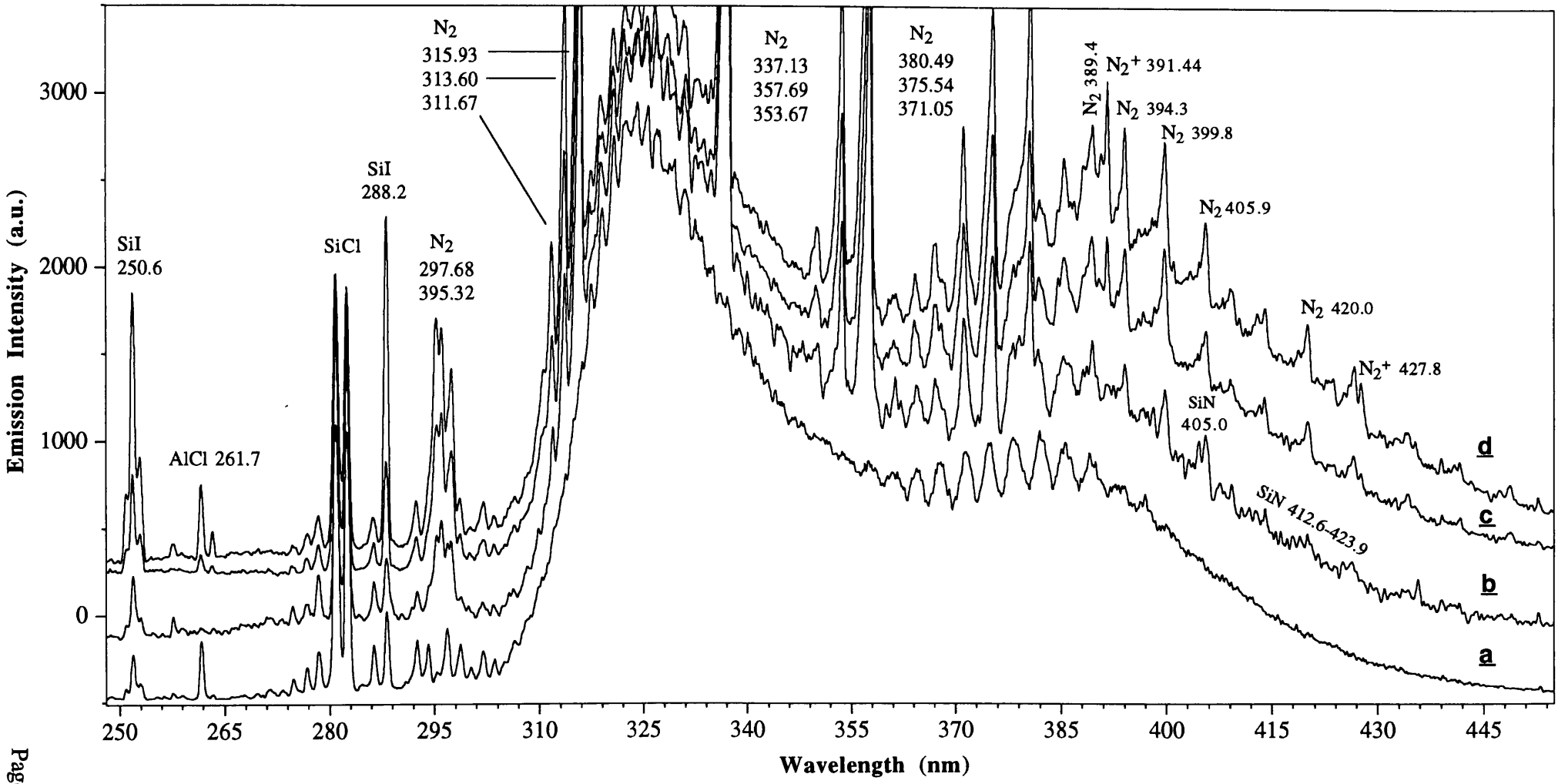

Fig.3.13: (a); Spectrum of pure $SiCl_4$ plasma recorded at power of 15 W, flow rate of 9 sccm and pressure of 25 mtorr. (b, c, and d); spectra of $SiCl_4/N_2$ plasmas, using a flow rate ratio of 9/0.3 sccm, a pressure of 25 mtorr and powers of 15, 25 and 40 W respectively, which shows the emission from N_2, SiN and N_2^+.

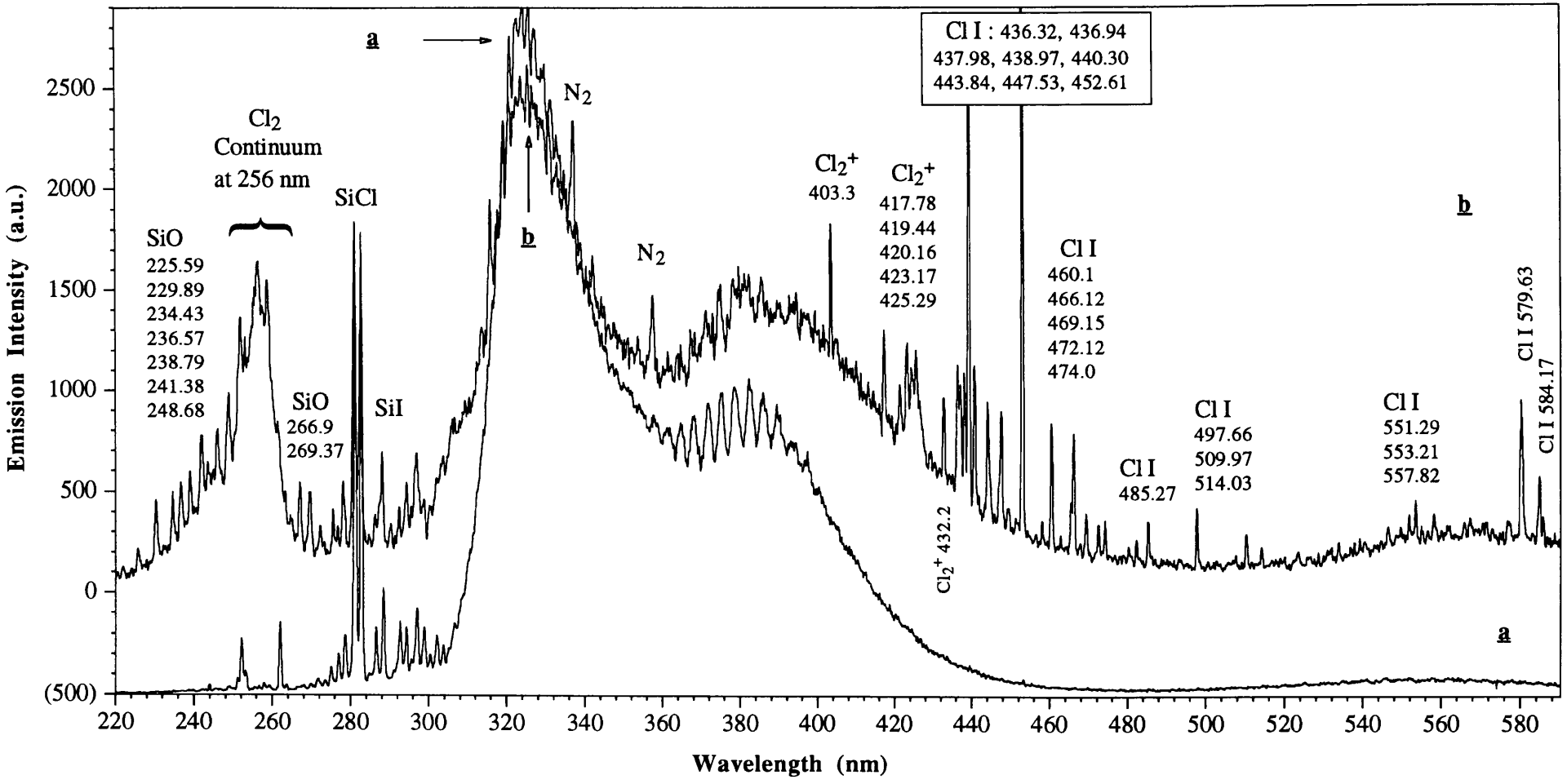

Fig.3.14: Spectra of $SiCl_4$ plasmas. a; pure $SiCl_4$ using flow rate of 9 sccm, pressure of 25 mtorr and power of 15W. b; $SiCl_4/O_2$ at flow rate ratio of 9/0.3 sccm and using the same conditions of pressure and power as a, which shows the emission from Cl_2, Cl_2^+ and intense emission from ClI lines, also shows emission lines from SiO which has been formed due to the addition of O_2 in small amounts to the discharge. The emission from N_2 is due to trace of N_2 in the chamber.

The emission from AlCl is no longer detected which again suggests that the etching of electrodes has stopped. The formation of Cl_2 molecules and the increase in emission from Cl atoms is attributed to the addition of O_2 which significantly enhances the dissociation of $SiCl_4$ molecules and their fragments such as $SiCl_2$ and SiCl radicals into Cl_2 molecules or Cl atoms by the following reactions.

$2SiCl_4 + O_2 \rightarrow 4Cl_2 + 2SiO$ ..... (3.5.2.1)

$2SiCl_2 + O_2 \rightarrow 4Cl + 2SiO$ ..... (3.5.2.2)

$2SiCl + O_2 \rightarrow 2Cl\ (or\ Cl_2) + 2SiO$ ..... (3.5.2.3)

As a result of enhanced formation of Cl_2 and Cl reactive species, O_2 addition can be considered advantageous from the etching point of view as it oxidizes the etched surfaces and in particular the sidewalls which helps to achieve vertical profiles. However the formation of involatile SiO hinders the advantages of the addition of O_2 and turns into disadvantages since SiO is involatile, it deposits on the chamber surfaces. This is not necessarily true for very low pressure plasmas ≤ 0.5 mtorr and for low O_2 to $SiCl_4$ flow rate ratios, for example Song et.al [43] have recently reported the use of a mixture of $SiCl_4/O_2$ plasma using a flow rate ratio of 9:1 sccm in ECR/RIE for GaAs etching with minimum SiO_x formation.

3.4.3 Spectrum of $SiCl_4/H_2$ plasma

The spectrum of a mixture of $SiCl_4/H_2$ plasma for a flow rate ratio of 9/3 sccm together with the spectrum of pure $SiCl_4$ for comparison is given in fig.3.15. The discharges were performed using a pressure of 9 mtorr and rf power of 120 W, and in case of pure $SiCl_4$ a flow rate of 9 sccm was used. The spectrum of $SiCl_4/H_2$ plasma is significantly different from that emitted from pure $SiCl_4$ plasma in a number of points.

1. The emission from $SiCl_2$ which dominates the spectrum of pure $SiCl_4$ plasma has been reduced greatly and it is no longer distinguishable.
2. Strong emission lines from HCl^+ at (283.5 - 386.78) nm were detected.
3. Emission lines from H_2 and H species were detected.
4. Increase in the emission of Cl was observed.

The most significant is the disappearance of the emission from $SiCl_2$ and the formation of HCl^+ molecules. This can be ascribed to the reaction of H_2 with $SiCl_4$ molecules and their fragments to form volatile species through the following reactions.

$SiCl_4 + H_2 \rightarrow 2HCl + SiCl_2$ ..... (3.5.3.1)

$SiCl_2 + H_2 \rightarrow HCl + SiCl + H$ ..... (3.5.3.2)

$HCl + e \rightarrow HCl^+ + 2e \qquad E_{th} = 12.747\ eV$

The reaction (3.5.3.2) is important because it converts $SiCl_2$ radicals which are considered as polymeric deposits into volatile products of HCl, SiCl and H atoms and since HCl may be ionized or dissociated it can play a significant role in the etching process. From this

discussion it seems that the addition of H_2 to $SiCl_4$ discharge brings about more volatile species by enhancing the dissociation rate of secondary polymeric products that form from $SiCl_4$ dissociation. However, the presence of H_2 itself may not be desirable for some etching applications for the reasons related with dry etch damage (the subject of chapter 6). The addition of H_2 was also found to have a long time effect on the repeatability of the etch rate.

3.5 Comparison between ECR generated and rf generated $SiCl_4$ plasmas

In order to widen our understanding of how the applied power and electron energy can influence the dissociation of $SiCl_4$ into its fragments, a comparison between the emission spectra of an Electron Cyclotron Resonance (ECR) generated plasma and conventional rf generated plasma has been carried out. The ECR generated plasma was carried out using an Oxford Plasma Technology ECR machine, driven by 2.45 GHz microwave power source. The electrode is driven by an rf power generator to extract the plasma from the ECR chamber down to the etching chamber. The emission was collected from the ECR chamber where the plasma was most dense . In fig.3.16 the spectra in the range of 200-600 nm of an ECR generated and a rf generated $SiCl_4$ plasmas are given. The spectra in the range of 500-970 nm are in fig.3.17. The ECR discharge was performed using microwave power of 150 W, flow rate of 9 sccm and pressure of 0.65 mtorr, while the rf discharge was performed using power of 150 W, flow rate of 9 sccm and pressure of 9 mtorr. The spectra differ in a number of ways.

1. In the ECR spectrum the emission from Si atoms is stronger by nearly an order of magnitude than in the RIE spectrum.
2. Detection of strong emissions from a large number of ionic lines of Cl^+ in the ECR plasma. The intensity of the emission from Cl^+ is over a 1000 time higher than in the RIE.
3. Detection of a large number of emission lines from Cl_2^+ in the ECR plasma , whereas no emission was detected from RIE plasma.
4. The emission from Cl atoms is stronger by a factor of about 5 in the ECR plasma.
5. The emission from $SiCl_2$ is weaker in the ECR plasma by a factor of about 3.
6. The emission from SiCl is stronger in the ECR by a factor of about 5.

The excitation and ionization of the species in the ECR plasma are expected to be by direct electron impact upon $SiCl_4$ molecules through a single step and not through excitation of the species in the ground state. As a result, the ECR plasma has higher ion and reactive species densities achieved by higher energy electrons present in ECR region. As a result of the high degree of dissociation, the ECR has a high density of gaseous Si which can form polymeric deposits on the chamber surfaces if recombined. From this discussion, it seems reasonable to conclude that the etching characteristics using $SiCl_4$ will differ markedly between an ECR/RIE and a RIE machine.

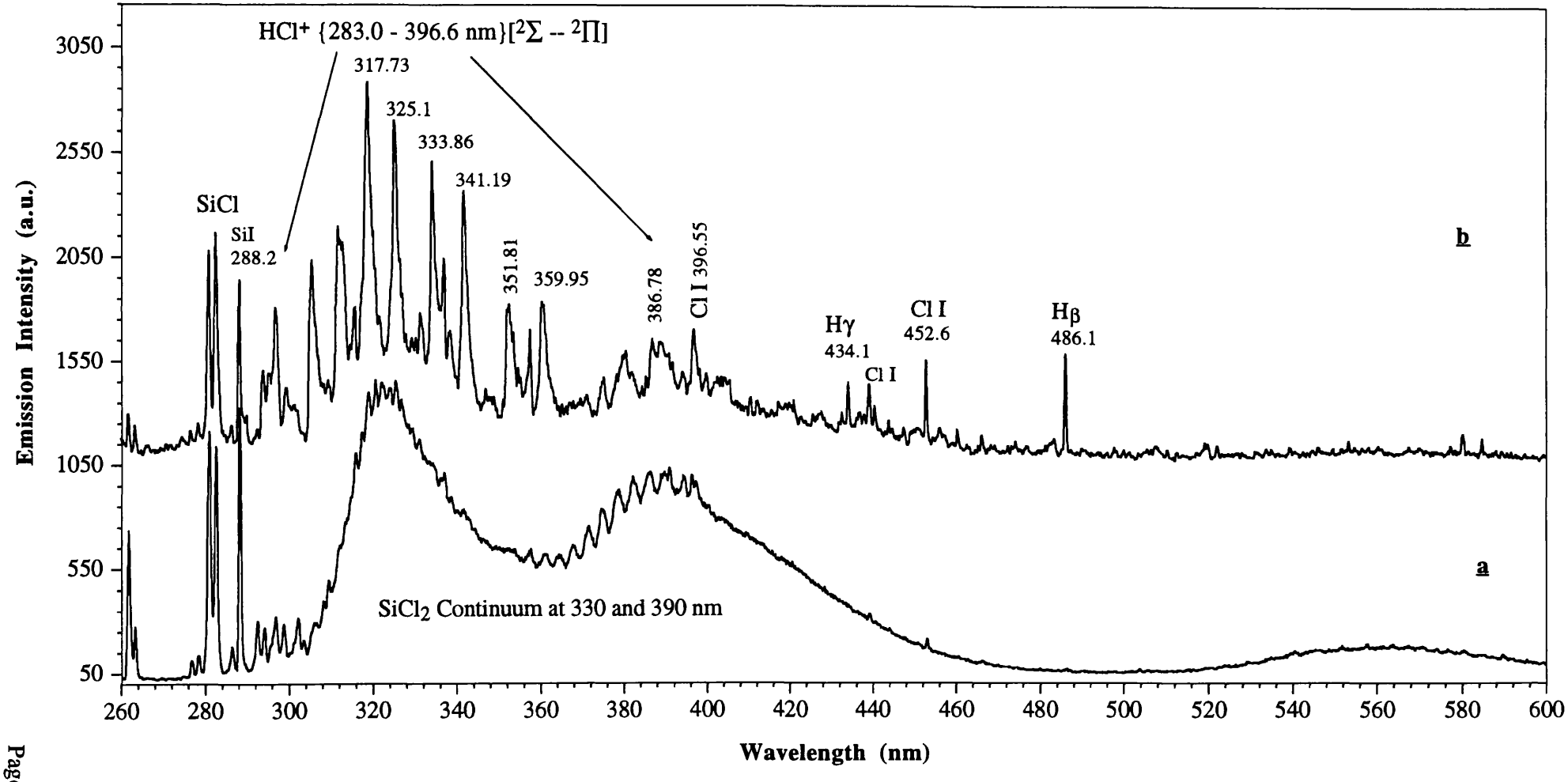

Fig.3.15: Spectra of a; pure $SiCl_4$ plasma using flow of 9 sccm, at pressure of 9 mtorr and power of 120 W, and b; $SiCl_4/H_2$ plasma using flow rate ratio of 9/3 sccm, pressure of 9 mtorr and 120 W. Shows the emission from HCl^+ which dominates the spectrum whilst the emission from $SiCl_2$ has been reduced remarkably.

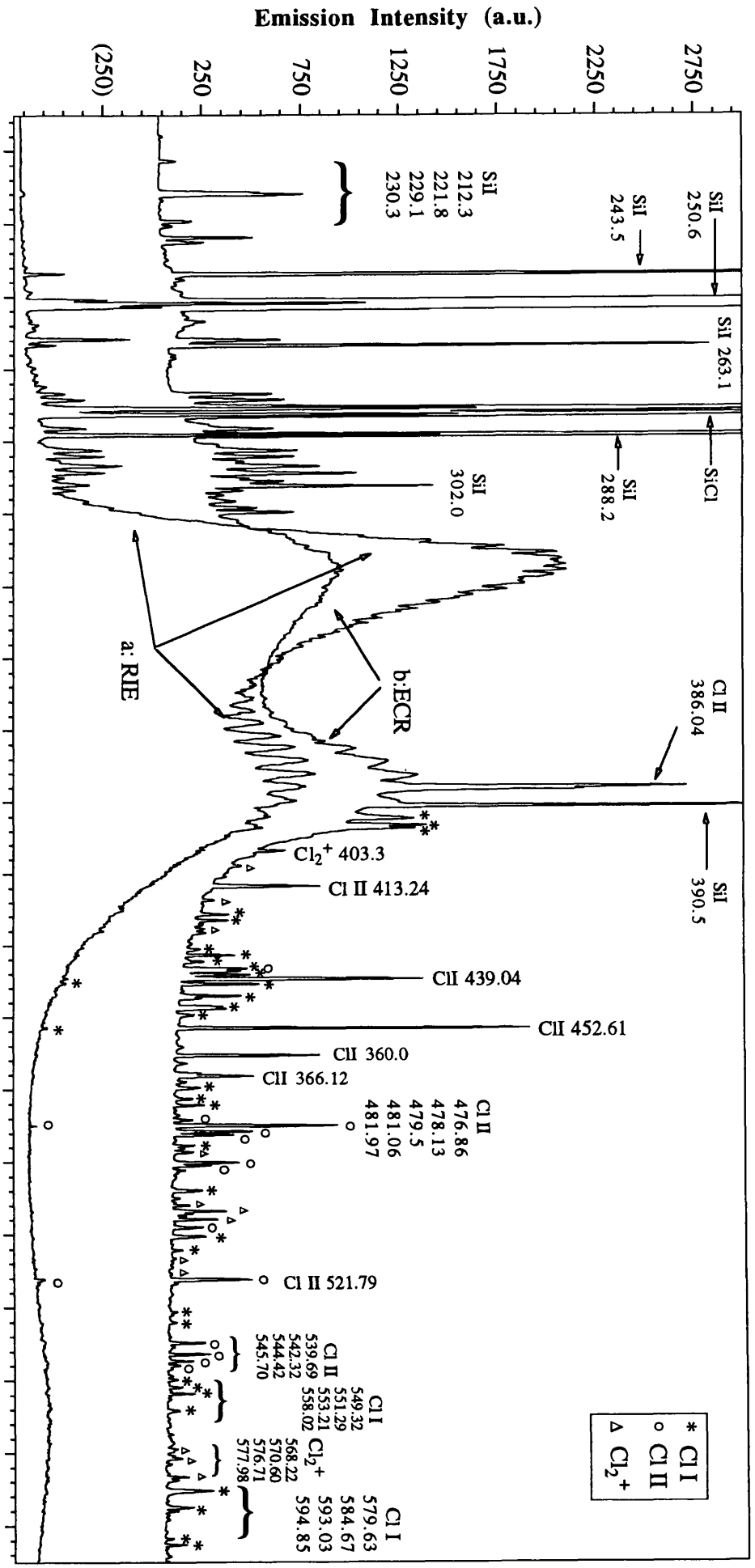

Fig. 3.16: Spectra of $SiCl_4$ plasmas. a: Rf generated plasma in a RIE machine using a power of 120 W, gas flow rate of 9 sccm and pressure of 12 mtorr. b: Microwave generated plasma using excitation frequency of 2.54 GHz in an ECR machine, μwave power of 200 W, gas flow rate of 9 sccm and pressure of 0.65 mtorr. Shows that the microwave excited plasma has a large degree of ionization compared to rf generated plasma.

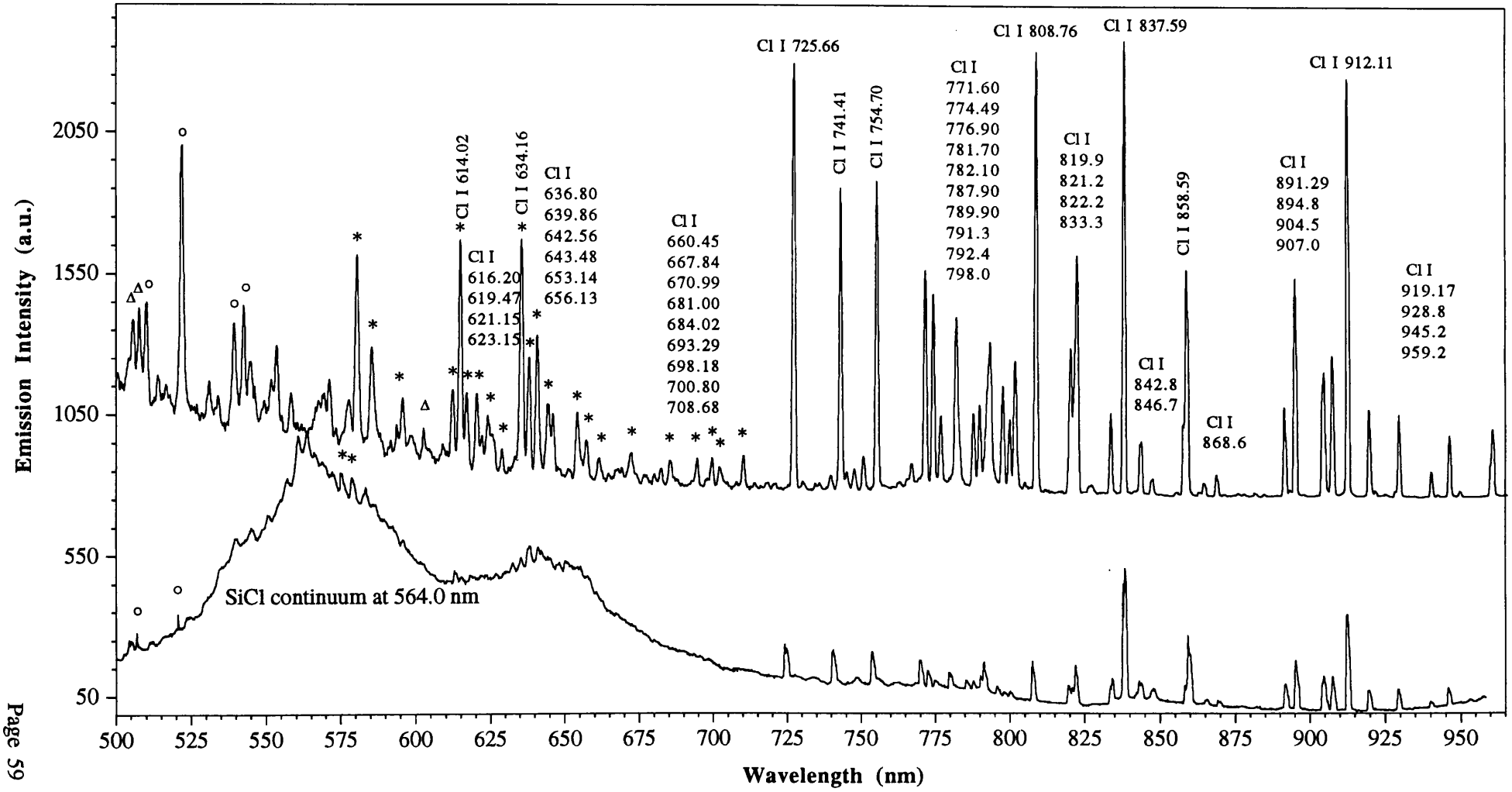

Fig.3.17: Spectra of $SiCl_4$ plasmas in the region of 500-975 nm. a: Rf generated plasma in a RIE machine using a power of 120 W, gas flow rate of 9 sccm and pressure of 12 mtorr. b: Microwave generated plasma using an ECR machine, μwave power of 200 W, gas flow rate of 9 sccm and pressure of 0.65 mtorr.

3.6 OES detection of etch products during etching GaAs in $SiCl_4$ plasma

Gas phase diagnosis using OES provides real time information on process stability and reliability. Detection of optical emissions from electronically excited states of etch reactants and products is an effective means to monitor dry etching of III-V heterostructures. Detection of etch products using the OES during etching of GaAs in $SiCl_4$ plasma has been carried out. The spectrum of $SiCl_4$ plasma during etching GaAs together with the spectrum without etching are given for comparison in fig.3.18. The discharges were performed using a rf power of 120 W, a flow rate of 12 sccm and a pressure of 15 mtorr. The etch rate of GaAs using these conditions is about 420 nm/min. Besides the emissions from $SiCl_4$ species, emissions from etch products were detected. These include emissions from Ga atoms at (294.4, 403.3 and 417.2) nm, As atomic lines at (235.0, 245.7 and 274.5)nm, GaCl lines at (307.0, 319.2, 326.0, 334.6, 338.1, 342.6, 353.0 and 360.0) nm. However no emission was detected from AsCl. It is believed that the emissions from As and Ga atoms originate from Ga and As chlorides that form as the GaAs is being etched as it is also evident from detection of GaCl lines. Unlike the etching in CH_4/H_2 chemistry where the etch products could not be detected because of low etch rates, the detection of etch products from etching GaAs in $SiCl_4$ plasma is readily obtained. A substrate area of only 4 mm^2 is sufficient to detect etch products as etch rates can be relatively high in $SiCl_4$ plasma.

3.6.1 Determination of etch initiation and an end point using OES

The OES has been used to determine the etch initiation period (the induction time) and the end point during etching of multiple layers of GaAs/AlAs in $SiCl_4$ plasma. The etching was performed using discharge conditions of 120 W, a flow rate of 12 sccm and a pressure of 15 mtorr. The expected etch rate for both GaAs and AlAs layers is about 400-420 nm/min.

Using the time dependence of the Ga atomic line at 417.2 nm as shown in fig.3.19, one can easily determine the induction time: the time between when the plasma was turned 'on' but before the emission from Ga is detected which was found to be about 12 sec. The induction time occurs because of the presence of a native oxide layer on the top surface of the GaAs which usually is harder to etch than the material itself. The end point of any of the 20 layers of AlAs or the 19 layers of GaAs can also be determined from fig.3.19, as the emission from Ga will be in the minimum position in AlAs layer and will be in the maximum position in GaAs layer.

The resolution for which the detection of end point can be achieved using this method is not greater than 5 nm due to various factors. One factor is the uniformity of the etching over various layers, if the uniformity is poor then the etching will proceed into layers with different compositions at different rates.

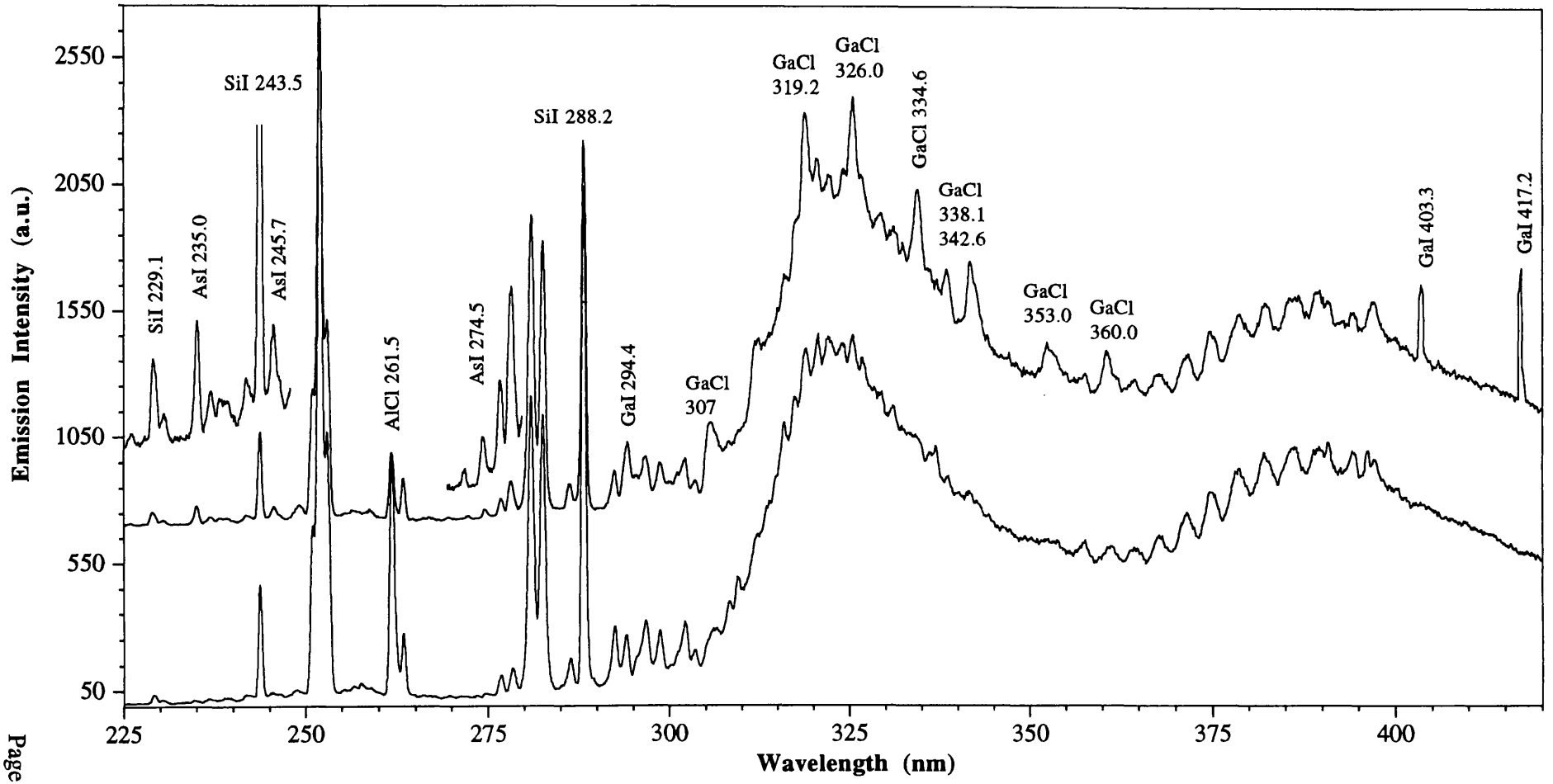

Fig.3.18: Spectra of $SiCl_4$ plasma, A: whilst etching GaAs and B; with no etching. Shows the emissions from etch products of atomic GaI and AsI lines as well as the emission from the GaCl lines but no emission from AsCl was detected. The emission from AlCl is due to contamination from electrodes. The etching was carried out using a flow rate of 9 sccm, a pressure of 12 mtorr and a rf power of 120 W.

As a result, the sample will be etched in some places deeper than others, therefore we can end up etching layers with similar composition placed at different depths.

The pumping system used is another factor, the efficiency and the speed by which the etch products have been pumped out have a big influence, the more efficient and faster the pump in pumping out the etch products, the better the chance of higher resolution. To summarise, we have shown that the OES can well be used to monitor the etch products and determine the etch initiation and end point accurately. The accuracy of with which the etching can be stopped at the desired point depends on several factors but the most significant is the uniformity of the etching over layers with different compositions.

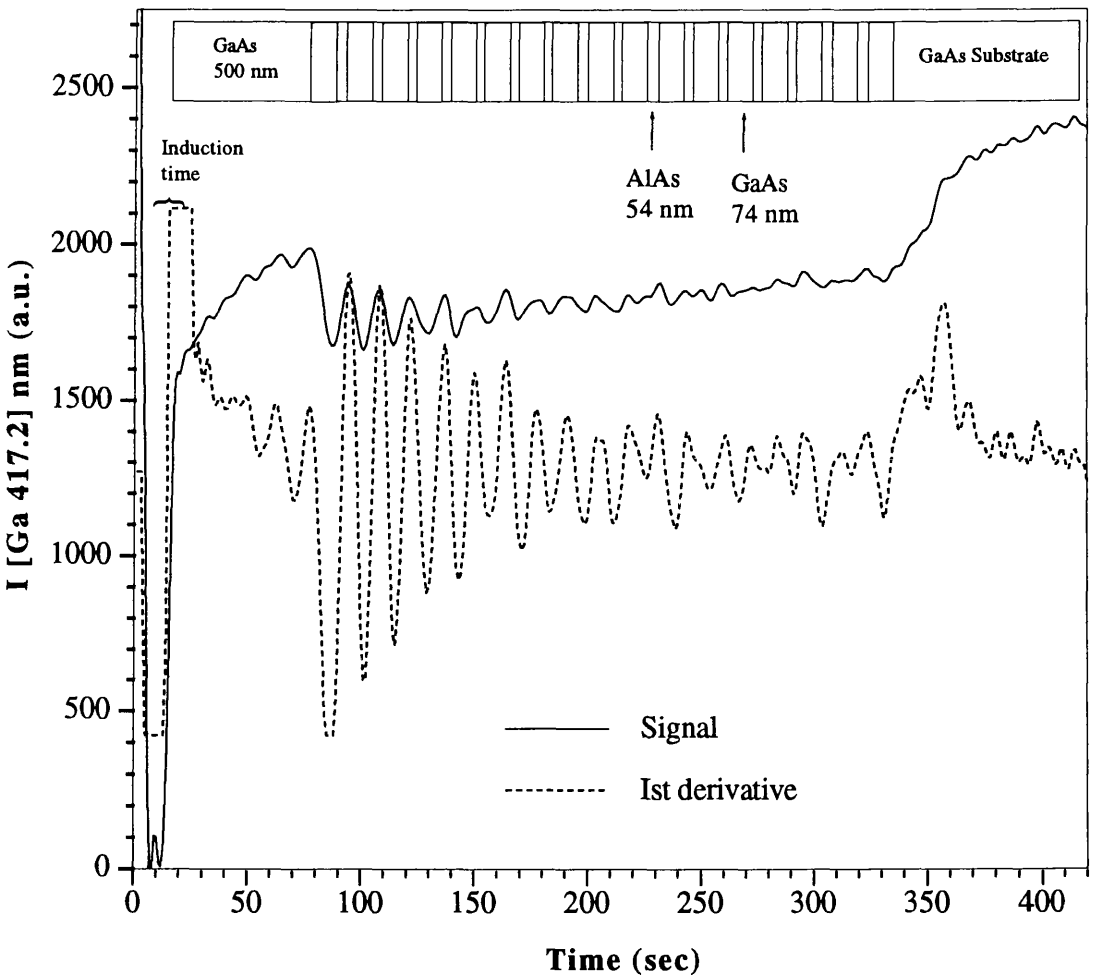

Fig.3.19: The emission intensity of Ga line 417.2 nm as a function of time during RIE of multilayers of GaAs/AlAs in $SiCl_4$ plasma.

3.7 Chapter summary

In this chapter a comprehensive analysis of Optical Emission Spectroscopy of $SiCl_4$ plasmas was given. The analysis showed that the applied rf power plays a decisive role in the way $SiCl_4$ breaks down to its constitutent radicals and atoms. Two power regimes were identified: low power regime and high power regime. In the low power regime $SiCl_4$ molecules break down gradually by multistep electron impact dissociation and excitation processes, whereas in the high power regime $SiCl_4$ molecules break down more rapidly through single electron impact dissociative excitation and ionization processes. The main ions detected in the plasma in the low power regime are Cl_2^+, whereas in the high power regime the main ions are Cl^+. The effect of adding small amounts of N_2, O_2 and H_2 (each separately) to $SiCl_4$ plasma was found to alter the discharge chemistry radically. Results showed that N_2 addition leads to SiN_x deposition on the chamber surfaces, in the case of O_2 addition SiO_x is deposited, whereas the addition of H_2 lead to the formation of HCl ions. Results from a comparison between rf generated and microwave generated $SiCl_4$ plasma showed that the microwave plasma has a superior degree of ionization compared to the rf plasma. Results presented in this chapter showed that OES can be used to detect etch products from a number of III-V compounds and can be used to in situ monitor etch initiation and end point detection successfully. The results also showed that the resolution for which the detection of end point can be achieved using this method is not greater than 5 nm due to various factors such as the uniformity of the etching over various layers and the pumping system.

Table 3.1: Detailed wavelength, transitions and energies of the emitting state (upper state) of the species in the spectra of (a): a (RIE) rf generated $SiCl_4$ plasma, (b): an (ECR) microwave generated $SiCl_4$ plasma, (c): a (RIE) rf generated $SiCl_4/N_2$ plasma, (d): a (RIE) rf generated $SiCl_4/O_2$ plasma, and (e): a (RIE) rf generated $SiCl_4/H_2$ plasma.

Wavelengths (nm)	Species	E (ev)	Plasma	Transitions	Refer. No.
205.813	Si	6.803	a + b	$3p\ ^1D_2 \rightarrow 5s\ ^1P_1^0$	13-15
221.089	Si	5.615	a + b	$3p\ ^3P_1 \rightarrow 3s3p^2\ ^3D_2^0$	
221.666	Si	5.619	a + b	$3p\ ^3P_2 \rightarrow 3s3p^2\ ^3D_3^0$	
243.515	Si	5.870	a + b	$3p\ ^1D_2 \rightarrow 3d\ ^1D_2$	
250.689	Si	4.953	a + b	$3p\ ^3P_1 \rightarrow 4s\ ^3P_2$	
251.431	Si	4.929	a + b	$3p\ ^3P_0 \rightarrow 4s\ ^3P_1$	
251.611	Si	4.953	a + b	$3p\ ^3P_2 \rightarrow 4s\ ^3P_2$	

Table 3.1 continued

251.920	Si	4.929	a + b	$3p\ ^3P_1 \rightarrow 4s\ ^3P_1$	13-15
252.410	Si	4.920	a + b	$3p\ ^3P_1 \rightarrow 4s\ ^3P_0$	
252.850	Si	4.929	a + b	$3p\ ^3P_2 \rightarrow 4s\ ^3P_1$	
263.128	Si	6.619	a+b+c +e	$3p\ ^1S_0 \rightarrow 3d\ ^1P_1{}^0$	
288.157	Si	5.082	all	$3p^2\ ^1D_2 \rightarrow 4s\ ^1P^0$	
298.764	Si	4.929	b	$3p^2\ ^1D_2 \rightarrow 4s\ ^3P_1$	
302.00	Si	4.131	b	$3p\ ^3P_1 \rightarrow 3s3p^2\ ^3S_1{}^0$	
390.522	Si	1.908	b	$3p\ ^1S_0 \rightarrow 4s\ ^1P^0$	
276.8-278.3 280.7-282.2 285.0-310.0	SiCl SiCl SiCl	4.243	all	$B\ ^2\Delta \rightarrow X\ ^2\Pi$ {(v`,v``) (1,0)} $B`\ ^2\Delta \rightarrow X\ ^2\Pi$ {(v`,v``) (0,0)} $B\ ^2\Sigma^+ \rightarrow X\ ^2\Pi$	12,16, 18
455.6 to 630.9	SiCl	2.852	a	$A\ ^2\Sigma^+ \rightarrow X\ ^2\Pi$ {(v`,v``) from (0,2) to (3,15} has a maximum at 563.94 nm	19
315.8-330.9 330.9-356.4 350.0 to 410.0	$SiCl_2$ $SiCl_2$ $SiCl_2$	3.76	all	$\tilde{A}\ ^1B_1 \rightarrow \tilde{X}\ ^1A_1$ {(v_2`,v_2``)(0,9) to (0,0)} $\tilde{A}\ ^1B_1 \rightarrow \tilde{X}\ ^1A_1$ {($v_2$`,$v_2$``)(1,0) to (8,0)} $\tilde{A}\ ^1B_1 \rightarrow \tilde{X}\ ^1A_1$ {(v_1`,$v_2$`,v_3`)(0,1,0) to (v_1``,$v_2$``,v_3``)(0,0,0)} "super-position of valence-and deformation vibration within the transition"	3-7, 10 11,12, 8,9
386.08	Cl^+	19.17	b	$4d\ ^5D_4^0 \rightarrow 4p\ ^5P_3$	14,17,23
413.249	Cl^+	19.00	a + b	$4s\ ^1D_2^0 \rightarrow 4p\ ^1D_2$	
479.45	Cl^+	15.96	b	$4s\ ^1S_2^0 \rightarrow 4p\ ^5P_3$	
481.06	Cl^+	15.95	a + b	$4s\ ^5S_2^0 \rightarrow 4p\ ^5P_2$	
481.947	Cl^+	15.94	a + b	$4s\ ^5S_2^0 \rightarrow 4p\ ^5P_1$	
507.82	Cl^+	18.16	a + b	$4s\ ^3D_3^0 \rightarrow 4p\ ^3D_3$	

Table 3.1 continued

521.79	Cl^+	16.33	a + b	$4s\ ^3S_1^0 \rightarrow 4p\ ^3P_0$	14,17,23
522.13	Cl^+	16.33	a + b	$4s\ ^3S_1^0 \rightarrow 4p\ ^3P_1$	
539.21	Cl^+	18.30	b	$4s\ ^1D_2^0 \rightarrow 4p\ ^1F_3$	
542.32	Cl^+	15.96	a + b	$3d\ ^5D_4^0 \rightarrow 4p\ ^5P_3$	
544.33	Cl^+	15.95	a + b	$3d\ ^5D_3^0 \rightarrow 4p\ ^5P_2$	
256.0	Cl_2^+	2.48	d	Continuum	12,
403.3, 417.87, 419.44, 431.62, 502.01, 505.98			b + d	Bands which belong to system I and II	24,25
396.55	Cl	12.32	b	$4s^4\ P \rightarrow 5p^2\ P$	14,22
420.96	Cl	11.86	b + d	$4s^4\ P \rightarrow 5p^2\ D^0$	
422.64	Cl	11.85	b	$4s^4\ P \rightarrow 5p^2\ S^0$	
432.33	Cl	11.85	b	$4s^4\ P \rightarrow 5p^2\ D^0$	
436.32	Cl	11.83	a +b +d		
436.94	Cl	11.86	a +b +d		
437.98	Cl	11.82	a +b +d	$4s^4\ P \rightarrow 5p^4\ D^0$	
438.97	Cl	11.74	a +b +d		
440.30	Cl	11.73	a +b +d	$4s^4\ P \rightarrow 5p^4\ P^0$	
443.84	Cl	11.71	a +b +d		
446.93	Cl	11.97	b + d	$4s^2\ P \rightarrow 5p^2\ P^0$	
452.62	Cl	11.94	a +b +d		
460.10	Cl	11.97	b + d		
466.12	Cl	11.94	b+ d		
497.07	Cl	11.81	b+ d	$4s^2\ P \rightarrow 4p^2\ D^0$	
579.63	Cl	12.53	b+ d	$4p^4\ P \rightarrow 6d^2\ F^0$	

Table 3.1 continued

594.85	Cl	12.41	b	$4p^4\ P \rightarrow 5d^4\ P$	14,22
601.98	Cl	12.39	b	$4p^4\ P \rightarrow 5d^4\ P$	
611.44	Cl	12.30	b	$4p^4\ P^0 \rightarrow 5d^4\ D$	
614.02	Cl	12.30	b		
616.21	Cl	12.32	b		
619.47	Cl	12.30	b		
634.17	Cl	12.42	b		
639.86	Cl	12.34	b	$4p^4\ D^0 \rightarrow 5d^4\ F$	
643.48	Cl	12.35	b		
653.14	Cl	12.3	b	$4p^4\ D^0 \rightarrow 5d^4\ D$	
725.66	Cl	10.62	a + b	$4s^4\ P \rightarrow 4p^4\ S$	14,20,22
741.41	Cl	10.59	a + b	$4s^4\ P \rightarrow 4p^2\ P$	
754.70	Cl	10.62	a + b	$4s^4\ P \rightarrow 4p^4\ S$	
771.76	Cl	10.59	a + b	$4s^4\ P \rightarrow 4p^2\ P$	
776.91	Cl	11.87	a + b	$4s^4\ P \rightarrow 4p^4\ S$	
777.78	Cl	12.06	a + b		
782.13	Cl	11.86	a + b	$4p^4\ P^0 \rightarrow 4d^4\ D$	
783.07	Cl	11.89	a + b		
787.82	Cl	10.49	a + b	$4s^4\ P \rightarrow 4p^2\ D^0$	
789.92	Cl	11.87	a + b	$4p^4\ P^0 \rightarrow 4d^4\ D$	
791.50	Cl	11.90	a + b		
793.38	Cl	11.96	a + b		
797.47	Cl	12.05	a + b		
799.78	Cl	10.53	a + b	$4s^4\ P \rightarrow 4p^2\ D^0$	
802.33	Cl	12.02	a + b	$4p^4\ D^0 \rightarrow 4d^4\ F$	
805.10	Cl	10.57	a + b		

Table 3.1 continued

808.67	Cl	11.95	a + b	$4p^2\ D^0 \rightarrow 4s^2\ D$	14,20,22
819.43	Cl	10.49	a + b	$4s^4\ P \rightarrow 4p^4\ D^0$	
820.02	Cl	11.94	a + b	$4s^2\ D \rightarrow 5p^2\ P^0$	
821.20	Cl	10.43	a + b	$4s^4\ P \rightarrow 4p^4\ D^0$	
822.17	Cl	10.49	a + b		
833.32	Cl	12.42	a + b		
837.59	Cl	10.40	a + b		
842.82	Cl	10.49	a + b		
846.73	Cl	11.87	a + b		
857.52	Cl	10.47	a + b		
858.59	Cl	10.43	a + b		
868.63	Cl	10.62	a + b	$4s^2\ P \rightarrow 4p^4\ S^0$	
891.29	Cl	10.59	a + b	$4s^2\ P \rightarrow 4p^2\ P^0$	
894.80	Cl	10.30	a + b		
903.89	Cl	11.80	a + b		
904.54	Cl	10.65	a + b		
906.96	Cl	11.79	a + b	$4s^2\ P \rightarrow 4p^2\ S^0$	
907.31	Cl	10.56	a + b		
912.11	Cl	10.28	a + b	$4s^4\ P \rightarrow 4p^4\ P^0$	
919.16	Cl	10.33	a + b		
928.88	Cl	10.53	a + b		
939.38	Cl	10.30	a + b		
945.20	Cl	10.59	a + b		14,20,22
261.7	AlCl	4.75	all	$A\ ^1\Pi \rightarrow X\ ^1\Sigma^+$	12,31

Table 3.1 continued

405.07 412.66 420.41 423.91	SiN	3.19	c	$^2\Sigma \rightarrow X\,^2\Sigma$	12,31
225.59 229.89 234.43 236.57 238.79 241.38 248.68 266.9 269.37	SiO	5.31	d	$A\,^1\Pi \rightarrow X\,^1\Sigma^+$	12,19
293.17 304.82 311.08 317.73 324.59 333.00 338.09 341.09 351.81 359.95 386.68 396.55	HCl^+	3.55	e	$A\,^2\Sigma \rightarrow X\,^2\Pi$	12,28

Table 3.2: Calculated minimum energies for the dissociation, excitation and ionization of the various species in $SiCl_4$ plasma.

No.	**Dissociation Processes**	**E_{th} (eV)**
1	$SiCl(X\,^2\Pi) + e \rightarrow SiCl^*(B\,^2\Sigma) + e$	4.24
2	$SiCl_4 + e \rightarrow SiCl(X\,^2\Pi) + Cl_2(X\,^1\Sigma_g^+) + Cl(^2P^0_{3/2}) + e$	10.07

Table 3.2 continued

3	$\rightarrow SiCl(X\,^2\Pi) + 3\,Cl(^2P^0_{3/2}) + e$	12.58
4	$\rightarrow SiCl^*(B\,^2\Sigma) + Cl_2(X\,^1\Sigma_g^+) + Cl(^2P^0_{3/2}) + e$	14.31
5	$\rightarrow SiCl^*(B\,^2\Sigma) + 3\,Cl(^2P^0_{3/2}) + e$	16.82
6	$SiCl_2(\tilde{X}\,^1A_1) + e \rightarrow SiCl_2^*(\tilde{A}\,^1B_1) + e$	3.76
7	$SiCl_4 + e \rightarrow SiCl_2(\tilde{X}\,^1A_1) + Cl_2(X\,^1\Sigma_g^+) + e$	5.12
8	$\rightarrow SiCl_2(\tilde{X}\,^1A_1) + 2\,Cl(^2P^0_{3/2}) + e$	7.63
9	$\rightarrow SiCl_2^*(\tilde{A}\,^1B_1) + Cl_2(X\,^1\Sigma_g^+) + e$	8.88
10	$\rightarrow SiCl_2^*(\tilde{A}\,^1B_1) + 2\,Cl(^2P^0_{3/2}) + e$	11.30
11	$\rightarrow Si(3p^2\,^3P_0) + 2\,Cl_2(X\,^1\Sigma_g^+) + e$	11.5
12	$\rightarrow Si(3p^2\,^3P_0) + 2\,Cl(^2P^0_{3/2}) + Cl_2(X\,^1\Sigma_g^+) + e$	14.02
13	$\rightarrow Si(3p^2\,^3P_0) + 4\,Cl(^2P^0_{3/2}) + e$	16.53
14	$SiCl(X\,^2\Pi) + e \rightarrow Si^*(4s\,^3P_0) + Cl(^2P^0_{3/2}) + e$	8.88
15	$SiCl_2(\tilde{X}\,^1A_1) + e \rightarrow Si^*(4s\,^3P_0) + Cl_2(X\,^1\Sigma_g^+) + e$	11.32
16	$SiCl_2(\tilde{X}\,^1A_1) + e \rightarrow Si^*(4s\,^3P_0) + 2\,Cl(^2P^0_{3/2}) + e$	13.83
17	$SiCl(X\,^2\Pi) + e \rightarrow Si(3p^2\,^3P_0) + Cl(^2P^0_{3/2}) + e$	3.96
18	$SiCl_2(\tilde{X}\,^1A_1) + e \rightarrow Si(3p^2\,^3P_0) + Cl_2(X\,^1\Sigma_g^+) + e$	6.40
19	$SiCl_2(\tilde{X}\,^1A_1) + e \rightarrow Si(3p^2\,^3P_0) + 2\,Cl(^2P^0_{3/2}) + e$	8.91
20	$Si(2p^2\,^3P_0) + e \rightarrow Si^*(4s\,^3P_0) + e$	4.92
21	$SiCl_4 + e \rightarrow Si^*(4s\,^3P_0) + 2\,Cl_2(X\,^1\Sigma_g^+) + e$	16.42
22	$\rightarrow Si^*(4s\,^3P_0) + 2\,Cl(^2P^0_{3/2}) + Cl_2(X\,^1\Sigma_g^+) + e$	18.94
23	$\rightarrow Si^*(4s\,^3P_0) + 4\,Cl(^2P^0_{3/2}) + e$	21.45
24	$Cl(^2P^0_{3/2}) + e \rightarrow Cl^*(4p\,^4P^0_{5/2}) + e$	10.28
25	$SiCl(X\,^2\Pi) + e \rightarrow Si(3p^2\,^3P_0) + Cl^*(4p\,^4P^0_{5/2}) + e$	14.24
26	$SiCl_2(\tilde{X}\,^1A_1) + e \rightarrow SiCl(X\,^2\Pi) + Cl^*(4p\,^4P^0_{5/2}) + e$	15.24

Table 3.2 continued

27	$SiCl_2(\tilde{X}\ ^1A_1) + e \rightarrow Si(3p^2\ ^3P_0) + Cl(^2P^0_{3/2}) + Cl^*(4p\ ^4P^0_{5/2}) + e$	19.19
28	$SiCl_4 + e \rightarrow SiCl_2(\tilde{X}\ ^1A_1) + Cl(^2P^0_{3/2}) + Cl^*(4p\ ^4P^0_{5/2}) + e$	17.91
29	$\rightarrow SiCl(X\ ^2\Pi) + Cl_2(X\ ^1\Sigma_g^+) + Cl^*(4p\ ^4P^0_{5/2}) + e$	20.35
30	$\rightarrow SiCl(X\ ^2\Pi) + 2Cl(^2P^0_{3/2}) + Cl^*(4p\ ^4P^0_{5/2}) + e$	22.86
31	$\rightarrow Si(3p^2\ ^3P_0) + Cl(^2P^0_{3/2}) + Cl^*(4p\ ^4P^0_{5/2}) + Cl_2(X\ ^1\Sigma_g^+) + e$	24.31
32	$\rightarrow Si(3p^2\ ^3P_0) + 3\,Cl(^2P^0_{3/2}) + Cl^*(4p\ ^4P^0_{5/2}) + e$	26.81
33	$Cl^+(^3P_2) + e \rightarrow [Cl^+]^*(4p\ ^5P_1) + e$	15.95
34	$Cl(^2P^0_{3/2}) + e \rightarrow [Cl^+]^*(4p\ ^5P_1) + 2e$	29.02
35	$SiCl_4 + e \rightarrow SiCl(X\ ^2\Pi) + Cl_2(X\ ^1\Sigma_g^+) + Cl^+(^3P_2) + 2e$	23.14
36	$\rightarrow SiCl_2(\tilde{X}\ ^1B_1) + Cl^+(^3P_2) + Cl(^2P^0_{3/2}) + 2e$	20.72
37	$SiCl_2(\tilde{X}\ ^1A_1) + e \rightarrow Si(3p^2\ ^3P_0) + Cl(^2P^0_{3/2}) + Cl^+(^3P_2) + 2e$	21.98
38	$SiCl(X\ ^2\Pi) + e \rightarrow Si(3p^2\ ^3P_0) + Cl^+(^3P_2) + 2e$	17.03
39	$SiCl_4 + e \rightarrow SiCl(X\ ^2\Pi) + Cl_2^+(X\ ^2\Pi_{3/2g}) + Cl(^2P^0_{3/2}) + 2e$	21.57
40	$\rightarrow SiCl_2(\tilde{X}\ ^1B_1) + Cl_2^+(X\ ^2\Pi_{3/2g}) + 2e$	16.64
41	$SiCl_2(\tilde{X}\ ^1A_1) + e \rightarrow Si(3p^2\ ^3P_0) + Cl_2^+(X\ ^2\Pi_{3/2g}) + 2e$	17.9
42	$Cl_2(X\ ^1\Sigma_g^+) + e \rightarrow [Cl_2^+]^*(A\ ^2\Pi_{3/2u}) + 2e$	13.96
43	$Cl_2^+(X\ ^2\Pi_{3/2g}) + e \rightarrow [Cl_2^+]^*(A\ ^2\Pi_{3/2u}) + e$	2.48

3.7 References

3.1. S. Thoms, S. P. Beaumont, C. D. W. Wilkinson, J. Frost, and C. R. Stanley, Microelectronic Engineering, **5**, 249, (1986).

3.2. M. B. Stern, H. G. Craighead, P. F. Liao, and P. M. Mankiewich, Appl. Phys. Lett., **45**, 410, (1984).

3.3. M. Sato, and H. Nakamura, J. Vac. Sci. Technol., **20**, 186, (1982).

3.4. B. J. Curtis, and H. R. Brunner, J. Electrochem. Soc., **136**, 1463, (1989).
3.5. R. K. Asundi, M. Karim, and R. Samuel, Proc. Phys. Soc. pp.**581**, (1938).
3.6. R. Cornet, and I. Dubois, J. Phys., B **10**, L69, (1977).
3.7. D. E. Milligan, and M. E. Jacox, J. Chem. Phys., **49**, 1938, (1968).
3.8. B. P. Ruzsicska, A. Jodhan, I. Safarik, O. P. Strausz, and T. N. Bell, Chem. Phys. Lett., 113, **67**, (1985).
3.9. N. Washida, Y. Matsumi, T. Hayashi, T. Ibuki, A. Hiraya, and K. Shobatake, J. Chem. Phys., **83**, 2769, (1985).
3.10. D. Sameith, J. P. Monch, H. J. Tiller, and K. Schade, Chem. Phys. Lett., **128**, 483, (1986).
3.11. H.-J. Tiller and D. Sameith, Contrib. Plasma Phys. **30**, 703, (1990).
3.12. The identification of molecular spectra by R. W. B. Pearse, and A. G. Gaydon, third edition (1963) and fourth edition (1978).
3.13. MIT Wavelength Tables by George R. Harrison, (1939).
3.14. Atomic energy levels by Charlotte E. Moore, Vol.**I**, National Bureau of standards, Circular **467**, (1949).
3.15. Leon J. Radziemski, and Kenneth L. Andrew, J. Opti. Soci. Amer., **55**, 474, (1965).
3.16. N. Sani and R. D. Verma, Can. J. Phys., **43**, 959, (1965).
3.17. Leon J. Radziemski, and Victor Kaufman, J. Opti. Soci. Amer., **64**, 366, (1974).
3.18. R. D. Verma, Can. J. Phys. **42**, 2345, (1964).
3.19. S. R. Singhal, and R. D. Verma, Can. J. Phys., **49**, 407, (1971).
3.20. C. J. Humphreys, and E. Paul, J. Opti. Soc. Amer., **49**,1180, (1959).
3.22. Leon J. Radziemski, and Victor Kaufman, J. Opti. Soci. Amer., **59**, 424, (1969).
3.23. C. C. Kiess, and T. L. deBruin, J. Res. Nat. Bure. Stand., **23**, 443, (1939).
3.24. P. B. V. Haranath, and P. Tiruvenganna Rao, J. Mol. Spect., **2**, 428, (1959), also Ind. J. Phys., 50, 401, (1958).
3.25. F. P. Huberman, J. Mol. Spect., **20**, 29, (1966).
3.26. Goran Norlen, Phys. Scripta, **8**, 249, (1973).
3.27. F. J. Kampas, and R. W. Griffith, J. Appl. Phys., **52**, 1285, (1981).
3.28. Handbook of chemistry and physics, 73 rd edition, CRC press, (1992-1993).
3.29. L. F. Wang, J. L. Margrave, and J. L. Franklin, J. Chem. Phys., **61**, 1357, (1974).
3.30. L. F. Wang, J. L. Margrave, and J. L. Franklin, J. Chem. Phys., **60**, 2158, (1974).
3.31. J. W. Hastie, and J. L. Margrave, J. Phys. Chem., **73**, 1105, (1969).
3.32. M. Tsuji, T. Toshinori, and Y. Nishimura, Can. J. Phys., **59**, 985, (1981).
3.33. Albert, D. Richards and Herbert H. Sawin, J. Appl. Phys., **62**, 799, (1987).
3.34. Albert, D. Richards, Brain E. Thompson, Kenneth D. Allen, and Herbert H. Sawin,

J. Appl. Phys., **62**, 792, (1987).

3.35. H. Uchiike, H. Shindo, H. Nishi, K. Arinaga, Y. Fukushima, and T. Tamaru, J. Appl. Phys., **61**, 4479, (1987).

3.36. E. G. Rochow, Comprehensive inorganic chemistery, Vol. **1**, pergamon press, (1973).

3.37. M. W. Rowe, The 5th International Conference on "Ion and Plasma Assisted Techniques" (IPAT), Munich-May 1985, pp. 87.

3.38. R. Avni, U. Carmi, A. Inspector, and I. Rosenthal, Thin Solid Films, **118**, 231, (1984).

3.39. R. Avni, U. Carmi, I. Rosenthal, R. Manory, and A. Grill, Thin Solid Films, **117**, 235, (1983).

3.40. N. Mayo, U. Carmi, I. Rosenthal, and R. Avni, J. Appl. Phys., **55**, 4404, (1984).

3.41. U. Carmi, A. Inspector, and R. Avni, Plasma Chem. Plasma Process., **1**, 233, (1981).

3.42. I. Haller, J. Vac. Sci. Technol. A **1**, 1376, (1983).

3.43. Y. P. Song, P. D. Wang, C. M. S. Torres, and C. D. Wilkinson, paper presented in EIPB'94 conference, New Orleans (1994).

Chapter 4

Reactive Ion Etching (RIE) of GaAs in $SiCl_4$ Plasma

4.1 Introduction

The dry etching of GaAs and related materials is of current interest in the fabrication of devices such as metal-semiconductor field transistors (MESFETs). The etching requirements vary with the application: fast etch rates for deep trenches, high selectivity of one material over another for etch stops to give a precise etch depth or conversely equi-rate etching in making vertical mirrors in optical waveguide material. There are two basic classes of gas mixtures used for etching GaAs based materials [1,2]. The first class is based on methane or ethane and hydrogen. In such plasmas which contain carbon radicals, the deposition of polymer films is a problem. Moreover the etch rates of GaAs based materials in CH_4/H_2 plasmas are very slow which makes this chemistry unsuitable for many applications such as the etching of deep laser waveguides. The presence of hydrogen further complicates the etching process as it leads to the passivation of dopants in GaAs by forming complexes associated with the dopant atoms [1,2]. These passivation effects are not desirable in the fabrication of devices, which further limits the application of hydrogen based chemistry. The second general class of gas mixtures is based on chlorine, Iodine or bromine, because both the gallium and arsenic halides are volatile at low temperatures. However the use of chlorinated gases have been most popular of all halides. A variety of Cl containing gases have been used, including Cl_2,[3,4] CCl_4,[5,6] $COCl_2$,[7] chlorofluorocarbons (CFCs) such as CCl_2F_2,[8,9] BCl_3[10,11] and $SiCl_4$ [12,13]. The use of CFCs will be severely restricted in a few years time because of the concern about the earth's ozone layer. On the other hand CCl_4 is less desirable for GaAs etching because polymer films which contain carbon and chlorine are formed during etching. These polymers degrade etching reproducibility, corrode patterns after etching because of high chlorine concentration, and are hard to remove even through O_2 plasma cleaning [14]. Moreover, the etching chamber and the rotary pump oil become heavily contaminated. Consequently, other chlorine compounds which have less potential for contamination and polymer formation are needed.

The use of $SiCl_4$ and BCl_3 has received great interest for etching GaAs based material because they have less polymer deposition as the Si or B do not form as many polymers as C. Reactive Ion Etching of GaAs employing $SiCl_4$ was first reported by Stern and co-workers[15,16], who developed a high resolution RIE process for etching GaAs using $SiCl_4$

at pressures of 5 mtorr and bias of 330 V with NiCr as the etch mask. Pearton [17] and co-workers have also investigated GaAs etching in $SiCl_4$ and Cl_2/Ar plasmas over a wide range of discharge parameters. They have concluded that etching in $SiCl_4$ offers a number of advantages over the use of Cl_2/Ar as it gives better surface morphologies, more anisotropic etching and fewer residues.

To produce anisotropic etching of GaAs in $SiCl_4$, all the researchers have had to use relatively high biases of the order of $\geq$ 300 V. RIE of GaAs in $SiCl_4$ at these biases has been reported by many researchers[18-21] to cause considerable degradation to the electrical and optical properties of devices. This degradation in the properties of the devices after RIE etching is known as the "dry etch damage". Rahman [21] and co-workers have carried out extensive work on the GaAs damage after etching in $SiCl_4$ at biases of $\geq$ 280 V and have concluded that considerable damage occurs at these bias levels. The possible sources of damage in RIE processes include: radiation damage by bombardment of ions, electrons and photons [3], contamination originating from deposition during etching or materials sputtered from the etching chamber; stoichiometry modification due to preferential etching or layer intermixing and passivation of donors in the case of hydrogen containing plasmas [23,24]. However, the extent of damage has been reported [18-22] to be largely dependent on the energies of ions bombarding the etched surfaces or sidewalls. Various methods have been adopted for reducing the dry etch damage by reducing the ion energies in the discharge while trying to maintain the integrity of the etching, i.e., the anisotropy, smooth surfaces, etc. These include the so called triode reactor in which a second plasma-generating electrode is included within the process chamber, or the addition of magnetic field configured to reduce the electron loss from the discharge and thus reduce the potential between it and the sample [24]. This form of magnetically enhanced etching is generally divided into two types: magnetron RIE and Electron Cyclotron Resonance (ECR) plasma etching. In ECR discharges, free electrons in the plasma are forced to orbit about external magnetic field lines while absorbing microwave energy. In the ECR region the plasma is most dense, the outer shell electrons from gas molecules in the discharge are liberated leading to a very high degree of ionization in the plasma as it was shown in section 3.6. Since the motion of electrons is constrained by the external magnetic field, few electrons may be lost in collisions with reactor walls, therefore the plasma potential relative to ground is low. The resultant energies of ions reaching the sample to be etched without the application of additional bias are low; typically $\leq$ 15 eV. Since this is less than the displacement threshold for damage in most semiconductors, ECR is expected to achieve low damage etching [25].

In RIE processes the energies by which the ions bombard the surface "the ion energies" are largely dependent on the sheath or the plasma potential to the ground, in other words the self dc bias. On the other hand, the dc bias largely depends on the applied rf power and to some extent on the pressure. Therefore to reduce the ion energies, one has to reduce the rf power levels provided that the discharge can be maintained. However, it is often difficult to

reduce the rf power while maintaining reasonable etch rates, anisotropic profiles and smooth surfaces. There is also the problem of deposition of nonvolatile species at such low levels of power. Moreover the presence of impurities and contaminants will have more prominent effect on the etching at such low power levels because of the low density of etchants in the plasma.

One of the aims of this work has been to develop a "damage-free" RIE process for GaAs while maintaining the integrity of the etching such as the smooth surfaces, reproducible etch rates and anisotropic profiles. As mentioned earlier $SiCl_4$ plasma has the potential for achieving such demanding etching requirements, therefore the development of RIE processes carried out in this work are based on $SiCl_4$ chemistry. First the chemistry of $SiCl_4$ discharge was studied as it was given in chapter 3. In this chapter a comprehensive analysis of GaAs etching in $SiCl_4$ plasmas has been carried out. Two mechanisms of GaAs etching are suggested one at low powers and one at high powers. The correlation of these mechanisms with emissions from plasma species is discussed. Anisotropic RIE process for etching GaAs in $SiCl_4$ plasma using low powers and low biases has been developed. The problems associated with contamination and low power etching and the possible cures are discussed in this chapter.

4.2 Experimental

All the etching was performed using an Oxford Plasma Technology RIE80 machine, with a bottom electrode driven at 13.56 MHz and normally partially covered by quartz plate of smaller diameter and the top electrode earthed. The area ratio of top/bottom electrode was 1/0.46. Both electrodes were covered with a thick layer of hard anodized aluminium and they were water cooled to 40 °C under normal working condition. The schematic diagram of the machine is shown in fig.4.1.

The samples used for dry etch depth measurements were undoped and grown by MBE (Molecular Beam Epitaxy) on (100) semi-insulating GaAs wafers. Standard photolithography was used to define the large patterns (1-10 μm wide and 100 - 300 μm long) used for etch depth measurements. A Leica-Cambridge EPBG-5HR Electron-beam writer was used in the definition of small patterns. The small patterns ranged in width from 50-500 nm. Photoresists and metal were used as dry etch masks. The photoresists used were Shipley S1400-31, and S1400-17 which were spun coated for 30 seconds at 4000 rpm to yield thicknesses of 1.8 and 0.4 μm respectively. These photoresists are generally considered to be good masks for etching in $SiCl_4$. The metal masks used were either NiCr or SrF_2 doped with AlF_3 which were transferred to the substrate by the evaporation and lift-off technique described in chapter 1. The metal masks were used in the definition of the small patterns by e-beam lithography. NiCr and SrF_2/AlF_3 are known to be very resistant to halogen containing gases and have small grain size which is necessary in the fabrication

of nanostructures. The etch depth measurements were made using Talystep after removing the photoresist, The anisotropy and the smoothness of etched structures were observed using the Hitachi (S 800, S 900) Scanning Electron Microscopes (SEM).

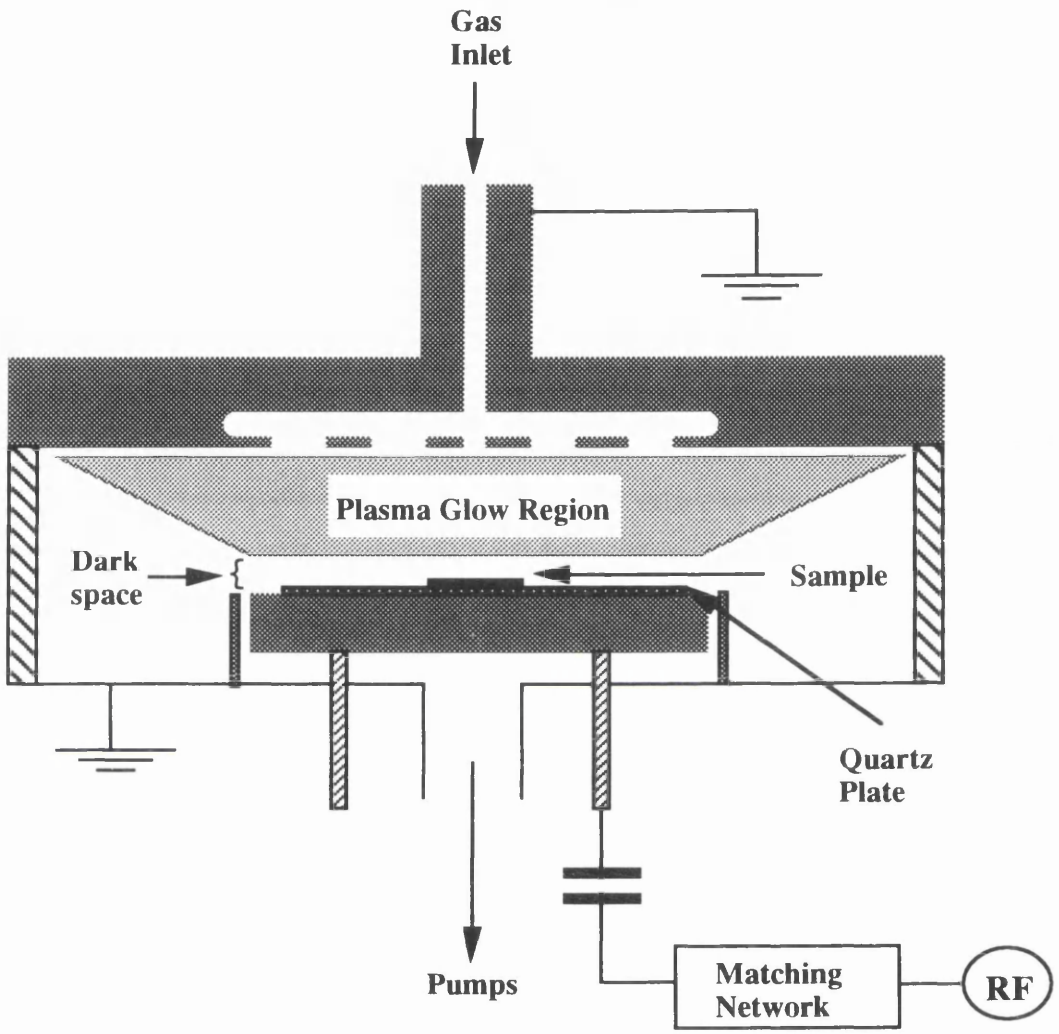

Fig.4.1: Schematic diagram of the Oxford Plasma Technology RIE 80 machine used in this work.

4.3 Presence of contaminants in the discharge

To address the problem of contamination we will first look at the sources of contamination in $SiCl_4$ plasma and the possible cures in the following sections.

4.3.1 The problems and the cures

As it was discussed in section 3.5, impurities can come from various sources and can change the dominant ions in the discharge. However, only few studies have been carried out on plasma impurity effects. Some workers have reported that the chamber

surface condition affects the etching processes, in particular the chlorine containing discharges have been reported to be very sensitive,[26-28] since the Cl loss can be significant and can affect the discharge chemistry. Seasoning of the chamber has been shown to affect the etching results by changing the recombination rates on stainless steal electrodes. Atomic Cl loss can also cause nonuniformity in Cl based etching processes, if the loss of the Cl on the electrodes is different from that of the wafers. The loss of the chlorine has also been identified as the cause for excess polymer formation in CCl_4 plasmas [29]. Zau and co-workers [30] have carried out an extensive study on the effect of contamination of atmospheric leaks on the etching processes in Cl based plasmas and other plasmas. They have concluded that the Cl based plasma is critically sensitive to H_2O and O_2 contamination which can affect the etching rate for hours to days after the contamination has been introduced depending on the pumping system .

Process contamination can cause micromasking effects in the etching of GaAs and other materials. Cluster-like forms of involatile materials deposited from the plasma at the etching surface can mask the etching and lead to a roughened etched surface especially at low powers because these clusters cannot be sputtered-off the surface because of the low biases at these low power levels. The formation of micromasking has also been attributed to insufficient descumming of photoresists, the presence of patchy oxides and to contamination by water vapour, oxygen and pump oil. Reduction of atmospheric contamination by use of load locks and elimination of pump oil backstreaming,[31] has been seen to reduce the micromasking effect. However, the use of these techniques is not sufficient to reduce the chamber contamination through deposition from the discharge itself. The method we have used to overcome these problems is making the etching chamber as clean as possible by regular plasma cleaning in a hydrogen and an oxygen discharge after each etching run.

4.3.1.1 Chamber cleaning in H_2 and O_2 plasmas

The treatment of the etching chamber with an H_2 discharge has been shown [32] to be more effective than treatment with an Ar discharge in removing carbon and oxygen contaminants. This is because H_2 reacts with these contaminants to form volatile species which reduces their deposition once they have been liberated. It was shown in section 3.3.4, that deposition of chlorosilicon species can occur in $SiCl_4$ plasmas. Therefore treatment of the etching chamber with H_2 plasma is likely to lead to formation of volatile species of hydrogenated chlorosilicons and HCl and hence lead to cleaning the chamber from deposits. To investigate these possibilities, a $SiCl_4$ discharge was run for 1 hour using a rf power of 15 W, a pressure of 30 mtorr and a flow rate of 9 sccm using a Plasma Technology RIE80 machine. Then H_2 plasma was performed to clean the chamber while OES was used to monitor the species emitted from H_2 plasma as a function of time. The

spectrum of a H_2 plasma was recorded immediately after striking the H_2 plasma, after 5 min and after 20 minutes running the plasma (see fig.4.2). The discharges conditions were: rf power of 200 W, flow rate of 30 sccm and pressure of 100 mtorr.

In addition to H and H_2 lines, emission lines from atomic Si at 251.6 and 288.2 nm and a large number of emission lines from HCl^+ in the range of 283-386.7 nm were detected in the spectra. After 5 minutes the intensity of the emission from both the Si and HCl^+ lines was reduced and then was no longer observable after 20 minutes, whereas the intensity of the emission from atomic H at 486.1 nm and molecular H_2 at 463.4 nm increased to over 30 % of their value at the beginning of the discharge. This suggests that Si had been deposited on the chamber surfaces during the 1 hour exposure to $SiCl_4$ plasma, presumably in the form of polymerized Si_xCl_y and that H_2 is reacting with these polymerized species to form volatile products of gaseous Si and HCl, that is to say;

$Si_xCl_y + H_2 \rightarrow Si\,(gas) + HCl\,(gas).$

From the discussion above it seems that the chamber treatment with H_2 plasma is an effective method for cleaning the chamber of deposited involatile compounds. However with no further treatment of the chamber, the etch rate of GaAs in $SiCl_4$ was found to vary from run to run by as much as 30-60 %, this effect could last up to a week to 10 days. Similar effects have been observed by some other researchers [30] but the reasons for this behaviour are not very well understood. To eliminate the effect of residual H_2, the chamber was further cleaned in an O_2 discharge. It is thought that the O_2 will react with any residual hydrogenated chlorosilicon species in the chamber and form volatile compounds of OH thereby reducing the residual H_2 in the chamber and eventually its effect on the repeatability of etch rates. Again, was investigated by the use of OES monitoring of the species in an O_2 plasma which was performed after a H_2 discharge. The spectra of the O_2 plasma as a function of time is shown in fig.4.3. The conditions of the discharge were: rf power of 120 W, flow rate of 20 sccm and pressure of 100 mtorr. As expected, emission from the OH lines at 306.4-312.6 nm was detected in the O_2 spectra in the first 15 minutes of running the plasma. The intensity of the emission then decreased and completely disappeared after running the O_2 discharge for 20-25 minutes. However no emission from any chlorosilicon species were detected. After regular cleaning in H_2 and then O_2 discharges, the variability of GaAs etch rate in $SiCl_4$ plasma was about 3-5%. It is reasonable to suggest that the O_2 discharge has indeed eliminated the effect of H_2 on the reproducibility of the etch rates. The effect of this cleaning procedure on the etch rate values, the smoothness and anisotropy of the etching is given in sections 4.3.3 and 4.4.5.

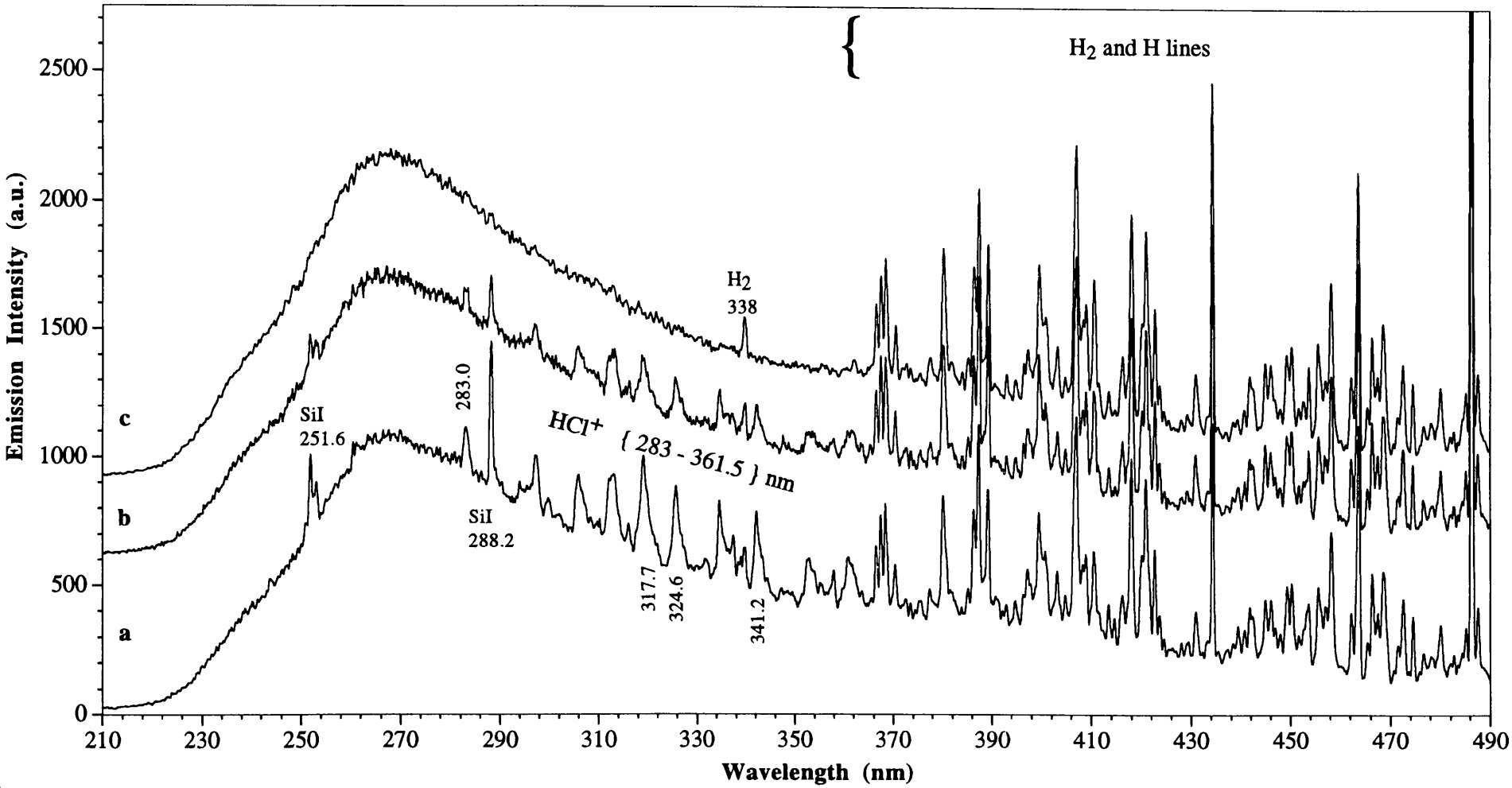

Fig.4.2: Spectra of H_2 plasma as a function of time, recorded after running the $SiCl_4$ plasma for one hour. The discharges were performed using a rf power of 200 W, flow rate of 30 sccm and a pressure of 100 mtorr. (a) recorded in the first 1-2 minutes from running the H_2 plasma, (b) recorded after 5 minutes and (c) recorded after 20 minutes. Shows the presence of the Si and HCl^+ emission lines in the spectra (a) and (b) and they disappear completely after running the H_2 plasma for long enough (20 minutes) to clean the chamber from deposits.

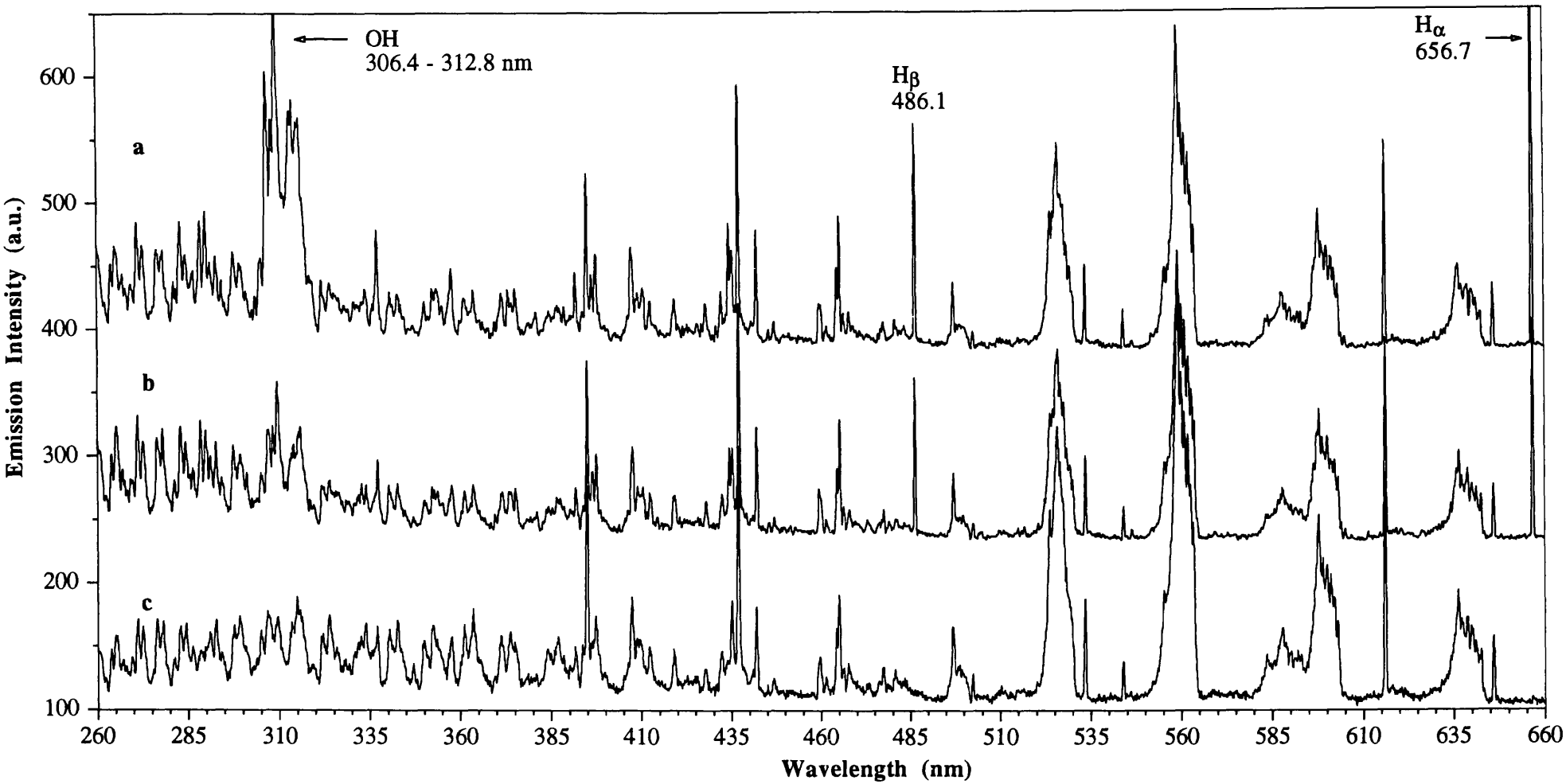

Fig.4.3: Spectra of O_2 plasma recorded at various times from striking the plasma whilest cleaning the chamber from the residual H_2 or hydrgenated and chlorosilicon species. The discharge was performed using a rf power of 100 W, flow rate of 30 sccm and a pressure of 100 mtorr. (a) recorded after 1 minute from running the plasma, (b) recorded after 10 minute and (c) recorded after 20 min. Shows the presence of OH and H lines in the spectra of (a) and (b) and then they disappear after a bout 20 minutes of running the plasma indicating that the residual H_2 has been fully depeleted from the chamber.

4.3.2 GaAs etch rate as a function of the rf power

In fig.4.4 the average etch rate of GaAs, the dc bias and the intensity of the emission from Cl line at 837.6 nm are given as a function of applied rf power from a chamber cleaned as described in section 4.3.1. The rf power was varied between 5-150 W (0.022-0.66 W/cm^2), whereas the flow rate and the pressure were kept constant at 9 sccm and 12 mtorr respectively. It can be seen that the dc bias increases linearly with power.

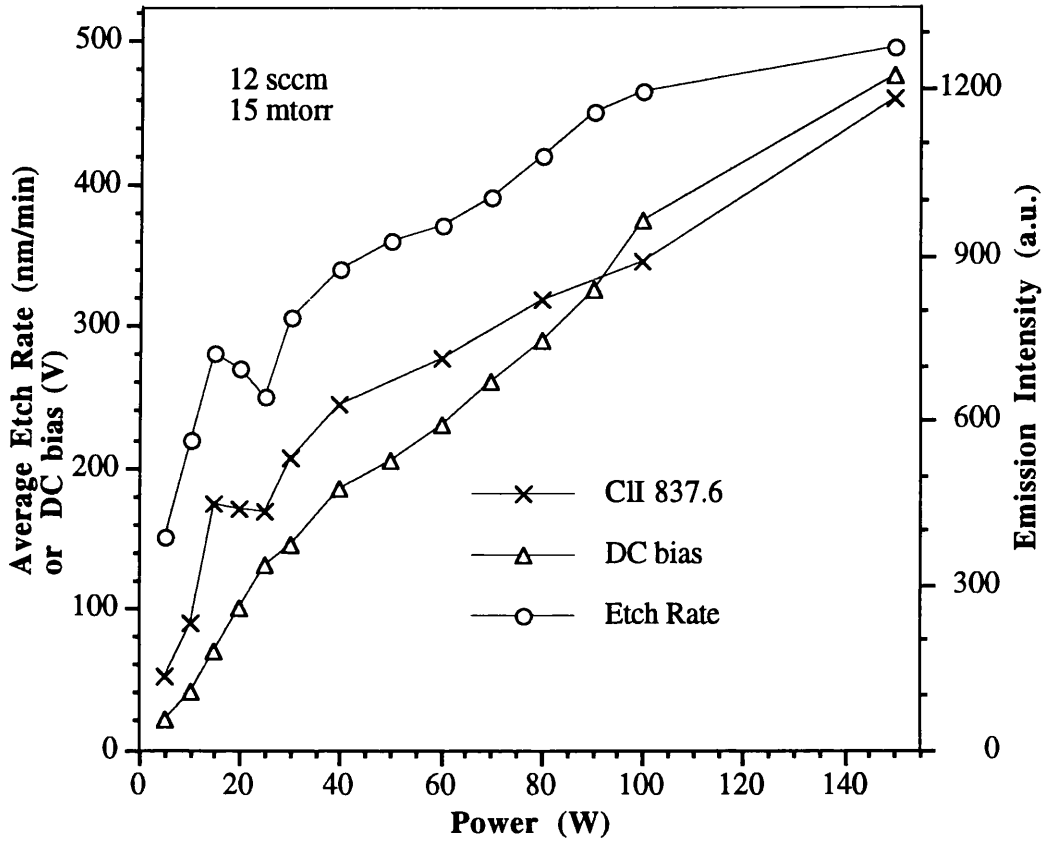

Fig.4.4: The etch rate of GaAs, the dc bias and and the ClI emission as a function of power in $SiCl_4$ plasma, using constant flow rate and pressure of 9 sccm and 15 mtorr respectively.

The behaviour of the etch rate as a function of power is remarkable, first it increases in the power range of 5-15 W, displays a minimum at a power of ~ 25 W and then, increase linearly, (for further increases in the power between 25-150 W). The etch rate of GaAs has been reported[10,33,34] to decrease with power for other Cl containing gases namely BCl_3, CCl_2F_2, Cl_2-CH_4-H_2-Ar and BCl_3-Cl_2 but at much higher power density (0.8-1 W/cm^2). They have assumed that the Cl radicals are desorbed from the GaAs surface before they have a chance to react with surface material. However, in this case the etching process seems to work in two different regimes, with the division between regimes occuring at

about 25 W. From our discussion about the origin of the emitting species in $SiCl_4$ plasma, (see section 3.3.2) we have shown that there are two different chemical regimes responsible for the production of the excited species which depend on the applied rf power and they were identified as the "low power regime" in the power range of 5-20 W and the "high power regime" in the power range 25-150 W.

It is clear from fig.4.4 that the etch rate follows a similar trend to that of the intensity of the emission from atomic Cl in the two power regimes. Therefore, there is a close correlation between the concentration of atomic Cl in the excited state, and the etching mechanism. As a result, the etching proceeds with a different mechanism in the "low power regime" (5-20) W from that in the "high power regime" (25-150) W. Since etching is dependent partly on the ions and partly on the neutrals, the type of the ions that exist in each power regime will play a significant role in determining the mechanism of etching. In the high power regime (power range 25-150 W), the principal ion species detected from the plasma emission was Cl^+, therefore the principal etchants in this power regime are expected to be Cl^+ ions and neutral atomic Cl. In the low power regime (power range 5-20 W), the Cl_2^+ ions were detected in the plasma emission spectrum and no emission from Cl^+ was detected, implying that the main etchants in this power regime are Cl_2^+ and neutral atomic Cl. As a result, two mechanisms of etching are initiated, the first is in the power range of 5-20 W "the low power regime" in which the etch rate will depend on the concentration of Cl_2^+. Hence it increases with increasing power up to a point where the concentration of Cl_2^+ begins to fall because of the dissociation-excitation processes that occur in the plasma, it decreases accordingly. The second mechanism of etching is in the power range of 25-150 W "the high power regime". In this mechanism the etch rate will depend on the concentration of Cl^+ ions and Cl neutrals and it increases with increasing concentration of both.

4.3.3 Effect of chamber cleaning on the etch rates

The effect of the cleaning the chamber with successive H_2 and O_2 plasmas was studied using two identical RIE machines, the Plasma Technology RIE80. The first machine (a), was regularly treated with H_2 and then O_2 plasmas for 20 minutes after each etching run, whereas the second machine (b), was not cleaned with any plasmas, however it was cleaned mechanically on a weekly base. The etch rate of GaAs as a function of power for the two machines is given in fig.4.5, using constant flow rate and pressure of 12 sccm and 15 mtorr. As it can be seen the etch rates at powers of 40-150 W are over 45% higher in the machine (a) than in the corresponding powers in machine (b). On the other hand for low powers 5-30 W the effect of the cleaning is even greater, the etch rates in machine (a) are higher by almost an order of magnitude than in machine (b) for the corresponding powers.

It should be noted that the discharge in machine (b) at powers of 5-10 W was difficult to

maintain for long etching times and usually the discharge was split up into three rotating arcs going round the edges of the lower electrode. No such effects were observed in machine (a) even with "1 W" discharge. Therefore it is clear that the cleaning the chamber with H_2 and O_2 plasmas has a dramatic effect on the etch rates especially at low powers.

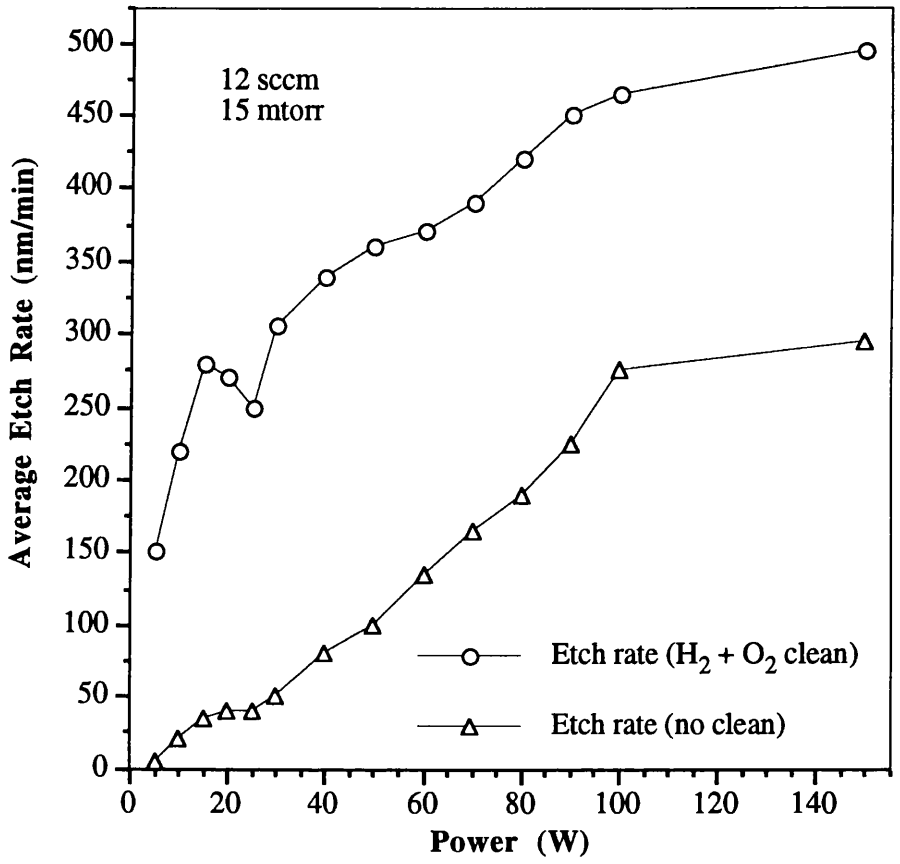

Fig.4.5: The effect of cleaning the chamber with H_2 and then O_2 plasmas on the etch rate of GaAs in $SiCl_4$ plasma as a function of rf power.

4.4 Low power etching of GaAs in $SiCl_4$

One of the aims of this work has been to develop a "damage-free" RIE process for GaAs while maintaining the integrity of the etching such as the smooth surfaces, reproducible etch rates and anisotropic profiles. Therefore the etching characteristics of GaAs has been studied under low power conditions and for the sake of comparison under high powers and over a wide range of pressures and $SiCl_4$ flows.

4.4.1 The effect of pressure and flow rate on the etch rates

The effect of the total chamber pressure and $SiCl_4$ flow rate on the etch rate has been studied in the pressure range of 9-35 mtorr and flow rate range of 2-15 sccm, all

at constant and low power of 15 W (0.066 W/cm^2). The resulting average dc bias fell in the range of 65-20 V. The etch rate as a function of the pressure at various flow rates, the intensity of the emission from the atomic Cl line at 837.6 nm and the dc bias as a function of the pressure at constant flow rate of 9 sccm are given in fig. 4.6.

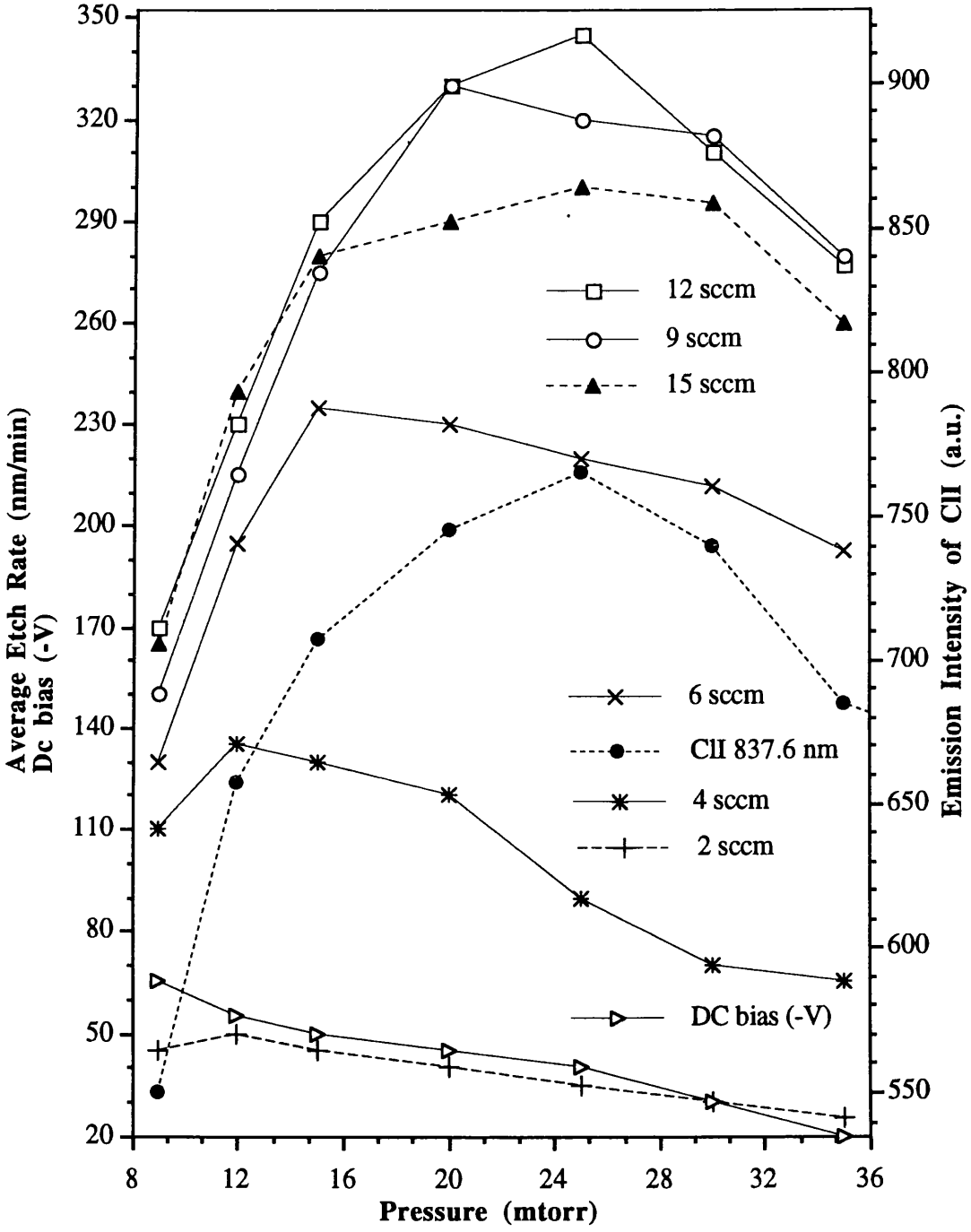

Fig.4.6: GaAs etch rate in $SiCl_4$ plasma as a function of the pressure and the flow rate at constant rf power of 15 W (0.066 W/cm^2). The dc bias and the emission intensity of CII at 837.6 nm are plotted for a flow rate of 9 sccm.

The average dc bias is given as the bias decreases during each run. It can be seen that the average dc bias decreases linearly with increasing pressure. This may be attributed to the fact that the dc bias is mainly determined by the ion energy and ion flux across the dark space region. As the pressure is increased, the ion energies decrease because the ions suffer more collisions and so the dc bias decreases.

As shown in fig.4.6, in the pressure range of 9-12 mtorr the etch rate increases with both the flow rate and the pressure and follows a similar trend as the emission from the atomic Cl line 837.6 nm. This clearly indicates that the etch rate depends on the amount of the chlorine supplied to the surface. At higher pressures the etch rate passes through a maximum at a pressure to flow rate ratio of approximately 2:1 (mtorr : sccm). The drop in the etch rates at higher pressures is accompanied by a decrease in the emission intensity from the atomic Cl and an increase in the emission of the less volatile species, such as $SiCl_2$, (see fig.3.11 in chapter 3). Therefore this fall in the etch rates may be attributed to the increase in formation of $SiCl_2$ through Cl, Si and SiCl recombination at higher pressures which inhibits the etching by retarding the surface reactions through deposition.

4.4.2 The etch rate of GaAs as a function of etching time in $SiCl_4$ plasma

The etch rate of GaAs as a function of etching time in $SiCl_4$ plasma has been studied in both high and low power regimes given in section 4.3.2, namely at 15 and 25 W. The etch rates of GaAs as a function of the etching time have been studied in terms of the differential etch rate which has been calculated as follows:

Differential etch rate at nth minute = $X_{(n)} - X_{(n-1)}$

where $X_{(n)}$ is the etch depth after etching (n) number of minutes and $X_{(n-1)}$ is the etch depth after etching (n-1) number of minutes. Therefore the etch rate during the: first, second, third, 10th minute, etc, can be calculated this way. The differential etch rate at rf power of 15 W and using various pressures and flow rates and at a power of 25 W while using a flow rate of 9 sccm and a pressure of 12 mtorr are given in fig.4.7.

The etch rate, using 15 W of rf power and low flow rates of 2-6 sccm at low pressure of 9 mtorr increases nonlinearly with time in the first 1-4 minutes, being very low during the first minute for the 4-6 sccm and almost no etching occurs in case of 2 sccm of flow rate. The etch rate then stablizes for longer etching times. For high flow rates of 9-12 sccm at high pressures of 15-25 mtorr and for the same power of 15 W, again the etch rate is nonlinear with time but only during the first minute, where it is low, then increses sharply during the second minute and then generally stablizes for longer etching times with a variability of about 5-10%.

The nonlinear behaviour of the etch rate in the first 1-4 minutes in the case of low flow rates of 2-6 sccm at low pressure of 9 mtorr is likely to be due to an oxide layer on the GaAs surface which is harder to etch than the GaAs itself. However, the source of the oxide layer

in this case can be a native oxide grown on the GaAs surface during sample preparation and transportation to the etching system since the surface is exposed to air. The thickness of this oxide layer for GaAs is believed to be about 3 nm. Therefore, we would expect the etching to take a definite time (induction time, the time between the plasma being "on" and before the onset of the actual etching) to etch through this oxide layer, say 40-50 seconds. After this layer (the native oxide) has been etched, the etch rate should be relatively constant with time (in the second, third and the 4th minute etc).

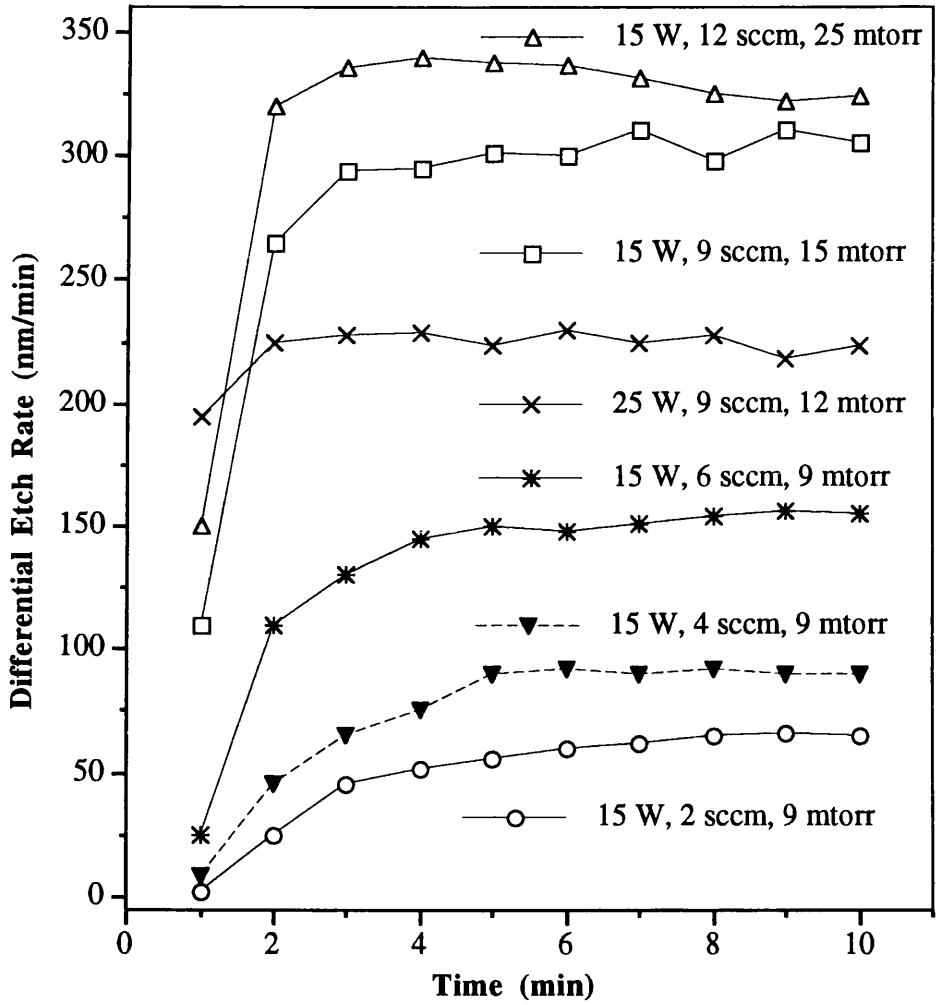

Fig.4.7: Etch rate of GaAs in $SiCl_4$ plasma as a function of the etching time at various flow and pressure conditions.

However this is not the case with low flow and at low pressure, which suggests that the source of the oxide layer is not just an native oxide grown before the etching but an oxide which is being continuously formed and etched (sputtered) during the first 1-4 minutes of etching. The formation of the oxide during the etching is likely to arise from the residual O_2 or water vapour in the chamber which can be effective at low flow rate and low pressure

since there are not enough gas molecules to mop up all the residual O_2 and water vapour at once. So it takes up to 4-5 minutes to scavenge the excess O_2 from the chamber, hence only then the etch rate stablizes. In the case of a high flow rate of 9-12 sccm and high pressure of 15-25 mtorr, the etch rate is different only for the first minute which suggests that a negligible oxide is being formed during the etching. Presumably because the density of gas molecules is high enough to mop up the residual O_2 and water vapour in a very short time, and so the etch rate is low only in the first minute due to the native oxide layer which takes about 30-35 seconds of induction time to be etched.

For the high power regime at 25 W, there is a little change in the etch rate as a function of time which suggests there is a negligible induction time. This may be attributed to the higher dc bias compared to the 15 W power which may help to sputter the native oxide.

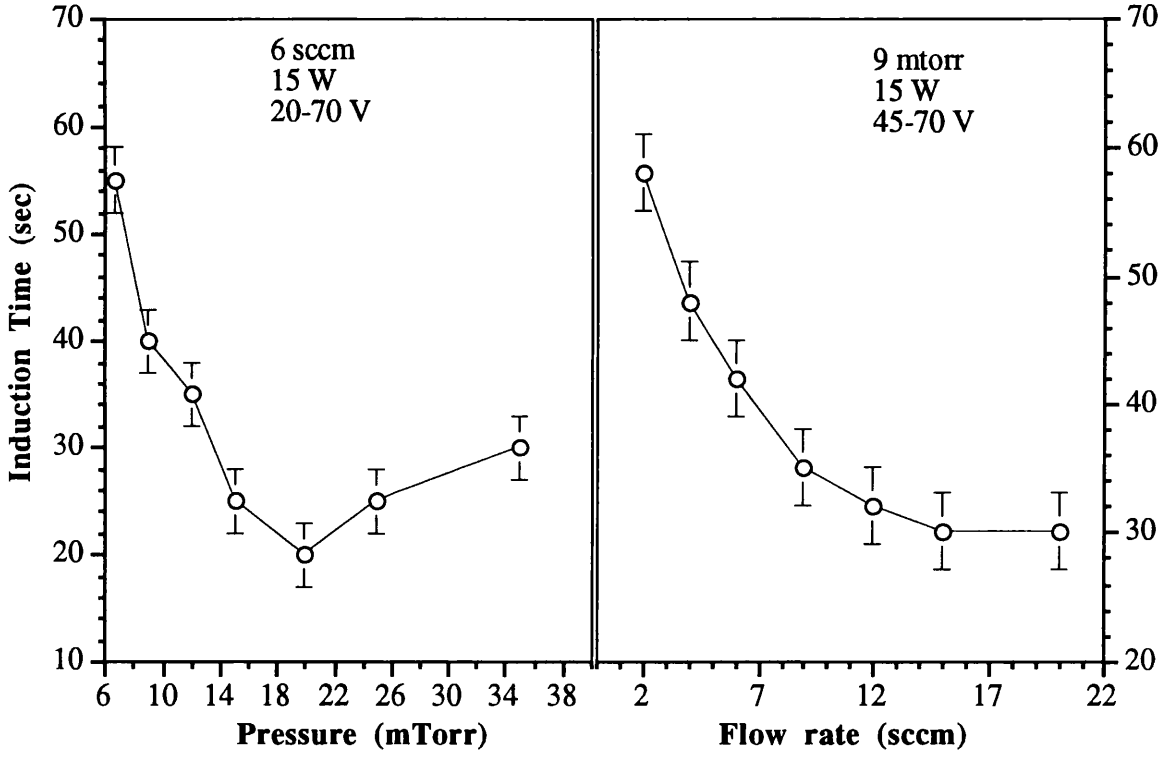

Fig.4.8: The resulting induction time as a function of the pressure and the flow rate during GaAs etching in $SiCl_4$ plasma at low power of 15 W and low bias of 65-20 V.

For the 15 W power regime, the induction time was measured by monitoring the Ga line at 417.2 nm as a function of time and observing the onset of Ga emission using Optical Emission Spectroscopy. The induction time was found to decrease with increasing both the flow rate in the range of 2-20 sccm and the pressure in the range of 6-25 mtorr, as shown in fig.4.8. However for higher values of the pressure > 25 mtorr, the induction was found to increase with increasing pressure. The decrease in the induction time with increasing

pressure and flow rate may be ascribed to more free atomic Cl available at the surface. On the other hand the increase in the induction time for higher pressures may be caused by the considerable decrease in the dc bias, which results in a decrease of overall etch rate at the same time.

4.4.3 The effect of the pressure and $SiCl_4$ flow rate on the anisotropy and surface smoothness at low powers

Generally Reactive Ion Etching of GaAs in $SiCl_4$ plasma can result in a smooth surfaces and anisotropic profiles when high dc biases are used. However, the biases we obtained at low powers, are low ≤70 V, therefore our task of obtaining vertical profiles and smooth surfaces is more difficult. The effect of the pressure and the flow rate on etch profiles and on surfaces was studied in the pressure range of 8-35 mtorr, in the flow rate range of 4-15 sccm and at powers of 10-15 W, the power being varied between 10-15 W to keep the dc bias in the range of 40-70 V. The profile changes at low pressures of 8-15 mtorr were studied by fabricating ribs with width ranging from 60-500 nm, rings of laser structures and gratings with wall thickness down to 40 nm. At pressures ≥ 20 mtorr, the profiles were studied by fabricating narrow and deep trenches 1-3 μm wide and up to 12 μm deep.

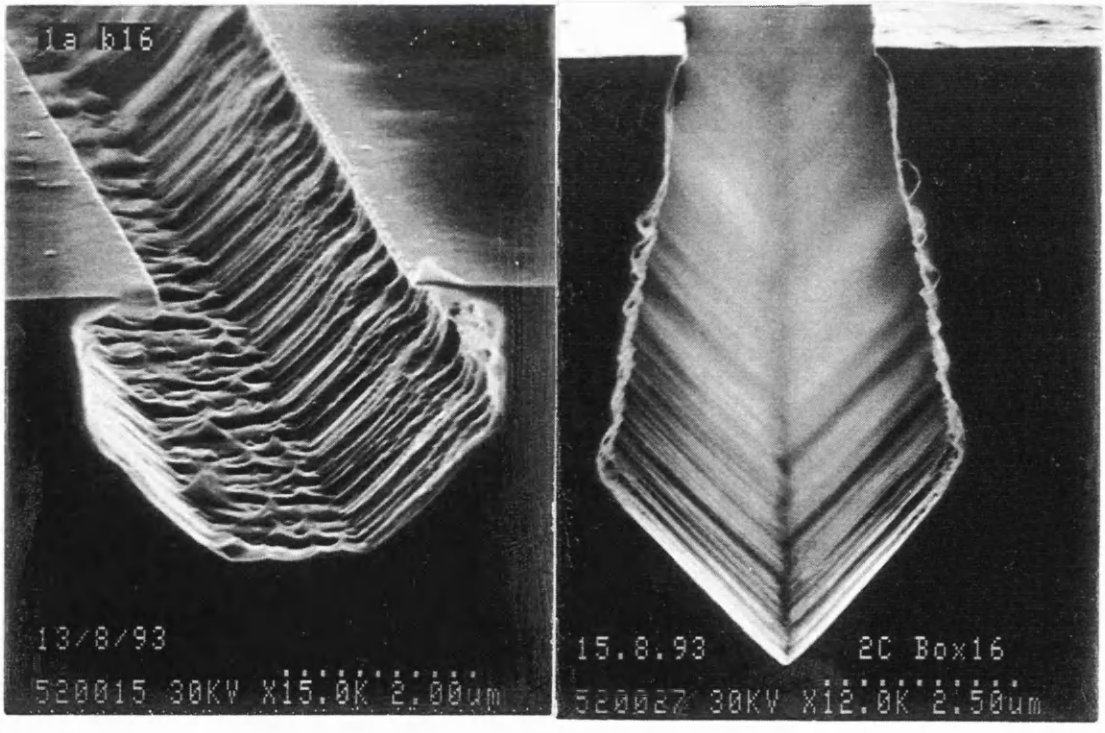

Fig.4.9: SEM micrographs of deep trench of GaAs etched in $SiCl_4$ plasma. (a) left, 2 μm wide, 5 μm deep etched at power of 15 W, flow rate of 12 sccm and pressure of 35 mtorr. (b) right, 2 μm wide, and 11.5 μm deep etched at 30 motrr and the same power and flow rate conditions as in (a). The masks are 75 nm thick NiCr which have not been removed.

Starting first, in the high pressure range ≥ 30 mtorr and with a high flow rate range 12-15 sccm and at 15 W (0.066 W/cm^2) (as shown in the SEM micrographs of fig.4.9) it was found that the etching starts by markedly undercutting the mask, then as the etching proceeds is along crystallographic directions with rough surfaces. The degree of undercutting depends on the pressure, being higher at higher pressures. Lowering the flow rates to 4-9 sccm while keeping the pressures at ≥ 30 mtorr, does not change the tendency of the etching to take place along the crystallographic axis, however the etch surfaces become rougher. This is may be due to the increased residence time of the etchants in the chamber at low flow rates while using high pressures which leads to even more chemical like etching.

In the pressure range 20-25 mtorr and at flow rates of 12-15 sccm, the etching is still along the crystallographic axis but the large undercutting under the mask has almost disappeared and the etched surfaces are smoother as shown in the SEM micrographs of fig.4.10, (a,b). Fixing the pressures at 20-25 mtorr and lowering the flow rate to 9-4 sccm the crystallographic nature of the etching has almost disappeared, however, the surfaces are slightly rougher than at higher flow rates as shown in SEM micrographs of fig.4.10, (c,d). At pressures < 20 mtorr no crystallographic etching was observed at all flow rate conditions. In the pressure range 8-15 mtorr the profile of the sidewalls is very sensitive to changes in both the flow rate and the pressure, while the surfaces are generally smooth and less sensitive to the changes in the pressure or the flow rate. At a pressure of 15 mtorr and flow rates of 12-15 sccm a key hole profile is obtained as shown in fig.4.11a. Reducing the flow rate to 9-4 sccm while keeping the pressure at 15 mtorr the profile is "straight undercut" with about 5-8 degrees off the normal as shown in SEM micrographs of fig.4.11b.

At pressures of 12 mtorr and high flow rates of 12-15 sccm, there is less undercutting, however, the profile has a large foot. Lowering the flow rate to 9 sccm while keeping the pressure at 12 mtorr, the foot is reduced. At a flow rate of 6 sccm, the foot disappears completely and the verticality improves however the there is still undercutting especially in the beginning of the etching as shown in the SEM micrographs of fig.4.12(a-d).

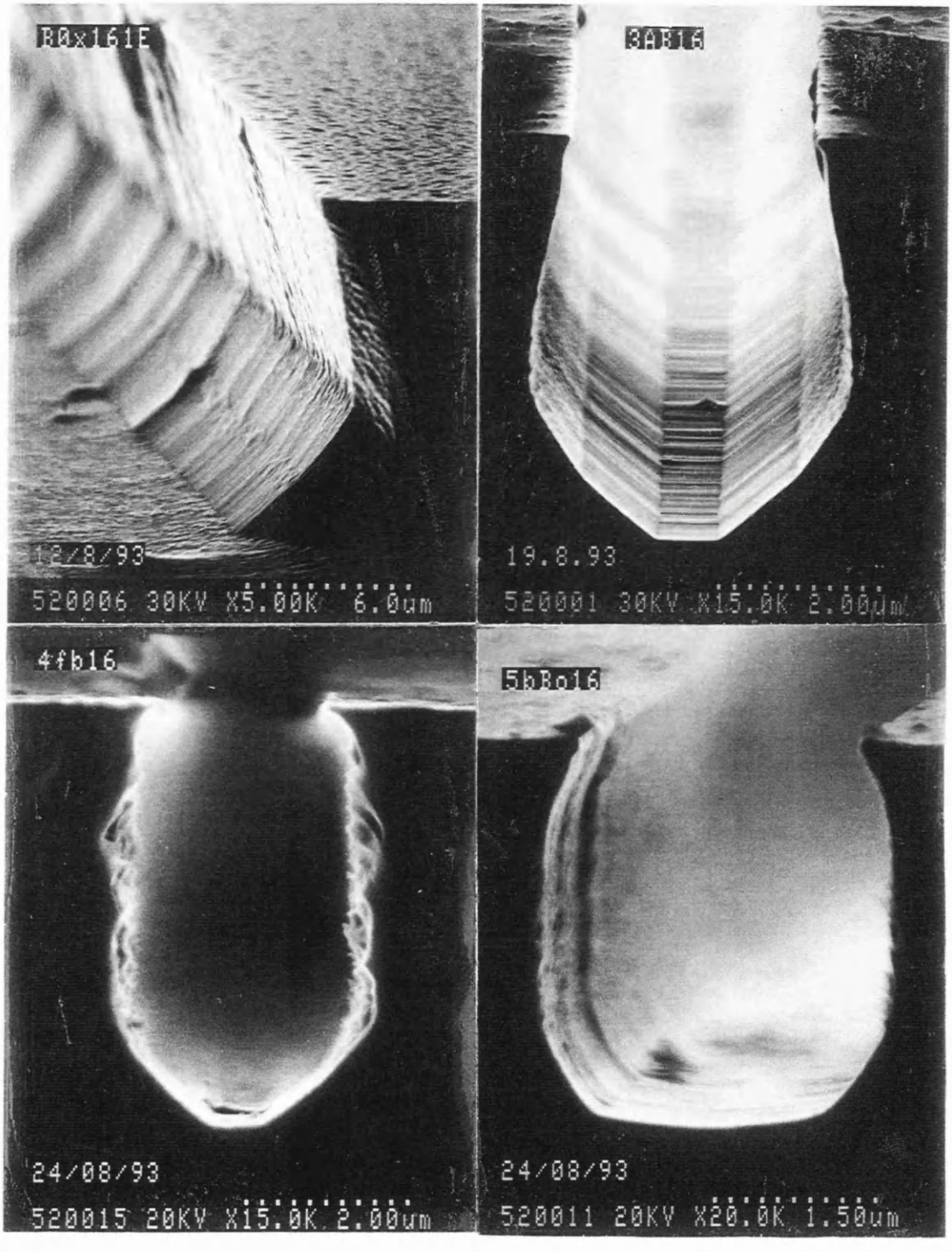

Fig.4.10: SEM micrographs of GaAs trenches etched in $SiCl_4$ plasma at 15 W power and the other etch parameters are; (a) top left, 12 sccm, 25 mtorr, (b) top right, 15 sccm, 20 mtorr, (c) bottom left, 6 sccm, 25 mtorr. and (d) bottom right, 9 sccm, 20 mtorr

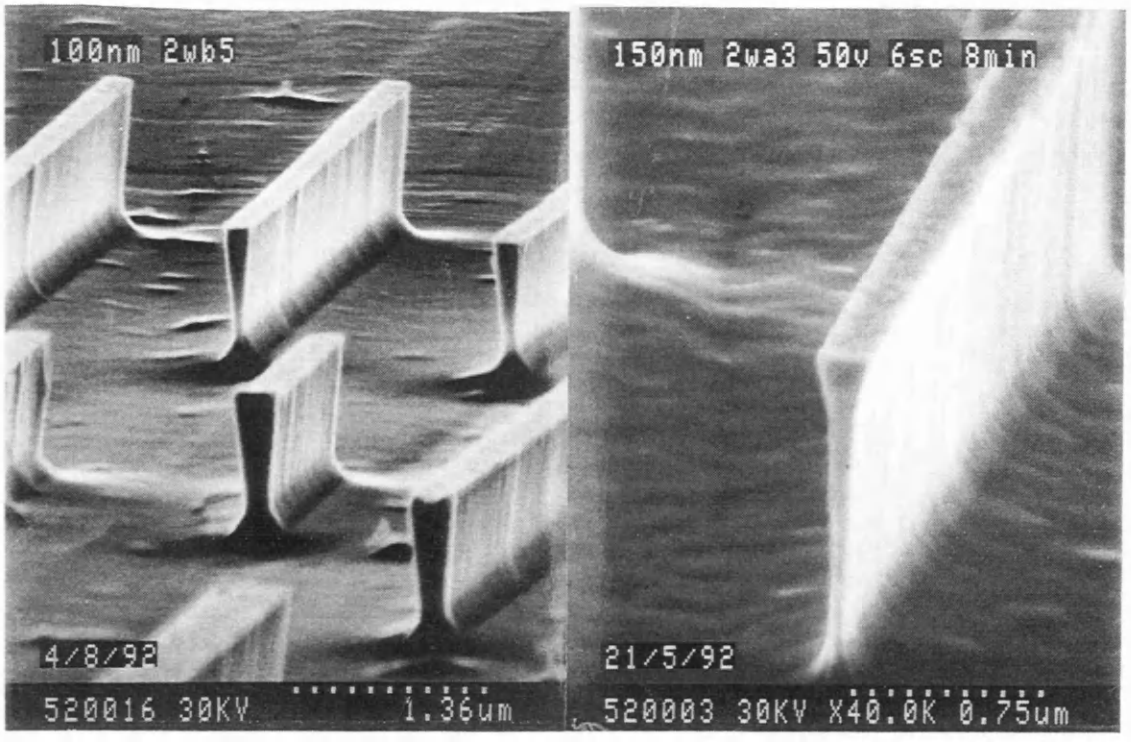

Fig.4.11: SEM micrographs of ribs etched in $SiCl_4$ plasma; (a) left etched using 12 sccm, 15 mtorr and power of 15 W. (b) right etched using 6 sccm, 15 mtorr and 15 W power.

At pressures of 8-9 mtorr, the etch profiles are vertical at all flow rates. However at high flow rate of 9-15 sccm the trenches are bowl shaped, with a larger degree at 15 sccm than 12 sccm as shown in fig.4.13 (a,b). Lowering the flow rate to 6-4 sccm very vertical profiles can be achieved with very smooth surfaces as shown in fig.4.13 (c,d). The summary of the results are given in table 4.1.

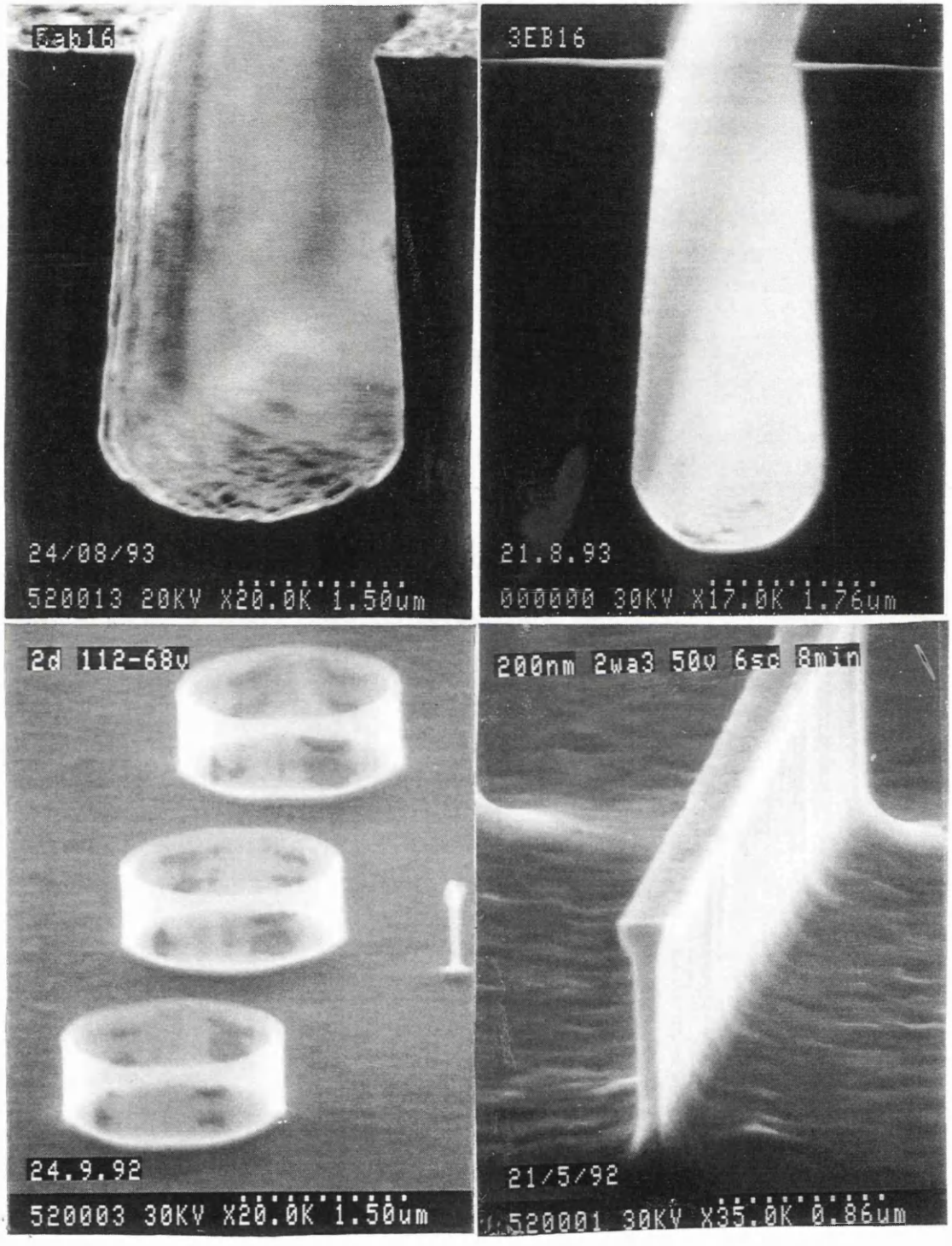

Fig.4.12: SEM micrographs of GaAs structures etched in $SiCl_4$ at power of 15 W. (a) top left, a trench etched using 15 sccm and 12 mtorr. (b) top right, a deep trench etched using 9 sccm and 12 mtorr. (c) bottom left, a laser like ring, 100 nm wall thickness etched using 6 sccm and 12 mtorr. (d) bottom right, a rib etched using 6 sccm and 12 mtorr.

Table 4.1: Summary of the GaAs etch profile changes with pressure and flow rate in RIE in $SiCl_4$ plasma.

Pressure / Flow Rate	9 mtorr	12 mtorr	15 mtorr	20-25 mtorr	≥ 30 mtorr
4-6 sccm	very vertical profiles and smooth surfaces	undercut at start of the etching, with smooth surfaces	throughout undercut at 5-8 degrees off the normal, smooth surfaces	undercut under the mask,10-15 degrees off the normal, rough surfaces and some evedance of small degree of crystallography	large undercut ≥ 20 degrees, very crystallographic and very rough surfaces
9 sccm	vertical profiles and smooth surfaces with bowl shape trenches	throughout undercut at 3-5 degrees off the normal, reduced foot, smooth surfaces	similar to 6 sccm but with small foot at the bottom of the ribs, smooth surfaces	same as 6 sccm but with larger degree of crystallography and smoother surfaces.	same as 6 sccm but with less rough surfaces
12-15 sccm	similar to 9 sccm but with increase in the bowl shape	undercut as in 9 sccm but with larger foot, smooth surfaces	key hole profile, large foot, smooth surfaces	similar to 9 sccm but with increased crystallography	same as 9 sccm

Crystallography: Crystallograhic effects mean that the etching takes place along the crystallographic planes as can seen by the SEM inspection.

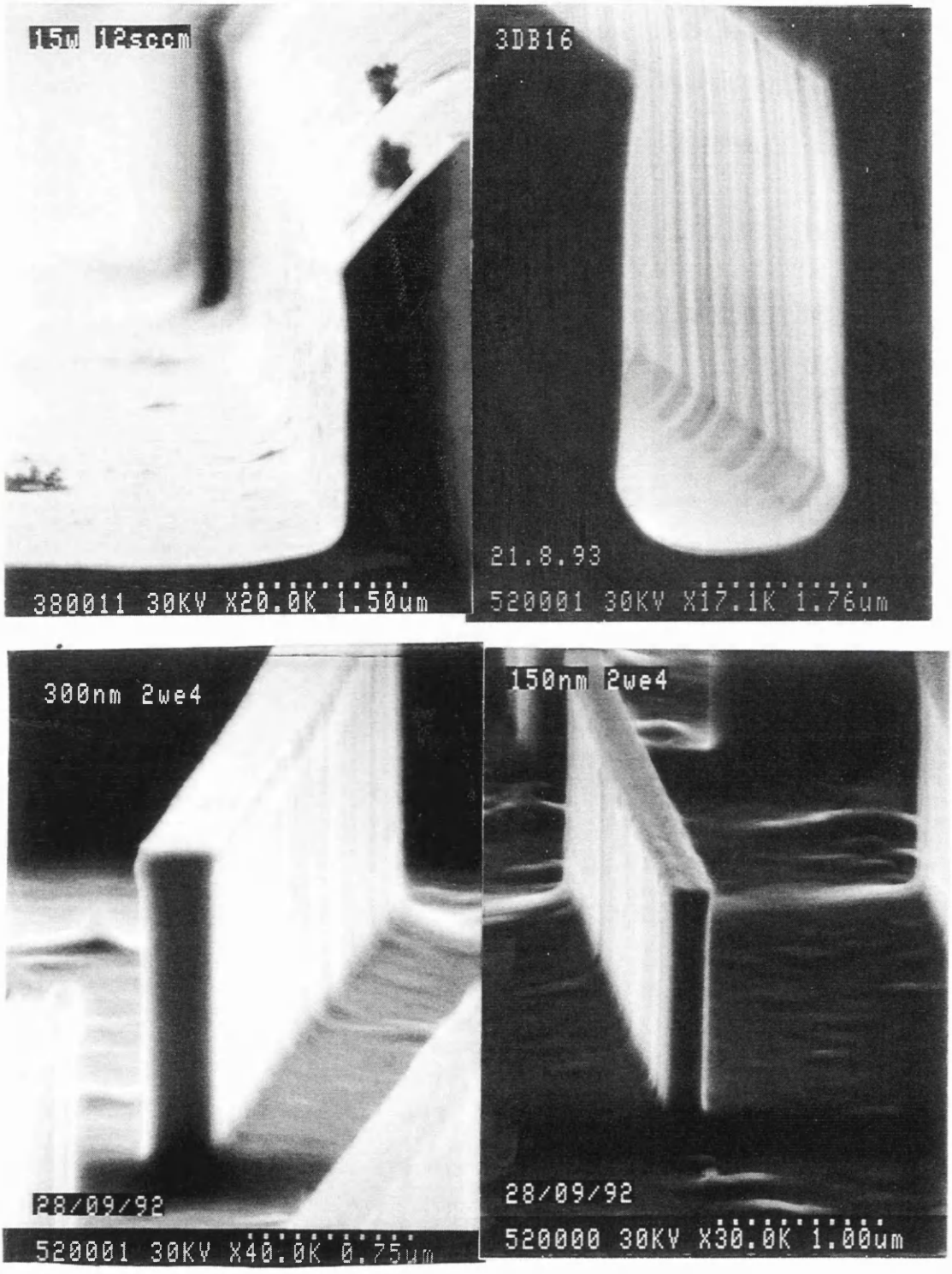

Fig.4.13: SEM micrographs of GaAs trenches and ribs etched in $SiCl_4$ plasma at 15 W, 45-70 V bias, pressures of 8-9 mtorr and at various flow rates. (a) top left, 12 sccm, (b) top right, 15 sccm, (c) bottom left, 6 sccm and (d) bottom right, 4 sccm.

4.4.4 The optimized etching conditions

It is clearly desirable to select etching parameters that will achieve high resolution, a vertical profile. An optimized etching conditions were found to be: a flow rate of 4-6 sccm, a pressure of 8-9 mtorr and powers of 10-15 W at biases of 40-70 V. To test these parameters, a variety of nanostructures were etched, as shown in the SEM micrographs of fig.4.14 and fig.4.15, where ribs 60-70 nm wide etched to a depth of 1.45 μm, gratings 50-60 nm line width and a 120 nm spacing etched to a depth of 0.7 μm and laser-like rings some of them with 40 nm wall thicknesses. It can seen that hese nanostructures have been etched with excellent verticality, smooth surfaces and some of them with a very high aspect ratio of an order of ≥ 20:1 all at low levels of power and low dc bias.

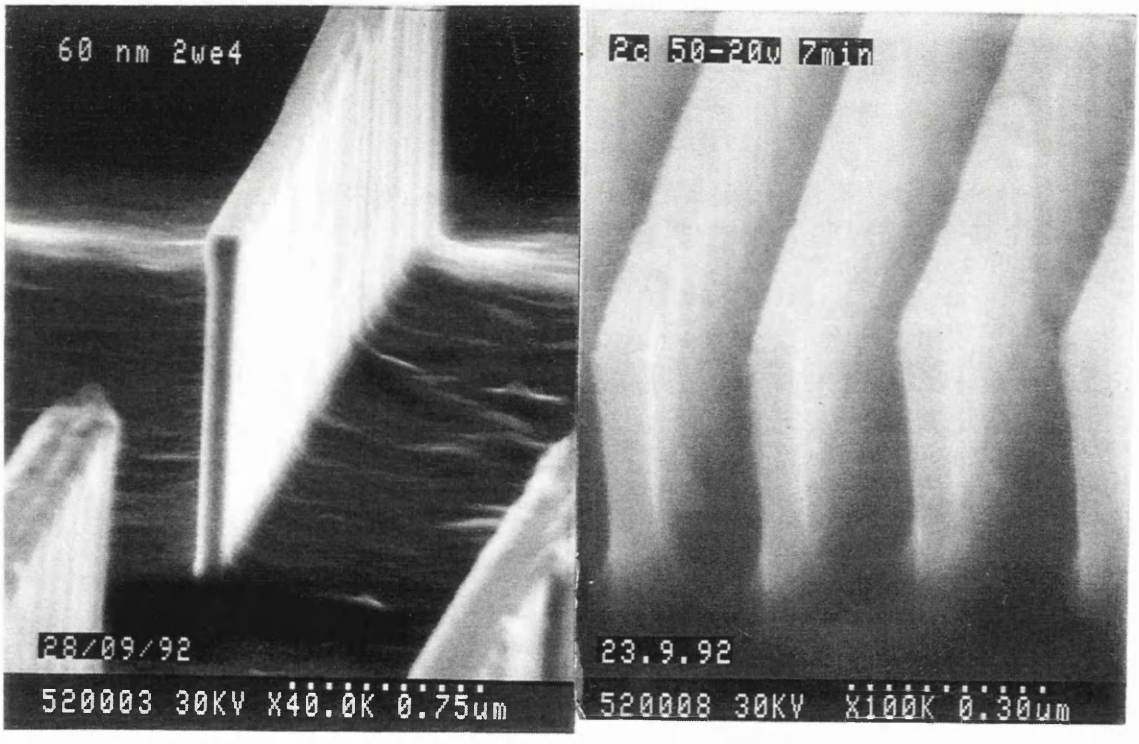

(a) **(b)**

Fig.4.14: SEM micrographs of GaAs nanostructures etched in $SiCl_4$ plasma. (a); ribs 60-70 nm wide etched to a depth of 1.45 μm (aspect ratio ≥20:1) using the optimized conditions: power of 15 W, bias of 70-45 V, flow rate of 6 sccm, pressure of 8 mtorr resulting in etch rate of 110 nm/min. (b); Gratings, 50-60 nm line width and 120 nm spacing etched to a depth of 420 nm using the optimized conditions as in (a) but with a flow rate of 4 sccm resulting in an etch rate of 70 nm/min.

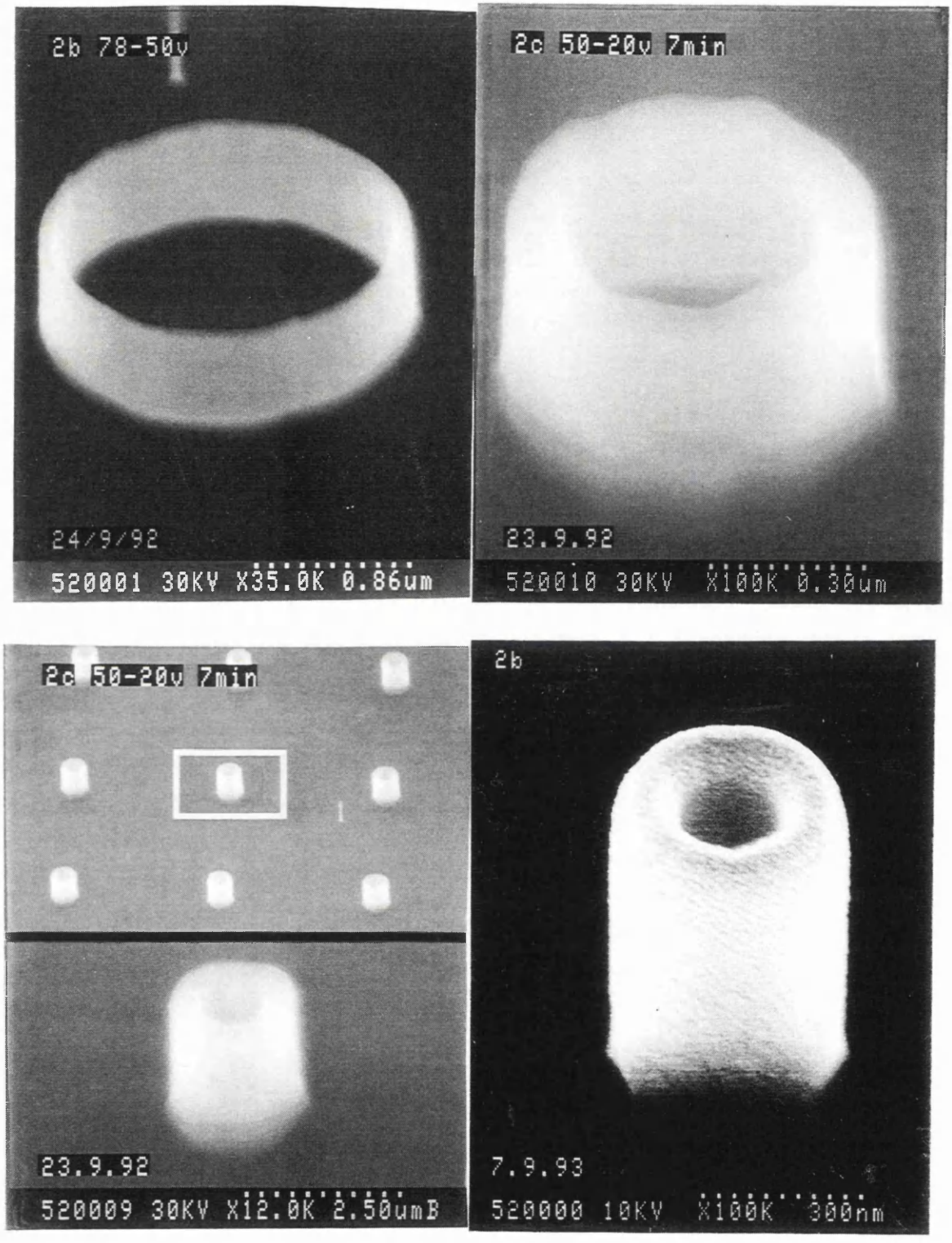

Fig.4.15: laser-like rings of GaAs etched in $SiCl_4$ plasma using the optimized conditions. (a) top left etched to a depth of 0.75 μm, (b) top right, (c) and (d) bottom left and right: Cylinders of different sizes etched to a depth of 0.45 μm at an etch rate of 65 nm/min with 4 sccm flow rate.

4.5 The effect of the chamber contamination on the anisotropy and smoothness

We discussed in section 4.3.3 the effect of the chamber cleaning with successive H_2 and O_2 plasmas on the etch rates of GaAs at various powers. It was shown that the etch rates at low powers are higher by as much as an order of magnitude in the RIE machine with cleaning than in an RIE machine with no cleaning. It has also been shown that anisotropic profiles and smooth surfaces can be obtained at low powers when using the optimized conditions with regular cleaning of the chamber. However if the chamber is not cleaned regularly very different etching characteristics are obtained. The surfaces are very grassy, the amount of grass increases with time which makes it very difficult to obtain anisotropic profiles. This is shown in the SEM micrographs of fig.4.16. The etching parameters used are the optimized etching conditions as in figures 4.14 and 4.15: power of 15 W, flow rate of 6 sccm and at pressure of 9 mtorr. The reasons for this big change in the etching characteristics are mainly the contamination from the discharge itself through the deposition of involatile compounds as discussed in the beginning of this chapter.

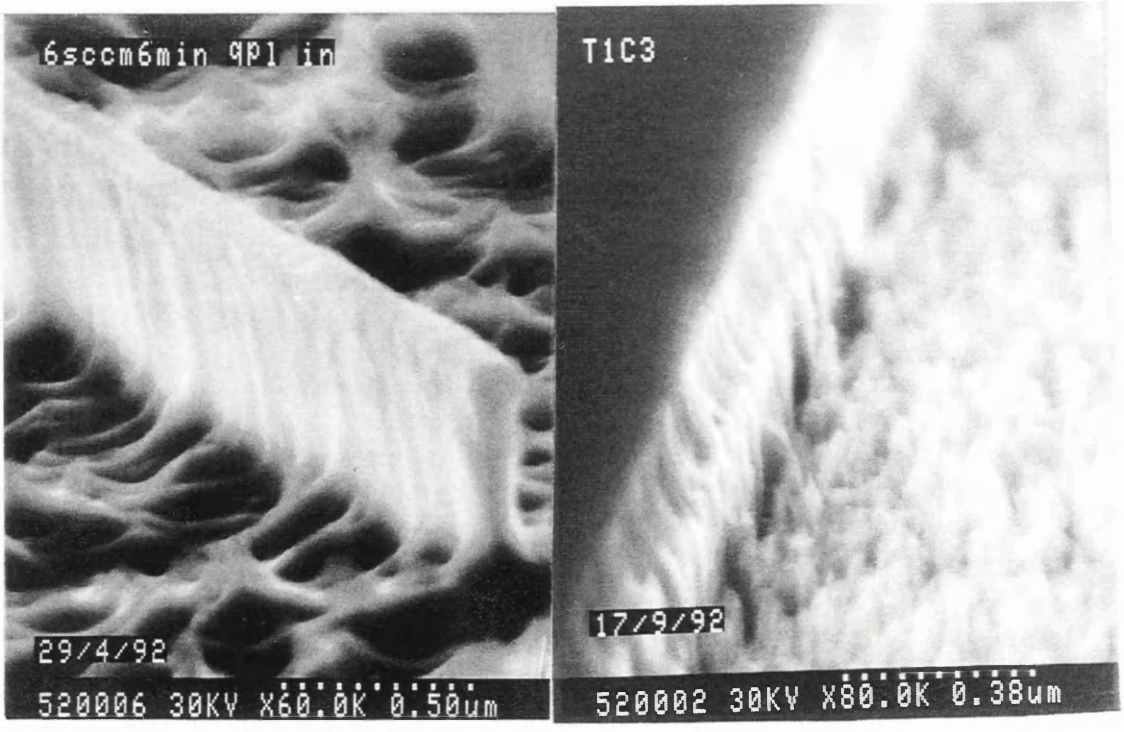

Fig.4.16: SEM micrographs etched in $SiCl_4$ plasma using the optimized conditions, however with no chamber cleaning. The picture on the left shows the effect on the anisotropy and on right shows the effect of grass on the smoothness of the surface. (to be compared with figures 4.14 and 4.15)

4.6 The effect of the lower electrode material on the etching in $SiCl_4$

The effect of different lower electrode materials on the etching characteristics was studied by covering the electrode with glass, quartz, hard anodized aluminium and unanodized aluminium electrode. However the top electrode was not changed which was hard anodized aluminium. The etch rates were found insensitive to change in the lower electrode material from glass, quartz to hard anodized aluminium. By contrast, when an unanodized aluminium was used the etch rates dropped by more than 30-40 %. The fall in the etch rates with an aluminium electrode is likely to be caused by the formation of $AlCl_x$ from etching the electrode which loads the etching. Whereas hard anodized aluminium, glass or quartz do not etch in $SiCl_4$ so there is a little on the etch rate. On the other hand, the effect of electrode material on the formation of grass on the etched surfaces or the smoothness of the surfaces was found to be very sensitive to electrode material. Etching with a bare aluminium electrode was found to be worse of all, the surface being very grassy. The use of a hard anodized aluminium improves the situation but not much as shown in the SEM micrographs of fig.4.17. Generally less grass was found when the electrode was covered with glass, however the surface has some roughness. Covering the electrode with a quartz plate was found to be best, the formation of grass was almost eliminated, as shown in the SEM micrographs of the last section (for example see figs. 4.14, 4.15)

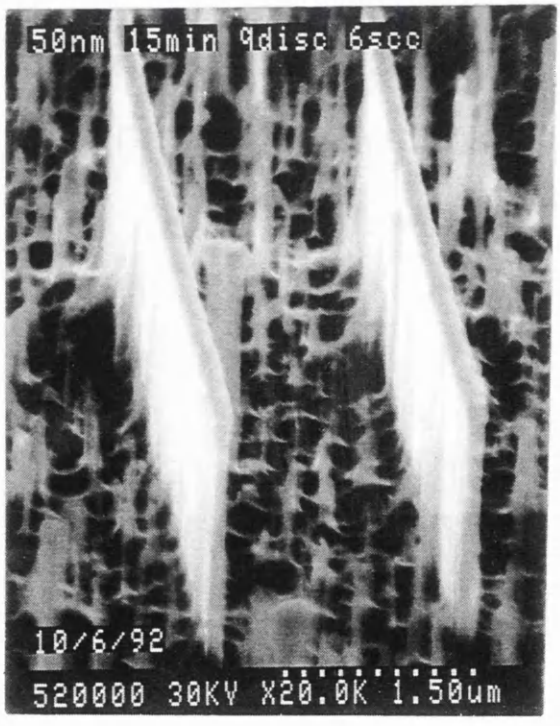

Fig.4.17: SEM micrographs of ribs etched in $SiCl_4$ under the optimized condition but on a bare hard anodized aluminium electrode, which shows that the surface can be covered with a dense grass.

4.7 Chapter discussions and conclusions

In this chapter the possible sources of contamination in RIE processes using $SiCl_4$ plasma have been identified. A procedure for cleaning the etching chamber was developed which ensures that the plasma instabilities at low powers are avoided. This opened up the possibility of developing a Reactive Ion Etching process using $SiCl_4$ plasma at very low levels of rf power (10-15) W and hence low dc bias (20-50) V while maintaining the integrity of etching (i.e. anisotropy, smooth surfaces, low damage etching, etc.). This cleaning procedure relies on treating the chamber with a H_2 plasma followed by an O_2 plasma. Optical Emission Spectroscopic analysis given in this chapter showed that chamber treatment with H_2 plasma leads to formation of volatile species of hydrogenated chlorosilicons and HCl, thus removing earlier chlorosilicon deposits from the chamber. However, a further treatment of the chamber with O_2 plasma was required to remove the residual H_2 in the chamber which was observed to affect the reproducibility of etching. The results of GaAs etch rate as a function of rf power clearly showed that there is a close correlation between the concentration of atomic Cl in the excited state, the type of ions in the plasma on one side and the mechanism of etching on the other side. As a result the etching proceeds with a different mechanism depending on the type of ions in the plasma. Consequently, two mechanisms of etching were identified. The first mechanism occurs at rf power of (5-20) W "the low power regime" in which the etch rate depends on the concentration of Cl_2^+ ions as well as Cl atoms. The second mechanism is in the power range of (25-150) W "the high power regime". In this regime the etch rate depends on the concentration of Cl^+ ions and Cl atoms.

In this chapter a comprehensive analysis of low power RIE of GaAs in $SiCl_4$ plasma was described. The results showed that the etch rate of GaAs can be as high as 300 nm/min at very low rf power of (10-15) W, (0.033-0.066 W/cm^2) and with a low bias of 20-50 V. However, the etch rate decreases dramatically to below 20 nm/min if no chamber cleaning is used which again emphasises the significance of chamber cleaning. The results of GaAs etch rate as a function of $SiCl_4$ flow rate and pressure at low rf power of 15 W, showed that the etch rate passes through a maximum at a pressure to flow rate ratio of approximately 2:1 (mtorr : sccm). The drop in the etch rate at higher pressure is attributed to the increase in the formation of less volatile species in the plasma such as $SiCl_2$. On the other hand, GaAs etch rate as a function of time at low power of 15 W, showed that the etching is nonlinear in the first 1-4 minutes due to continuous formation of oxide on the GaAs surface. This was ascribed to the low density of the reactive molecules in the discharge at such low level of power. This low density of reactive species makes the initial residual O_2 and water vapour very significant and therefore the plasma takes a longer time (more than 1-4 min depending on the flow rate and the pressure) to reduce their effect on the etch rate. Moreover, the induction time at low rf power of 10-15 W can be as high as 50-60 seconds for low pressures and was found to decrease with increasing flow rate.

The variation of etch profile of GaAs with pressure and $SiCl_4$ flow rate at low power of 10-15 W was studied extensively in this chapter. The results showed that at high pressures of ≥ 30 mtorr, crystallographic etching with rough surfaces are obtained, whereas below 20 mtorr no crystallographic etching occurs and the surfaces are smoother. Vertical etching and smooth surfaces are obtained at low pressures of 8-12 mtorr. To achieve a high resolution, vertical profile and smooth etching while using very low rf power and bias, optimised etching conditions were found to be a pressure of 8-10 mtorr, flow rates of 4-6 sccm at 10-15 W power and 40-70 V dc bias. Using the optimized etching conditions, a variety of nanostructures 50-70 nm wide were etched to a depth of 1.45 μm with vertical sidewalls and smooth surfaces.

4.8 References

4.1. R. H. Burton, R. A. Gottscho and G. Smolinsky, Dry Etching for Microelectronics, Edited by R. A. Powell (Elsevier, 1984).

4.2. D. L. Flamm, Plasma Etching, Edited by D. M. Manos and D. L. Flamm, (Academic Press, 1989)

4.3. S. W. Pang, J. Electrochem. Soc., **133**, 784, (1986).

4.4. E. L. Hu, and R. E. Howard, J. Vac. Sci. Technol., B **2**, 85, (1984).

4.5. R. E. Klinger, and J. E. Greene, J. Appl. Phys, **54**, 1595, (1983).

4.6. G. Smolinsky, R. P. H. Chang, and T. M. Magler, J. Vac. Sci. Technol., **18**, 12, (1981).

4.7. E. L. Hu, and R. E. Howard, Appl. Phys. Lett., **37**, 1022, (1980).

4.8. K. L. Seaward, N. J. Moll, D. J. Coulman, and W. F. Stickle, J. Appl. Phys., **61**, 2358, (1987).

4.9. R. E. Klinger, and J. E. Greene, Appl. Phys. Lett., **38**, 620, (1981).

4.10. S. J. Sonek, and J. M. Ballantyne, J. Vac. Sci. Technol., B **2**, 653, (1984).

4.11. A. Scherer, H. G. Craighead, and E. D. Deebe, J. Vac. Sci. Technol., B **5**, 1599, (1987).

4.12. S. Saliman, C. B. Copper, III, J. Electrochem. Soc., **136**, 2420, (1989).

4.13. R. A. Gottscho, G. Smolinsky, and R. H. Burton, J. Appl. Phys., **53**, 5908, (1982).

4.14. M. Sato, and H. Nakamura, J. Vac. Sci. Technol., **20**, 186, (1982).

4.15. M. B. Stern, and P. F. Liao, J. Vac. Sci. Technol., B **1**, 1053, (1983).

4.16. M. B. Stern, H. G. Craighead, P. F. Liao, and P. M. Mankiewich, Appl. Phys. Lett., **45**, 410, (1984).

4.17. S. J. Pearton, U. K. Chakrabarti, W. S. Hobson, and A. P. Kinsella, J. Vac. Sci. Technol., B **8**, 607, (1990).

4.18. M. Rahman, N. P. Johnson, M. A. Foad, A. R. Long, M. C. Holland, and C. D. W. Wilkinson, Appl. Phys. Lett., **61**, 2335, (1992).

4.19. R. Cheung, S. Thoms, M. Watt, M. A. Foad, C. M. Sotomayor-Torres, C. D. W. Wilkinson, U. J. Cox, R. A. Cowley, C. Dunscombe, and R. H. Williams, Semicond. Sci. Technol., **7**, 1189, (1992).

4.20. D. Lootens, P. Van Daele, P. Demeester, and P. Clauws, J. Appl. Phys., **70**, 221, (1991).

4.21. M. W. Cole, S. Salimian, C. B. Cooper, H. S. Lee, M. Mutta, Scanning, **14**, 31, (1992).

4.22. M. Rahman, Ph D Thesis, Glasgow University, (1992) unpublished.

4.23. S. J. Pearton, J. Appl. Phys., **53**, 4509, (1982).

4.24. R. Cheung, S. Thoms, I. McIntyre, C. D. W. Wilkinson, and S. P. Beaumont, J. Vac. Sci. Technol., B **6**, 1911, (1988).

4.25. S. J. Pearton, Mat. Res. Soc. Symp. Proc., **216**, 277, (1991) and references therein.

4.26. H. H. Sawin, B. E. Thomson, and A. D. Richardson in "Plasma Processing". The Electrochemical Society Softbound proceedings Series, Pennington, NJ, pp.434-544, (1985). Editors, G. S. Mathad, G. C. Schwartz, and G. Smolinsky.

4.27. K. D. Allen, H. H. Sawin, and A. Yokozeki, J. Electrochem. Soc., **133**, 2331, (1986).

4.28. A. D. Richards and H. H. Sawin, J. Appl. Phys., **62**, 799, (1987).

4.29. G. Smolinsky, R. A. Gottscho, and S. M. Abys, J. Appl. Phys., **54**, 3518, (1983).

4.30. G. C. H. Zau, L. D. Baston, D. C. Gray, I. Tepermeister, H. H. Sawin, and M. T. Mocella, J. Electrochem. Soc., **137**, 3526, (1990).

4.31. E. R. Sirkin, and R. D. Powell, J. Vac. Sci. Technol., B **1**, 74, (1983).

4.32. Y. Matsuzaki, N. Suzuki, and T. Hirayama, Jpn. J. Appl. Phys., **25**, 253, (1987).

4.33. R. J. Contonili, and L. A. D, Asaro, J. Vac. Sci. Technol., B **4**, 706, (1987).

4.34. N. Voddjdani, and P. Parrnes, Vac. Sci. Technol., B **5**, 1591, (1987).

Chapter 5

Selective and Nonselective RIE of GaAs/AlGaAs in $SiCl_4$, $SiCl_4/N_2$, $SiCl_4/O_2$ and $SiCl_4/SiF_4$ Plasmas

5.1 Introduction

Selective RIE techniques simplify the processing of heterostructure devices. In particular, the selective removal of GaAs over AlGaAs has received great interest for gate recessing in MESFET and HEMTs fabrication.[1] Selective RIE of GaAs over AlGaAs in CCl_2F_2 - based plasmas [2-5], $SiCl_4/SiF_4$ [6-8] and $SiCl_4/SF_6$ [9,10] has been reported. In these processes, etching ceases when a nonvolatile layer of AlF_3 is formed. However, the formation of such a layer requires the use of relatively high pressures and low dc biases which result in isotropic profiles. On the other hand, nonselective or equi-etch rate etching of GaAs/AlGaAs is important for the fabrication of optoelectronic devices such as laser facets.

In chapter 4, we studied the etching characteristics of GaAs in $SiCl_4$ plasma in detail. In this chapter, the characteristics of the AlGaAs etching in $SiCl_4$ plasma are given with special emphasis on the selective and nonselective etching of GaAs over AlGaAs and the etching parameters that control the degree of selectivity.

New selective and anisotropic RIE processes for etching GaAs/AlGaAs in pure $SiCl_4$ and $SiCl_4/N_2$ plasmas have been developed which can stop on an extremely thin AlGaAs layer (1.13 nm; 4 monolayers). The selectivities obtained can virtually reach infinity. Moreover, new mechanisms for selectivity are suggested, which rely on the formation of Aluminium oxide, Silicon and Aluminium nitrides for the etching to stop on a very thin AlGaAs layer.

Selective RIE etching of GaAs/AlGaAs utilizing a mixture of $SiCl_4/SiF_4$ has been reported by many authors [6-8], however the selectivities obtained are $\leq 350:1$ which are not as high as the in case of CCl_2F_2 [2-5] plasmas. In an attempt to improve the selectivity of etching GaAs/AlGaAs in $SiCl_4/SiF_4$ plasma. Selective etching of GaAs/AlGaAs in a mixture of $SiCl_4/SiF_4$ has also been studied. Optical Emission Spectroscopy of $SiCl_4/SiF_4$ plasma has been studied to investigate the relative concentration of the various species and their effect on the selectivity at various etching parameters.

T-gate recesses in MESFET and HEMT's material using the selective processes in pure $SiCl_4$ and $SiCl_4/SiF_4$ have been performed. The resulting gate profiles from these processes are compared. The advantages of having a more controllable gate profile are discussed.

5.2 Experimental

All the etching was performed in an Oxford Plasma Technology RIE80 machine which has been described in previous chapters. The etching chamber is usually pumped down to a base pressure of 4-5 mtorr. All the material used here was grown by MBE on semi-insulating (100) GaAs substrates. The measurements of the AlGaAs etch rates were made (using a Talystep) on 2 μm thick $Al_{0.3}Ga_{0.7}As$ layer capped with a 10 nm GaAs layer. The capping layer eliminates the problem of oxide growth on air exposed AlGaAs surfaces and insures that the same initial surface is presented to the RIE system on each occasion. The etch rate of AlAs was measured using multiple quantum well material which consisted of 20 periods of GaAs/AlAs with thickness of 54/74 nm giving a total thickness of [20 x 128] nm. The etch rate of AlAs was worked out after subtracting the etch rate of GaAs which was measured on a separate GaAs sample with identical masking patterns etched on the same run . The selectivities were measured by simultaneously etching GaAs, AlGaAs and GaAs/AlAs and comparing the resulting etch rates. In case of small flow rates a mass flow controller of 0-1 sccm full scale (N_2 calibrated) was used. The surface quality and the anisotropy of AlGaAs was obtained using a Hitachi (S800, S900) Scanning Electron Microscopes (SEM). The small patterns were defined using electron-beam lithography and the large patterns were defined using standard photolithography. NiCr was used as an etch mask. The method used for the definition of the T-shaped gate is given later in the chapter.

5.3 $Al_xGa_{1-x}As$ etching in pure $SiCl_4$ plasma

When $Al_xGa_{1-x}As$ is etched in $SiCl_4$ plasma (at high dc biases ≥ 300 V)[11-13], both GaAs and AlGaAs are etched at the same rate and anisotropic profiles are obtained. As mentioned in chapter 3, (at these biases) considerable damage is inflicted on the etched material. As we are concerned with low damage etching, the etching characteristics of AlGaAs have been extensively studied under low power and bias conditions while using the same cleaning procedure carried out with GaAs etching as discussed in chapter 3. First we will examine the AlGaAs and AlAs etch rates as a function of power and then describe the characteristics of the etching as a function of the $SiCl_4$ flow rate and the pressure.

5.3.1 $Al_{0.3}Ga_{0.7}As$ and AlAs etch rates as a function of rf power

The etch rates of both AlGaAs and AlAs as a function of power have been studied in the power range of 5-150 W at constant flow rate and pressure. The etch rates of $Al_{0.3}Ga_{0.7}As$, AlAs, the Cl emission at 837.6 nm and the etch rate of GaAs for comparison as a function of rf power are given in fig.5.1. The etching was carried out at constant flow rate and pressure of 12 sccm and 15 mtorr respectively. The etch rate dependence of GaAs on rf power has been discussed in chapter 3. In the low power regime

(5-20 W), in contrast to GaAs etch rate behaviour, the AlGaAs and AlAs etch rates do not follow the same trend as the emission from atomic Cl . This suggest that the AlGaAs and AlAs etching is more dependent on the dc bias than the GaAs.

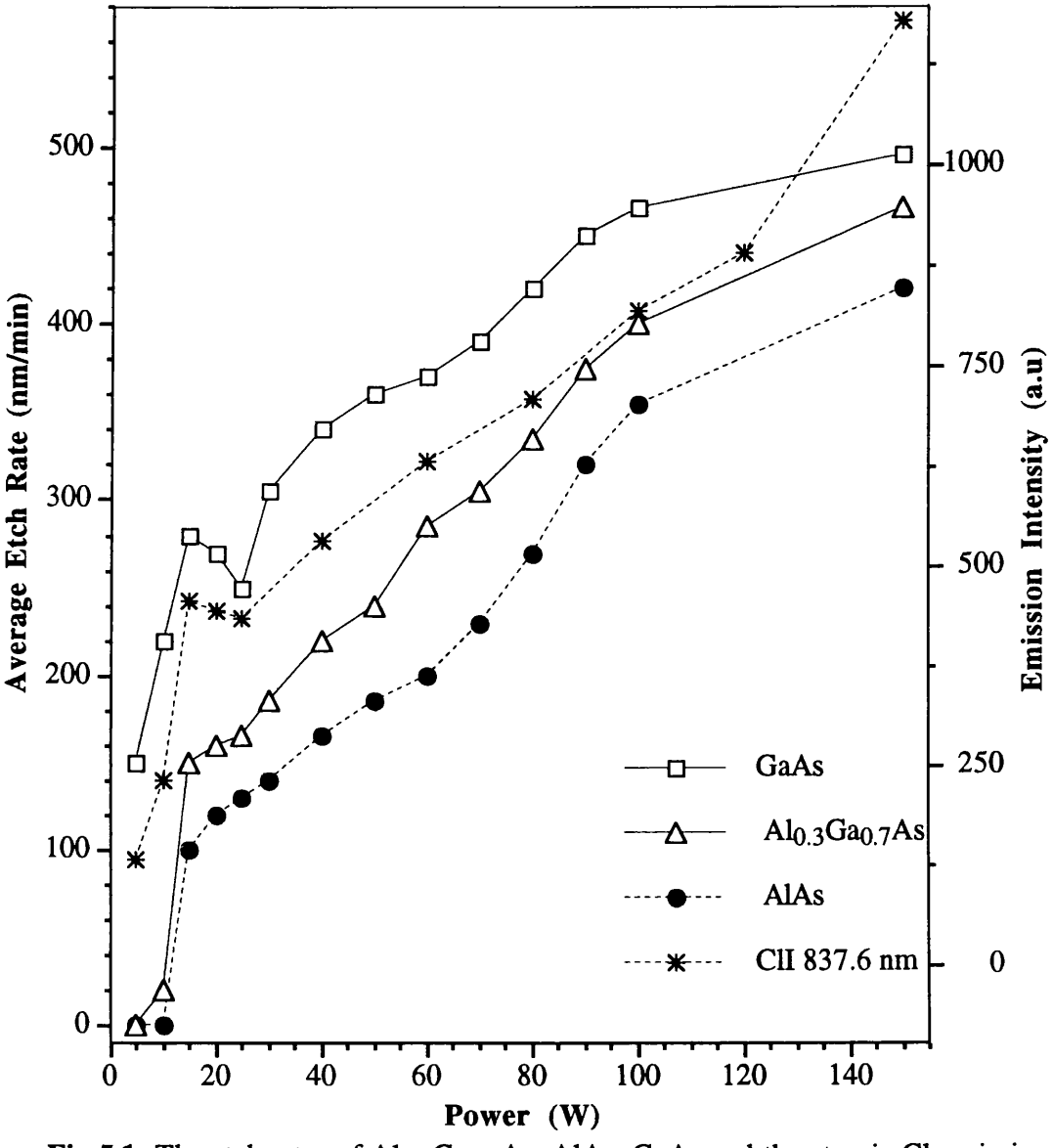

Fig.5.1: The etch rates of $Al_{0.3}Ga_{0.7}As$, AlAs, GaAs and the atomic Cl emission at 837.6 nm in $SiCl_4$ plasma as a function of rf power at constant flow rate and pressure of 12 sccm and 15 mtorr respectively.

Moreover the etch rates of AlGaAs and AlAs at 5-10 W are very low, being lower for the latter in which they are less than 1 nm/min for AlGaAs and almost (zero) for AlAs. This very low rate of etching especially for AlAs suggest that ions do not have sufficient energy or the minimum energy to initiate the etching of aluminium oxide which forms on the surface of AlAs. The aluminium oxide is thought to be formed from the residual oxygen, air or water vapour in the chamber. Increasing the rf powers ≥ 15 W, the etch rates of

AlGaAs and AlAs increase rapidly with power increase and nonselective etching of GaAs/AlAs with almost equi-rate etching is easily obtained.

5.3.2 The effects of the pressure and the flow rate on AlGaAs and AlAs etch rates at low power

The effects of the pressure and the flow rate on the etch rates of $Al_{0.3}Ga_{0.7}As$ and AlAs have been studied under low power condition of 15 W, in the pressure and flow rate ranges of 9-35 mtorr and 2-15 sccm respectively. The resulting dc biases fell in the range of 70-30 V. The etch rates of $Al_{0.3}Ga_{0.7}As$ as a function of the pressure for five values of the flow rate and at constant rf power of 15 W are shown in fig.5.2.

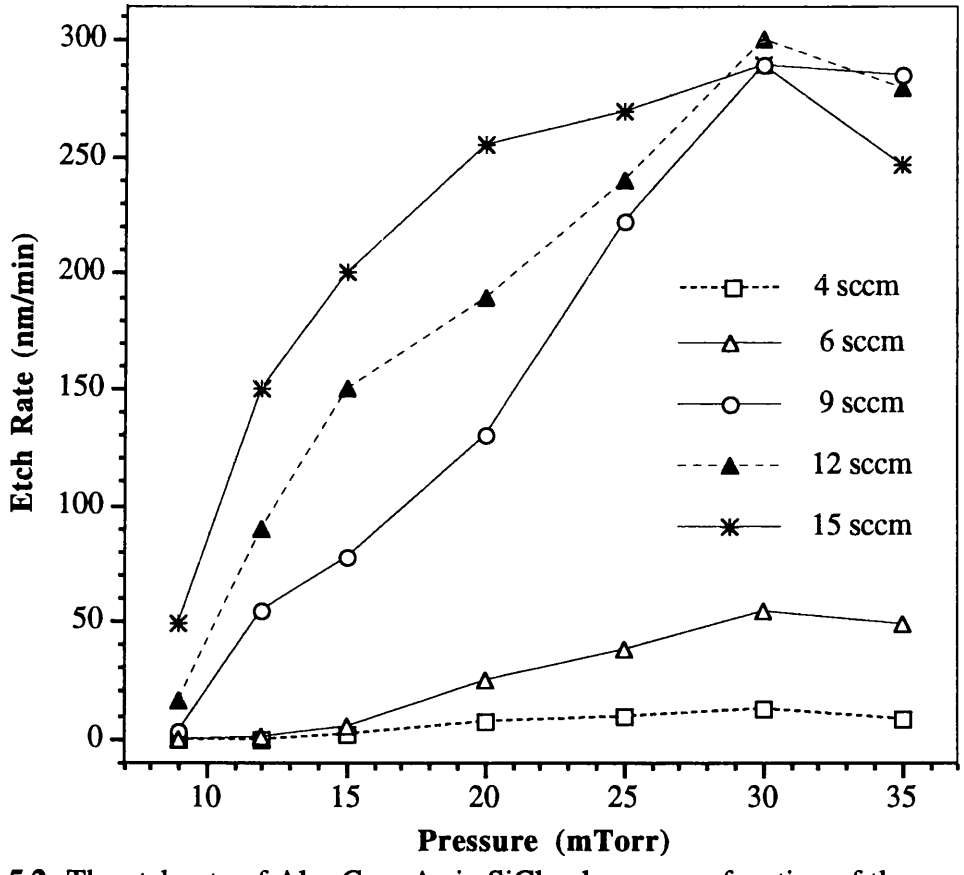

Fig.5.2: The etch rate of $Al_{0.3}Ga_{0.7}As$ in $SiCl_4$ plasma as a function of the pressure for five values of the gas flow rate; 4 -15 sccm. The etching was performed at constant rf power of 15 W and the resulting dc biases fell in the range of 70 - 30 V.

It is clear from fig.5.2 that the etch rate of AlGaAs increases with both the pressure and the flow rate. In the pressure range 9-12 mtorr and with 4-6 sccm flow rate the etch rate is almost (zero), then it increases slowly with increasing pressure. Keeping the pressure in the range of 9-12 mtorr while increasing the flow rate ≥ 12 sccm, the etch rate increases

considerably and it continues to increase with increasing pressure until it levels off at a pressure of about 30 mtorr and then it begins to fall with further increase in the pressure. The increase in the etch rate with pressure at high flow rates may be attributed to increase in the amount of Cl supplied to the surface. However, this does not explain the very low or nonetching behaviour at low flow rates and still at high pressures. One of the ideas to explain this behaviour, is that at low flow rates, the amount of Cl available is not sufficient to initiate the surface oxide etching thus inhibiting the etching.

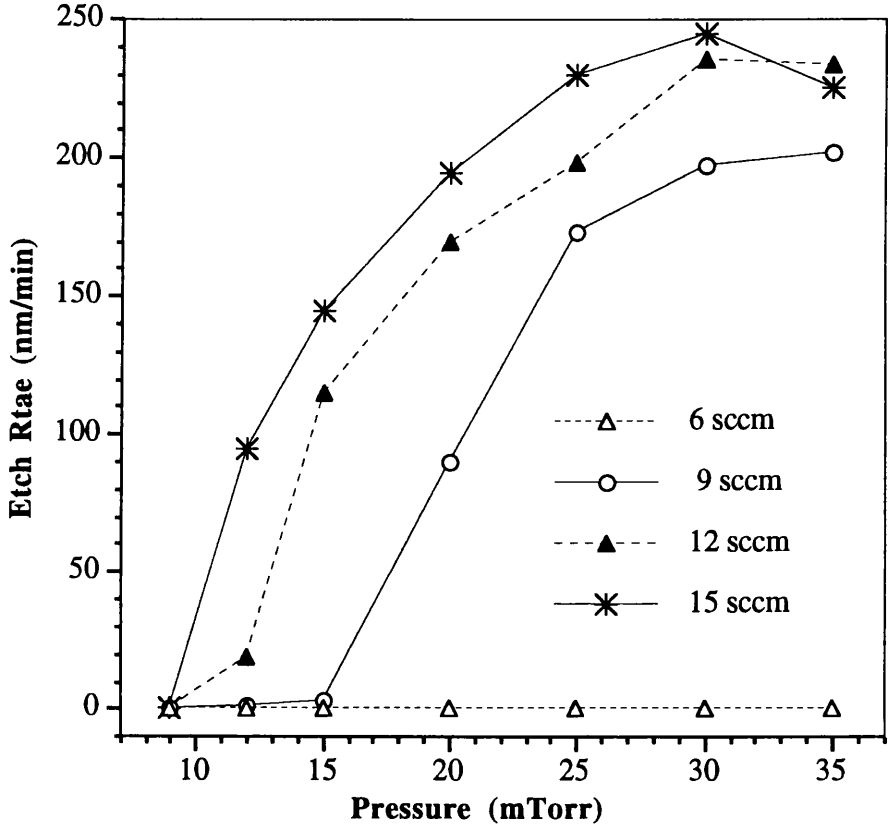

Fig.5.3: AlAs etch rate in $SiCl_4$ plasma a function of the pressure for four values of the flow rate (6, 9,12, 15) sccm. The etching is carried out at constant rf power of 15 W and the dc biases fell in the range of 70 - 30 V.

The etch rate of AlAs as a function of the pressure for four values of the $SiCl_4$ flow rate and at constant power of 15 W is shown in fig.5.3. As in the case of the AlGaAs the etch rate of AlAs has a similar dependence on the pressure and the flow rate except that it can not be etched at pressures lower than 12 mtorr and it also cannot be etched at flow rate lower than 9 sccm. This behaviour may be ascribed to the fact that the AlAs can form an oxide layer more rapidly and possibly of greater thickness than $Al_{0.3}Ga_{0.7}As$. Therefore it seems that the formation of Aluminium oxide from residual oxygen or water vapour is the limiting factor for AlGaAs etching at low powers. The residual O_2 is likely to be due to the cleaning the chamber with H_2 and O_2 plasmas before the etching which are essential for the plasma to be sustained at low powers.

5.4 Development of a selective and an anisotropic RIE of GaAs/AlGaAs in $SiCl_4$ plasma

Most of the selective RIE processes of GaAs//AlGaAs reported in the literature [2-9,14,31] have used some form of fluorinated compounds in addition to the Cl containing gases so that the fluorine reacts with Al to form an etch stop layer of AlF_3. However the formation of such a layer is not effective unless high pressures are used at relatively low biases which results in isotropic profiles and lateral etching which is difficult to control. The formation of involatile etch stop layers other than AlF_3 seem to have been over looked by most workers. For example any form of aluminium oxide Al_xO_y or any form of aluminium nitride Al_xN_y is nonvolatile and may be used as an etch stop [15]. Hu et. al.[16] have reported the use of Cl_2/O_2 mixture for selective etching of GaAs/AlGaAs, however the selectivities were an order of magnitude smaller than in the fluorine containing gases. The reasons for poor selectivities is the reduction in both GaAs and AlGaAs etching rates due to the addition of O_2 which oxidizes all the etchants and surfaces. Around the time of publication of this work, Agrawala, et.al.[17] has reported the use of HBr plasma for selective etching of InGaAs/AlInAs material systems in which the selectivity depends on the formation of Al_2O_3 from residual O_2 or water vapour in the chamber.

In the last two sections we have shown that the etch rates of AlGaAs or AlAs are either very low or the etching stops at low powers, low pressures and low flow rates. On the other hand, under these conditions of power, pressure and flow rate we have shown in chapter 4 that high etch rates can be obtained for GaAs etching. Therefore a selective etching for GaAs/AlGaAs is possible under these discharge conditions. To optimize the selectivities, first we will examine the selectivity as a function of power at high flow rates and pressures and at low flow rates and pressures, then we will study the effect of the flow rate and the pressure on selectivities at constant and low power.

5.4.1. Effect of rf power on GaAs/AlGaAs selectivity

The effect of rf power on selective etching of GaAs/AlGaAs or GaAs/AlAs has been studied in the power range of 5-150 W for two values of pressure and flow rate; 9 mtorr using 6 sccm and 15 mtorr using 12 sccm. The selectivities were measured by taking the ratio of the etch rates of GaAs/AlGaAs or GaAs/AlAs. As shown in fig.5.4, the selectivities are very high at low powers as expected and the etching is nonselective at high powers. However the range of power for which high selectivities are obtained depends on the pressure and on the flow rate. At pressure of 15 mtorr and flow rate of 12 sccm, the selectivities are high in the power range of 5-10 W only. For flow of 6 sccm and pressure of 9 mtorr the selectivities are high in a wider range of power; 5-20 W. Therefore there are two regimes of GaAs/AlGaAs etching, the first is selective and the other is nonselective with respect to AlGaAs, depending on the pressure and the flow rate. This behaviour may be explained by the density of the etchants compared to that of residual O_2 or air in the

chamber and by the ion energies in each regime. In the first regime, the etching is selective up to a power of about 20 W, because of the low flow rate and low pressure, the density of etching species is so low that a very small O_2 or air residuals can stop the surface reaction by oxidation and as Al_2O_3 is not volatile, the etching stops. This happens until such a point (at powers ≥25 W) where the ion energies are high enough to sputter off the thin Aluminium oxide layers which continuously form on the surface and lead to AlGaAs etching.

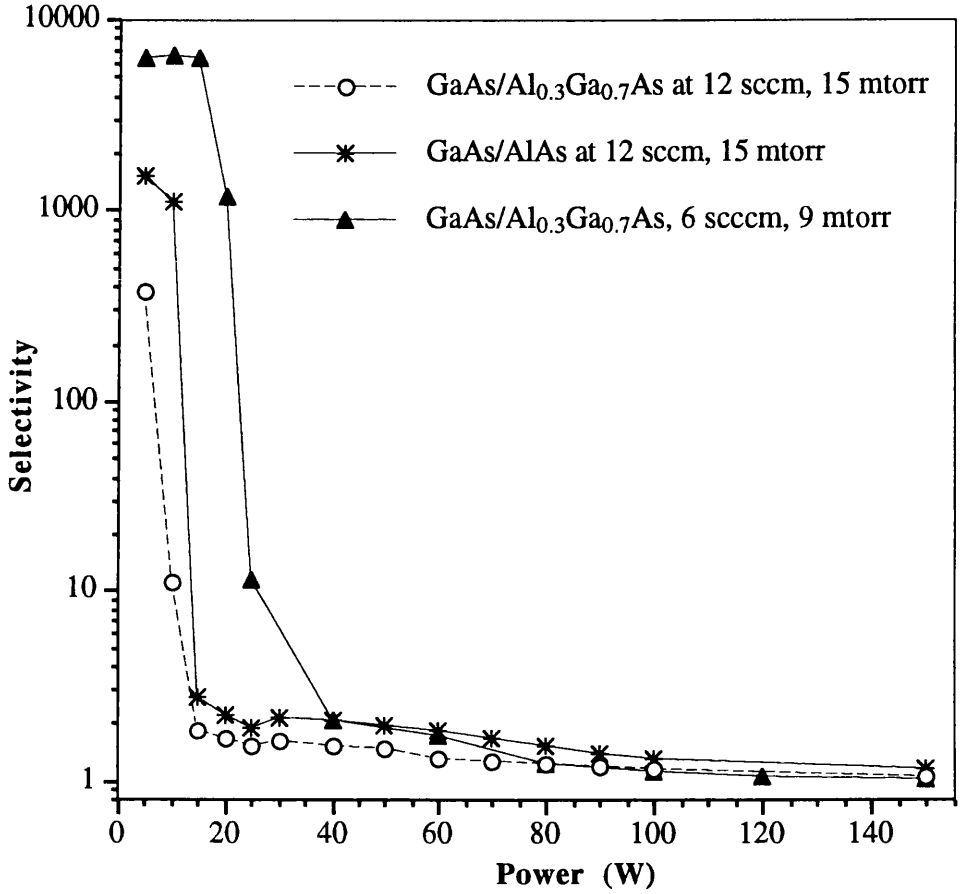

Fig.5.4: The etch rate ratios (the selectivity) of GaAs/$Al_{0.3}Ga_{0.7}$As and GaAs/AlAs in $SiCl_4$ plasma as a function of rf power for two values of flow rate and pressure; 12 sccm at 15 mtorr and 6 sccm at 9 mtorr.

In the second regime "high flow rate and high pressures" the etching is "nonselective" down to power of 10 W. Because of the high pressures and high flow rates, the density of the etching species is higher than in the case of low pressure and low flow rate for the same power. Therefore the etching species will outnumber the microscopic residual O_2 or air molecules which will prevent further oxide formation on the surface after the initial oxide had been etched and will lead to the etching of AlGaAs up to a point or power of ≤10 W where the ion energy and ion density are so low that they are not sufficient to initiate the AlGaAs surface oxide etching. To summarise, the GaAs/AlGaAs is always selective at

powers ≤ 10 W, it is selective only at low pressures and low flow rates for higher powers of 15-20 W and it is nonselective for powers ≥ 25 W regardless of the pressures and flow rates.

5.4.2 Optimization of the GaAs/AlGaAs etching for high selectivity and high anisotropy

In section 4.4.4 we set an optimized etching conditions for GaAs etching to produce anisotropic profiles at low rf power, the optimized conditions were set to 8-9 mtorr pressure and 4-6 sccm flow rate and power of 15 W. Very anisotropic profiles were obtained. In this case to optimize the etching process to achieve high selectivities for etching GaAs/AlGaAs and at the same time produce anisotropic profile, the selectivity changes with pressure and the flow rate were investigated in more detail at a constant rf power of 15 W. In fig.5.5 the selectivity of etching GaAs/AlGaAs as a function of the pressure and the flow rate at constant rf power of 15 W is given.

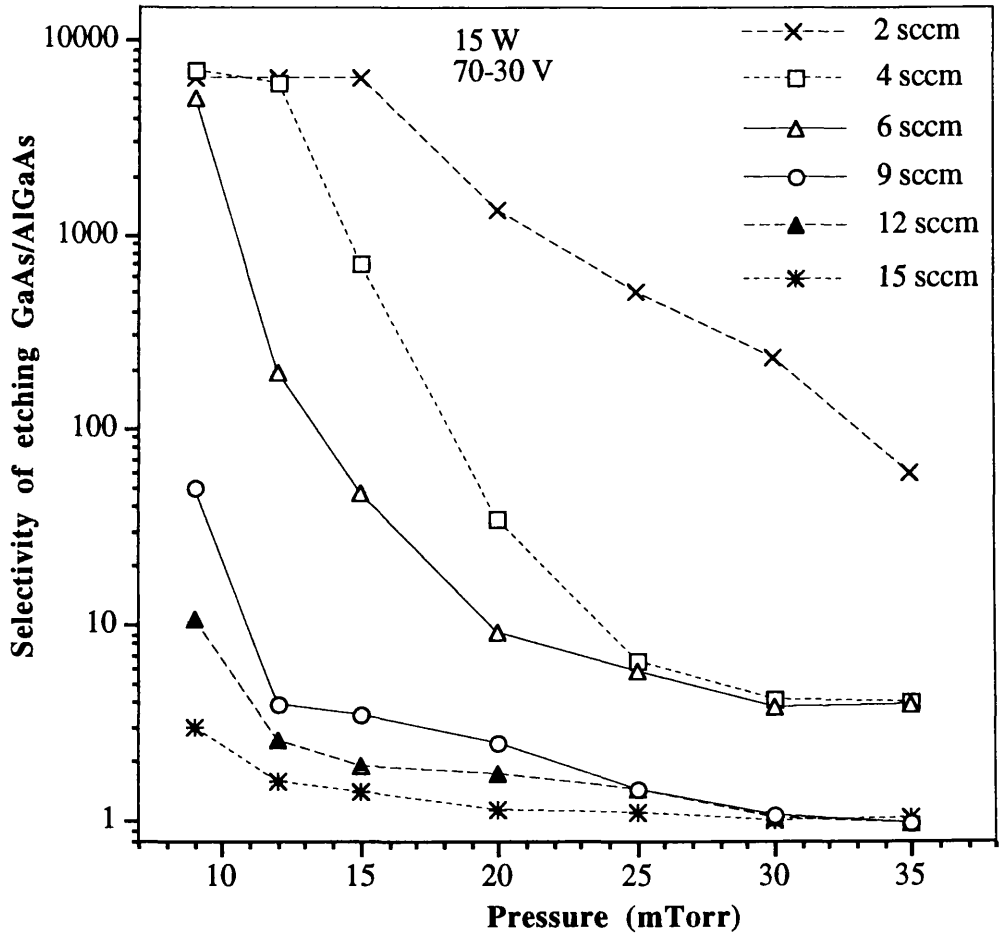

Fig.5.5: Selectivity of etching GaAs/AlGaAs in $SiCl_4$ plasma as a function of pressure for flow rate values of (2, 4, 6, 9, 12 and 15 sccm), all at constant rf power of 15 W and bias range of 35-70 V.

As expected the selectivity is extraordinarily high at 2, 4 and 6 sccm while using 9 mtorr, then decreases rapidly as the pressure increases in the case of 6 and 4 sccm, whereas the selectivity remains very high in case of the 2 sccm and pressures as high as 25 mtorr where selectivities of an order of 500:1 can still be obtained. For flow rates of 9, 12 and 15 sccm and at pressures ≥12 mtorr the maximum obtainable selectivity is about 10:1 compared to a selectivity of ≥ 5000:1 at 2 sccm and 12 mtorr. At pressures above ≥20 mtorr and flow rates of ≥ 9 sccm nonselective etching can be obtained with power of 15 W and bias of 40-60 V. The etch rate ratio of GaAs/AlGaAs is about 1.25:1. Therefore a very high selectivity is obtained at the optimized conditions for anisotropic etching of GaAs which are 4-6 sccm and 9 mtorr and a power of 15 W. To test the selectivity further using these parameters, the etching was carried out on samples consisting of a very thin layer (1.13 nm, 4 monolayers thick) of $Al_{0.3}Ga_{0.7}As$, sandwiched between a 110 nm thick GaAs layer and GaAs substrate. As shown in fig.5.6, the etch was stopped by the very thin AlGaAs layer for as long as 30 minutes. Therefore we have shown that this process is highly selective and yet very anisotropic for GaAs/AlGaAs etching.

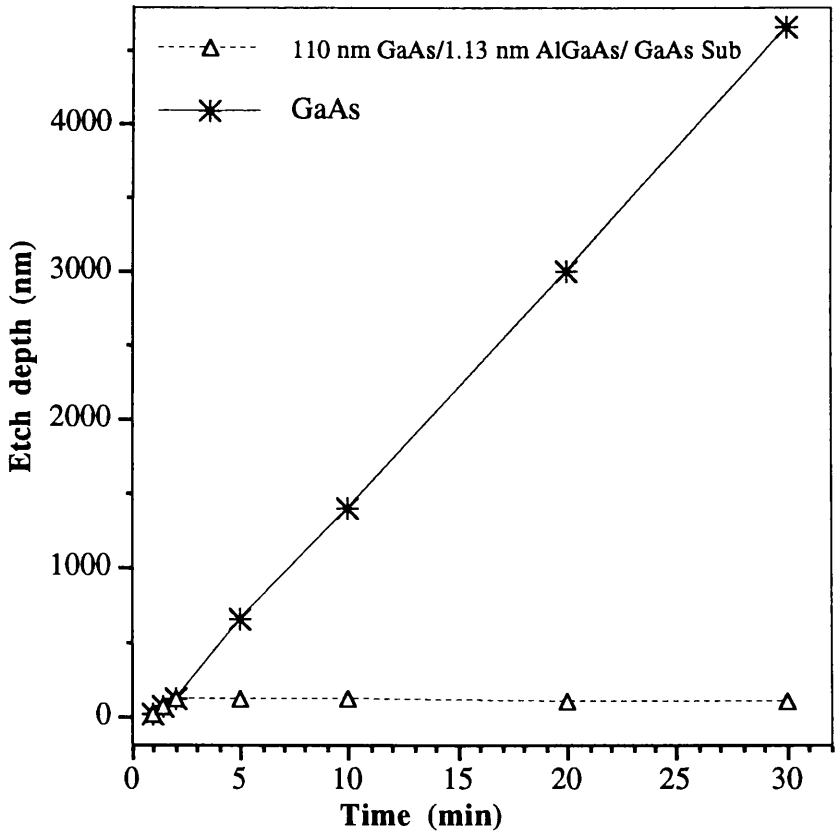

Fig.5.6: The etch depth of a 5 μm thick GaAs layer and 1.13 nm thick $Al_{0.3}Ga_{0.7}As$ layer sandwiched between 110 nm GaAs layer and GaAs substrate as a function of time. The etching is in $SiCl_4$ plasma using the optimized etching conditions.

5.5 Mechanisms of Selectivity

In the last few sections it has been shown that very selective etching of GaAs/AlGaAs is obtained when using low pressures, flow rates and at low powers. The formation of Al_xO_y during the etching was suggested to play a major role in stopping the etching. To investigate this mechanism or any other possible mechanisms responsible for selectivity, N_2 or O_2 was added to $SiCl_4$ at high pressure and at power of 15 W, where the selectivity is normally low. N_2 was added to simulate the effect of the residual air in the chamber on the selectivity, whereas O_2 was added to simulate the effect of the residual O_2 in the chamber on selectivity. Small percentages of N_2, 0.55% to 10% of the total flow were added, whereas the flow rate of $SiCl_4$ was fixed at 9 sccm, the pressure was 30 mtorr and the power of 15 W was used which resulted in a bias of 45-35 V. The etch rates of GaAs, AlGaAs and the selectivities as a function of the percentage of N_2 in the total flow are given in fig.5.7.

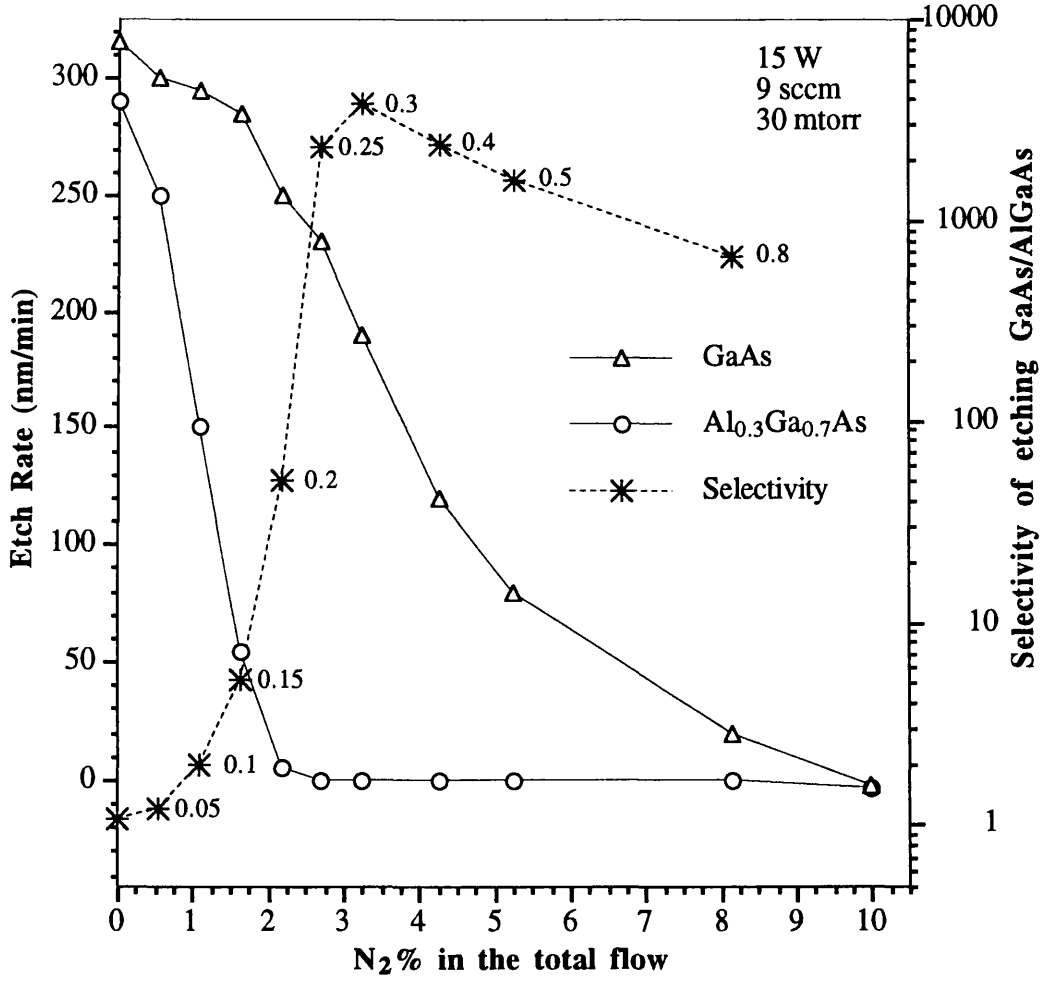

Fig.5.7: The etch rates of GaAs, $Al_{0.3}Ga_{0.7}As$ and the selectivity in $SiCl_4/N_2$ plasma as a function of N_2 percentage in the total flow with corresponding values of N_2 flow rate in sccm plotted. The etching was carried out using rf power of 15 W, $SiCl_4$ flow rate of 9 sccm and pressure of 30 mtorr.

The etch rate of both GaAs and AlGaAs decrease steadily with a very small increase in the N_2 flow. However, the etch rate of AlGaAs decreases much faster than the etch rate of GaAs leading to a very sharp increase in the selectivity. The selectivity increased from a ratio of 1.2:1 without N_2 to ≥ 3500:1 with only 3.2% N_2 added for the same pressure and flow rate of $SiCl_4$. These percentages of N_2 correspond to an increase in the N_2 flow rate from zero to only 0.3 sccm. The etch rate of AlGaAs under these conditions is practically zero, whereas the etch rate of GaAs is about 180-200 nm/min. At a N_2 flow rate of 0.8-1 sccm which corresponds to 8.2-10 % N_2 in the total flow, deposition occurs at a rate of about 0.5-1 nm/min with no etching of either materials. The deposited material is likely to be some form of Si_xN_y as it is evident from the optical emission spectrum of $SiCl_4/N_2$ of fig.3.15 (see chapter 3), where emission lines from SiN could be detected even with N_2 flow rate as small as 0.3 sccm, 3.2% of the total flow.

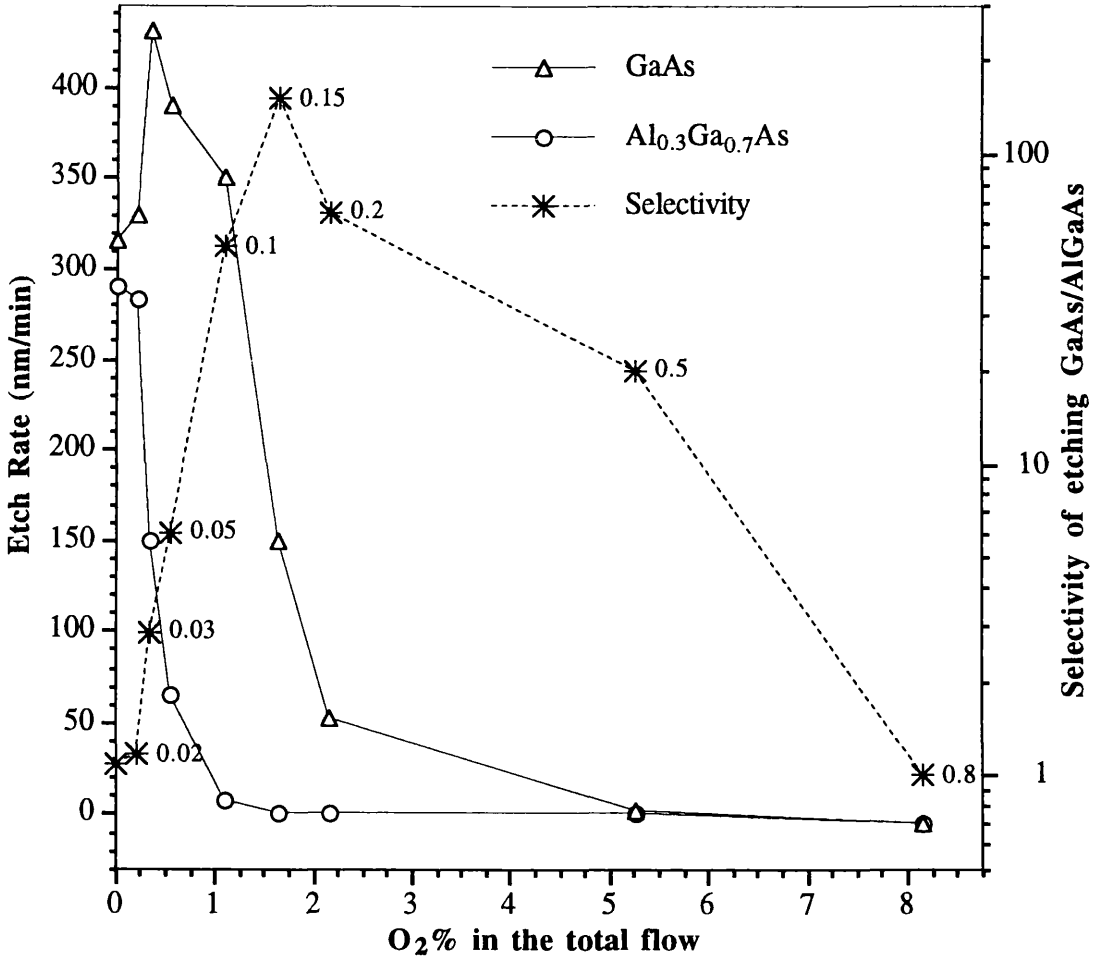

Fig.5.8: The etch rates of GaAs, $Al_{0.3}Ga_{0.7}As$ and the selectivity in $SiCl_4/O_2$ plasma as a function of O_2 percentage in the total flow with corresponding values of O_2 flow rate in sccm plotted. The etching was carried out using rf power of 15 W, $SiCl_4$ flow rate of 9 sccm and pressure of 30 mtorr.

These results suggest that the presence of N_2 in $SiCl_4$ discharge is responsible for the cessation of etching on AlGaAs layer through the formation of an etch stop layer of an involatile nature. Therefore one can only think of these layer being some form of nitrides as most are involatile such as Si_xN_y or Al_xN_y. The formation of SiN has indeed been detected in the emission spectrum of $SiCl_4/N_2$, but the assumption that the presence of SiN in the discharge stops the etching of AlGaAs and not GaAs is difficult to interpret. A possible interpretation is that the adsorption of SiN on the respective surfaces of GaAs and AlGaAs is different and that this adsorption influences the kinetics of surface reaction in such a way that it totally inhibits the reactions on the AlGaAs surface but not on GaAs.

The second mechanism of the etch stop might be through the formation of Al_xN_y layer. In this case the interpretation of the etch stop is similar to the formation of AlF_3 layer in fluorine containing gases, where the AlF_3 layer is formed when the etching encounters the AlGaAs layer and thereby stopping the etching.

The effect of adding O_2 to $SiCl_4$ on the etch rate of GaAs, AlGaAs and on the selectivity was then investigated as shown in Fig.5.8. The pressure and $SiCl_4$ flow rate were kept constant at 30 mtorr and 9 sccm respectively, the O_2 flow rate was increased from 0.025 sccm to 0.8 sccm which corresponds to 0.25% to 8.2% of O_2 in the total flow. The etch rate of GaAs was increased from 315 nm/min to 440 nm/min as the O_2 was increased from zero to 0.1sccm (1.1%), then decreased steadily with further increase in O_2 flow rate. In contrast, the etch rate of AlGaAs decreased immediately even with smallest O_2 addition. However, because of the more rapid reduction of GaAs etch rate with O_2 addition than with the N_2 addition to $SiCl_4$, the selectivities obtained are at least an order of magnitude less than in the case of N_2 addition. The selectivity in this case is due to the formation of an involatile layer of Al_xO_y. The highest selectivity is obtained at O_2 flow rate of 0.15 sccm or 1.64% in the total flow. At O_2 flow rate $\geq$ 0.5 sccm deposition occurs, the deposited material is thought to be SiO_x as it is evident from the emission spectrum of $SiCl_4/O_2$ (see fig.3.14) where emission lines from SiO can be detected at O_2 flow rates of $\geq$ 0.5 sccm. Therefore it seems that the mechanism responsible for selective etching of GaAs/AlGaAs in a mixture of $SiCl_4/N_2$ plasma is the formation of either Al_xN_y or Si_xN_y layers, whereas the mechanism responsible for selectivity in $SiCl_4$ and $SiCl_4/O_2$ Plasmas is the formation of Al_xO_y.

5.5.1 XPS analysis of the AlGaAs etch stop layer

To study the nature of etch stop layer, XPS (X-ray Photoelectron Spectroscopy) measurements were made on samples etched with $SiCl_4/N_2$ at high pressures of 30 mtorr, power of 15 W and on samples etched in $SiCl_4$ alone at low pressures of 9 mtorr and low power of 15 W where the selectivity in both cases is very high, the samples consisted of 500 nm thick $Al_{0.3}Ga_{0.7}As$ layer of capped with 10 nm thick GaAs. The samples were over

etched for 5 minutes in each case so as to provide thick enough etch stop layer to perform the XPS measurements.

As the XPS equipments are unfortunately not available in Glasgow university, the XPS measurements were performed on these samples in Aston University by Dr. John Sullivan after about three weeks from being etched. This delay will inevitably lead to a high degree of oxidation of the surface and possible contamination. The measurements were performed with a wide range of binding energies 0-550 eV with a take off angle of 45 degree. The XPS peak of each element was converted to its relative atomic concentration in %, the results are summarised in table 5.1. For sample 1 which is etched in $SiCl_4/N_2$, the initial examination reviled very high concentrations of C, O, Si and Cl and low concentrations of Ga, As and Al and significantly the presence of N with a concentration of only 1.3%. The presence of C and O in air exposed reactive ion etched AlGaAs surfaces has been reported by many workers [5,7,18] to be due to environmental contamination.

Table 5.1: The relative atomic concentration extracted from the XPS spectra performed on AlGaAs etch stop layers etched in $SiCl_4$ and $SiCl_4/N_2$.

Element	(Sample 1) Atomic concentrations in %	(Sample 1) Concentrations in % (after Ar ion etch)	(Sample 2) Concentrations in % (after Ar ion etch)
C	32.6	18.7	13.1
O	25.1	28.5	50.9
Si	27.0	0	0
Cl	6.9	0	0
N	1.3	3.0	0.06
As	2.2	18.9	0
Al	2.7	15.6	2.0
Ga	2.2	15.2	33.8

To remove the contaminated layer the sample was Ar ion etched for 15 minutes with an etching rate of 0.24 nm/min, therefore a layer of 3.6 nm thick was removed from the surface and XPS measurements were performed. After removing this contaminated layer, the Si and Cl were completely removed, whereas the relative atomic concentration of Ga, Al and As was sharply increased. On the other hand the concentration of C was halved and that for the O was unchanged. Interestingly the concentration of N was more than doubled to 3% as shown in table 5.1. The presence of Si and Cl is due to deposition of chlorosilicon species (see section 3.3.4 in chapter 3), gallium halides and possibly silicon nitrides (see fig.3.15) incorporation in the etch stop. For sample 2 which is etched in pure $SiCl_4$ plasma

at low pressure and flow rate with high selectivity, initial XPS results showed similar domination by the C, Si and O. However unlike sample 1 after Ar ion etching, the relative concentration of O remained high whereas the Cl, Si and C concentration were reduced drastically. At the same time the surface was Ga rich with no As detected. This suggests that the stoichiometry of surface is either GaAs oxide or AlGaAs oxide. This is in agreement with studies [24] which found that the native oxide of the AlGaAs surface has a large degree of As deficiency.

As the XPS spectra were taken in wide scans, the measured binding energies are only approximate, nonetheless they provide a guide to the possible compounds from which they originate. The binding energies measured from XPS spectra on both samples for the Al 2p and Si 2p photoelectrons, were 75.5 eV and 104 eV respectively. The binding energy for the N 1s peak as measured from sample 1 (etched in $SiCl_4/N_2$) was 399.3 eV. The literature values [7] for the Al 2p line from Al_2O_3 is about 75 eV and from AlN is 74.5 eV, whereas for the N 1s line from AlN is about 397.4 eV [19] and N 1s from SiN_x (x=1.5) [20] is 398.2 eV. As the measured energies are not very accurate because of the low resolution of the XPS spectra, it is not clear which compound the Al is bonded to, Al_2O_3 or AlN or both. The Si 2p peak is known to be in the vicinity of 99.4 eV for elemental Si, [21] at 102.7 eV for SiO, [22], at 103.4 eV for SiO_2 [23] and at 102.8 eV for SiN_x (x=1.5) [20]. The binding energy of the peak that appears on the AlGaAs surface is clearly too high for elemental Si, but it is near the binding energies of SiO, SiO_2 and $SiN_{1.5}$. The mere presence of the nitrogen especially in sample 1, may suggest that the N_2 is incorporated in the etch stop as some form of nitrides, but again it is not clear from either the position of N 1s or Si 2p which nitride, AlN or SiN_x. Therefore to have a full picture of the chemistry of the etch stop layer a comprehensive XPS analysis are required which unfortunately was not available by the time this project was completed.

5.6 The effects of pressure and rf power on AlGaAs and AlAs etch profiles

The etch profiles of AlGaAs and AlAs have been studied at low (15 W) and high (≥100 W) powers and at pressures ≥12 mtorr as the etch rate of the AlGaAs is very low at low pressures while using low powers. At low power of 15 W, pressures of 12-15 mtorr and flow rate of 12-15 sccm the etch profiles of AlGaAs have a large undercutting with a lateral etch rate of about 35-40 nm/min and vertical etch rate of about 120-130 nm/min. Therefore the vertical etch rate/ lateral etch rate ratio is about 3.1:1. This is shown in the SEM micrographs of fig.5.9, where a sample consisting of 1 μm thick $Al_{0.3}Ga_{0.7}As$ layer on a GaAs substrate was etched to a depth of 8 μm to show the lateral etching/vertical etching ratio of AlGaAs compared to almost vertical etching on the GaAs substrate. The degree of undercutting in AlGaAs is far larger than that of GaAs under the same conditions. Increasing the pressure to > 15 mtorr the lateral etching of AlGaAs

increases to 50 nm/min. The etch profiles for the AlAs was investigated using multiple quantum well material of 20 periods of GaAs/AlAs 54/74 nm capped with a 500 nm thick layer of GaAs so that the etching begins with a small undercut as the GaAs etching have undercutting as well at high pressure. The etching was carried out at pressure of 15 sccm and flow rate of 12 sccm and power of 15 W. As shown in the SEM micrographs of fig.5.10 the etching starts with small undercutting in the top 500 nm layer of GaAs and then it laterally etches every AlAs layer at a rate of about 45 nm/min compared to a vertical etch rate of 90-100 nm/min. Therefore the vertical etch rate/lateral etch rate ratio is only (2.1:1) under these discharge conditions which is lower than that of AlGaAs under similar conditions. The lateral etching of both AlAs and AlGaAs increases with pressure, however the vertical etching of both materials increases faster than their lateral etch rate with pressure increase as shown in fig.5.11. The lateral etching of Al itself in $SiCl_4$ plasma at pressures $\geq$ 10 mtorr and at power density of 0.16 W/cm^2 has been reported [25] to be caused by the high volatility of $AlCl_x$ and less deposited Si on the sidewalls compared to low pressures and high powers where the sidewalls of the Al were found to be coated with a thin film containing Si.

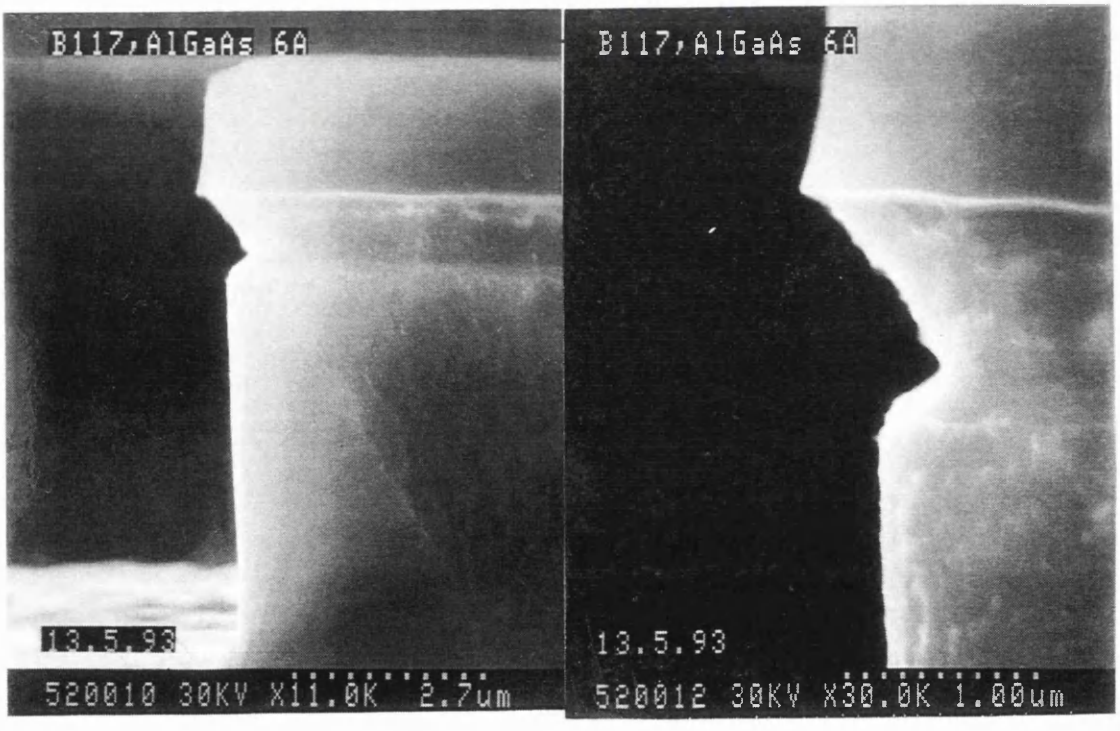

Fig.5.9: SEM micrographs of 1 μm $Al_{0.3}Ga_{0.7}As$ on GaAs substrate etched in $SiCl_4$ plasma to a depth of 7 μm. The 1.8 μm photoresist mask is still in place which show the lateral etching of AlGaAs and almost a vertical etching of GaAs. The discharge conditions are: power of 15 W, flow rate of 12 sccm and pressure of 15 mtorr. The left micrograph is the whole structure and the right in more detail.

To suppress the lateral etching of AlAs, low pressures must be used (as was the case for GaAs), however it is not possible to etch AlAs or AlGaAs at low pressures and under low power conditions because of the residual O_2 or air in the chamber as discussed in the last few sections. Therefore, the residual O_2 and air in the chamber has to be reduced greatly or eliminated completely before the we can etch the AlAs at low pressures and under low power conditions. To reduce the residual O_2 or in the chamber a RIE system with load lock and very low base pressure < 0.1-0.01 mtorr is required. This should enable us to etch the AlAs or AlGaAs at low pressures and hence vertically under low power conditions.

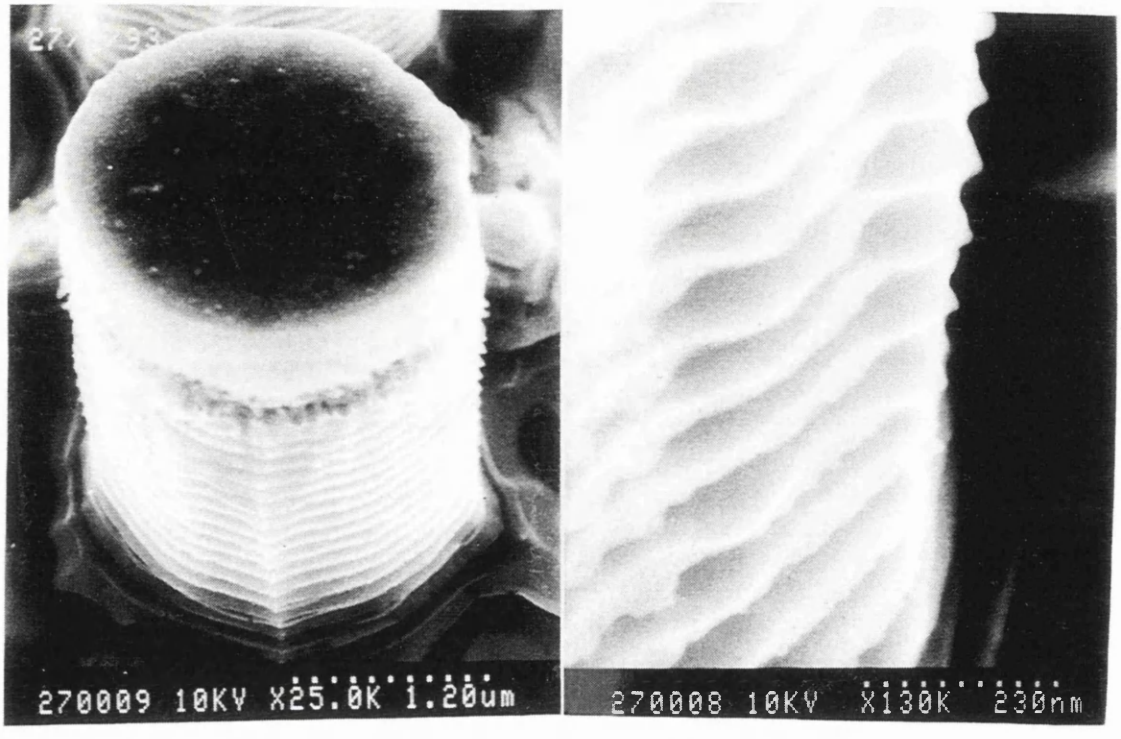

Fig.5.10: SEM micrographs of MQW material of AlAs/GaAs, etched in $SiCl_4$ plasma using pressure of 15 mtorr, flow rate of 12 sccm, dc bias of 45 V and power of 15 W. Right; the whole structure and left: the texture of the sidewalls which shows the lateral etching in the AlAs layers.

The lateral etching of both AlGaAs and AlAs can be completely suppressed and very anisotropic profiles can be obtained with very smooth surfaces and sidewalls by using high powers ≥ 40 W and high dc biases ≥ 200 V and at ≤ 15 mtorr. This is shown in SEM micrographs of fig.5.12, where the MQW material shown in fig.5.10 has been etched under the same conditions of pressure and flow rate as in fig.5.10, but at a power of 120 W and a dc bias of 360 V to a depth of about 23 μm with a dot diameter of 2.5 μm. To summarise, the etch profiles of AlGaAs or AlAs have a large lateral etching at low powers and high pressures, whereas the lateral etching can be suppressed and very smooth surfaces and sidewalls are obtained by using high powers. To improve the verticality of AlAs etching at low power RIE systems with load lock and low base pressure are required.

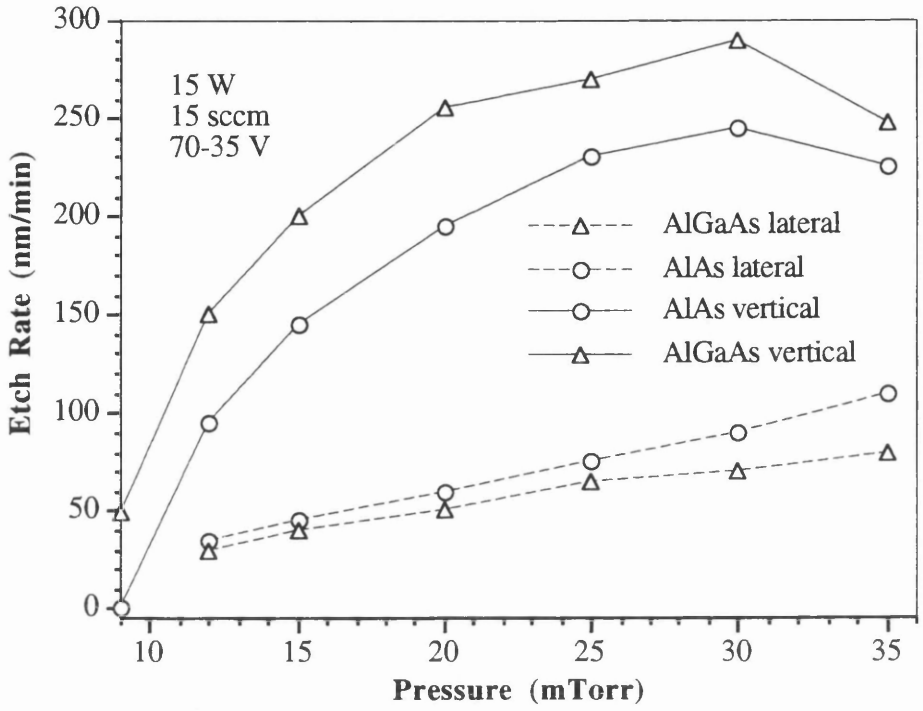

Fig.5.11: The lateral and vertical etch rates of AlGaAs and AlAs in $SiCl_4$ plasma as a function of the total pressure using a constant flow rate of 15 sccm and power of 15 W.

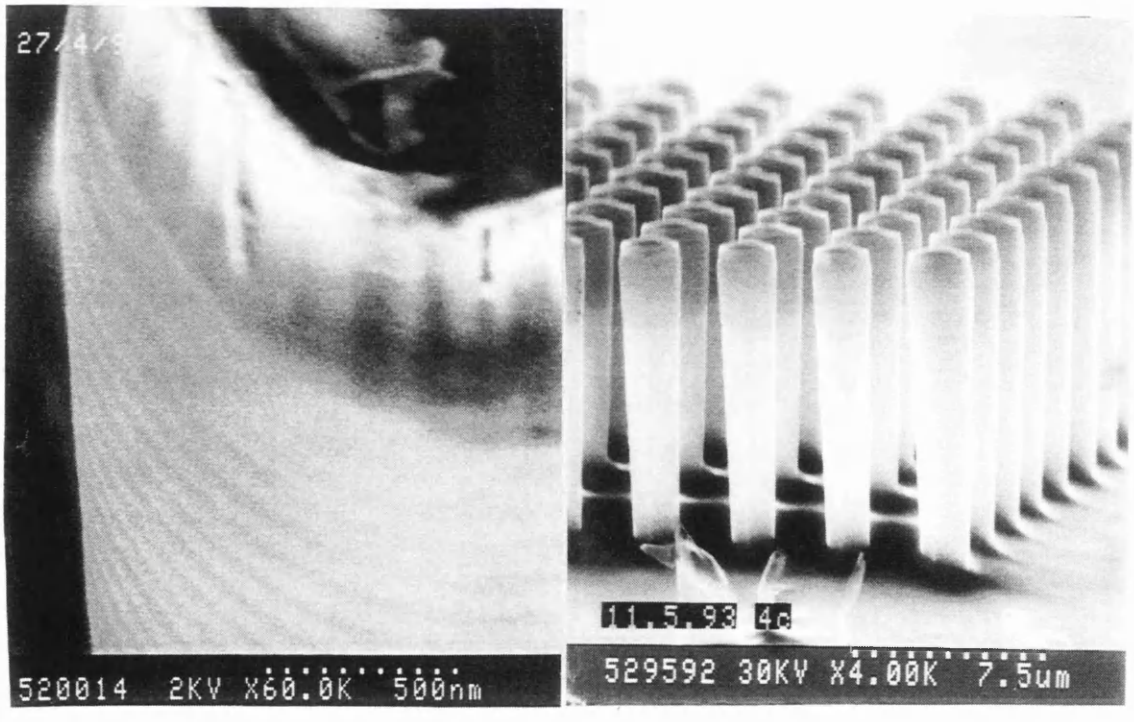

Fig.5.12: SEM micrographs of MQW material AlAs/GaAs etched to a depth of 11 μm at rf power of 120 W, dc bias of 360 V, flow rate of 12 sccm and pressure of 15 mtorr. (left) Shows the smoothness of the sidewalls for both layers, AlAs and GaAs and (right) shows the whole structure.

5.7 Selective and nonselective RIE of GaAs and AlGaAs in a mixture of $SiCl_4/SiF_4$ plasma

Selective RIE etching of GaAs/AlGaAs utilizing a mixture of $SiCl_4/SiF_4$ has been reported by many authors [6-8], however the selectivities obtained are ≤ 350:1 which are not as high as the in case of CCl_2F_2 [2-5] plasmas or $SiCl_4$ plasmas given in the last few sections. In an attempt to improve the selectivity of etching GaAs/AlGaAs in $SiCl_4/SiF_4$ plasma and to examine the etching parameters that are closely related to the achievement of selectivity, a comprehensive study of the $SiF_4/SiCl_4$ plasma chemistry has been carried out using Optical Emission spectroscopy (OES). The selectivity was studied over a wide range of $SiCl_4/SiF_4$ flow rate ratio and a wide pressure range of 20-150 mtorr, all at low powers and low biases of 12-15 W and 20-50 V respectively.

5.7.1 Optical Emission Spectroscopy of SiF_4 and $SiCl_4/SiF_4$ plasmas

5.7.1.1 OES of SiF_4 plasma

The Silicon Tetrafluoride (SiF_4) plasma has an emission spectrum similar to $SiCl_4$ in many aspects, with many overlapping systems and continuums belonging to various species of Silicon fluorides in the discharge. The spectra of pure SiF_4 plasma in the range of 200-600 nm and 700-840 nm are given in fig.5.13, and fig.5.14 respectively. The discharge conditions are: a rf power of 15 W, SiF_4 gas flow rate of 9 sccm and at a pressure of 150 mtorr. A very complicated overlapping emission system which belongs to SiF and SiF_3 radicals are detected in the region of 220-280 nm. The emission from SiF_3 has its strongest band heads at (245.25, 244.73, 242.74, 240.73, 240.22 and 238.27) nm. Further intense emission bands from SiF at (334.6, 336.3, 436.82 and 440.05) nm were detected. Intense and regularly spaced emission bands from SiF_2 in the region of 364-418 nm were also detected. No emission from F was detected in the range of 200-600 nm, whereas a very weak emission from Si was detected at 288.16 nm. In the Infrared region (700-840) nm, the spectrum is again dominated by the emission from SiF radicals however a very weak emission from atomic F at 703.75 nm was detected. The wavelengths of the observed emission lines and bands are obtained from references [26-27].

The probable basic dissociation reactions resulting from the collisions between SiF_4 molecules and electrons in the discharge are thought to be as follows:

$$SiF_4 + e \rightarrow SiF_3 + F + e \qquad E_{th} = 5.6\ eV \qquad (5.7.1.1)$$

$$SiF_4 + e \rightarrow SiF_2 + 2F + e \qquad E_{th} = 11.2\ eV \qquad (5.7.1.2)$$

$$SiF_4 + e \rightarrow SiF + 3F + e \qquad E_{th} = 16.8\ eV \qquad (5.7.1.3)$$

$$SiF + e \rightarrow Si + F + e \qquad E_{th} = 5.72\ eV \qquad (5.7.1.4)$$

The reaction energies given were calculated from the standard enthalpy of formation and bond dissociation energies for each radical.

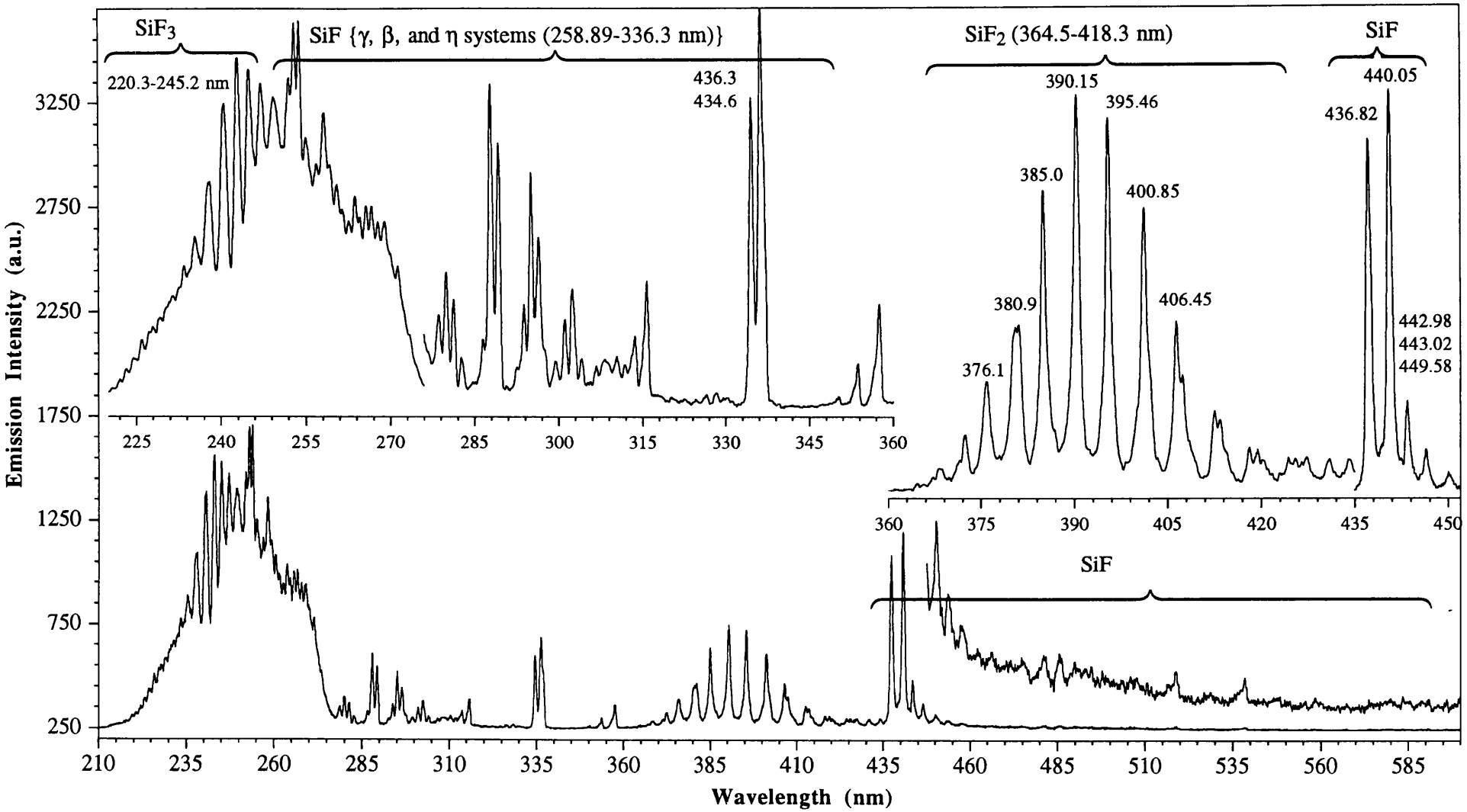

Fig.5.13: Spectrum of SiF_4 plasma in the range of 210-600 nm, the discharge conditions are: a pressure of 150 mtorr , a flow rate of 9 sccm and a power of 15 W. Shows the emission from SiF, SiF_2 and SiF_3 but not from Si or F atoms. The various parts of the spectrum have been enlarged with different scales to show the details in every part.

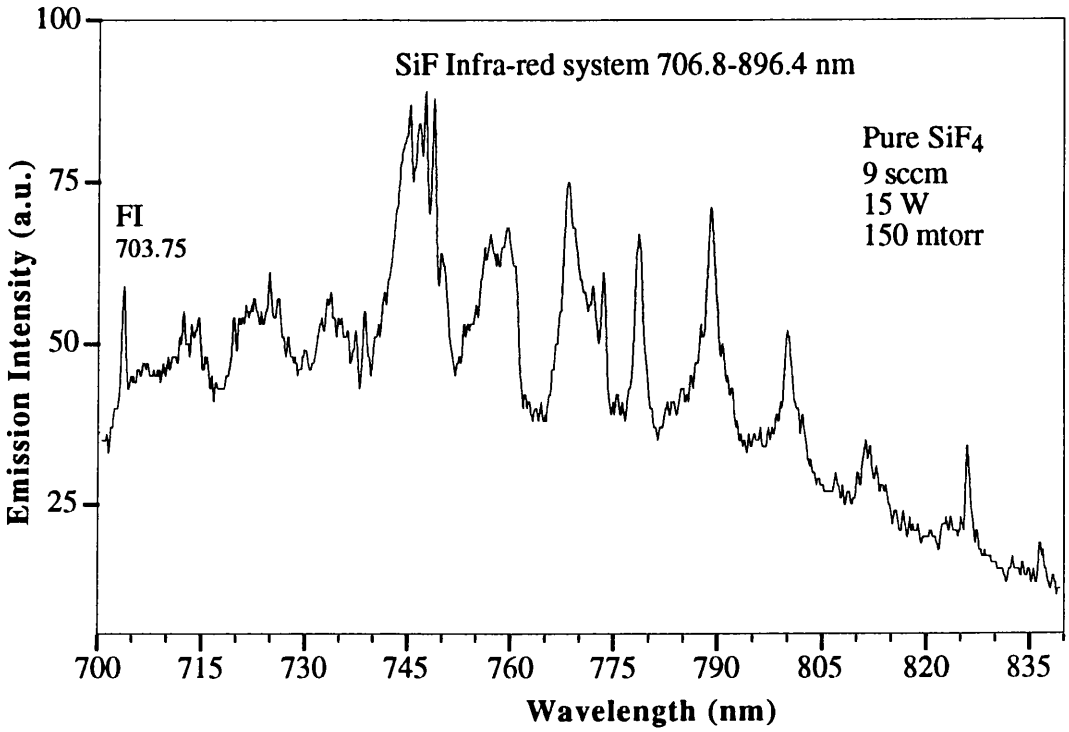

Fig.5.14: Spectrum of SiF_4 plasma in the infrared region, recorded from a discharge at rf power of 15 W, gas flow rate of 9 sccm and at a pressure of 150 mtorr.

5.7.1.2 OES of $SiCl_4/SiF_4$ plasma

The spectrum of a mixture of SiC_4/SiF_4 plasma is more complicated than the spectrum of any of the two gases alone due to increase overlapping in the emission systems from the large variety of species in this plasma. The spectra of $SiCl_4/SiF_4$ plasma in the wavelength range of 220-500 nm from a discharge using flow rate ratios of $SiCl_4$:SiF_4; 2:9, 6:9 and 9:2, pressure of 150 mtorr and a power of 15 W, together with the spectrum of pure SiF_4 plasma are given for comparison in fig.4.15. At low flow rate ratio of $SiCl_4$:SiF_4 of (2:9), the spectrum is dominated by the emission from SiF_4 decomposition species: SiF, SiF_2, SiF_3 and the only indication of the $SiCl_4$ presence in the discharge is the emission from SiCl radicals at 280.7 and 282.3 nm. The emission from atomic Si is unexpectedly stronger with a small percentage of $SiCl_4$ in the discharge than with just SiF_4 alone. Increasing the flow rate ratio to (6:9), a very complicated spectrum is obtained in the range of (220-500) nm with detection of SiF, SiF_2, SiF_3, SiCl, $SiCl_2$ and Si. At high flow rate ratio (9:2) of $SiCl_4$:SiF_4 the spectrum is dominated by the emission from $SiCl_2$ radicals (the continuum maximum at 330 and 390 nm) as well as SiCl radicals at 280 nm. However the presence of SiF_4 in the discharge is well established by the strong emission from SiF and SiF_3 radicals, whereas no emission from SiF_2 was detected in this case. No emissions from Cl or F were detected in all spectra in this wavelength range.

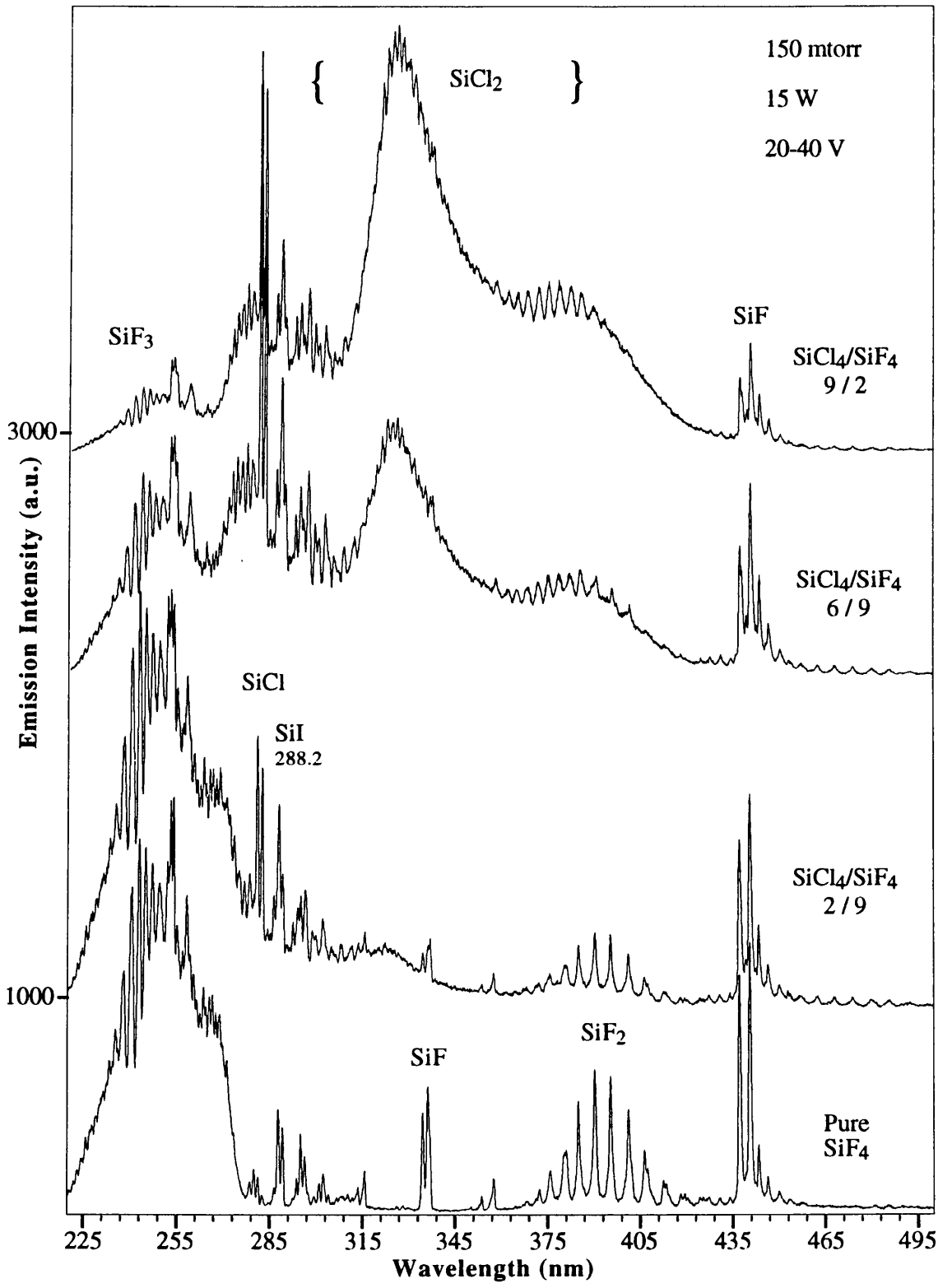

Fig.5.15: Spectra of $SiCl_4/SiF_4$ plasmas recorded for various $SiCl_4/SiF_4$ flow rate ratios, constant pressure of 150 mtorr and power of 15 W.

The spectrum of $SiCl_4/SiF_4$ plasma using a flow rate ratio of 2:9 sccm together with the spectrum of pure SiF_4 plasma in the Infra-red region (700-840) nm are given for comparison in fig.5.16.

The spectrum of $SiCl_4/SiF_4$ plasma in this region is dominated by the emission from the atomic Cl and surprisingly no emission from F can be detected even though the flow rate ratio is only 2 $SiCl_4$: 9 SiF_4. This is most likely to be due to the bond strength between Si-F which is 5.72 eV being higher than that of Si-Cl which is 3.96 eV. This leads to higher dissociation energies for SiF_4 and its decomposition products than their counterpart in $SiCl_4$. For example, the energy required for the dissociation of SiF_4 to SiF_2 radical and 2F atom is 11.2 eV, whereas the energy required for the dissociation of $SiCl_4$ to $SiCl_2$ radical and 2Cl atom is only 5.12 eV, see table 3.1 in chapter 3 for more detail about the dissociation energies of chlorosilicon species.

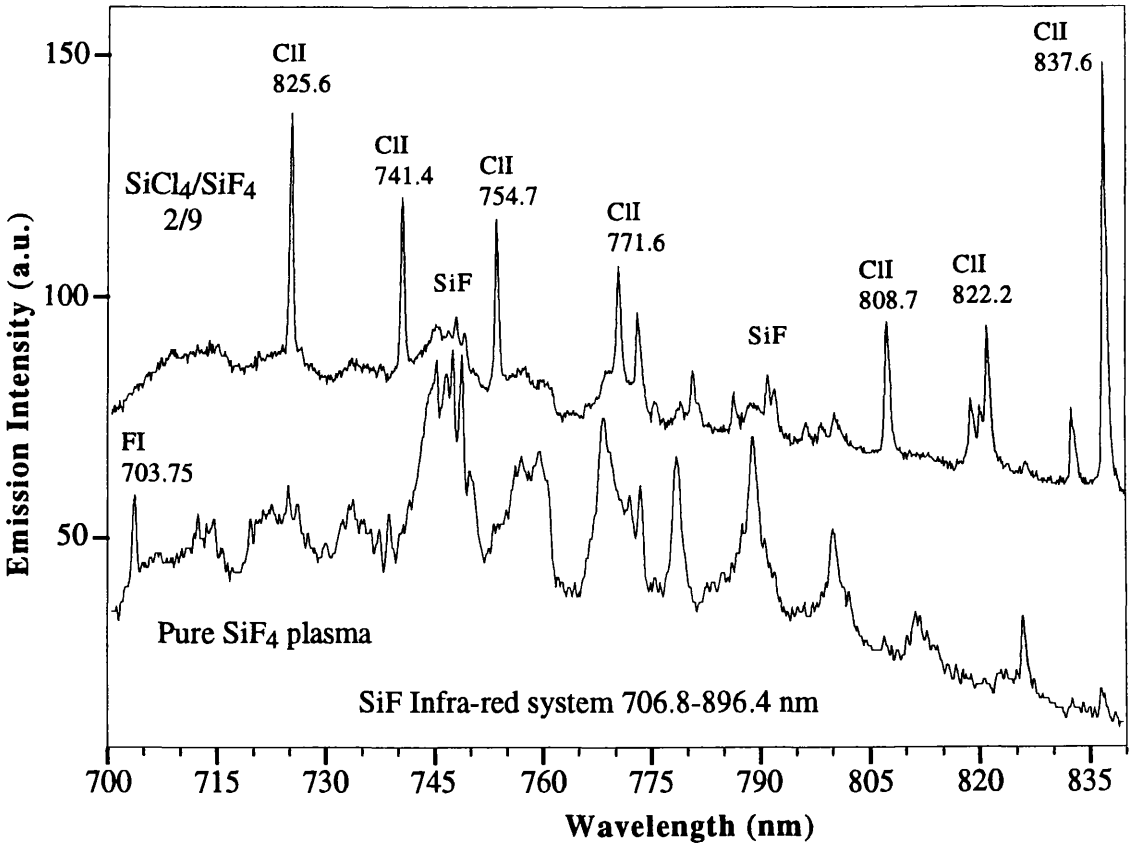

Fig.5.16: Spectra of $SiCl_4/SiF_4$ and SiF_4 plasmas in the infrared region, recorded from a discharge at rf power of 15 W, gas flow rate ratio of $SiCl_4/SiF_4$ of 2/9 and at pressure of 150 mtorr. The SiF_4 spectrum was recorded using 9 sccm, 150 mtorr and 15 W.

5.7.1.3 Effect of $SiCl_4/SiF_4$ flow rate ratio on the emission intensities of the discharge species

The effect of $SiCl_4$ percentage in the total gas flow rate, which is the flow rate of ($SiCl_4$ + SiF_4), on the emission intensities of the various species in the discharge was studied over a wide range of $SiCl_4/SiF_4$ flow rate ratio and over a total gas flow rate of 9 to 18 sccm, powers of 12-15 W and at two values of the pressure 50 and 150 mtorr. The emission intensities of SiF at 440 nm, SiF_2 at 390.15 nm, SiF_3 at 240.7 nm, F at 703.75 nm, Si at 288.16 nm, SiCl at 280 nm, $SiCl_2$ at 330 nm and Cl at 837.6 nm as a function of the $SiCl_4$ percentage in the total flow at constant rf power of 15 W and constant pressure of 150 mtorr is given in fig.5.17. The emission intensity of SiF increases with increasing $SiCl_4$ % between 0-30%, then begins to decrease slowly between 30-50% $SiCl_4$ in the discharge and then decreases faster for further increase in $SiCl_4$ %. The emission intensity of SiF_3 increases in a similar way as SiF between 0-30% $SiCl_4$, however it decreases for further increase in $SiCl_4$ % in the total flow. On the other hand, the emission intensity of SiF_2 decreases immediately with smallest addition of $SiCl_4$ to SiF_4 discharge. The emission from atomic F could not be detected at all as soon as the $SiCl_4$ was introduced to the SiF_4 discharge.

Having described how the fluorinated species react to the addition of $SiCl_4$, to complete the analysis we must consider the behaviour of the chlorinated species at the same time. The emission intensity of SiCl increases sharply between 0-30% $SiCl_4$ in the discharge, then it increases slowly between 30-50% $SiCl_4$ and then decreases sharply for further increase in $SiCl_4$ % in the discharge. In contrast to SiCl the emission from $SiCl_2$ is very low and it increases slowly between 0-25% $SiCl_4$, then increases very sharply between 25-50% $SiCl_4$ and it continues to increase for further increase in the $SiCl_4$ % in the discharge. The emission intensity of Si increases between 0-30% $SiCl_4$ and it is remarkably constant between 30-50% $SiCl_4$ in the total flow and then it decreases with further increase in the $SiCl_4$ %. The emission behaviour from Cl is similar to that of Si except it has a higher value at very low percentages of $SiCl_4$, the Cl emission increases with $SiCl_4$ % between 0-25% and it stays constant over $SiCl_4$ % range of 30-50% and then it decreases for further increase in the $SiCl_4$ %.

It is obvious that it is a very difficult task if not impossible to account for all the changes in the emission intensities of all the species in the discharge. Nonetheless, closer examination of the emission intensity plots in fig.5.17, one can identify three regions in the graph where most of the species behave differently. The first region is between 0-30 % $SiCl_4$ in the discharge, the second region is between 30-50% $SiCl_4$ in the discharge and the third region is between 50-100 % or Pure $SiCl_4$ discharge. Therefore there are three chemical regimes in the discharge depending on the $SiCl_4$ percentage in the discharge.

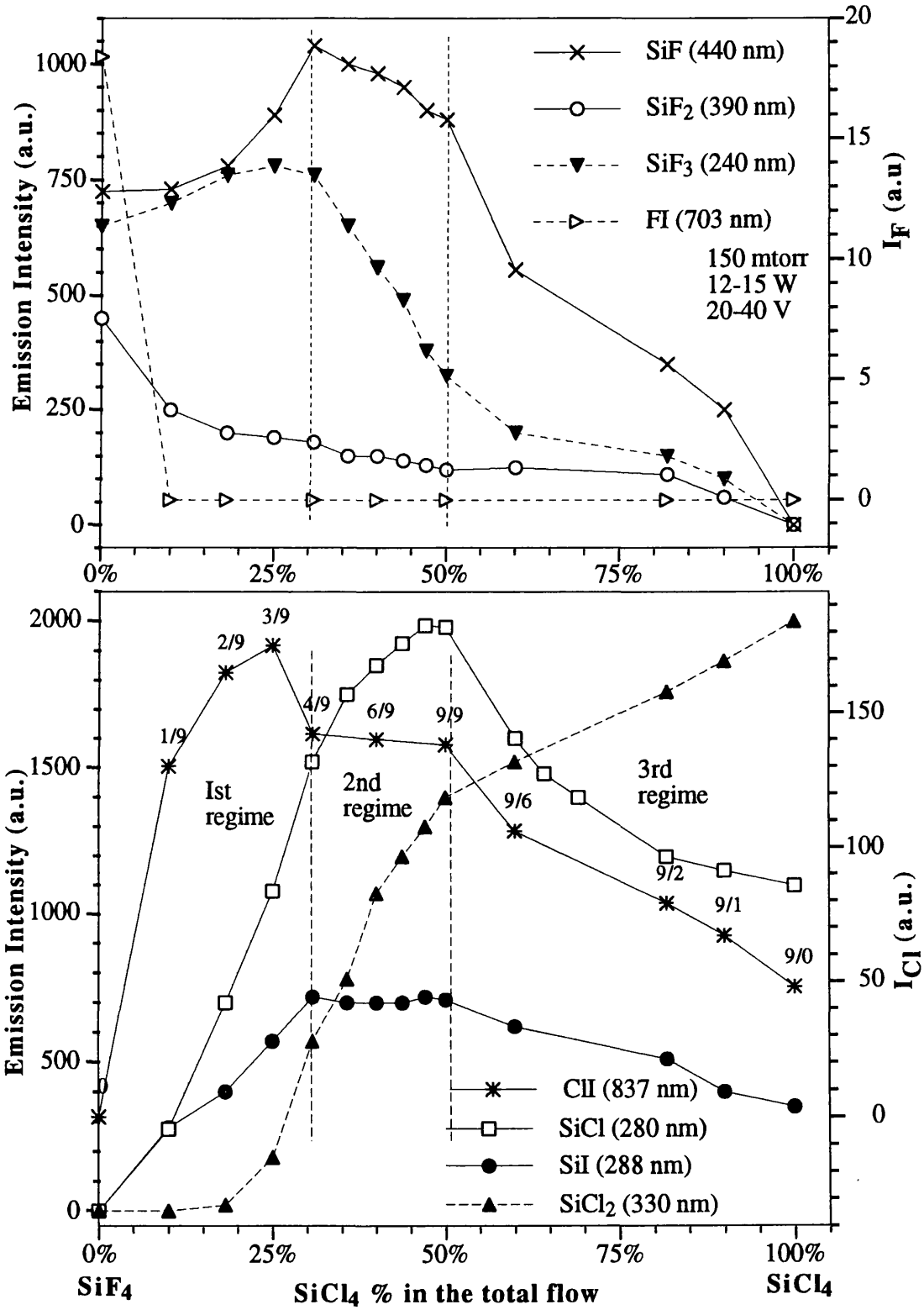

Fig.5.17: Emission intensities of the various species of $SiCl_4/SiF_4$ plasma as a function of the $SiCl_4$ percentage in the total gas flow rate with the corresponding values of $SiCl_4/SiF_4$ flow rates plotted. The discharges were performed at rf powers of 15 W and pressures of 150 mtorr.

In the first regime "0-30% $SiCl_4$" the chemistry of the plasma is likely to be dominated by the fluorosilicon species such as SiF and SiF_3, in other word the plasma is mostly fluorine species. In this regime, the discharge in the beginning is pure SiF_4 which has a certain degree of SiF_4 dissociation into SiFs and free F atoms, as the $SiCl_4$ is introduced to SiF_4 discharge, the F atoms react immediately with $SiCl_4$ molecules and their dissociative products to form more SiF and SiF_3 radicals and liberating at the same time large amounts of free Cl. This leads to the increase in the emission intensities of the SiF and SiF_3, whereas the amount of free F available is decreasing significantly as the $SiCl_4$ flow rate or % is increased. This process continues up to the point where the free F is fully depleted from the discharge at about 30% $SiCl_4$ or 4/9 sccm flow rates of $SiCl_4/SiF_4$.

The second chemical regime is initiated in the range of 30-50% $SiCl_4$ in the total flow or 4/9 - 9/9 sccm flow rates of $SiCl_4/SiF_4$. In this regime the plasma has a very complex chemistry where there is a strong competition between the formation of the silicon fluorides and silicon chlorides species, as the free atomic F is fully depleted, the production of Cl and Si seems to have reached equilibrium where the extra $SiCl_4$ molecules do not lead to the formation of more Cl or Si but the formation of mainly $SiCl_2$ which increases sharply in this regime and to lesser degree the formation of SiCl. Although the SiF_4 flow rate in this regime is constant at 9 sccm , the emission from fluorides of silicon (SiF_{1-3}) is decreasing with increasing $SiCl_4$ flow, this may suggest that there is some kind of preferential dissociation of $SiCl_4$ molecules over SiF_4 molecules because of the lower dissociation energies of $SiCl_4$ compared to SiF_4 molecules.

The third chemical regime begins at about 50% $SiCl_4$ (9/9 sccm $SiCl_4/SiF_4$ flow rates) up to pure $SiCl_4$ discharge, as the SiF_4 flow rate is being decreased, there will be even less and less fluorinated species as they are swamped by the chlorinated species, therefore the plasma chemistry is dominated by chlorine species with little effect of the fluorinated species. Similar results were obtained when the pressure was changed to 50 mtorr instead of 150 mtorr.

To summarise, the chemistry of $SiCl_4/SiF_4$ plasma seems to obey three chemical regimes depending on the percentage $SiCl_4$ in the discharge. At low percentages of $SiCl_4$ "0-30%" the plasma chemistry is mainly fluorinated, at "30-50%" of $SiCl_4$, there is no overall domination of either the fluorine or the chlorine chemistries and at high percentages of $SiCl_4$ "50-100%" the plasma chemistry is mainly chlorinated with little effect of the fluorine species.

5.7.2 Effect of $SiCl_4/SiF_4$ flow rate ratio on the GaAs, AlGaAs etch rates and on the selectivity

In the last section we identified three chemical regimes responsible for the formation of the reactive species in the plasma. In this section the etch rates of the GaAs,

AlGaAs and the selectivity in each regime are studied. The etch rates of GaAs, AlGaAs and the ratio of the etch rates of GaAs/AlGaAs as a function of the $SiCl_4$ % in the total flow at constant pressure of 150 mtorr, at powers of 12-15 W and biases of 20-45 V are given in fig.5.18. No etching occurs for either material at $SiCl_4$ % of ≤ 10%, however there is some deposition, the deposited material is likely to some form of fluorosilicon species. Increasing the $SiCl_4$ % to 18% (2/9) sccm, the GaAs etch rate increases dramatically to 155 nm/min, whereas the etch rate of AlGaAs is almost zero, this leads to a selectivity of GaAs/AlGaAs etching of almost infinity. Increasing the $SiCl_4$ % to 30% (4/9) sccm, the GaAs etch rate increases slowly but the AlGaAs etch rate is still very low, therefore the selectivity is still very high, ≥ 2000:1. Consequently the selectivity for etching GaAs/AlGaAs is very high in the first chemical regime (0-30 % $SiCl_4$) in an agreement with optical emission observation which suggested that the plasma is dominated by the fluorine chemistry which is important for the etching to stop on AlGaAs by the formation of involatile layer of AlF_3, whereas the formation of Ga and As fluorides should not slow down the etch rate of GaAs as they are volatile.

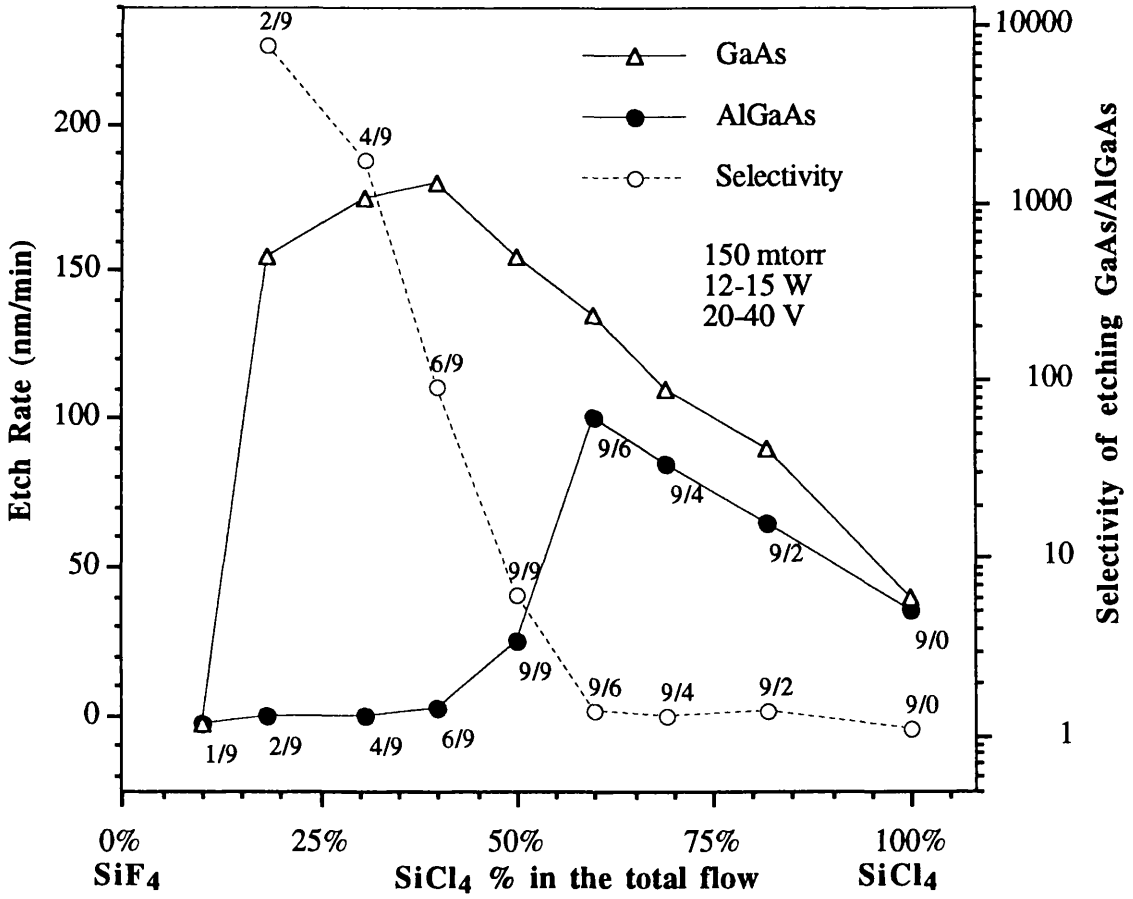

Fig.5.18: The etch rates of GaAs, AlGaAs and the selectivity of etching GaAs/AlGaAs in the mixture of $SiCl_4/SiF_4$ plasma as a function of the $SiCl_4$ % in the total flow at low powers of 12-15 W, a pressure of 150 mtorr and dc biases of 20-45 V.

In $SiCl_4$ % range of 30-50% "the second chemical regime" the etch rate of GaAs decreases, whereas the etch rate of AlGaAs increases which lead to decrease in the selectivity which is ≤ 60:1. The increase in the AlGaAs etch rate may be attributed to the less efficient formation of the AlF_3 etch stop layer since the plasma chemistry is no longer dominated by the fluorine species, however the decrease in the GaAs etch rate with increasing $SiCl_4$ % may be ascribed to less Cl available due to the recombination processes to form $SiCl_2$ at high pressure, this again agrees with the optical emission observation in the second regime. Increasing the $SiCl_4$ % in the total flow between 50% to 100% "the third chemical regime" by decreasing the SiF_4 flow rate, the etch rates of both GaAs and AlGaAs decrease however the selectivities are only ≤ 1.5:1. This due to the fact that the plasma chemistry in this case is similar to the pure $SiCl_4$ at high pressure where it can readily etch both the GaAs and AlGaAs at an almost equal etch rate. To summarise the results, very high selectivities of an order of ≥ 5000:1 can be obtained at low $SiCl_4$ percentages (18-30%) in $SiCl_4/SiF_4$ plasma at pressure of 150 mtorr, low selectivities are obtained in the $SiCl_4$ percentage range of 30-50 % and nonselective etching is obtained for higher percentages of $SiCl_4$. These results are well correlated with optical emission observation of the $SiCl_4/SiF_4$ plasmas.

5.7.3 Effect of the pressure on the selectivity of GaAs/AlGaAs etching in $SiCl_4/SiF_4$ plasma

The effect of the pressure on the selective etching of GaAs/AlGaAs in $SiCl_4/SiF_4$ plasma has been studied in the pressure range of 20-150 mtorr at constant rf power of 12-15 W and for two values of the flow rate ratio of $SiCl_4/SiF_4$ of 2/9 and 4/9 sccm as shown in fig.5.19.

As it can be seen the etch rate of GaAs increases with pressure, being higher for the ratio of 4/9 than 2/9, the etch rate of AlGaAs remains low even at the lowest pressure. The selectivities however, are low below 50 mtorr, then increase steadily with pressure, being higher for the flow rate ratio of 2/9 than 4/9. This is likely to be due to the formation of AlF_3 which is more effective at high pressures than low pressures. However this is in sharp contrast to the high selectivities obtained by using pure $SiCl_4$ at low flow rates of 2 sccm and pressures as high as 25 mtorr.

The selectivity obtained in pure $SiCl_4$ plasma using 2 sccm flow rate and at 20 mtorr pressure is ≥1000:1 (see fig.5.5) compared to selectivity of only about 20:1 in a mixture of (2/9) sccm, $SiCl_4/SiF_4$ and at the same pressure of 20 mtorr and power of 12-15 W respectively . The selectivity in pure $SiCl_4$ plasma is due to the presence of residual O_2 or water vapour in the chamber which outnumbers the etching species at low flow rates and leads to inhibition of the etching on the AlGaAs layer by the formation of Al_xO_y. The

addition of the SiF_4 to $SiCl_4$ disrupts the process of oxide formation on the AlGaAs layer as the SiF_4 and its dissociative species are very reactive, they react with any residual O_2 or water vapour to form HF and oxidized SiF_x species and thereby reducing the effectiveness of any residual O_2 or water vapour in forming the etch stop layer of Al_xO_y. Therefore the addition of SiF_4 to $SiCl_4$ at low pressures enhances the AlGaAs etching by mopping up the residual O_2 and water vapour in the chamber instead of inhibiting the etching on the AlGaAs by the formation of the AlF_3 layer.

To test the degree of selectivity at high pressure of 150 mtorr and at pressure of 50 mtorr using flow rate ratio of 2/9 and at power of 15 W, samples consisting of 1.13 nm thick $Al_{0.3}Ga_{0.7}As$ sandwiched between 110 nm GaAs and GaAs substrate were over etched for various times. As shown in Fig.5.20, in the case of 150 mtorr the etching is stopped by the thin AlGaAs layer for as long as 30 minutes etching leading to an extremely high selectivity of an order of $\geq$ 5000:1. However in the case of 50 mtorr it took about 7.5 minutes to etch through 1.13 nm thick AlGaAs layer which results in an etch rate of about 0.15 nm/min for the AlGaAs, on the other hand the etch rate of GaAs under these conditions is about 145 nm/min therefore the selectivity is about 900:1 as it is also shown in fig.5.19.

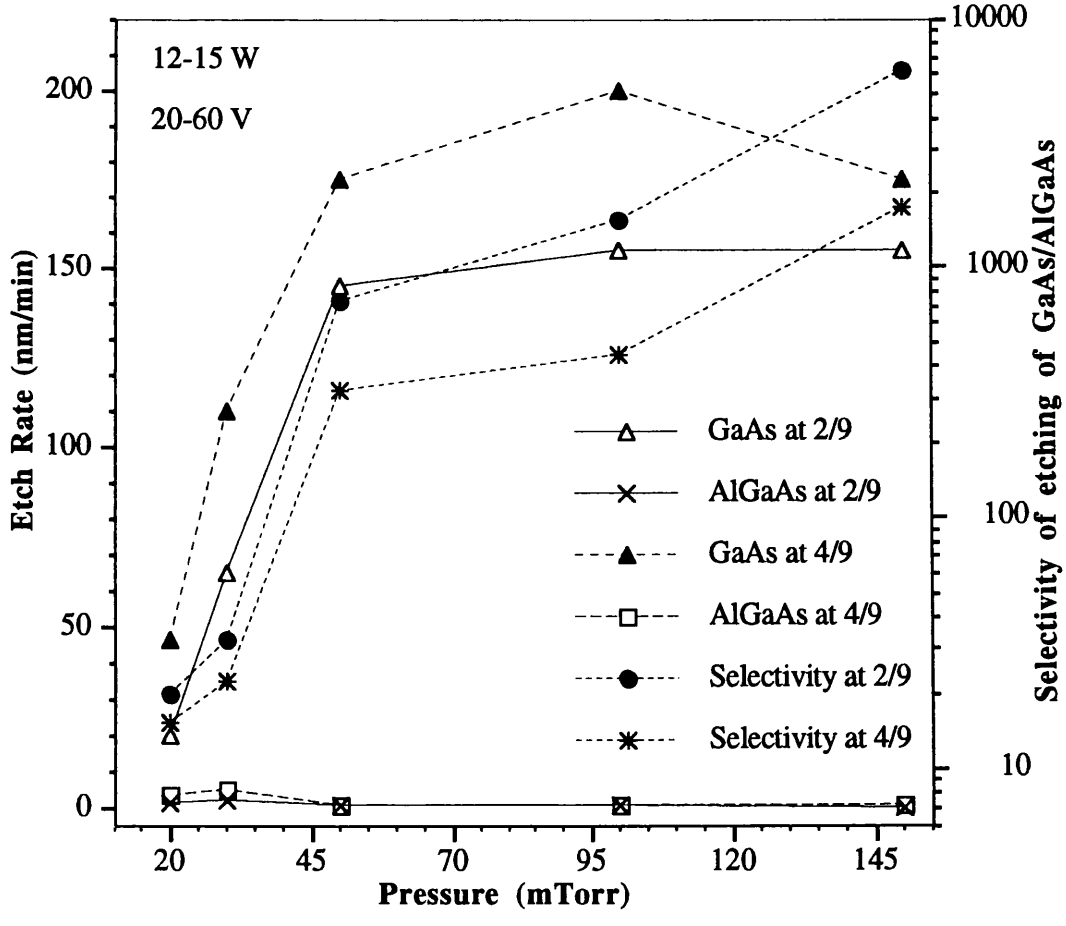

Fig.5.19: The etch rates of GaAs and AlGaAs and the selectivity of etching GaAs/AlGaAs in $SiCl_4/SiF_4$ plasma as a function of the pressure for two values of the $SiCl_4/SiF_4$ flow rate ratio of 2/9 and 4/9 and at constant power of 12-15 W.

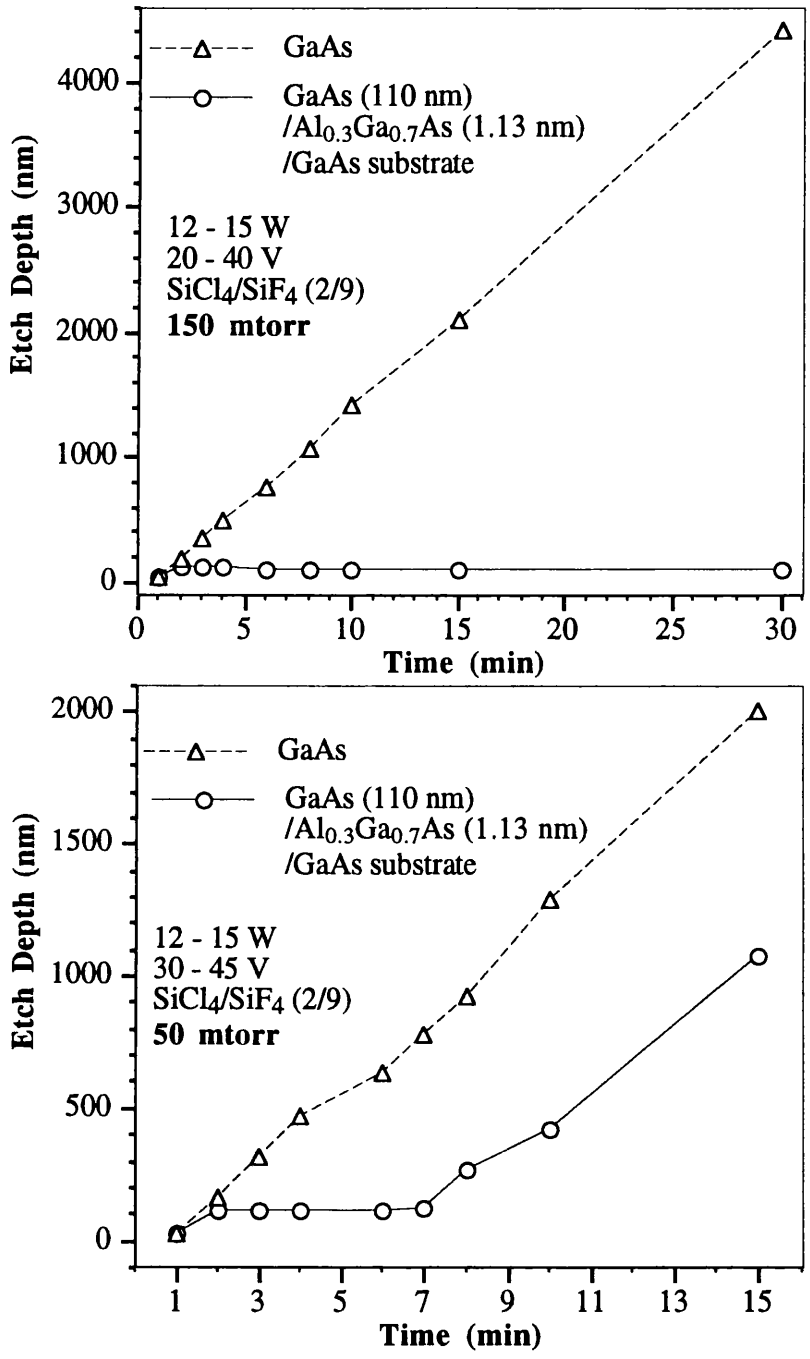

Fig.5.20: The etch depth of GaAs and 1.13 nm thick layer of $Al_{0.3}Ga_{0.7}As$ sandwiched between 110 nm GaAs and GaAs substrate in $SiCl_4/SiF_4$ plasma as a function of time, using 2/9 sccm of $SiCl_4/SiF_4$, 12 W and top; pressure of 150 mtorr, bottom; 50 mtorr.

5.7.4 Effect of rf power on selectivity in $SiCl_4/SiF_4$ plasma

The effect of power or dc bias on the selectivity of etching GaAs/AlGaAs in $SiCl_4/SiF_4$ plasma has been studied for two values of the rf power 12 and 30 W and as a function of the $SiCl_4$ % in the total flow. The resulting average dc biases were 30 and 100

V respectively. As shown in fig.5.21 the maximum obtainable selectivity in case of 30 W, 100 V bias is about 250:1 which occurs at 10% $SiCl_4$ or flow rate ratio of 1/9 sccm then it decreases as expected with the increasing $SiCl_4$ %. In the case of 12 W, 30 V as it was discussed earlier no etching occurs at 10% $SiCl_4$ or 1/9 sccm and the highest selectivity occurs at 2/9 sccm. It is known [2,6] that the formation of AlF_3 provides the etch stopping mechanism in fluorine containing plasmas. However, the low values of selectivity obtained at power of 30 W suggest that there is a competition between the formation of AlF_3 and the chemical etching of AlGaAs by $SiCl_4$ species and because the dc bias is high; 100 V, the AlF_3 is being sputtered which decreases the effectiveness of the etch stop mechanism and thereby allowing the etching of AlGaAs to proceed.

To summarise, the conditions at which high selectivities can be obtained for etching GaAs/AlGaAs in $SiCl_4/SiF_4$ plasma are: high pressure of > 50 mtorr, low $SiCl_4/SiF_4$ ratios of the order of 2-3/9 or 20-30 % of $SiCl_4$, and at the same time low biases are required. Moreover the selectivities obtained are higher by more than an order of magnitude than the reported values (≤ 350:1) in the literature[6-8].

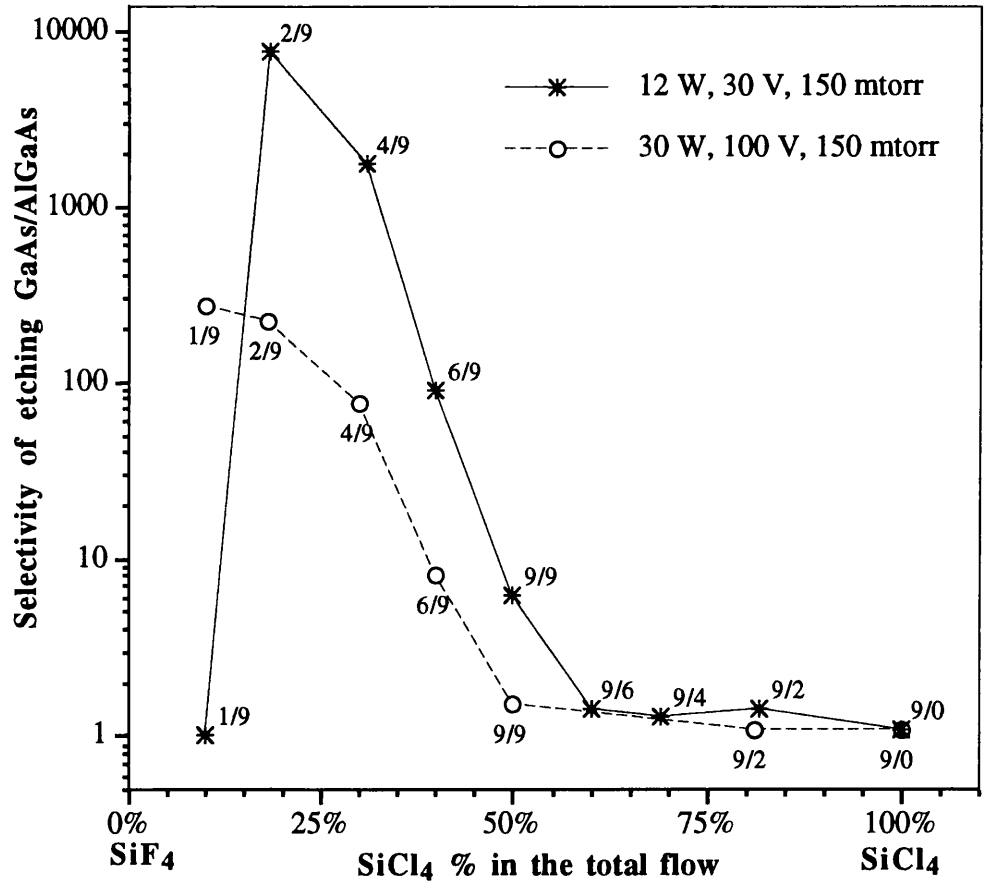

Fig.5.21: The selectivity of etching GaAs/AlGaAs in $SiCl_4/SiF_4$ plasma as a function of $SiCl_4$ % in the total flow for two values of the rf power 12 and 30 W and at constant pressure of 150 mtorr. The resulting biases were 30 and 100 V respectively. The actual $SiCl_4/SiF_4$ flow rate values are also plotted.

5.7.5 Etch profiles, microloading effects and the smoothness of GaAs under selective and nonselective etching conditions in $SiCl_4/SiF_4$ plasma

As the selective etching of GaAs/AlGaAs in $SiCl_4/SiF_4$ plasma requires high pressures, the etch profiles of GaAs at the selective etching pressures or conditions (2/9 - 4/9 sccm of $SiCl_4/SiF_4$ at ≥100 mtorr) have large undercutting or lateral etching under the mask as shown in fig.5.22. The degree of undercutting depends on the pressure being higher for higher pressures. Moreover both the vertical and the lateral etching rates at these high pressures depend on the trench width being higher for wider trenches. The lateral etch rate was measured on samples consisting of etch stop layer of AlGaAs 1.1 nm thick sandwiched between 110 nm GaAs cap layer and GaAs substrate, as the etching is stopped vertically it continued laterally, hence it easy to measure the lateral etch rate by the SEM. The vertical etch rate depends more strongly on the trench width than the lateral etch rate which is not so sensitive to trenches narrower than 200 nm even when the vertical etching has stopped, as shown in fig.5.23. Moreover the lateral etching is negligible for small trenches < 200 nm in case of nonselective etching and for the same pressure as the selective etching condition as shown in SEM micrographs of fig.5.24.

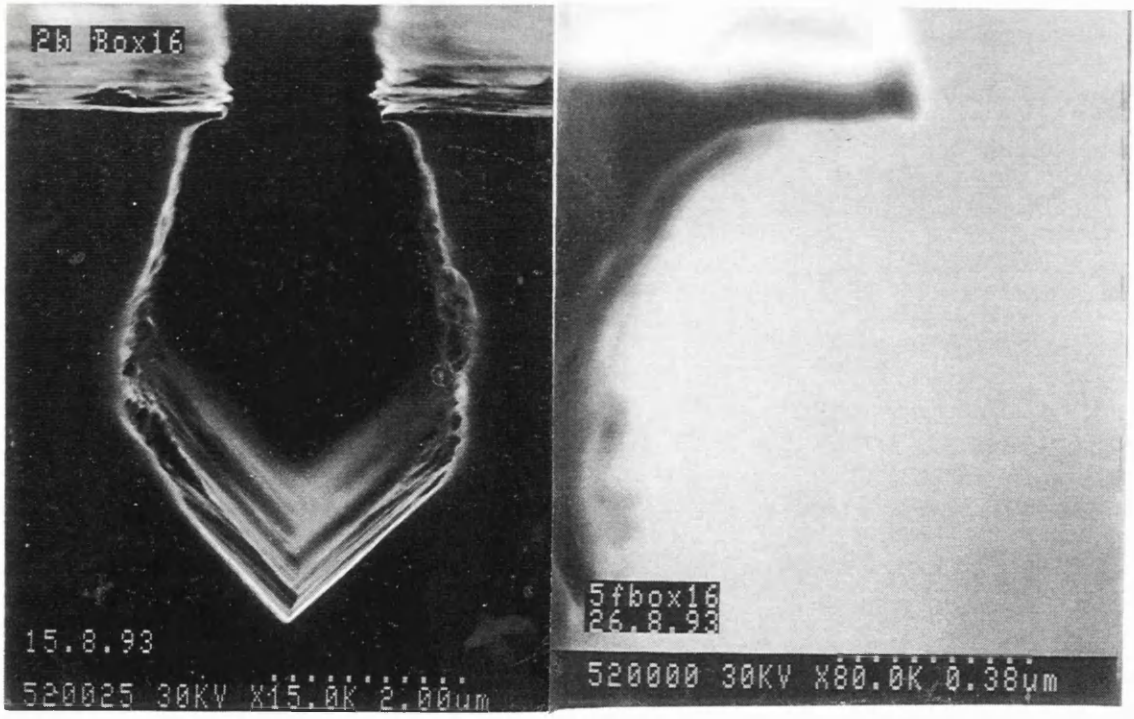

Fig.5.22: SEM micrographs of GaAs etched in $SiCl_4/SiF_4$ plasma under the selective etching conditions of 2/9 sccm of $SiCl_4/SiF_4$, pressure of 150 mtorr and rf power of 12 W. Shows the undercutting profile of the GaAs under these conditions.

In small trenches the lateral etching starts only when the vertical etching has been stopped on the bottom of the trench on an etch stop layer of AlGaAs, whereas for very wide

trenches of ≥ 1 μm, the lateral etching starts at the same time as the vertical etching or in the beginning of the etching and that is why there is a large undercutting under the mask in fig.5.22 and not in fig.5.24. This is due to "microloading effect": the microloading effect is a phenomenon which occurs when narrow trenches are being etched shallower than wide trenches usually at high pressures. The reasons for the occurrence of microloading effect is due to less ions being directed vertically in the plasma at high pressures, so narrow trenches will receive a lower density of ions than the larger trenches. This phenomenon should not be confused with the well known phenomenon of "loading effect" in plasma etching processes where the etch rate decreases when the area of the material to be etched is increased due to the depletion of the reactive species in the gas phase by increasing consumption by the open surfaces [28].

The etch surfaces of GaAs in $SiCl_4/SiF_4$ plasma are somewhat rough but generally the surfaces are smoother than for etching in pure $SiCl_4$ plasma for the same pressure. This is likely to be due to chemical etching effects at high pressures which is higher in pure $SiCl_4$ due to more chlorinated species in the $SiCl_4$ plasma than in $SiCl_4/SiF_4$ plasmas.

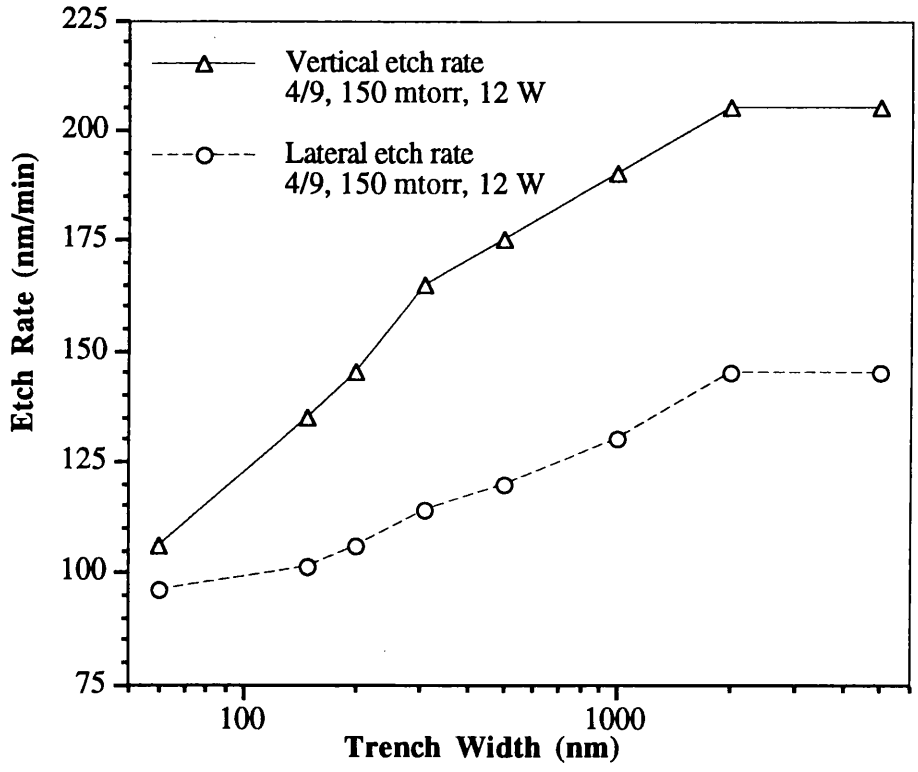

Fig.5.23: The vertical and lateral etch rates in $SiCl_4/SiF_4$ plasma as a function of the trench width. The vertical etch rate was measured on GaAs samples, whereas the lateral etching was measured on samples consisting of etch stop of 1.1nm thick AlGaAs layer sandwiched between 110 nm GaAs cap layer and GaAs substrate.

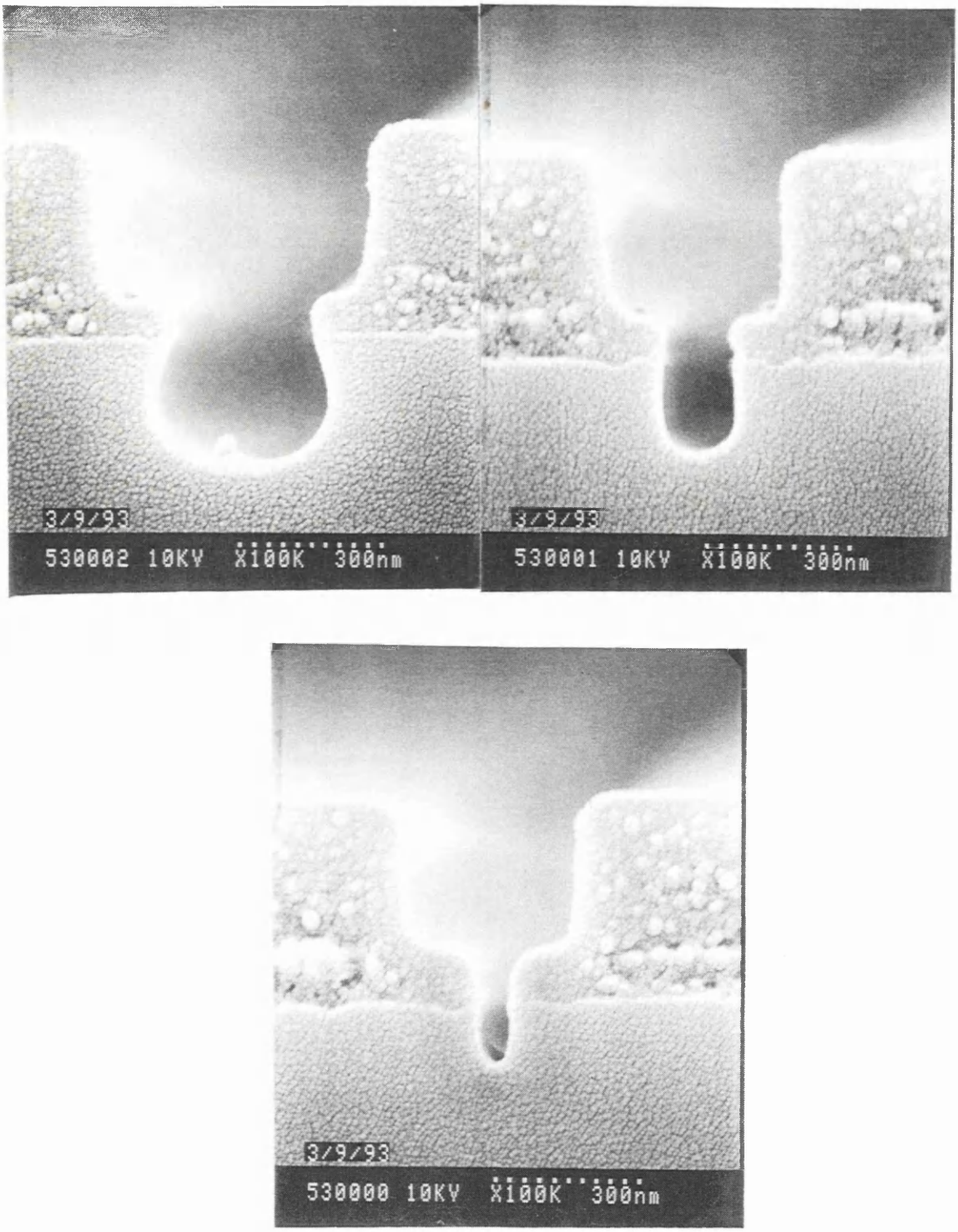

Fig.5.24: SEM Micrographs of various trench widths (T- shaped) etched for 2 minutes in $SiCl_4/SiF_4$ plasma under nonselective etching conditions of 100 mtorr, $SiCl_4/SiF_4$ flow rates of 9/4 sccm and rf power of 12 W. This shows that the lateral etching is negligible and also shows the effect of "microloading" where the wider trenches have been etched deeper than narrower ones.

5.8 T-gate recess etching for MESFET and HEMTs fabrication

It has been shown [29,30] that reducing the gate length in metal-semiconductor field effect transistors (MESFETs) and high electron mobility transistors (HEMTs) enhances the high frequency performance of these devices. In addition to shorter gate lengths, to produce high frequency devices, the gate recess depth and gate off-set (the gate off-set is the distance between the gate footprint and the gate recess edges) have to be accurately controlled and easily reproduced. For devices operating at very high frequencies ≥ 30 GHz, the required gate lengths are less than 300 nm. Conventionally, wet etch techniques have been used for the gate recess etching. However, the wet recess etching has been shown [29] to be increasingly problematic at nanometer gate lengths because of the nonuniform recess depth etching, large gate off-set due to isotropic nature of the wet etching and the poor repeatability of wet etching. Reactive Ion Etching (RIE) provides better dimensional and profile control, enhanced uniformity and repeatability over the conventional wet etching. For these reasons, the RIE as a mean for gate recess etching has received great attention over the past few years. Previous worker have used selective RIE of GaAs/AlGaAs in CCl_2F_2 [31], $SiCl_4/SiF_4$ [6], and $SiCl_4/SF_6$ [10] for gate recessing of GaAs-based MESFET and HEMTs. As these processes allow accurate recess depth control, stopping the etching at a thin AlGaAs layer placed within the channel or on top of the AlGaAs supply layer, the standard deviation of the threshold uniformity has been considerably improved [31]. However concern about RIE induced damage of the active layer of the device during dry etch gate recessing and particularly in low noise devices has restricted the application of the dry etch recessing. Moreover, most common SRIE processes used for dry etch gate recessing use fluorinated chemistry as a mean for the selective etching. As we discussed in the last few sections, in fluorinated chemistry, high pressures have to be used for the etching to stop on a thin AlGaAs layer. At these high pressures the gate recess is undercut by lateral etching. The lateral etching is difficult to control for various reasons such as variation in the etch initiation period before the on set of the etching (the induction time) and hence it inevitably leads to undesirable variation in the recess off-set. Therefore a selective RIE process with minimum or no lateral etching would have a distinct advantage in this regard. In section 5.4 we have shown that a very high selectivity can be obtained in pure $SiCl_4$ plasma and yet the profiles are very anisotropic. Therefore both SRIE in pure $SiCl_4$ plasma and for comparison SRIE in $SiCl_4/SiF_4$ plasma discussed earlier have been applied for gate recessing and the differences are given in the next two sections.

5.8.1 Definition of the T-shaped gate by E-beam lithography

As the gate length decreases, its cross-sectional area decreases too, resulting in increased gate resistance. High gate resistance has undesirable effects on device performance such as the voltage or power gain, therefore it has to be minimized. Few gate shapes have been adopted in the literature for this purpose such as " T " shape [32] or " Γ "

shape [33], etc. In principle by using the properties of the E-beam resists of different sensitivities, it is possible to achieve the desired structure.

The definition of the T- gates in this work was carried out in collaboration with Nigel Cameron in the Department of Electronics and Electrical Engineering in Glasgow University. The samples consisted of 39 nm thick, 2.5 x 10^{18} cm^{-3} Si doped GaAs capping layer, 5 nm undoped $Al_{0.3}Ga_{0.7}As$ layer as an etch stop layer, 56 nm thick, 5 x 10^{17} cm^{-3} Si doped GaAs active layer on 100 nm thick p-type GaAs buffer layer, all grown by MBE on a semi-insulating GaAs substrate.

The definition of the T-gates requires tri-layer e-beams resists with different molecular weights and hence different sensitivity to the e-beam. The definition process is illustrated in fig.5.25 and was carried out as follows:

1. A high molecular weight (350 K), low sensitivity e-beam resist of PMMA (Poly-Methyl Methacrylate) known as Elvacite with (4% concentration in a solution of Chlorobenzene) was spin coated at 5000 rpm for 60 sec which resulted in a thickness of 100 nm, oven baked at 180 °C for 1 hour. This resist layer requires a high e-beam dose and it is used to define the gate footprint.
2. A thick layer (400 nm) of P(MMA/MAA) (Co-polymer Methyl Methacrylate and Methacrylate Acid) with 9% concentration was spin coated at 5000 rpm for 60 sec, oven baked for 1 hour. This resist has a higher sensitivity than the PMMA and it used to produce the wide top part of the T.
3. A low molecular weight (85 K) of PMMA, 4% BDH, is spin coated at 5000 rpm for 60 sec, oven baked over night. The thickness of this layer is about 100-120 nm, this top layer of resist is used to provide an overhanging profile and improve lift-off yield.
4. The exposure process.

A Leica-Cambridge EPBG-5HR e-beam writer was used in the exposure process. Patterns consisting of a central line with an exposure high enough to develop out the small footprint, two side lines of low exposure dose and two edge lines with a medium exposure dose were written. The large sensitivity difference between the P(MMA/MAA) and the 350K mw PMMA allow the edge lines to be developed without affecting the footprint size, the edge lines provide increased area for the " T " and provide an overhanging profile to increase the lift-off yield, whereas the two side lines are to reduce the size of the overhang produced by the 85K mw PMMA.

5. Development: The samples were developed in 2.5:1 IPA : MIBK (Isopropyl Alcohol : Methyl Isobutyl Keton) for 30 secs at 23 °C and rinsed in IPA for another 30 sec, then blown dry with dry nitrogen.

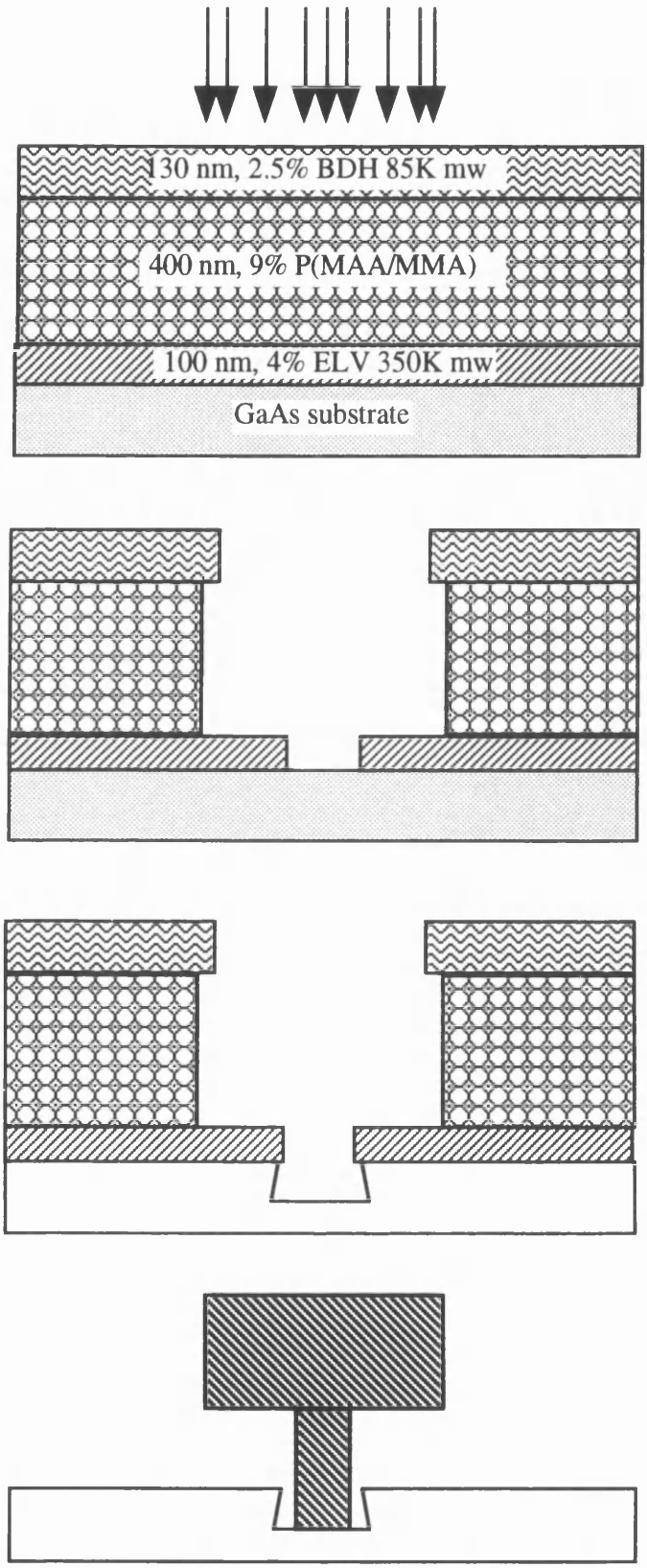

1- Spin coat tri-layer of e-beam resists that have different sensitivity to electron beam.

2. Oven bake each layer at 180 °C (see text for detail).

3. E-beam expose with high dose for the footprint, medium dose for edges and low dose for the side lines.

4. Resists development in 2.5: (IPA:MBIK) for 30 sec at 23 °C and rise in IPA for 30 sec.

5. Dry etch the recess in a selective RIE process.

6. Metallization and lift off in warm acetone .

Fig.5.25: The fabrication steps of the T- gate.

5.8.2 T-gate recessing in pure $SiCl_4$ plasma

The selective RIE in pure $SiCl_4$ as described in section 5.4 was used to dry etch the gate recess. The etching was carried out for 2 minutes at a power of 12 W, a $SiCl_4$ flow rate of 6 sccm, at a pressure of 9 mtorr and dc bias of 60 V. As shown in the SEM micrographs of fig.5.26 the etching was stopped on the AlGaAs layer after etching the 39 nm GaAs capping layer and the profile of the gate is vertical whereas the gate lengths was varied between 60-200 nm and all have the same gate profile.

This vertical profile of the gate makes the gate off-set very small even with long over etching times, since there is no lateral etching. This gate profile could have a very big advantage because the gate off-set is very small and because all gate sizes are etched with equal etch rate and no lateral etching occurs. Moreover, devices with various gate lengths can be fabricated on the same chip with the same gate off-set. However this puts the gate metal too close to the recess edges as shown in the SEM micrographs of fig.5.27 which might cause problems of increased gate leakage for very high doping concentrations of the capped layer. Because of the depletion regions of the gate recess edges, this problem should be minimized by choosing either fully depleted capping layers or lightly doped which will not affect the high frequency operation of the devices since the effective gate length has been reduced greatly by the vertical profile of the gate recess.

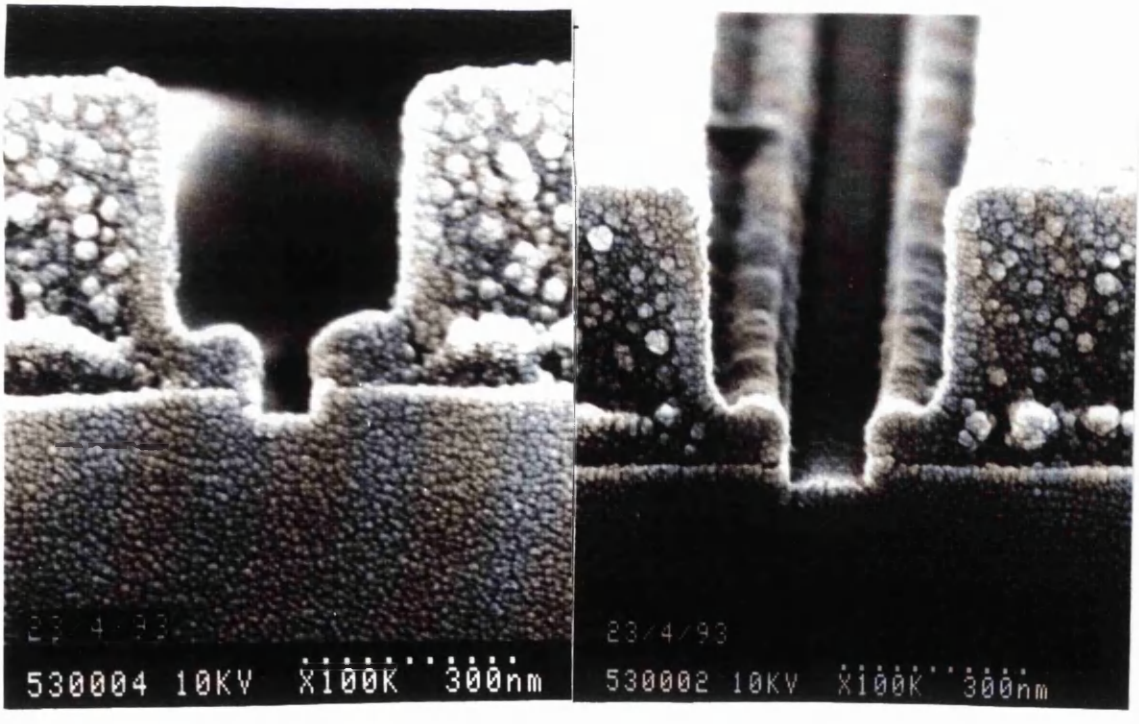

Fig.5.26: Cross-sectional view of T- gates etched in pure $SiCl_4$ plasma using the optimized conditions for high selectivity and high verticality. The conditions were; rf power of 12 W, flow rate of 6 sccm, pressure of 9 mtorr, dc bias of 40 - 60 V. The gate lengths are 60 for the left micrographs and 130 nm for the right.

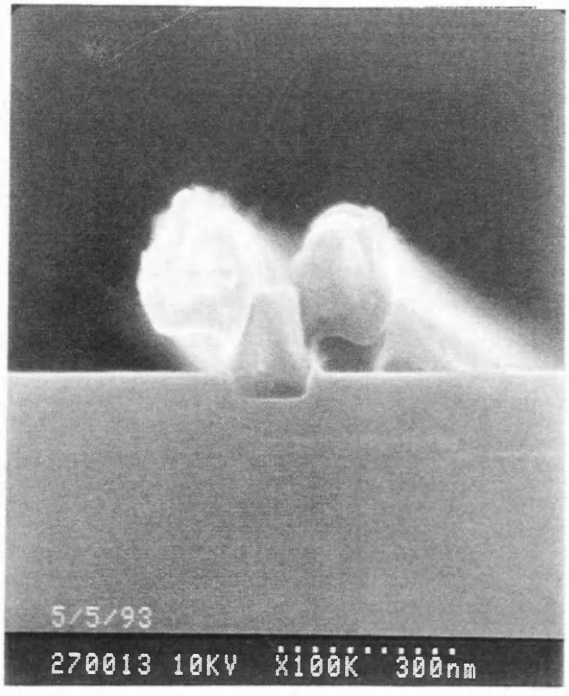

Fig.5.27: SEM micrograph of a T- gate after Metallization and lift off which shows that there is no gate off-set.

5.8.3 T-gate recessing in a mixture of $SiCl_4/SiF_4$ plasma

T- gate recess etching have been carried out in a mixture of $SiCl_4/SiF_4$ plasma using highly selective etching conditions which are: flow rate ratio of 2/9 sccm, pressure of 150 mtorr, rf powerof 12 W, 20-40 dc bias and the etching was for 2.5 minutes. The gate lengths varied between 120-310 nm. As shown in the SEM micrographs of fig.5.28, the etching stopped on the 5 nm thick AlGaAs layer after etching the 40 nm GaAs capping layer. As it can be seen the gates have a very wide lateral etching even though the etching was only for 2.5 minutes. The vertical etch rate is ranged from 145-175 nm/min for gate lengths of 120-320 nm. This means that the etching takes about 17 seconds to etch through the 40 nm GaAs capping layer for the gate length of 120 nm, whereas it takes 13 seconds for the gate length of 320 nm. These times are after subtracting the induction time in both cases which is about 15-20 seconds at these etching conditions. This results in a slightly wider gate off-set for the longer gates which can be seen in SEM micrographs of 5.28. However the difference in the gate off-set for gates $\leq$ 300 nm is very small and should not cause any problems regarding the fabrication of devices with various gate lengths on the same chip. The gate off-set for example of 120 nm long gate after 2 minutes overetching is about 240 nm whereas for a 320 nm gate length is about 285 nm. It is obvious that one can obtain shorter gate off-sets by minimizing the overetching time.

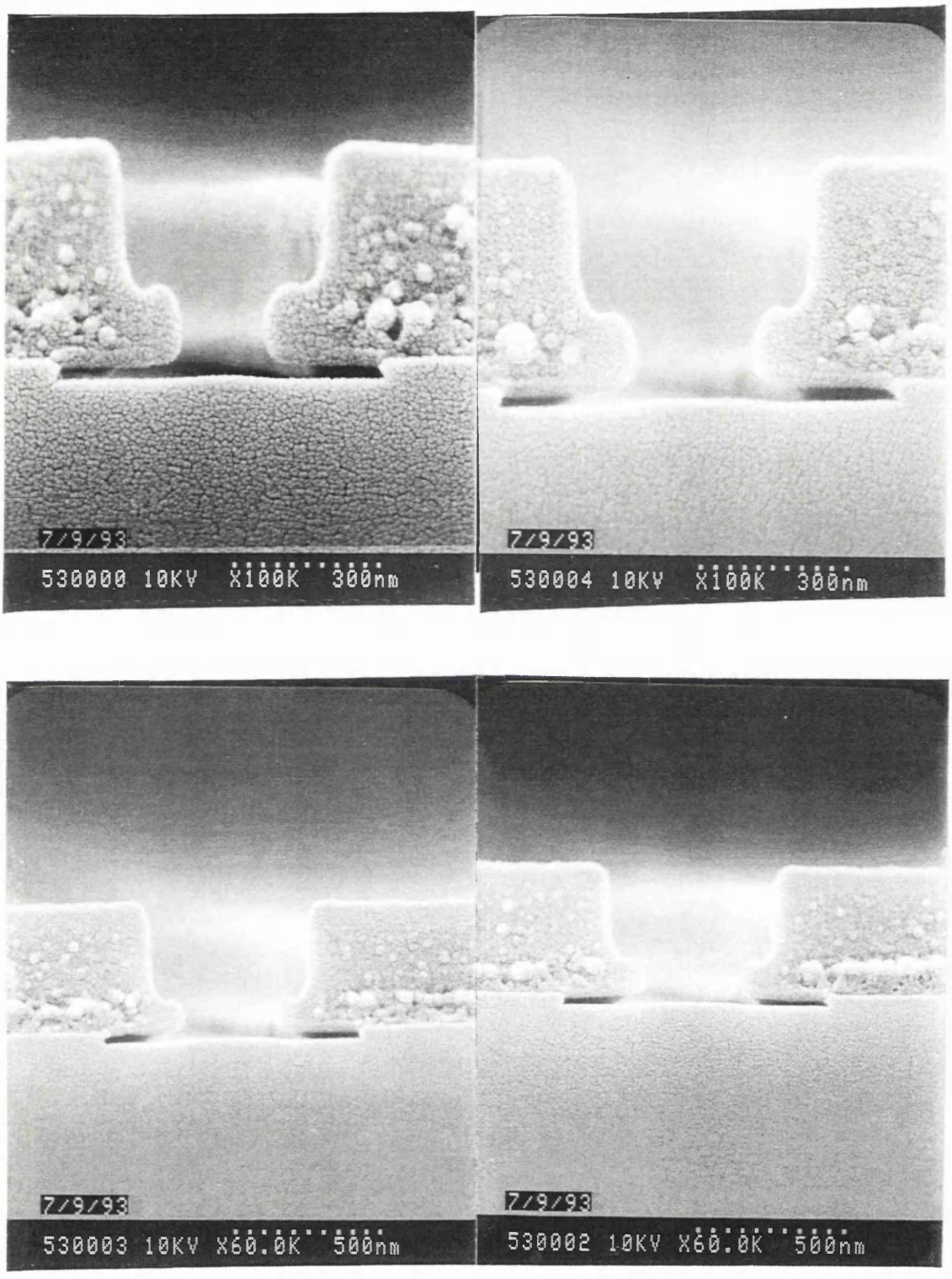

Fig.5.28: Cross-sectional view of different size T- gates etched in $SiCl_4/SiF_4$ plasma for 2.5 minutes using highly selective etching conditions of 2/9 sccm of flow rates, pressure of 150 mtorr, power of 12 W, and bias of 20-40 V. The lateral etching is slightly greater in longer gates due to microloading effect.

5.8.4 The ideal T-gate shape and comparison between gate recessing in $SiCl_4$ and $SiCl_4/SiF_4$ plasmas

The ideal T- gate shape is a gate with a very small gate off-set and with gate recess profile of 5-10 degree from the normal to increase the lift-off yield of the gate footprint, and a small off-set to decreases the gate leakage and at the same time is essential for making the effective gate length as short as possible. Such a shape is illustrated in fig.5.25. The gate recessing in pure $SiCl_4$ is very near the ideal gate shape, however the gate profile needs to be more undercut so as to provide small gate off-set. The etch profiles in pure $SiCl_4$ plasma are very sensitive to the pressure as discussed in chapter 4, section 4.4.3. At pressures of 20-25 mtorr the etch profiles were 15-20 degrees from the normal (see fig.4.9) which could be ideal for the gate recess shape. However the selectivity in pure $SiCl_4$ plasma at these pressures and for flow rates of > 4 sccm is not high ($\leq$90:1) see fig.5.5, therefore these conditions are not suitable for gate recessing. A possible answer to the problem of selectivity at high pressure of 20-25 mtorr is by lowering the $SiCl_4$ flow rate to $\leq$ 2 sccm, where the selectivity at 25 mtorr is about 500:1 which is sufficient for the gate recessing. However, the induction time using 2 sccm and 25 mtorr is very long, it can be as high as 2 minutes. Another possible answer is to use a mixture of $SiCl_4/N_2$ at pressures of $\geq$ 25 mtorr where the selectivity is very high ($\geq$ 2000:1), see fig.5.7. As stated earlier the etch profiles are about 15-20 degrees from the vertical and at the same time the selectivity is very high, making this process very attractive for use in gate recessing.

The gate recessing in a mixture of $SiCl_4/SiF_4$ plasma like all other fluorine dependent selective etching, results in a large gate off-set which has a serious implication on prolonging the effective gate length.

To summarise, an ideal T- gate shape may be obtained in $SiCl_4$ or $SiCl_4/N_2$ plasma which has a small gate off-set with recess profile of 15-20 degrees off the vertical. The gate recessing in $SiCl_4/SiF_4$ plasma has the disadvantage of a large gate off-set.

5.9 Chapter summary

In this chapter a new selective RIE process for etching GaAs/AlGaAs in pure $SiCl_4$ plasma has been developed, the selectivities obtained can virtually reach infinity at low pressures and low flow rates. Moreover this process is highly anisotropic. A new selective RIE process for GaAs/AlGaAs etching in $SiCl_4/N_2$ plasma has also been developed, the mechanism of selectivity maybe relying on the formation of Al_xN_y or Si_xN_y's. A highly selective etching in a mixture of $SiCl_4/SiF_4$ plasma has been realised in which the selectivities obtained are over a magnitude higher than the reported values in the literature for this etching system. Meanwhile the selectivity was found to be closely correlated to the chemistry of $SiCl_4/SiF_4$ plasma which was found to be fluorine dominated up to 25 % $SiCl_4$ in the discharge, a very complex chemistry between 30-50 % $SiCl_4$ and being

chlorine dominated for ≥ 50 % $SiCl_4$. T- gate recessing in pure $SiCl_4$ plasma has been successfully carried out resulting in a vertical gate recess profile and controllable gate off-set which can have a considerable advantage over the most common methods used in the literature which use the fluorinated chemistry at high pressure to selectively etch the GaAs/AlGaAs leading to an uncontrollable gate off-set.

5.10 References

5.1. J. Vatus, J. Chevrier, P. Delescluse, and J. F. Rochette, IEEE Trans. Electron Devices, **33**, 934, (1986).

5.2. A. Seabough, J. Vac. Sci. Technol., B **6**, 77, (1988).

5.3. C. M. Knoedler and T. F. Kuech, J. Vac. Sci. Technol., B **4**, 1233, (1986) .

5.4. K. Hikosaka, T. Mimura and K. Joshin, Jpn. J. Appl. Phys., **20**, L847, (1981).

5.5. K. L. Seaword, N. J. Moll, D. J. Coulman and W. F. Stickle, J. Appl. Phys., **61**, 2358, (1987).

5.6. A. A. Ketterson , E. Andideh, I. Adesida, T. L. Brock, J. Baillargeon, J. Laskar, K. Y. Cheng and J. Kolodzey, J. Vac. Sci. Technol., B **7**, 1493, (1989).

5.7. W. H. Guggina, A. A. Ketterson, E. Andideh, I. Adesida, S. Caracci and J. Kolodzey, J. Vac. Sci. Technol., B **8**, 1956, (1990) .

5.8. D. G. Ballegeer, S. Agarwala, M. Tong, K. Nummila, A. A. Ketterson and I. Adesida, J. Vac. Sci. Tecnol., B **11**, 618, (1993).

5.9. S. Salimian and C. B. Copper, J. Vac. Sci. Technol., B **6**, 1641, (1988).

5.10. S. Salimian, C. Yuen, C. Shih, C. Smith and C. B. Cooper, J. Vac. Sci. Technol., B **9**, 114, (1991).

5.11. S. J. Pearton, U. K. Chakrabarti, W. S. Hobson, and A. P. Kinsella, J. Vac. Sci. Technol., B **8**, 607, (1990).

5.12. S. Thoms, I. McIntyre, S. P. Beaumont, M. Al-Mudares, R. Cheung, and C. D. W. Wilkinson, J. Vac. Sci. Technol., B **6**, 127, (1988).

5.13. H. Arnot, S. R. Andrews, and S. P. Beaumont, Microelectronic Engineering, **9**, 365, (1989).

5.14. N. I. Cameron, S. Ferguson, M. R. S. Taylor, S. P. Beaummot, M. Holland, C. Tronche, M. Soulard, and P. H. Ladbrooke, J. Vac. Sci. Technol., B **11**, 2244, (1993).

4.15. S. K. Murad, S. P. Beaumont, and C. D. W. Wilkinson, Microelectronic Engineering, **23**, 357, (1994).

5.16. E. L. Hu and L. A. Coldren, in Proceedings of SPIE: Advanced Processing of Semiconductor Devices, edited by S. D. Mukherjee (The International Society for Optical Engineering,Vol.**797**, 1987).

5.17. S. Agrawala, and I. Adesida, Appl. Phys. Lett. **62**, 2830, (1993).

5.18. K. L. Seaward, N. J. Moll, and W. F. Stickle, J. Vac. Sci. Technol., B **6**, 1645, (1988).

5.19. Private communication with Dr. John Sullivan (Aston University, England)

2.20. R. Karcher, L. Ley, and R. L. Johnson, Physical Review, B **30**, 1896, (1984).

5.21. K. L. Smith, and K. M. Black, J. Vac. Sci. Technol., A **2**, 744, (1984).

5.22. J. A. Taylor, G. M. Lancaster, A. Ignatiev, and J. W. Rabalais, J. Chem. Phys. **68**, 1776, (1978).

5.23. M. Klasson, A. Berndtsson, J. Hedman, R. Nillson, R. Nyholm, and C. Nording, J. Electron. Spectrosc. Relat. Phenom. **3**, 427, (1974).

5.24. Properties of Aluminium Gallium Arsenide, edited by Sadao Adachi, (1993).

5.25. Masaaki Sato, H. Nakamura, A. Yoshikawa, and Y. Arita, Jpn. J. Appl. Phys., **26**, 1568, (1987).

5.26. Identification of Molecular Spectra by A. G. Gaydon and R. W. B. Pearse, 4th edition, 1976.

5.27. N. Mutsukura, M. Ohuchi, S. Satoh, and Y. Matchi, Thin Solid Films, **47**, 109, (1983)

5.28. Guy Turban, Pure and Applied Chemistry, **56**, 215, (1984) and references therein.

5.29. I. Thayne, PhD. Thesis, Glasgow University, (1993).

5.30. J. A. Adams, PhD. Thesis, Glasgow University, (1990).

5.31. N. I. Cameron, G. Hopkins, I. G. Thayne, S. P. Beaumont, C. D. W. Wilkinson, M. Holland, A. H. Kean, and C. R. Stanley, J. Vac. Sci. Technol., B **9**, 3538, (1991).

5.32. P. C. Chao, P. M. Smith, S. C. Palmateer, J. C. M. Hwang, IEEE Trans. Elect. Devices, ED **32**, No.**6**, 1042, (1985).

5.33. M. A. Thomson, L. M. Jelloin, L. D. Nguyen, and U. K. Mishra, J. Vac. Sci. Technol., B **8**, 1339, (1990) and references therein.

Chapter 6

Dry Etch Damage and Results

6.1 Introduction

The degradation of the electrical or optical properties of materials after reactive ion etching (RIE) is known as "dry etch damage". Over the past few years the dry etch damage has become one of the major issues concerning the application of RIE for device fabrication. The sources of damage in dry etching include: radiation damage by bombardment of ions, electrons and photons; contamination originating from deposition during etching or material sputtered from the etching chamber. However damage caused by ion bombardment is thought to be the most significant. Such damage introduces defects and traps of carriers by energy or momentum transfer from bombarding ions to the lattice, and so, in principle, can degrade the electronic properties of the material. Dry etching can also cause structural damage to the lattice, stoichiometric modification due to preferential etching or layer intermixing.

There are numerous studies in the literature [1-10] about dry etch damage, its effects on the material characteristics and the methods used to measure it. The dry etching can damage both the surfaces, and the sidewalls of the masked regions. The damage may be manifested in a variety of ways: in the reduced transconductance of MESFETs where gate recess etching has been carried out using RIE [1-2], in the degradation of Schottky barrier characteristics of metal to dry etched semiconductor surfaces [3-4], and in the reduced photoluminescence efficiency in optical materials by the generation of nonradiative centres [5]. In addition, damage to the etched sidewalls may inhibit the observation of quantum effects in nanostructures [6]. However, the degree of damage due to dry etching varies from plasma to plasma. Generally, the processing plasmas may be divided into three categories according to the nature and degree of the damage: (i) those containing hydrogen, (ii) inert gas plasmas, and (iii) reactive molecular gas plasmas which do not contain hydrogen. The effect of hydrogen containing plasmas on GaAs based materials, Si and InP based materials have been studied by many workers [11-15]. The consensus from these studies is that hydrogen leads to the reduction of the carrier concentration through the passivation of donors or acceptors by forming complexes associated with dopant atoms, and that these complexes can be broken up by rapid thermal annealing which restores the activity of the dopants. Moreover, hydrogen has been found at depths that are more than an order of magnitude deeper than the predicted values by the theory of Linhard, Scharf and Schiott

(LSS) [15] using the plasma dc bias as an estimate of the hydrogen ion energy. The behaviour of hydrogen is diffusive or may be channelled, however the lattice damage is not thought to be involved during the dopant deactivation by thermal annealing. Inert gas plasmas are often added to plasmas used for etching GaAs and related materials, and so it is important to assess the role they play in the damage. There is a large number of studies which have used ion beams and plasmas of He, Ne, Ar, and Xe to study the effects of ion mass and energy on semiconductor damage. The general conclusion on work on GaAs involving Schottky diodes,[16] Van der Pauw measurments,[17] Rutherford backscattering measurments,[18] and cathodoluminescence intensity [19] is that the carrier loss is proportional to the inverse of the ion mass. These studies also show that this type of damage is proportional to the plasma dc bias or ion beam accelerating voltage. In contrast to the damage caused by hydrogen, annealing of damage from inert ions does not recover the carrier loss.

The dependence of the damage in reactive ion etching plasmas which do not contain hydrogen or inert gases, on the ion masses and types is not an easy task because one can not differentiate between the effect of various molecular and atomic ions which exist in every plasma. However, it well known that the damage in these plasmas depends on the dc bias and that the material cannot be recovered to its original state by annealing.

Various methods have been adopted for reducing the dry etch damage by reducing the ion energies in the discharge while trying to maintain the integrity of etching, i.e., anisotropy, smooth surfaces, etc, as it was discussed in section 4.3. In chapter 4 and 5 we discussed the development of a very anisotropic RIE process for etching GaAs in $SiCl_4$ at low powers and low bias voltages and this process can also be selective or nonselective over AlGaAs. We have also shown a selective RIE process for etching GaAs in $SiCl_4/SiF_4$ at very low powers and bias voltages. In this chapter to assess these processes from the dry etch damage point of view, a comprehensive analysis of the damage in mainly GaAs after etching in $SiCl_4$ plasmas has been carried out using a variety of techniques. These techniques include: conductivity measurements on n^+- GaAs wires etched in $SiCl_4$ plasma for the measurement of the sidewall damage, Raman scattering measurements for surface damage assessment, Schottky, TLM, Van der Pauw, characterisation of MESFET performance after gate recessing, DLTS measurements and damage measurement using photoluminescence from multiple quantum wells (MQWs).

6.2 Sidewall damage and the Characterization methods

It is important to note that dry etch damage is not just limited to the vertically etched surfaces but occurs on the sidewalls of the masked regions too. In RIE and ECR-RIE, etc, while the surface may suffer damage from the direct bombardment of directional ions and reactive radicals, effects from nondirectional ions, reactive radicals, possibly

deposition and ricocheting particles from the bottom surface may account for the damage created on the sidewalls. However, the sidewall damage is more difficult to measure than the surface damage due to the impracticality of the device fabrication on the sidewalls. There are few methods to measure the sidewall damage such as the measurement of Schottky diodes characteristics made on the sidewalls, direct TEM observations of wires and conductance measurements of the narrow wires which relies on the determination of the cut-off width of the wires. R. Cheung and co-workers [20] have fabricated Schottky diodes on the sidewalls of etched structures as a method to assess the sidewall damage, however this method is complicated from the fabrication point of view. M. Foad [21,23] have used the direct Transmission Electron Microscopy to measure the sidewall damage on quantum wires fabricated in GaAs and etched in $SiCl_4$ plasma using $\leq$ 300 V bias and CH_4/H_2 plasmas using $\leq$ 800 V bias and hava concluded that there is a stoichiometry change near the edges of the wires in CH_4/H_2 etching which may be related to formation of point defects. Perhaps the most popular method for sidewall damage assessment is the conductance measurement of narrow quantum-like wires, a technique which was first reported by Thoms et.al. (1986)[23]. The principle behind this technique is that any damage in the wires will be manifest as a region of zero or low conductance. Therefore narrow wires with different widths are expected to show no conductance when the width of the wire is smaller or equal to twice the depletion depth of the sidewall which arising from the surface states at the air-GaAs surface plus the depletion caused by dry etch damage (details of this technique is given in the next section).

6.3 Characterization of "Sidewall damage" after RIE in $SiCl_4$ plasma

The sidewall damage measurement after RIE in $SiCl_4$ plasma has been carried out using the conductance measurement technique on narrow wires, fabricated in n^+- GaAs. First, we will describe the measurement method and then the fabrication procedure of narrow wires using the E-beam lithography.

6.3.1 The wire's conductance measurement technique

A wire is a rib of conducting material such as GaAs as shown in fig.6.1. The wires are usually formed from a thin epitaxial layer of heavily doped material, in this case n^+- GaAs on an undoped or p- type doped GaAs buffer layer, etched in a dry etching process, to give vertical and smooth sidewalls as much as possible.

The conductance of the wires is measured by applying current through the wires and measuring the voltage using a four terminal measuring technique. The measured value of conductance is related to the resistance of the wire and the depletion depths by the resistance formula: $R = \frac{\rho L}{A}$ (6.3.1).

From fig.6.1, the conducting cross-sectional area of the wire is,

$$A = (w - 2x_d)(t - x_0) \qquad (6.3.2)$$

Where t is the active epilayer thickness, x_d is the sidewall depletion depth, w is the wire width, and x_0 is the top surface depletion thickness due to air- GaAs interface. The conductance (G) of a wire of such a cross-sectional area as A, is given by:

$$G = \frac{w - 2x_d}{R_s L} \qquad (6.3.3)$$

Where L is the wire length and R_s is the sheet resistance of the epilayer which is given by;

$$R_s = \frac{1}{ne\mu(t - x_0)} \qquad (6.3.4)$$

Where n is the carrier concentration, e is the electron charge, and μ is the electron mobility. In practice R_s and the μ may be obtained from TLM and Van der Pauw measurements respectively.

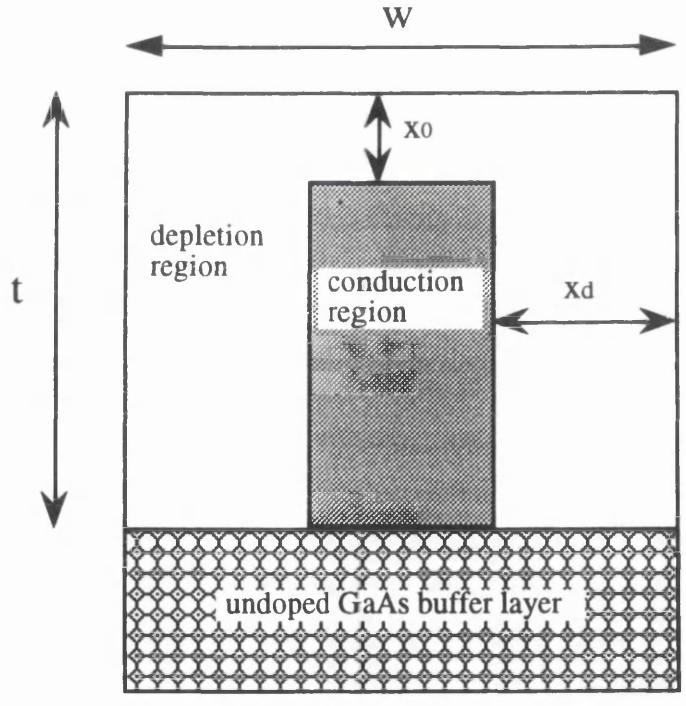

Fig.6.1: Cross-sectional area of the n^+- GaAs wire shows the conducting part and depleted part of the wire.

By measuring the conductance of wires of varying widths, a plot of conductance versus wire width is obtained. From such a plot, the cut-off width of the wire can be obtained by extrapolating the plot to zero conductance, since the cut-off width of the wire is the width at which the wire conductance should become zero. As the cut-off width of the wire is equal to $2x_d$ from Eq.6.3.3, one can obtain the value of x_d which represents the sidewall depletion thickness resulting from the depletion from surface states (x_0) plus the depletion resulting from dry etch damage (d_d), i.e. $x_d = (x_0 + d_d)$. (6.3.5)

For completely undamaged wires d_d is equal to zero, hence x_d is equal to x_0, theoretically x_0 is given by [24];

$$x_0 = \sqrt{\frac{2ef_s}{\varepsilon n}} \qquad (6.3.6)$$

Where $\varepsilon = \varepsilon_0 \varepsilon_r$ is the permitivity, and f_s is Fermi level, for GaAs, the Fermi level is pinned near the mid-gap at the surface, so $f_s = 0.7$ eV at room temperature.

In principle, knowing the value of x_d one can obtain R_s from Eq.(6.3.3) which can then be used in Eq.(6.3.4) to calculate the value of μ. For a well measured conductance, the values of μ, and R_s obtained from the conductance measurements should agree with those obtained by other methods.

6.3.2 Fabrication procedure of quantum-like wires.

The material used in the fabrication of wires was grown by MBE which consisted off: 100 nm thick, 4 x 10^{18} cm^{-3} Si doped GaAs active layer, 500 nm thick undoped GaAs buffer layer on a semi-insulating GaAs substrate. The fabrication was carried out as below:

1. Two (10 x 15) mm^2 samples were cut from the original wafer and processed. The samples were first cleaned in four step cleaning procedure by dipping and ultrasonic agitation for 5 minutes in trichloromethane, acetone, methanol and water successively, then blown dry with dry nitrogen.
2. A low molecular weight (85K), high sensitivity e-beam resist obtained from BDH, consisting of 15% of PMMA (Poly-Methyl Methacrylate) in Chlorobenzene, was spin coated at 5000 rpm for 60 seconds which gave a thickness of 1400 nm, oven baked at 180 °C for 2 hours.
3. Patterns for ohmic contacts and alignment marks were exposed using a Leica-Cambridge EPBG-5 HR e-beam writer operating at 50 kV.
4. The patterns were developed in 1:1 IPA : MIBK (Iso-Propyl Alcohol : Methyl Iso-Butyl Ketone) for 60 seconds at 23 °C.
5. Low resistivity ohmic contacts of (Au/Ge/Au/Ni/Au), thicknesses of (14/14/14/11/240) nm were evaporated using a Plassys MEB 450 evaporator and lift-off was performed in warm acetone. The ohmic contacts were then alloyed at 360 °C for 30 seconds.
6. Two layers of e-beam resists (low molecular weight 85 K, 4% BDH and high molecular weight 350 K, known as Elvacite with concentration of 4% in Chlorobenzene) were successively spin coated at 5000 rpm for 60 seconds to yield a total thickness of about 200 nm, then oven backed for 2 hours at 180 °C.
7. Wire patterns 10 μm long with widths ranging from 55-600 nm were exposed using e-beam writer and subsequently developed in 2.5:1 IPA : MIBK for 60 seconds at 23 °C.

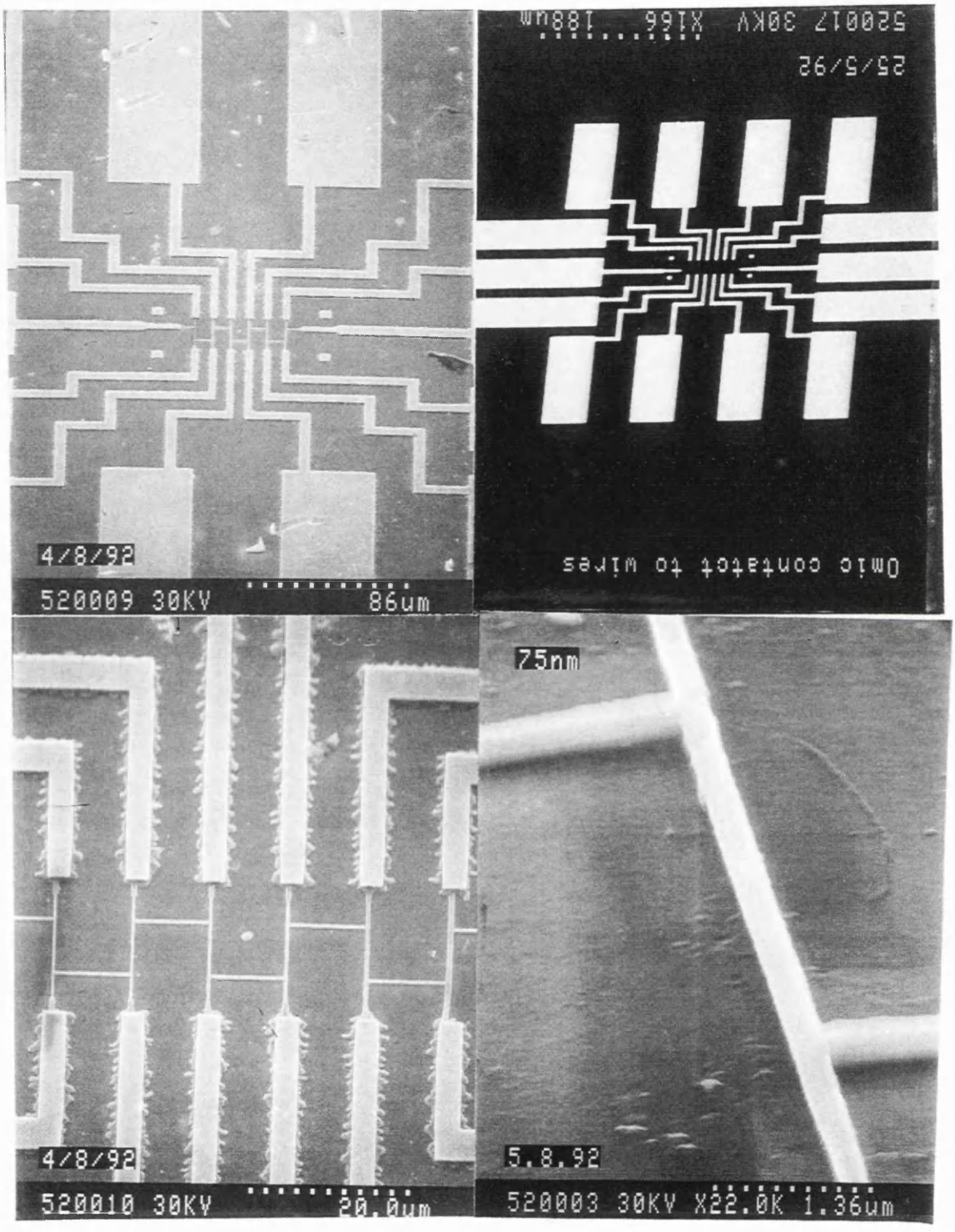

Fig.6.2: SEM micrographs of wires with the ohmic contacts. Top, shows the ohmic contact patterns and the bottom show a single wire.

8. Finally NiCr 30 nm thick was evaporated on one of the samples while a 30 nm thick SrF_2 doped with AlF_3 was evaporated on the other, so any differences between the NiCr and SnF_2 as a mask for small structures could be found. Lift-off was performed in warm

acetone to act as a dry etch mask. Each sample was then cleaved into 6 pieces and each piece was inspected using an optical microscope. The total number of wires fabricated exceeded 250. The whole pattern of the wires is shown in the SEM micrographs of fig.6.2.

6.3.3 Results of sidewall damage from wires etched in $SiCl_4$ plasma

Different samples with wire width ranging from 55-600 nm were etched for 2, 3, and 5 minutes using $SiCl_4$ plasma at low power of 15 W (0.06 W/cm^2), dc bias of 40-70 V, flow rate of 6 sccm and pressure 9-10 mtorr (in the low power regime and with the optimized conditions for high verticality, see chapter 3 and 4), also for 2 minutes using power of 40 W, (0.2 W/cm^2, the high power regime) dc bias of 200 V, flow rate of 6 sccm, pressure of 9 mtorr. The samples with NiCr mask were rinsed in 1:1 HCl : H_2O for 3 minutes to remove the NiCr, whereas the samples with SrF_2 were rinsed in H_2O for 5 minutes with ultrasonic agitation which was found to be sufficient for the removal of SrF_2. The conductance of the wires was then measured (in the dark) by applying current through the wires and measuring the voltage using four terminal measuring technique and Hewlett - Packard 4145B semiconductor parameter analyzer. Since the wires are rarely of uniform width due to various lithographic reasons, a single measurement is not sufficient to determine the wire width. Therefore, the width of the wires was taken as an average of 11 measurement made along the 10 μm length of the wires in 1 μm steps using the Hitachi S900 SEM.

In fig.6.3, the conductance of the wires is plotted as a function of width and since the measurements lay on straight lines, we can determine the cut-off width of each line by extrapolating it to zero conductance. The cut-off width of wires etched at 40-70 V for 2 min was 32 nm, for 3 min it increased to 40 nm and for 5 min was increased to 54 nm. These etches correspond to depths of 120, 230, and 430 nm, respectively. While the cut-off width of wires etched at 200 V for 2 min was 66 nm. Therefore the sidewall depletion depths (x_d) for wires etched at 40-70V for 2, 3, and 5 min are 16, 20, and 27 nm. On the other hand the sidewall depletion depth for wires etched at 200 V for 2 min is 33 nm. The value of x_0 (depletion due to surface states) can be calculated using Eq.6.3.6 which is found to be 15 nm. This means that the value of d_d (depletion due to dry etch damage) from Eq.6.3.5, for wires etched at 40-70 V for 2 min is only 1 nm/sidewall, for 3 min is 5 nm/sidewall and for 5 min etching the depletion was increased to 12 nm/sidewall. For the wires etched at 200 V and for 2 min the value of depletion due to dry etch damage was increased to 18 nm/sidewall. From these results it seems that exposing the sidewalls to the plasma for longer times, the damage on the sidewall has an accumulating effect. These results also suggest that the dc bias and hence the ion energy have a significant effect on the sidewall damage. However the amount of damage in the wires etched at low power of 15 W, bias of 40-70 V and for 2-3 min is significantly lower than most reported damage values in the literature [25]. Rahman [26] and co-workers for example, have shown that the

cut-off width of wires etched at 280 V dc bias has increased from 60 nm to 250 nm for an increase in the etching time form 30 to 90 sec. Therefore the above results are a clear indication that the etching process we have used is capable of producing a very low damage etching, while maintaining vertical walls and smooth surfaces (see chapter 4 concerning the verticality of the this process).

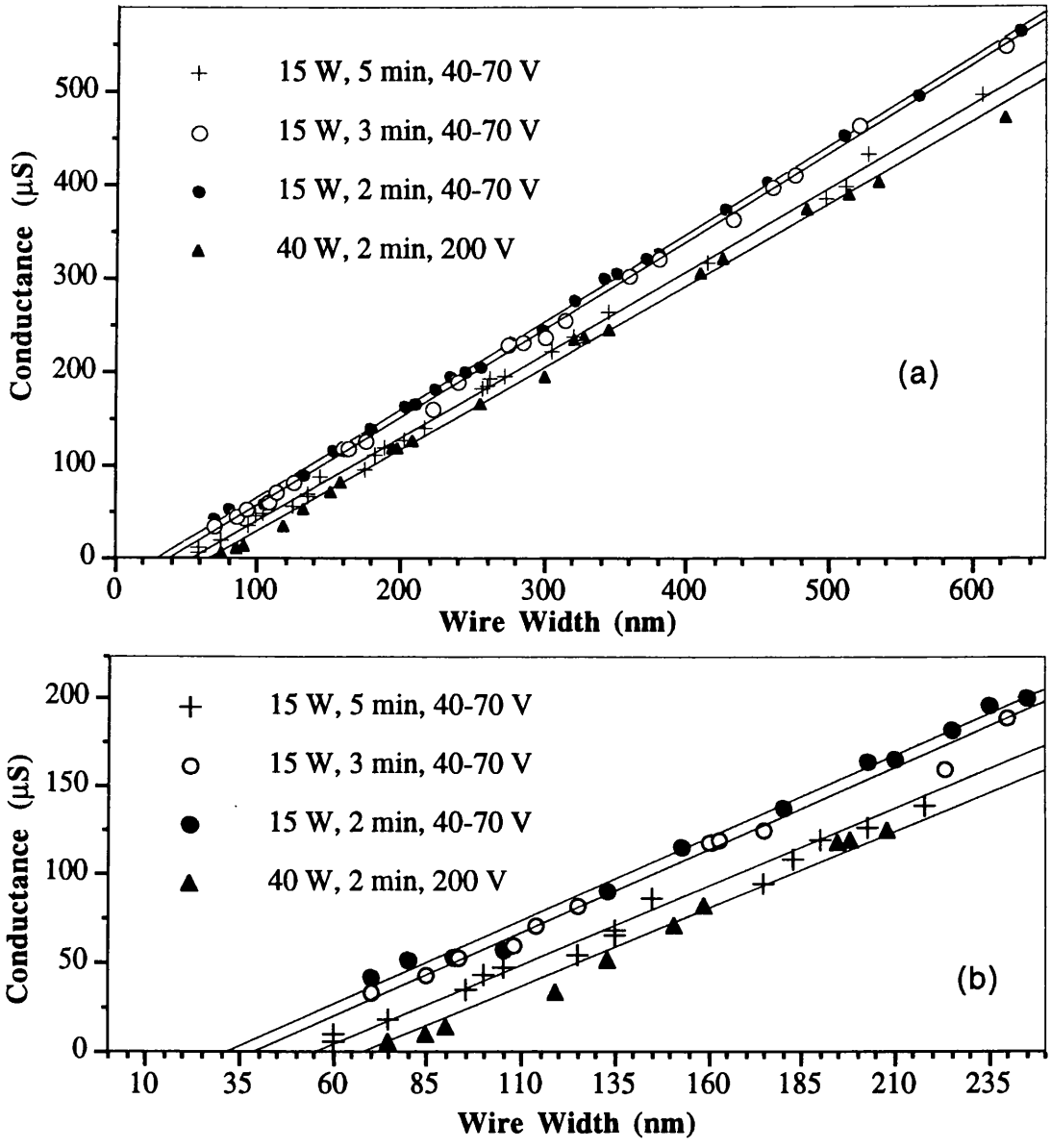

Fig.6.3: Conductance of the wires versus wire width for 2, 3, and 5 min etching at 40-70 V dc bias and for 2 min at 200 V bias. The etching was with $SiCl_4$ using a flow rate of 6 sccm and pressure of 8-9 mtorr, a; full data, and b; cut-off details.

The mechanism by which the damage is lower when low dc bias is used is not very clear, however it is likely that low voltage across the sheath in the plasma produces less energetic ions and hence less momentum transfer to the lattice upon collision. It is interesting to note

that low damage etching condition occurs in a plasma chemistry which has significant differences from the chemistry at which high damage occurs. In sections 3.3 and 4.3, it was found that the principal ions in the plasma and the dependence of etching mechanism at which low damage occur (rf power of 10-15 W) are Cl_2^+ ions. The principal ions and the dependence of etching mechanism at which high damage occur (rf power of ≥25 W) are Cl^+ ions. Therefore it seems likely that the ion masses in both cases play an important role in determining the extent of damage. In the low damage case, as the Cl_2^+ ion is twice as heavy as the Cl^+ ion and at the same time is accelerated to a lower voltage or bias therefore produces minimum damage to the lattice. In the high damage case, rf power of ≥ 25 W, as Cl^+ is half of the mass of Cl_2^+ and it is accelerated to higher bias, therefore, it is likely it will cause more damage. However, the mechanism by which lighter ions cause more damage that the heavy ones is not clear. Therefore it seems that the dominant ions in the plasma or the plasma chemistry has a significant role in determining the extent of damage.

6.4 Surface damage, and the characterization methods.

The surface of dry etched materials is under direct bombardment of ions which are accelerated by the plasma sheath or the dc bias, therefore it is likely it will suffer most. Dry etch induced damage on the surface can be both structural and electronic. The structural damage can occur in the form of surface roughness, lattice damage due to ion bombardment, or through the formation of vacancies and interstitials and their diffusion. More severely, as in the case of ion implantation processes where energetic ions of tens or hundreds of keV are used, polycrystalline and amorphous layers can be formed.

The electronic damage is mainly manifest as electronic traps which can reduce or deplete the free carriers in the material. Perhaps one of the most critical aspects of the damage in the dry etched surfaces is in devices that use very thin epitaxial layers such as MESFETs or HEMTs which consist of an etch stop layer within or on top of the active layer. As selective etching is required for these devices, any amount of damage is very significant because the damage will have a cumulative effect as the same active layer is being bombarded after the etching stop on the etch stop layer.

There is a host of methods to observe or measure the dry etch surface damage: surface science methods such as XPS (X-ray photoelectron spectroscopy), Auger spectroscopy and low angle X-ray scattering, electrical methods based on the characteristics of semiconductor-metal junctions or by the measurement of electrical properties of thin epitaxial layers, and optical methods such as photoluminescence and Raman spectroscopy. Each one of these methods has some advantages and disadvantages concerning the accuracy, the type of data it can provide and the ease of applicability. The surface science methods are mainly concerned with surface stoichiometric modification of the etched surfaces, such as polymer formation during etching, elemental deficiency due to

preferential removal of one element of the lattice over another. These methods can detect structural damage to the lattice, therefore they can be used for characterization of the surface damage in the bulk doped or undoped materials. The electrical techniques used to study the surface damage are Schottky diodes, TLM (Transmission Line Model), Van der Pauw, DLTS (deep level transient spectroscopy) and the recently reported [28] method of conductance measurement of the surface as a function of etch depth which is similar to the wire cut-off method in sidewall damage measurement. However unlike the damage on sidewalls, as the surface is constantly removed or etched, the degree of damage has been reported [27] to be constant with etching time after an initial rise in the beginning of the etching.

The Schottky, TLM and Van der Pauw methods do not provide information on the nature or the physical extend of damage, and they are also not sensitive when a bulk or a thick epitaxial layers are involved. However these methods are sensitive to any damage in thin epitaxial layers especially when selective etching is involved as they can provide if combined a wealth of information on the electron mobility, sheet resistivity, sheet carrier concentration, barrier height, etc, therefore any damage in such layers is easily observed and measured. On the other hand, DLTS measurements can provide information on the concentration, activation energy and profile of the deep level defects and electron traps created by dry etch surface damage. For example Johnson et.al. and co-workers [29], have reported to have resolved five distinct defect levels in n^+- GaAs after RIE in $SiCl_4$ plasma, these were labelled N1-N5 which were majority carrier (electron) traps Measurements of the defect density showed a near exponential dependence with depth for most of the traps. However DLTS measurements were not capable of detecting the very shallow traps. The optical techniques used for damage assessment (Raman scattering and photoluminescence) can provide information about the bulk as well as thin epitaxial layers and can also provide information about the electrical or structural and optical damage. However to have a complete understanding of the damage from any etching process, the damage assessment has to be carried out using at least three techniques from those discussed above. In this work, the damage due to $SiCl_4$ RIE at low power and bias has been studied using the optical method of Raman scattering and various electrical methods such as TLM, Van der Pauw, Schottky contacts, and characterization of MESFET performance. The damage from RIE in $SiCl_4/SiF_4$ plasma has been carried out using Van der Pauw and Raman scattering. The results and discussions are given in the following sections.

6.4.1 Surface damage measurements using Raman scattering

Raman scattering is a very useful tool for the investigation of any structural or electrical damage on the surface region caused by dry etching through the examination of the shifts and broadening of the phonon peaks [30]. It has been used by many workers to

investigate RIE damage on undoped and doped GaAs material [31,32]. Study of the plasmon peaks can yield information on the electrical properties of doped materials, such as carrier concentration, electron mobility, and depletion layer depth [32,33]. In addition the Raman scattering is contactless, nondestructive and has been demonstrated to be a powerful in situ technique, as it can be used for studying the etch damage without exposing the material to air.

6.4.1.1 The theory of Raman scattering of coupled phonon-plasmon modes

The Raman spectrum of the GaAs is well documented [34]. The features arise from the interaction between the electromagnetic field of the incident laser light and the variation in the crystal potential caused by the quantized vibrations (phonons). The dominant features of the Raman spectrum of the undoped GaAs are the longitudinal optical (LO) phonons and the transverse optical (TO) phonons which occur at 292 cm^{-1} and 269 cm^{-1} respectively. Raman group-theoretical selection rules determine whether the peaks are observable for any given scattering geometry. The selection rules for cubic crystal of T_d symmetry (such as GaAs), in backscattering geometry, show that only LO phonons are allowed to scatter; the TO scattering mode is forbidden by symmetry. In undoped semiconductors such as GaAs, for the (100) surface, these rules are usually obeyed very well for undamaged material, where the scattering from LO modes is observed but not from TO [31]. However in damaged material such as dry etched and undoped GaAs both the TO and LO modes are usually observed, indicating that the crystal damage (dry etch structural damage) has destroyed the selection rules [30].

In highly doped semiconductors such as GaAs, Mooradian and co-workers [34] were first to show that it is possible to observe coupled LO phonon plasmon modes using Raman scattering. The frequencies of the coupled mode are: a low frequency mode L_1 and a high frequency mode L_2. These frequencies can be obtained by solving Drude expression for dielectric function of the electron system $\varepsilon(\omega)=0$, for longitudinal modes, [35]

$$\varepsilon(\omega)=\varepsilon_\infty\left\{\frac{\omega^2-\omega_L^2}{\omega^2-\omega_T^2}-\frac{\omega_L^2(q)}{\omega^2}\right\}, \qquad (6.4.1)$$

Where ω_L and ω_T are the LO and TO phonon frequency, respectively. ε_∞ is the high frequency dielectric constant, and $\omega_p(q)$ is the wave vector dependent on the plasma frequency which is given by, [27]

$$\omega_p^2(q)=\frac{Ne^2}{\varepsilon_0\varepsilon_r m^*}+0.6q^2v_f^2 \qquad (6.4.2)$$

The wave vector q of the plasmon-phonon mode, for back scattering configuration, is equal to $q=2\nu n$, where v is the wave vector of the excitation light, n is the refractive index of the material at the excitation frequency, and N is the carrier density. ε_0 is the vacuum

dielectric constant, ε_r is the static dielectric constant of the material, m^* is the electron effective mass of the material, and v_f is the Fermi velocity.
For low values of q, the term $0.6q^2v_f^2$ in Eq.6.4.2, is negligible and ω_p is independent of q in three dimensional system. For GaAs the plasma frequency varies from 100 cm^{-1} to 700 cm^{-1} for doping concentration between 10^{17} to 10^{19} cm^{-3}. In heavily doped materials the position of L_1 approaches the TO phonon frequency (269 cm^{-1} for GaAs at room temperature) with longitudinal characteristics, and it depends only weakly on the carrier concentration. The position of L_2 is closer to the plasma frequency and shifts strongly to higher frequency or energies if the carrier concentration is increased. Therefore this allows an independent determination of the carrier concentration [35].
The unscreened LO phonons can also be detected in n^+- GaAs by Raman scattering due to the presence of surface depletion layer. Assuming an abrupt change of carrier density from the depletion region to the bulk region, then one should be able to calculate the thickness d of the surface depletion layer, from the integrated intensity *I(LO)* of LO phonons compared to the LO phonon intensity $I_0(LO)$ of undoped or semi-insulating GaAs substrate (n< $1x10^{14}$ cm^{-1}) [36], i.e.,

$$I(LO) = I_0(LO)(1 - e^{-2\alpha d}), \qquad (6.4.3)$$

where α is the absorption coefficient of GaAs at the excitation frequency. Therefore the intensity of the LO phonons decreases as the doping concentration increases. Assuming $I(LO) - I_0(LO)$ is proportional to the intensity of the coupled LO phonon-plasmon intensity $I(L_1)$, one can get:

$$\frac{I(LO)}{I(L_1)} = \beta(e^{2\alpha d} - 1), \qquad (6.4.5)$$

where β is the scattering constant given by

$$I_0(LO) - I(LO) = \beta I(L_1) \qquad (6.4.5)$$

The relative change in the intensity between L_1 and the unscreened LO modes reveals information about the depletion layer thickness, which in turn is related to the damage caused by dry etching. On the other hand, the unscreened LO mode itself provides information about crystal quality in the depletion region. [37,38]

6.4.1.2 Experimental

The surface damage in GaAs samples from RIE in $SiCl_4$ plasma and $SiCl_4/SiF_4$ plasma has been measured using Raman scattering. The damage has been studied in terms of depletion depth, since it is associated with etch induced electronic traps as discussed earlier. The samples used were Si doped, 4.4 x 10^{18} cm^{-3}, 1 μm thick GaAs active layer on 500 nm thick undoped GaAs buffer layer, grown by MBE on semi-insulating (100) GaAs substrate. In the case of $SiCl_4$ plasma the etching was carried out using a low power of 12-

15 W (0.06 W/cm^2), a dc bias of 40-70 V, a pressure of 9-10 mtorr and flow rate of 6 sccm (the same conditions used in sidewall damage measurements) and various samples were etched for different depths and times. In $SiCl_4/SiF_4$ plasma, the etching was carried out at a power of 12 W, a dc bias of 15-35 V, a flow rate ratio of 2/9 sccm and a pressure of 150 mtorr. Again, various samples were etched for different depths and times.
The Raman scattering experiments were carried out at room temperature using the 514 nm and 488 nm lines of an Ar ion laser. The absorption coefficients [39] of this laser at these wavelengths in GaAs are 7 x 10^4 cm^{-1} and 1.27 x 10^5 cm^{-1} which correspond to penetration depths of 105.2 nm and 78.8 nm respectively. The scattered light was dispersed by JY-U1000 1 m double spectrometer and detected by cooled GaAs photomultiplier or an Astromed multichanal system using a charge coupled device. There are two important limitation concerning the analysis of Raman scattering in dry etched GaAs. One is that the Raman scattering cannot probe damage at a greater depth than the penetration depth of the laser line. Therefore by employing the 488 nm laser line, the maximum damage depth assessable is about 80 nm. Second is that the thickness of the epitaxial layer remaining after etching must be greater than the laser line penetration depth so the Raman scattering does not probe the substrate volume.

6.4.1.3 Results of Raman scattering in GaAs after RIE in $SiCl_4$ plasma

In fig.6.4 the Raman spectra of GaAs recorded at room temperature as a function of etch depth and etching time. The etching was carried out in a $SiCl_4$ plasma using the conditions mentioned earlier with an etch rate of about 110-100 nm/min. The Raman scattering was carried out using an Ar laser at 514 nm. As it can be seen from fig.6.4, both the unscreened LO phonon and L_1 modes are detected and it is evident that the relative intensity of LO has increased very slightly from the control sample compared to that of 8 minute etching. This indicates that the change in the depletion layer thickness after RIE in $SiCl_4$ plasma is very small. To quantify the change in the depletion layer after RIE, the surface depletion layer thickness was calculated in every sample using the Eq.6.4.3-5 discussed in the last section. The surface depletion layer thickness of the control sample (unetched) was found to be 11±1 nm which in agreement with theoretical value calculated using Eq.6.3.6 (see section 6.3.1). The depletion depths as measured from Raman scattering as a function of etch depth is shown in fig.6.5a. It is clear that the depletion depth, and hence the damage, increases very slowly and saturates with a constant depletion depth of about 20 nm. This corresponds to a total etch depth of 320 nm and it also corresponds to an etching time of 4 min as shown in fig.6.5b.

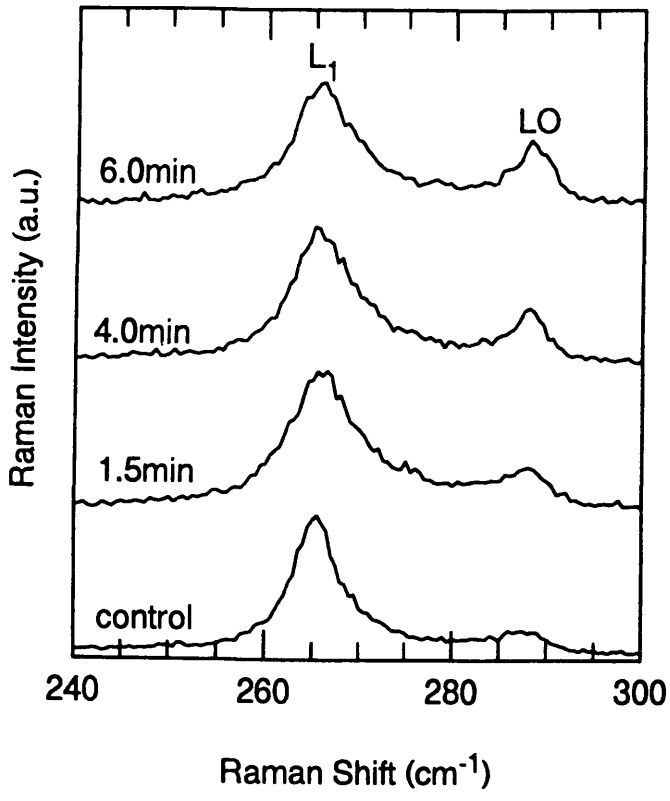

Fig.6.4: Raman spectra of GaAs as a function of etch depth and etching time. The etching was carried out in $SiCl_4$ plasma using the optimized conditions of high verticality (12-15 W, 6 sccm, 9-10 mtorr, 40-70 V dc bias).

These results suggest that the damage caused to the material surface due to RIE in $SiCl_4$ plasma using the above conditions is negligible in the first 3 minutes, then increases very slowly and saturates after 4 minutes of etching at a damage depth of about 7-8 nm. The saturation of the surface damage after an initial rise in the beginning has been reported previously [27]. The amount of damage on the surface obtained using Raman scattering is slightly higher than that obtained from the sidewall measurement. This is likely to be due to the fact that damage mechanism on the sidewalls is different from that on the surface. The damage on the sidewalls tends to be accumulative as the sidewalls are exposed to the plasma constantly, whereas the damaged layer on the surface is removed by etching in a continuous cycle and what we measure is a residual damage. To summarise, the results of damage measurements using Raman scattering on GaAs samples etched in $SiCl_4$ plasma at low power and bias clearly shows that the surface damage is very small and that no damage occurs at all in the first 2 min of etching, the damage for longer etching times saturates after about 4 min of etching .

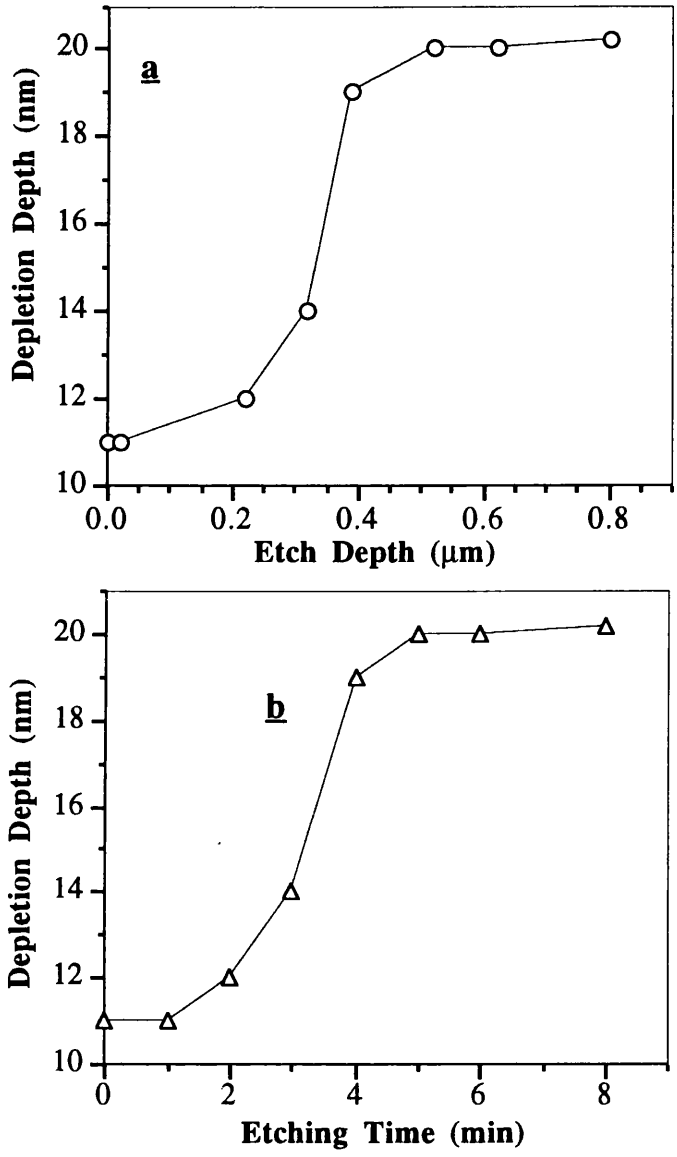

Fig.6.5: Depletion depth of GaAs as a function of (a); etch depth and (b) etching time. The etching is in $SiCl_4$ plasma using the optimized conditions of 12-15 W powers, dc bias of 40-70 V, flow of 6 sccm and pressure of 9-10 mtorr. The depletion depth increases very slowly and saturates after 4 minutes of etching and 320 nm etch depth.

6.4.1.4 Results of Raman scattering in GaAs after RIE in $SiCl_4/SiF_4$ plasma

Surface damage assessment of GaAs after RIE in $SiCl_4/SiF_4$ plasma has been carried out using the Raman scattering. The etching condition were 12 W of rf power, flow rates of 2/9 sccm and a pressure of 150 mtorr, which results in a dc bias of 15-36 V only. Using these parameters the etching of GaAs/AlGaAs is very selective (see chapter 5). In fig.6.6 the spectra Raman scattering of GaAs at room temperature for various etch depths and etching times are given. It is evident from fig.6.6, that the changes in the signal intensity from both the LO and L_1 are very small; however by a careful comparison of the

intensity ratio of L_1/LO from the spectra shows that the etched samples have higher ratios than the control sample (the unetched sample). This suggests that after etching the original surface layer and as much as 670 nm from the surface or 6 min etching time, the depleted region has been reduced. The surface depletion region was reduced from 11 nm to 9 nm after etching as shown in fig.6.7.

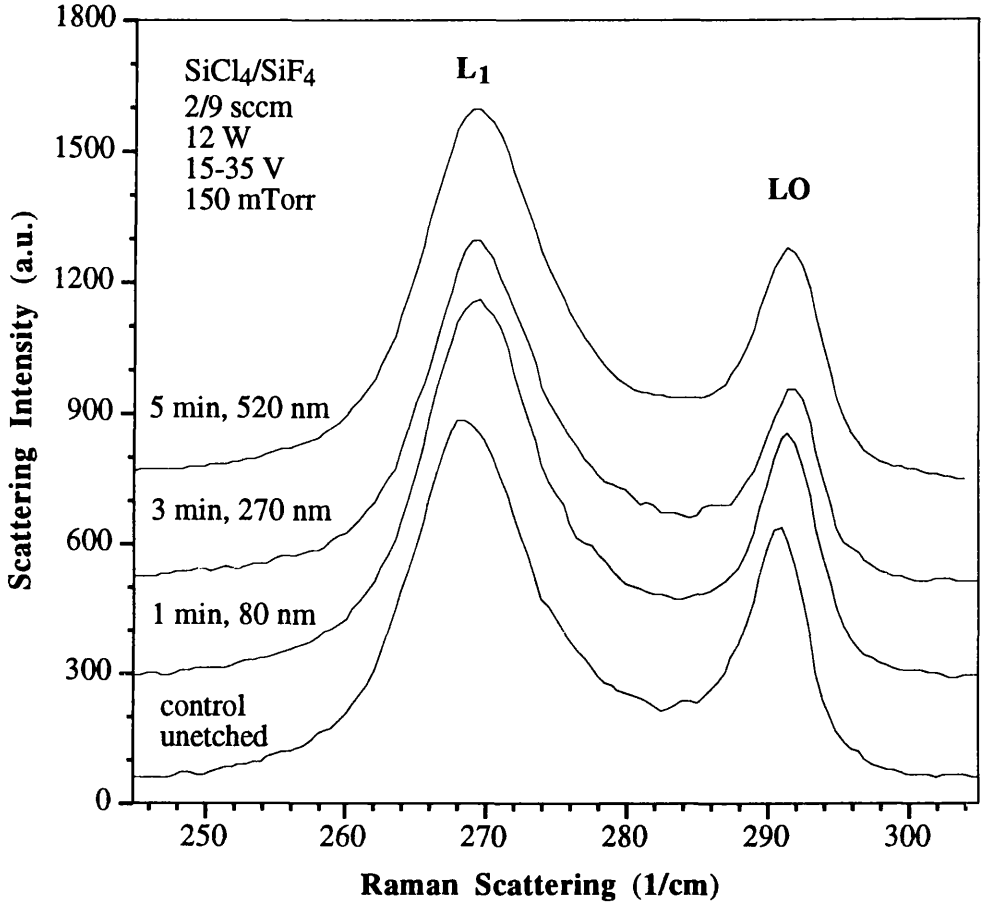

Fig.6.6: Raman spectra of GaAs as a function of etch depth and etching time, the etching was carried out in $SiCl_4/SiF_4$ plasma using selective etching conditions of a power of 12 W, a flow rates of 2/9 sccm a pressure of 150 mtorr and dc bias of 15-35 V.

This is in contrast to the results obtained during RIE in $SiCl_4$ from the last section and indeed it is in sharp contrast to all the reports in the literature regarding RIE [27-35]. The possibility that the RIE in $SiCl_4/SiF_4$ plasma which uses very low bias at high pressure is "damage free" and therefore can reduce the original surface defects by removing surface contaminations is not ruled out. Similar behaviour has been reported,[27] when wet etching was used which led to the increases in the ratio of L_1/LO implying that the surface depletion region has been reduced. The authors have attributed this to the removal of contamination by wet etching, on the other hand the wet etching has been reported to lead to formation of

residues on the surface. The mechanism by which the RIE in $SiCl_4/SiF_4$ leads to the reduction of the surface depletion region according to the above results is not clear. One of the possibilities is that Raman scattering method of damage assessment is not sensitive enough in case of low damage. Diffusion of Si, Silicon fluorides and Silicon chlorides into the surface at such low bias and at low temperature is unlikely and in any case diffusion leads to severe modification of the material and introduces defects, hence diffusion can be ruled out. The deposition of some form of conducting polymeric deposits from the plasma may act as a protecting layer for the surface. To judge whether the RIE in $SiCl_4/SiF_4$ can really be "damage free", damage assessment using Van der Pauw technique was made on samples consisting of thin and highly doped epitaxial layer containing an etch stop layer, therefore any damage on the surface will accumulate with time as the same surface is bombarded. The results are given in the next few sections.

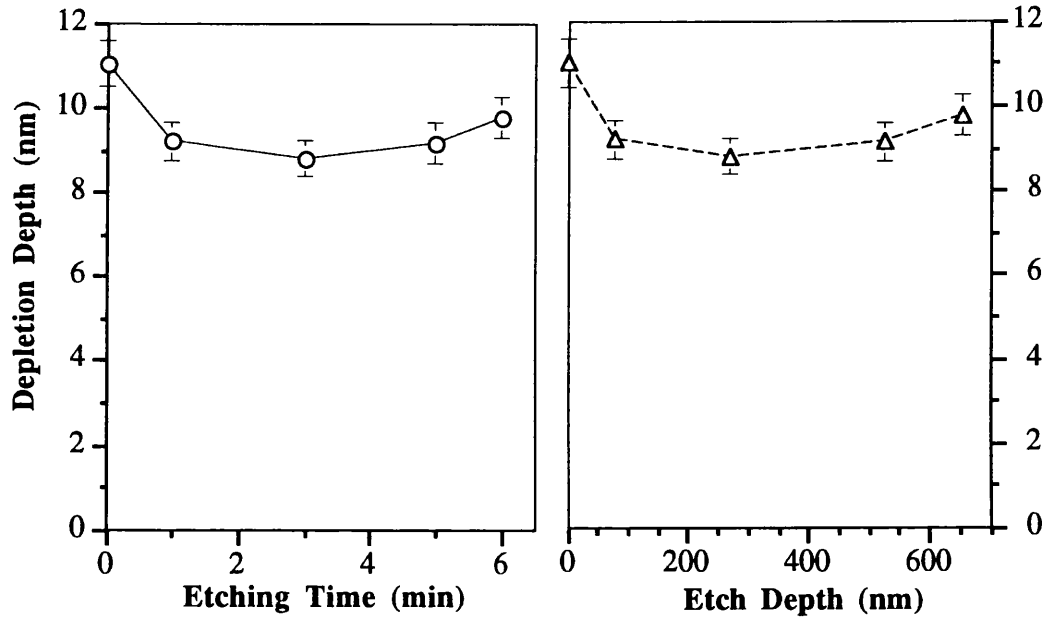

Fig.6.7: Depletion depth of GaAs as a function of etch depth and etching time as derived from the Raman scattering measurements. The etching is carried out in $SiCl_4/SiF_4$ plasma using 12 W, 2/9 sccm, 150 mtorr and 15-35 V.

6.4.2 Characterization of surface damage using Van der Paw, TLM and Schottky diodes on thin GaAs layers with AlGaAs etch stop layer

Damage to semiconductor materials caused by dry etching has frequently been evaluated by examining the electrical characteristics of Schottky diodes or electrical characteristics derived from Transmission Line Model (TLM) and Van der Pauw structures. These measurements are usually made on bulk, heavily or moderately doped semiconductors such as GaAs. The dry etching of bulk material will lead to the creation of

a damaged layer, however this layer will be continuously removed, hence the damage on the surface of the bulk layer does not accumulate. Therefore one cannot evaluate fully the degree of damage which has occurred nor the damage due to prolonged etching or overetching, especially if the damage was low, as in the case of $SiCl_4$ etching given in the last few sections. Therefore etching to a preknown etch depth by using selective etching and continuously bombarding the thin and nonetchable layer, is a better way to measure the damage caused to the underlying layers. In this method however, the etching has to be highly selective as in the case of GaAs/AlGaAs/GaAs materials using $SiCl_4$ or $SiCl_4/SiF_4$ plasmas. The damage caused by overetching, to the thin GaAs layers directly under the nonetchable and usually very thin AlGaAs layer can be determined easily by fabricating TLM, Van der Pauw and Schottky diodes on materials with such a composition.

6.4.2.1 The Transmission Line Model

A simple method for the electrical characterization damage due to RIE is the Transfer Length Model or Transmission Line Model (TLM). The method was first reported by Shockley for ohmic contact characterisation then developed by others. In the TLM method a line of ohmic contacts with an increasing separation is formed and if the resistance between adjacent contacts is plotted against the separation distance, then the resulting straight line has as its slope the sheet resistance of the semiconductor layer and the intercept at zero separation is the contact resistance of the ohmics. The contact resistance is usually expressed in Ωmm and the sheet resistance in Ω/sq, both of which can be determined this way. The structure used in this study comprised ohmic contact pads with areas of 30 x 30 μm^2 or 100 x 100 μm^2. The ohmic contacts were separated by gaps between 1.5 μm and 25 μm.

6.4.2.2 The Hall effect

The Hall effect was discovered by Hall in 1879 when he investigated the nature of the force acting on a conductor carrying a current in a magnetic field. Hall found that a magnetic field applied to a conductor perpendicular to the current flow produces an electric field (Hall field or Hall voltage) perpendicular to both the magnetic field and the current.

In n-type semiconductors the Hall theory predicts the Hall coefficient R_H as

$$R_H = -\frac{r}{qn} \qquad (6.4.2.1)$$

This equation shows that a knowledge of the Hall coefficient leads to the determination of the carrier concentration n per unit area or volume, q is electron charge and r is assumed to be unity.

The Hall voltage V_H is correlated to Hall coefficient through the formula

$$R_H = \frac{tV_H}{BI} \qquad (6.4.2.2),$$

where t is the layer thickness, I is the current, and B is the magnetic field. The active layer thickness is not the total layer thickness, but it is the thickness of the layer after taking into account the depletion depth of the layer.

The theoretical foundation of Hall measurement evaluation for irregularly shaped samples is based on conformal mapping developed by Van der Pauw [40]. He showed that the resistivity, carrier concentration and mobility of a flat sample of arbitrary shape can be determined without knowing the current pattern provided that there is a uniform current flow through the thickness of the sheet. The Hall mobility μ_H is related to Hall coefficient through the formula $R_H = \frac{\mu_H}{\rho}$ (6.4.2.3),

where ρ is the sheet resistivity. Van der Pauw method allow Hall measurement to be made on samples of arbitrary shape. The resistance is measured using four ohmic contacts on the circumference of the sample by applying current through two contacts and measuring the potential difference developed on the other two contacts. In this way the resistivity can be measured which is related to Hall mobility and Hall coefficient through Eq.(6.4.5.2 - 3) and it is related to sheet resistance R_{sh} by the formula,

$R_{sh} = \rho t$ (6.4.2.4)

Therefore by knowing the R_H and ρ, the carrier mobility in the layer, the sheet carrier concentration and the sheet resistance can be obtained.

6.4.2.3 Experimental

In this work the damage caused to the GaAs due to selective RIE in pure $SiCl_4$ plasma has been studied in material with composition shown in table 6.4.1. The materials were grown by MBE on a semi-insulating GaAs substrate. The damage was measured by electrical charaterization techniques, such as current-voltage and capacitance-voltage measurements of Schottky contacts, Van der Pauw measurements of the mobility, sheets carrier concentration and sheet resistance. Transmission Line Model measurements of sheet resistance were also made. An optical mask set of three levels (ohmics, isolation and Schottky contacts) comprising all the above structures and additional structures for MESFETs was used in the fabrication process. This mask set allowed a comprehensive analysis of all the electrical characteristics of the samples. The etching was carried out in pure $SiCl_4$ plasma at a rf power of 12 W, a dc bias of 40-60 V, a flow rate of 6 sccm and a pressure of 9 mtorr. This plasma condition leads to a very selective etching of GaAs/AlGaAs (see chapter 5). Various samples were etched for 2, 3, 5, and 12 minutes. Etching for 2 min of bulk GaAs without etch stop layer results in an etch depth of about

110-130 nm, whereas etching the 39 nm capping layers in the material of table 6.4.1, takes about 75 secs, after taking into account the long induction time of 45 sec using this plasma condition. Therefore etching for ≥ 2 min is more than sufficient to etch the 39 nm capping layers and arrive at the etch stop layer. Selective reactive ion etching for 2, 3, 5, and 12 min result in overetching for 45, 105, 225, and 645 sec respectively. By etching the 39 nm capping layers, the RIE damage is in the layers below; the 5 nm AlGaAs etch stop layer and the 56 nm thick GaAs active layer. As the 56 nm GaAs layer is doped to 5 x 10^{17} cm^{-3}, it has a natural depletion thickness of about 45 nm which was calculated using (Eq.6.3.6 see section 6.3) , therefore the conduction is only in the 11 nm from the 56 nm thick active layer. Hence any damage (even very low) to the 56 nm will be readily detected as a manifest of the decrease in the conduction layer thickness or increase in the depletion layer thickness. After RIE, Schottky contacts of Ti/Au (33/160) nm in thickness were evaporated and lift-off was performed in warm acetone. The Schottky contacts were in the form of 100 μm diameter dots.

15 nm n- GaAs	1.1 x 10^{18} cm^{-3}
24 nm n- GaAs	5 x 10^{17} cm^{-3}
5 nm n-AlGaAs	5 x 10^{17} cm^{-3}
56 nm n- GaAs	5 x 10^{17} cm^{-3}
100 nm p- GaAs	5 x 10^{15} cm^{-3}
100 nm GaAs	undoped
17 nm GaAs	undoped
S.I. GaAs Substrate	

Table 6.4.1: Material composition used to evaluate RIE damage and in MESFET fabrication in $SiCl_4$ plasma.

6.4.2.4 Results of SRIE damage in $SiCl_4$ plasma

The combined measurements from TLM, Van der Pauw and Schottky contacts are presented here giving a wealth of information about the extent of damage in the very thin layer of GaAs.

TLM measurements: In fig.6.8 the resistances as a function of separation distance as measured from TLM structures are given from samples etched in $SiCl_4$ plasma using the discharge conditions given earlier. As it can be seen from fig.6.8, the measured resistances increase sharply after etching the 39 nm capping layers, and they also increase as the etching time increase from 2 to 12 minutes. The sheet resistances as measured from the slop of the plots, increase with etching time or with overetching time as the etching stops

on the 5 nm AlGaAs layer, as shown in fig.6.9. The increase in the sheet resistance with increasing overetching time from 100% to 3600% which correspond to 45 sec to 645 sec, is due to accumulative etch induced damage in the 56 nm active layer. The sheet resistance was increased from 3600 Ω/sq. to 5300 Ω/sq. due to the above overetching increase.

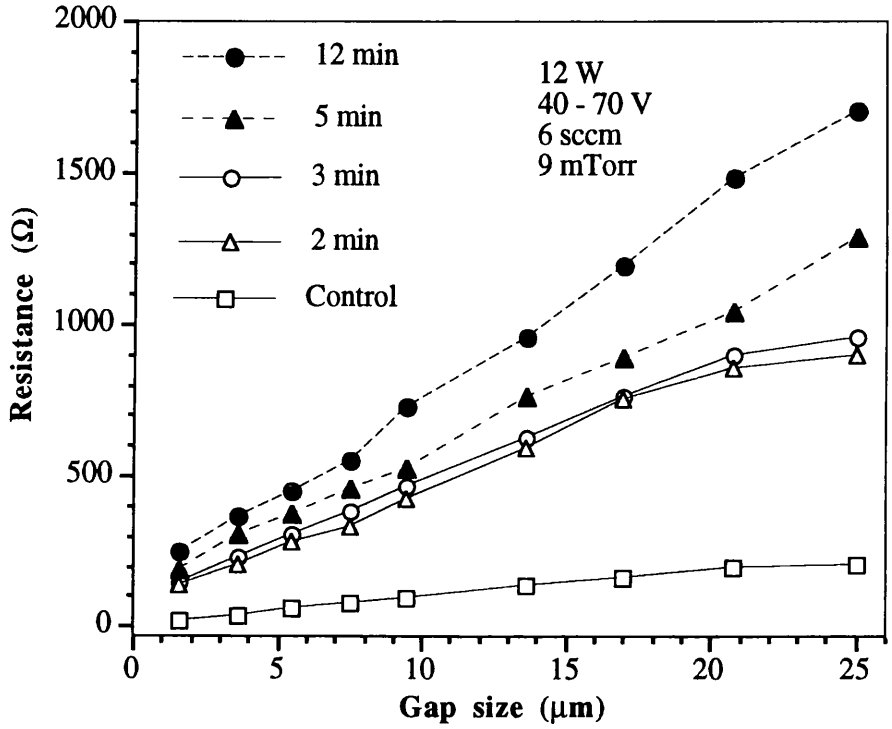

Fig.6.8: The resistance as a function of separating distance as measured for TLM patterns for various etching time in $SiCl_4$ plasma using a rf power of 12 W, a dc bias of 40-60 V, a flow rate of 6 sccm and a pressure of 9 mtorr.

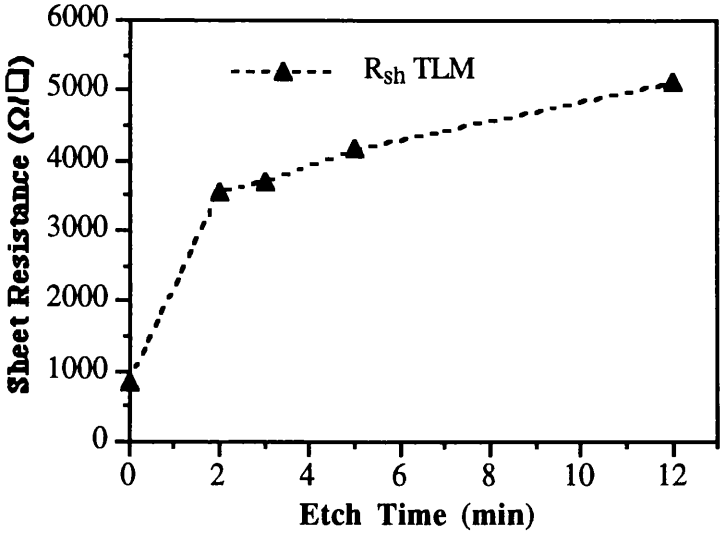

Fig.6.9: The sheet resistance as a function etching time and overetching time as measured from TLM structures on samples etched in $SiCl_4$ plasma using a rf power of 12 W, a dc bias of 40-60 V, a flow rate of 6 sccm and a pressure of 9 mtorr.

This increase in sheet resistance might give the impression that the damage is very large. However if we remember that the actual conducting layer thickness is only 11 nm thick, then this suggests that even with 645 sec of overetching time, the 11 nm thick layer has not been completely destroyed and that the damage rate is certainly <1 nm/min. To justify this hypothesis, the results from Van der Pauw and Schottky contacts are given below.

Hall measurements: The measurements of sheet carrier concentration, calculated sheet carrier concentration for zero damage etching, sheet resistance and mobility as measured by Van der Pauw method as a function of etching time and overetching are given in fig.6.10.

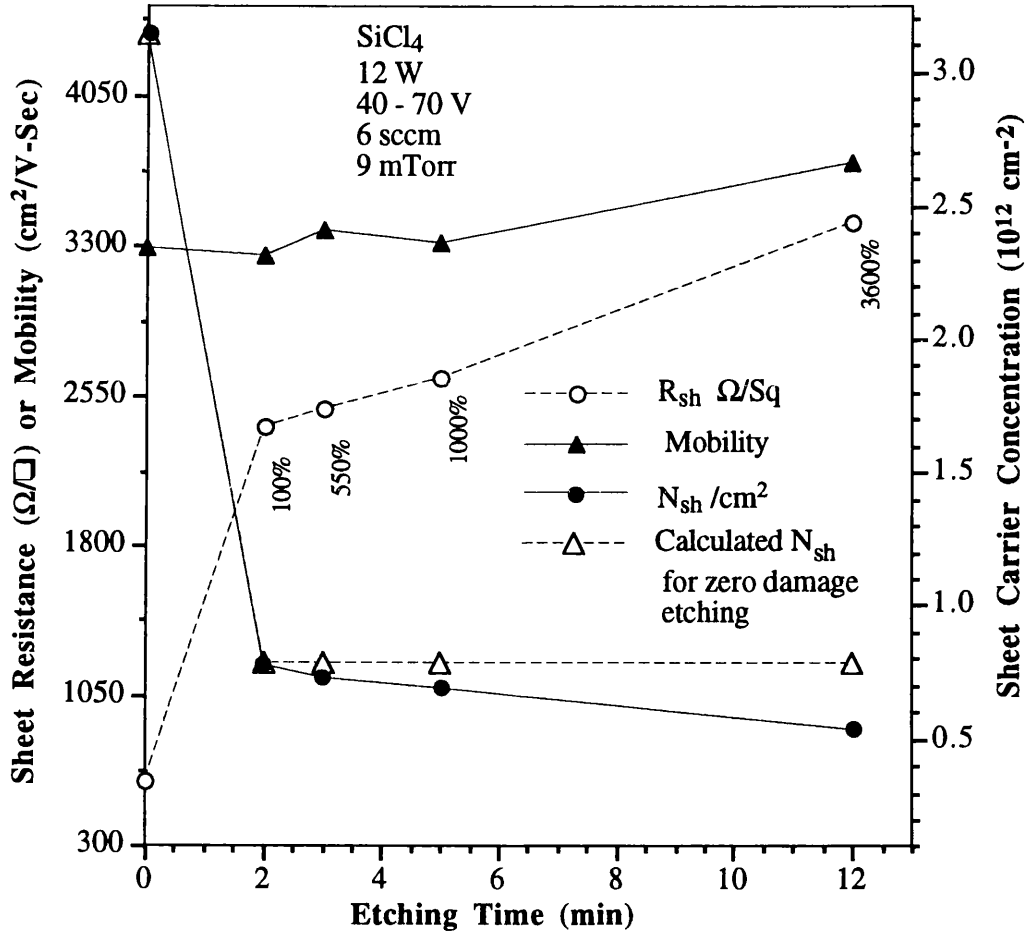

Fig.6.10: The sheet resistance, the sheet carrier concentration, the mobility, and the calculated sheet carrier concentration as a function of etching time as measured by Van der Pauw method on samples etched in $SiCl_4$ plasma using the same conditions as in TLM.

Hall measurements show a decrease in sheet concentration, N_{sh}, from 3.1 x10^{12} cm^{-2} as the 39 nm capping layers etched, to 0.8 x 10^{12} cm^{-2}, 0.77 x 10^{12} cm^{-2}, 0.72 x 10^{12} cm^{-2}, and 0.54 x10^{12} cm^{-2} for 2, 3, 5, and 12 min etching. The sheet resistance increased from

2370 Ω/sq. for 2 min etching to 3360 Ω/sq. for 12 min of etching. However a small increase in the mobility was observed with etching for up to 12 min. The values of sheet resistance measured using Van der Pauw are 20% lower than those obtained from TLM method. The discrepancies may due to the Van der Pauw method for sheet resistance measurement. These measuremens may not be very accurate for sheet thicknesses of less than 100 nm which could be caused by nonuniform current flow or to the fact that the Van der Pauw experiment were performed under the laboratory light. On the other hand, the measured reductions in sheet concentration were compared with values calculated by the one-dimensional solution to Poisson's equation for this material composition. The calculation gave N_{sh} of 3.05 x 10^{12} cm^{-2} for unetched material, 0.81 x 10^{12} cm^{-2} with the 39 nm capping layers removed and 0.48 x 10^{12} cm^{-2} with the 39 nm GaAs capping layers and 5 nm AlGaAs etch stop layer removed.

The calculations are in excellent agreement with the measurement, at the very worst, the 12 minute etching which is 3600% of overetching (nearly 11 min of overetching) may have caused no more than 27% degradation in sheet concentration. Etching for up to 5 min (nearly 4 min of overetching) does not cause degradation of more than 7% in sheet concentration. Etching for 2-3 minutes which is up to 550% of overetching is almost damage free. If these measurements translated into percentage of damage in terms of the damage depth or damage rate in the actual conducting layer of which is 11 nm, then the damage rate will be 27% of the 11 nm over 12 min of etching. Assuming the damage rate is constant with time, this implies that the damage depth is only 3.0 nm over 12 minute of etching, in other words the damage rate is only 0.25 nm/min.

Schottky contact assessment: The barrier height and diode ideality factor measured from an unetched control sample and from samples selective reactive ion etched (SRIE) in $SiCl_4$ plasma using discharge conditions given earlier, as a function of etching and overetching times are given in fig.6.11.

The ideality factor was in the range of 1.07 to 1.05 for unetched sample and for the samples etched for 2-5 minutes, the ideality factor in the sample with 12 min etching was increased to 1.17. These small changes in the ideality factor indicates that the ideality factor is not a sensitive parameter for a very low damage etch. On the other hand the barrier height was observed to increase from 0.74 V for unetched sample to 0.76, 0.76, 0.77, and 0.83 V for samples etched for 2, 3, 5, and 12 min. These results indicate that even with nearly 11 min of overetching, the increase in the barrier height is only 12%, whereas the increase in the barrier height for increasing etching time from 2 to 5 min is negligible.

The barrier height was derived from the forward *IV* characteristics by extrapolating the ideal part of the *IV* characteristics to the voltage axis to obtain the saturation current I_s.

The saturation current I_s in turn is related to the barrier height ϕ_b through the formula,

$$I_s = AA^{**}T^2 \exp[\frac{-q\phi_b}{kT}] \qquad (6.4.5.4)$$

Where A is the diode area, A^{**} is Richardson constant which takes into account the optical phonon scattering and quantum mechanical reflection [41], k is Boltzmann's constant, T is temperature in Kelvin, and q is the electron charge. The saturation current I_s comprises both the thermionic emission current and tunnelling current I_t. The tunnelling current I_t decreases exponentially with the increasing surface depletion [42] and the surface depletion in turn is related to damage. Therefore changes in saturation current are directly related to the surface depletion and damage.

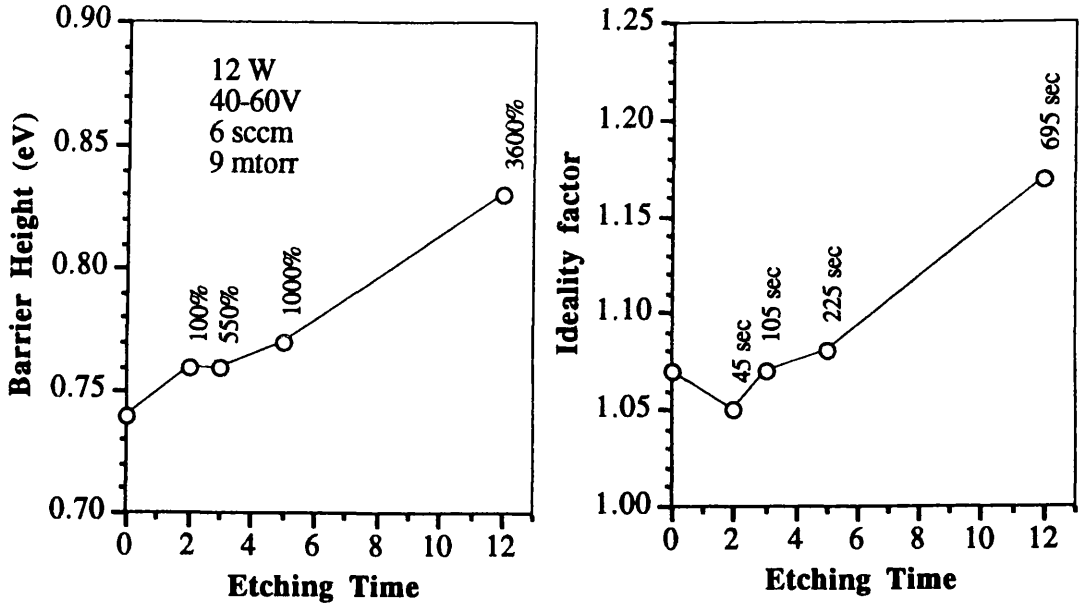

Fig.6.11: Schottky diode barrier height and diode Ideality factor as a function of overetching time in $SiCl_4$ plasma. The etching conditions are same as those used in TLM and Van der Pauw methods.

In fig.6.12 the Schottky diode saturation current, the reverse breakdown voltage and the zero bias capacitance are given as a function of the etching time. As expected, the saturation current decreases as the 39 nm capping layer is removed, then it decreases very slowly for 2-5 min etching. However the saturation current decrease to about 65% of its value at 2 min etching after 11 min of overetching. On the other hand, the reverse breakdown voltage improves on etching, this improvement is likely to be caused by increased depletion as the capping layers are etched, and can also be caused by the different nature of the surface of the GaAs oxide to AlGaAs oxide. The measurements of the zero bias capacitance show that a very small decease of less than 4% occurs when the etching time was increased from 2 to 5 min, the measurement also show that a decrease of about 28% for increase in overetching from 1 min to 11 min. The reduction of about 4% in zero bias capacitanceas as the etching

time increased from 2 to 5 min amounts to a negligible increase in the depletion layer thickness. On the other hand the reduction of 28% as the overetching time increased to 11 min is in agreement with results obtained from the sheet carrier concentration measurement from Van der Pauw.

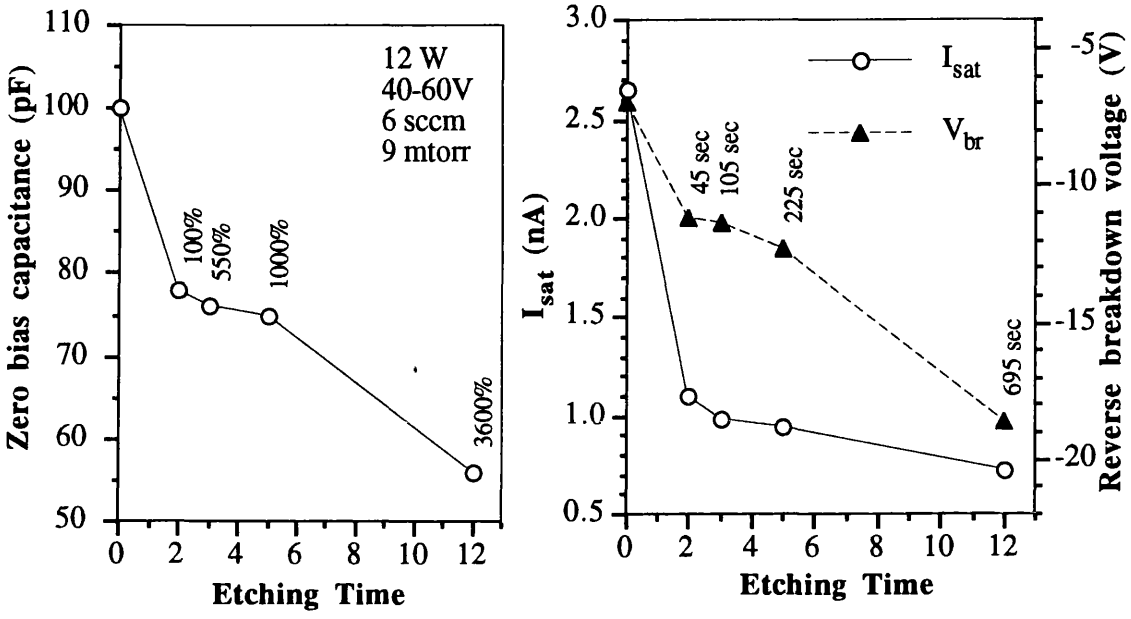

Fig 6.12: The zero bias capacitance, diode saturation current, and the reverse breakdown voltage as a function of etching or overetching time in $SiCl_4$ plasma.

6.4.2.5 Discussion of the results from SRIE in $SiCl_4$ plasma

The combined results of sheet resistance, sheet carrier concentration, electron mobility, Schottky barrier height, ideality factor, Schottky diode saturation current, reverse breakdown voltage and zero bias capacitance are summarised in table 6.4.2. These results consistently show that almost "damage free etching" can be obtained with 2-3 min of overetching, the active layer may suffer a damage of less than 4% for 4 min of overetching and 25-35% in case of 11 min of overetching. Knowing that the actual conducting layer thickness was only 11 nm which was still working very well even after 11 min of overetching. These results show that a damage depth of 7-8 nm suggested by Raman scattering method on samples with no etch stop layers (see section 6.4.1.3) is not realistic. However these results agree with damage measurements on the sidewalls of wires which were etched at the same conditions as the samples used here. This is not surprising since the damage on wire sidewalls have similar accumulating effect as in the case of materials with etch stop layer, however the mechanism by which the damage occur may be different. It is obvious that in device applications one need not overetch more than say 2-3 min at worst. Therefore the selective RIE in $SiCl_4$ plasma at low power of 10-15 W should cause no damage to GaAs devices for appropriate overetching times. The reasons behind the discrepancies in the damage results obtained from Raman scattering and those obtained by

electrical methods are still not very clear. One possible explanation is that Raman scattering may not be able to probe shallow damage or electronic traps, another possibility is the practical considerations, such the actual accuracy in the measurements may not be good enough to differentiate between samples with low damage.

Etching Time (min)	unetched	2	3	5	12
Sheet Carrier Concentration (10^{12} cm^{-2})	3.140	0.776	0.748	0.72	0.55
Hall Mobility (cm^2/V-s)	3290	3258	3386	3317	3516
Sheet Resistance from VDP (Ω/sq.)	628	2398	2495	2642	3315
Sheet Resistance from TLM (Ω/sq.)	842	3559	3698	4152	5105
Reverse Breakdown Voltage (V)	-7	-11.2	-11.4	-12.3	-18.6
Saturation Current (nA)	2.66	1.1	0.98	0.94	0.72
Ideality Factor	1.07	1.05	1.07	1.07	1.17
Barrier Height (V)	0.74	0.76	0.76	0.77	0.83
Zero Bias Capacitance (pF)	90	78	76	75	56

Table 6.4.2: Summary of the results from Hall measurements, TLM measurements IV and CV measurements of 100 μm diameter Schottky contacts to the layer shown in table 6.4.1, after selective RIE in $SiCl_4$ plasma at low rf power of 12 W and dc bias of 40-60 V.

6.4.2.6 Results of SRIE damage in $SiCl_4/SiF_4$ plasma

The damage due to selective reactive ion etching of GaAs/AlGaAs/InGaAs material structures in a mixture of $SiCl_4/SiF_4$ plasma has been studied using Van der Pauw structures made on two sets of pseudomorphic HEMTs wafers (A777, A778) with composition shown in table 6.4.3. The materials were grown by MBE on semi-insulting GaAs substrates. Both wafer structures feature a fully depleted doped cap. The etching of the depleted cap will have no effect on the sheet resistance, the mobility or the sheet carrier concentration, provided that the etching is damage free. Therefore these layer structure are ideal for studying the damage induced by selective reactive ion etching because one can have a direct comparison between unetched and etched samples unlike the material used in the case of $SiCl_4$ etching, see table 6.4.1. Various samples were etched for different times and the measurements of sheet concentration, Hall mobility and the sheet resistance were

carried out. The etching was carried out in $SiCl_4/SiF_4$ plasma using flow rates of 2/9 sccm, rf power of 12 W and dc bias of 15-35 V. These etching conditions result in a very high selectivity of the order of a few thousands to one, for etching GaAs/AlGaAs. The etch rate under these etching conditions is 130-150 nm/min, therefore the 20 nm capping layer takes about 25-30 sec to etch after taking into consideration the short induction time of 15-20 sec.

Layer	A 777	A 778
Cap	20 nm 1 x 10^{18} cm^{-3} Si doped GaAs	20 nm 1 x 10^{18} cm^{-3} Si doped GaAs
Schottky	25 nm $Al_{0.3}Ga_{0.7}As$	25 nm $Al_{0.3}Ga_{0.7}As$
Supply	2 ml GaAs 5 x 10^{12} cm^{-2} Si doped 3 ml GaAs	2 ml GaAs 5x10^{12} cm^{-2} Si doped 3 ml GaAs
Spacer	5 nm undoped $Al_{0.3}Ga_{0.7}As$	5 nm undoped $Al_{0.3}Ga_{0.7}As$
Channel	10 nm $In_{0.3}Ga_{0.7}As$	10 nm $In_{0.3}Ga_{0.7}As$
Buffer	10 nm undoped GaAs, 200 nm 1 x 10^{17} cm^{-3} Be doped GaAs	600 nm GaAs
Impurity trap	100 x (0.255 GaAs/0.225 $Al_{0.3}Ga_{0.7}As$) 1.1 μm GaAs	100 x (0.255 GaAs/0.225 $Al_{0.3}Ga_{0.7}As$) 1.1 μm GaAs
Substrate	S.I. GaAs Substrate	S.I. GaAs Substrate

Table 6.4.3: The Pseudomorphic HEMT layer structure used to study the dry etch damage in SRIE in $SiCl_4/SiF_4$ plasma.

In fig.6.12 the sheet carrier concentration and the Hall mobility for both layer structures (A 777, A 778) as a function of overetching time are given. The measurements of sheet resistance as a function of overetching time are given in fig.6.13. Hall measurements show that the sheet concentration for the two layer structures (A 777 and A 778) stayed remarkably constant with overetching time at 1.8 x 10^{12} and 2.4 x 10^{12} cm^{-2} respectively, even for as long as 10 min. On the other hand, the sheet resistances for both wafers stayed constant with overetching too. These results strongly indicate that the SRIE in $SiCl_4/SiF_4$ plasma has no any detectable effect or damage upon the electrical properties of these materials and that this reactive ion etching process is truly "Damage free". The damage results here agree well with the damage measurement results obtained from Raman scattering made on GaAs samples with no etch stop layers, etched under the same etching conditions, see section 6.4.1.4.

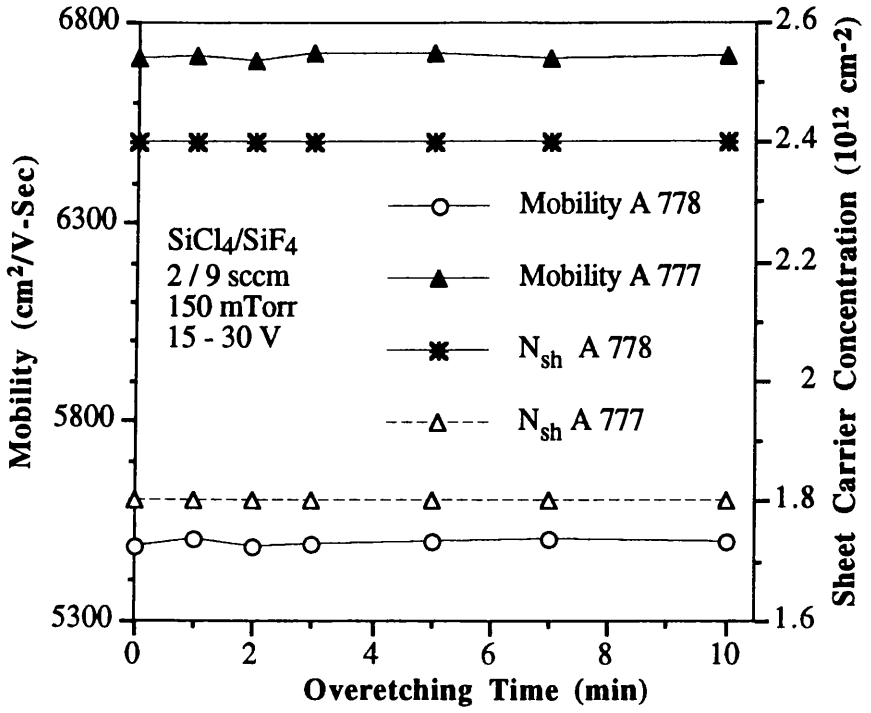

Fig.6.12: Hall mobility and sheet carrier concentration of the two wafer structures in table 6.4.3, as a function of overetching time in $SiCl_4/SiF_4$ plasma.

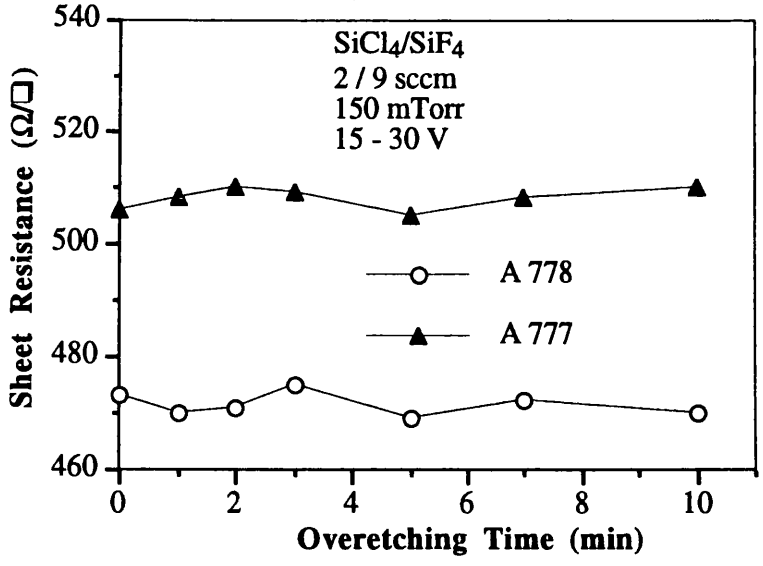

Fig.6.13: The sheet resistances of the material of table 6.4.3, as a function of overetching time in $SiCl_4/SiF_4$ plasma. The etching was carried out using rf power of 12 W, dc bias of 15-35 V and flow rates of 2/9 sccm.

The mechanism by which damage free etching may be obtained is likely to be connected with the ion energies in the discharge. It plausible to suggest that if the ions in the plasma have energies lower than the displacement threshold of semiconductor material in this case GaAs, then no damage is expected to occur. Since there are no easy means of measuring

the actual ion energies in the plasma, then the dc bias may give an indication to the energies by which the ions bombard the surface. As the bias is only in the range of 35-15 V and at the same time the pressure is high at 150 mtorr, therefore the ion energies may not be exceeding 15-30 eV. These ions are likely to suffer collisions in the sheath region due to high pressure which will further reduce their impact energy on the surface. This impact energy may be low enough not to cause damage. To conclude, the Hall measurements clearly shows that no detectable damage occurs due to selective reactive ion etching in $SiCl_4/SiF_4$ plasma. This agrees with the results obtained from Raman scattering measurements made on GaAs samples etched under the same conditions.

6.4.2.7 Damage results from gate recessing of MESFETs

To study the effect of selective reactive ion etching process in $SiCl_4$ plasma (which was given in chapter 5), on the characteristics of MESFETs, devices with gate lengths of 3-5 μm were made on the same samples that have TLM, Van der Pauw and Schottky contacts which were given in section 6.4.2.3. The material structure is given in table 6.4.1. The drain to source separation was 5 μm, on some of the samples, gate patterns 3 μm long were aligned between the source and drain separation using optical lithography and subsequently selective reactive ion etched in $SiCl_4$ plasma for 2, 3, 5, and 12 min using a rf power of 12 W, flow rate of 6 sccm a pressure of 9 mtorr and dc bias of 40-60V. On other samples, the whole distance between the drain and the source was selective reactive ion etched in $SiCl_4$ plasma before gate pattern definition and therefore the effective gate length in this case is 5 μm. The same etching conditions as in the case of 3 μm gate samples were used.

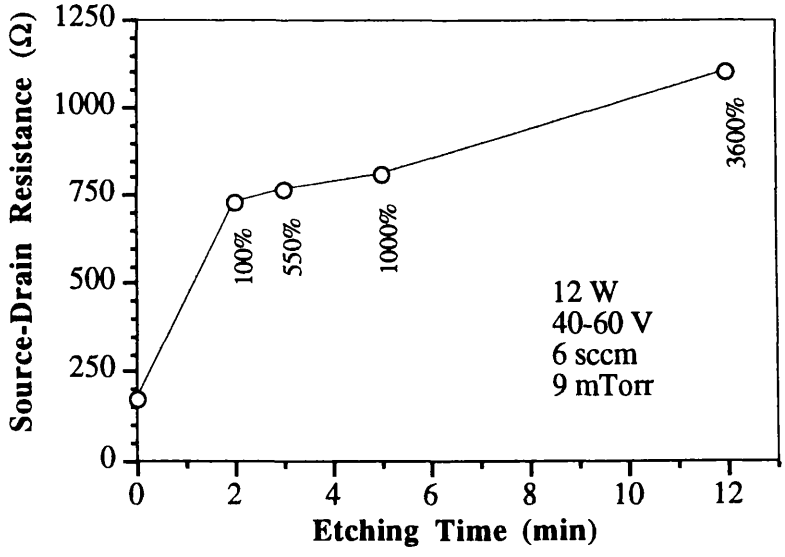

Fig.6.14: The drain-source resistance before gate metallization as a function of etching time in $SiCl_4$ plasma.

Measurements of the drain-source resistance R_{ds}, before gate metallization as a function of etching time are given in fig.6.14. As expected the resistance R_{ds} was increased sharply after the capping layers were removed, and then increased from 750 Ω for 2 min etching to 1100 Ω for 12 min of etching which is about 42 % increase in the resistance. These measurements are in line with resistance measurements from TLM and Van der Pauw structures. The current-voltage I_{ds} (V_{ds}, V_{gs}) and transconductance g_m (V_{gs}) characteristics of the devices for the unetched sample and 12 min etched sample are shown in figures 6.15-6.18. As it can be seen the devices with even 12 min of etching (11 min of overetching) can still work in the depletion mode, however with reduced drain saturation current I_{dss}, higher values of gate threshold voltage and lower transconductance. The I_{dss} was decreased from 8.5 mA for the unetched devices to 4.2, 4.1, 3.9 and 2.05 for samples etched for 2, 3, 5, and 12 min. These etching times correspond to overetching of 100% (45 sec), 550% (105 sec), 1000% (225 sec) and 3600% (645 sec) respectively.

As shown in fig.6.19, these data show that I_{dss} drops despite the fact that the etch has stopped on the AlGaAs layer, this is due to the decrease in the carrier concentration and the resulting increase in the depletion layer caused by the accumulative affect of ion bombardment induced damage. The reduction in I_{dss} from the unetched control sample cannot be compared with etched samples directly because of the existence of an extra 39 nm thick capping layers which contribute to I_{dss} in the control sample. Therefore the comparison should be made between the 2 min etched and the rest of the samples. The reduction in the I_{dss} due to increased etching from 2 to 5 min amounts only to less than 7%. I_{dss} decreases by more than 40% after 12 min of overetching.

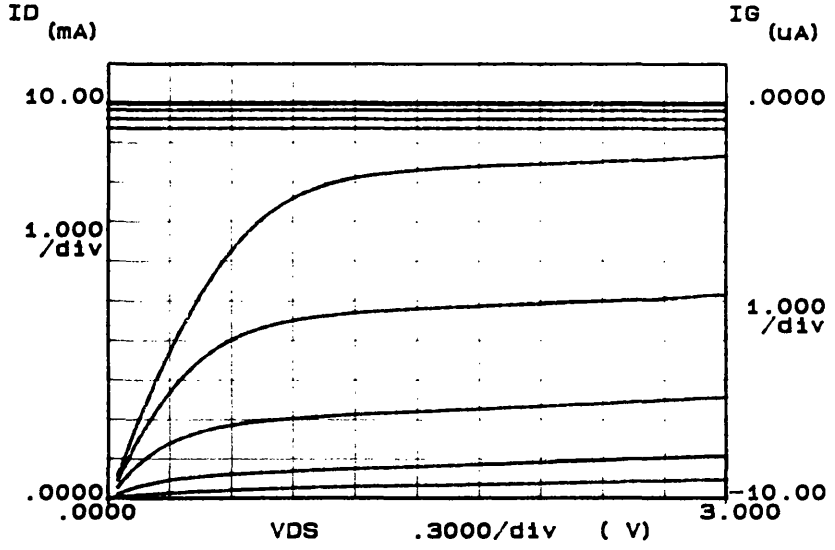

Fig.6.15: I_{ds} (V_{ds}, V_{gs}) Characteristics of 3 μm gate length MESFETs before gate recess etching. (V_{gs} start at 0 V, stop -0.8 V, step -0.2 V).

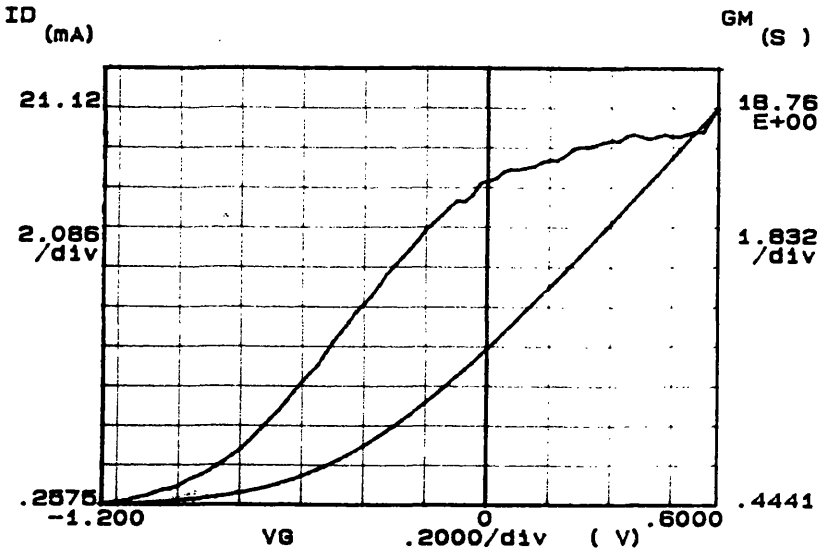

Fig.6.16: g_m (V_{gs}) Characteristics of 3 μm gate length MESFETs before gate recess etching. (V_{ds} = 2 V).

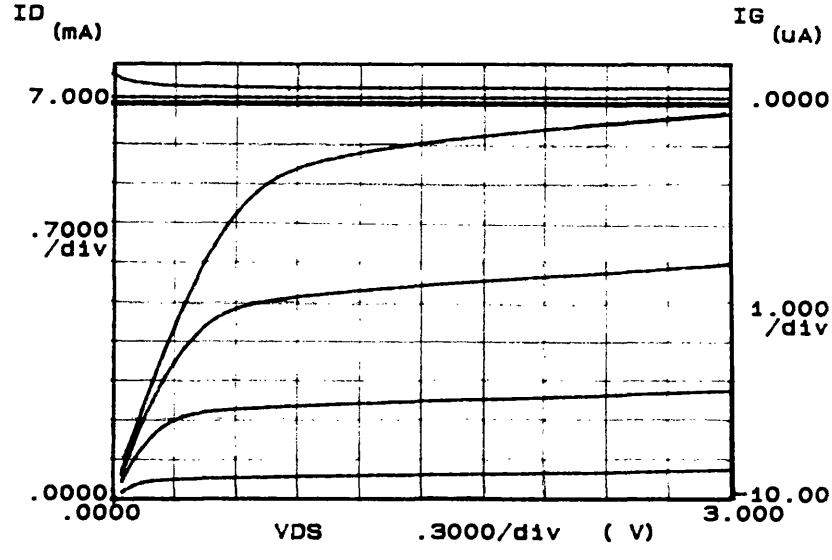

Fig.6.17: I_{ds} (V_{ds}, V_{gs}) Characteristics of 3 μm gate length MESFETs after gate recess overetching in $SiCl_4$ plasma for 11 min (total etching time of 12 min). The discharge condition are 12 W of rf power, 40-60 V dc bias flow rate of 9 sccm and pressure of 9 mtorr. (V_{gs} start at 0.5 V, stop -0.25 V, step -0.25 V).

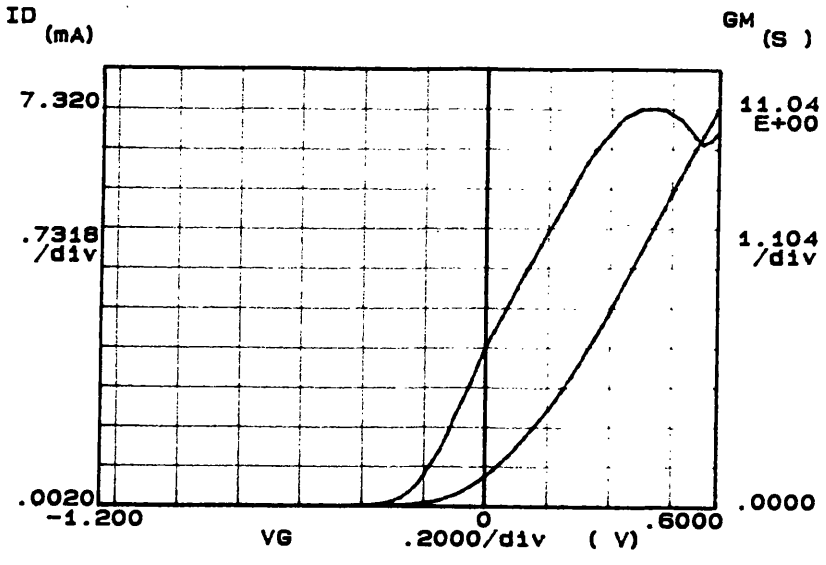

Fig.6.18: g_m (V_{gs}) Characteristics of 3 μm gate length MESFETs after gate recess overetching in $SiCl_4$ plasma for 11 min (total etching time of 12 min). (V_{ds} = 2 V).

Figure 6.20a shows the threshold voltage as a function of etching time. As it can be seen there is an increase in the threshold voltage with increasing overetching time. However this increase is very small, it amounts to less than 11% due to increase in the etching time from 2 to 5 min which corresponds to 1000% of overetching. For 12 min of etching or 11 min of overetching, the threshold voltage increased by around 30%, whereas the increase in the threshold voltage as a result of increased etching from 2 to 3 min amounts to less than 2%. The maximum transconductance of MESFETs with 3 μm long gate and the transconductance of devices with 5 μm long gates as a function of etching are shown in fig.6.20b. The transconductance of devices with effective gate length of 3 μm is 2-3 times higher than those with 5 μm gate length. The changes in the maximum transconductance with overetching time is about 23% even with 11 min of overetching time in both type of devices. The characteristics of MESFET or HEMTs as a function of gate overetching in either CCl_2F_2 or $SiCl_4/SiF_4$ plasmas has been studied by many authors [1,2,42-45]. These authors have concluded that the values of I_{dss} decreased to zero even with small amounts of overetch, furthermore, the gate threshold voltages increased to "positive values", as a result the devices worked only in the enhancement mode. Therefore the above results which have been obtained from selective reactive ion etching in $SiCl_4$ plasma are a clear indication of very low damage which agrees well with the results from Hall and Schottky diode measurements.

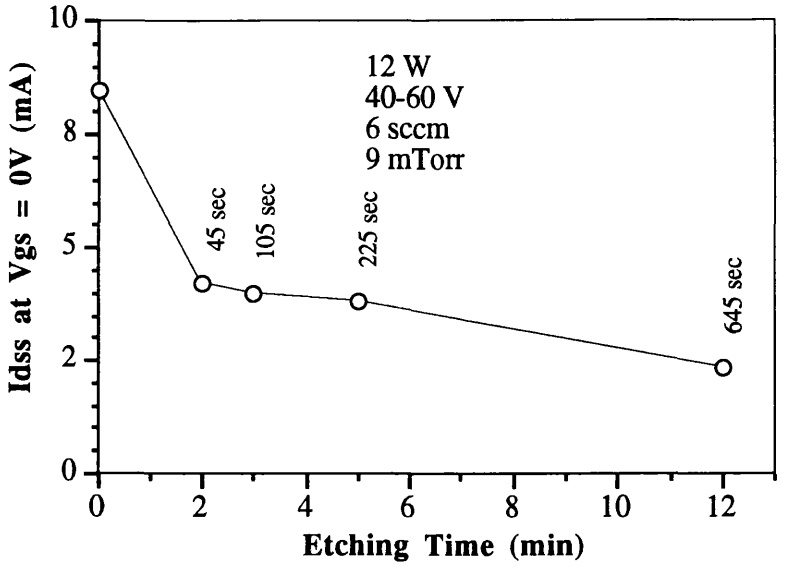

Fig.6.19: The drain saturation current I_{dss} as a function of etching time in $SiCl_4$ plasma.

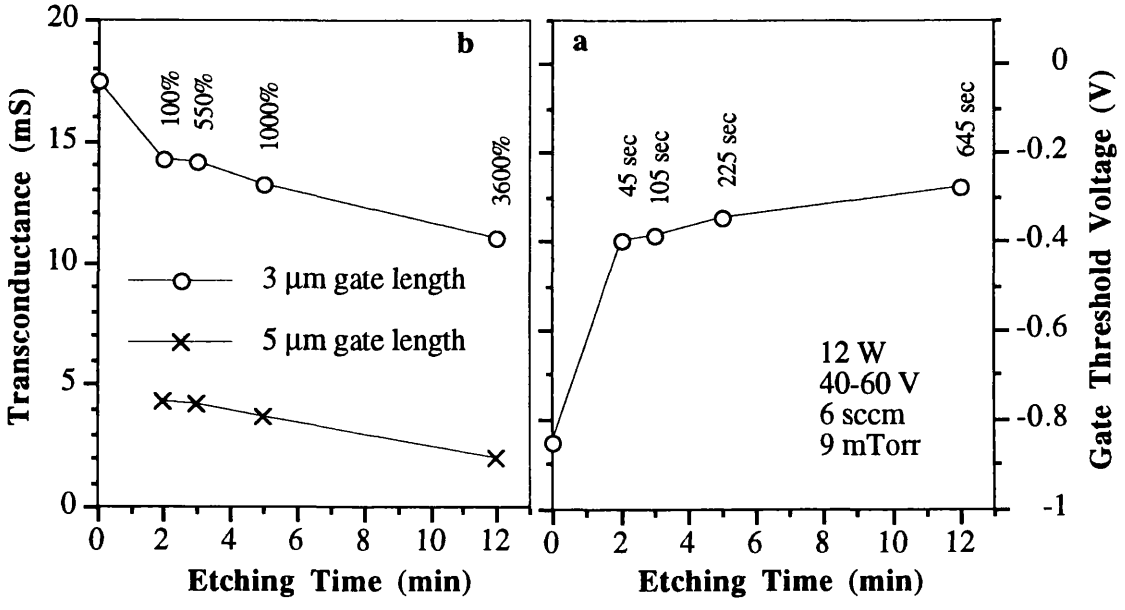

Fig.6.20: **(a)** The gate threshold voltage of MESFETs SRIE in $SiCl_4$ plasma as a function of etching time, and **(b)** the maximum transconductance at drain voltage of V_{ds}, of 2.5 V as a function of etching time.

To conclude, several important issues concerning the use of $SiCl_4$ plasma as a process for gate recess etching have been investigated. The measurements show that SRIE in $SiCl_4$ plasma using very low power of 12 W and low dc bias of 40-60 V causes no or minimum damage to the MESFET channels even with 5 min of overetching. The results also show

that even with unrealistic prolonged overetching periods of 11 min, the devices were still working in the depletion mode which again emphasizes the very low damage behaviour of this SRIE etching process. These results are summarised in table 6.4.4.

Etching Time (min) or Overetching (%)	unetched	2 100%	3 550%	5 1000%	12 3600%
Mode of Operation	Depletion + Enhancem.	Depletion + Enhancem.	Depletion + Enhancem.	Depletion + Enhancem.	Depletion + Enhancem.
Drain Saturation Current I_{dss} at V_{gs} = zero (mA)	8.51	4.2	4	3.8	2.05
Maximum Transconductance at V_{ds} = 2.0 V (mS)	17.5	14.2	14.1	13.2	11.4
Gate Threshold Voltage at V_{ds} = 2.0 V (V)	-1.1	-0.40	-0.39	-0.35	-0.28

Table 6.4.4: Summary of the MESFET characteristics which were selective reactive ion etched in $SiCl_4$ plasma.

6.5 Chapter discussions and conclusions

In this chapter two selective reactive ion etching processes for etching GaAs/AlGaAs in $SiCl_4$ and $SiCl_4/SiF_4$ plasmas have been assessed from the dry etch damage point of view. First in the $SiCl_4$ plasma, both sidewall and surface damage were measured. The sidewall damage was measured using conductance measurements on narrow wires made on n^+- GaAs. The results presented in this chapter showed that the sidewall damage has an accumulative effect with time. Moreover the sidewall damage is undoubtedly greater when high dc biases are used compared to low dc bias. The sidewall damage due to reactive ion etching in $SiCl_4$ plasma at very low power of 15 W (0.06 W/cm^2) was negligible (1 nm/sidewall) for the first 2 min of etching which was increased to 12 nm/sidewall for 5 min etching. On the other hand the sidewall damage increased to 18 nm/sidewall for 2 min etching at 200 V bias. The results from sidewall damage measurements also indicate that the plasma chemistry plays an important role (however not fully characterised) in determining the dominant type of ions in the discharge and in turn their contribution on damage. The results presented strongly indicate that the damage is very low in wires etched in a plasma chemistry dominated by molecular ions Cl_2^+, whereas the damage in wires etched in a plasma chemistry dominated by atomic ions was considerably higher. The surface damage assessment due to selective RIE in $SiCl_4$ plasma

was carried out using Raman scattering, electrical charaterization techniques such IV and CV measurements of Schottky diodes and Hall and TLM measurements made on a thin MESFET with AlGaAs etch stop layers. The damage assessment was confirmed by gate recess etching of MESFETs. The Raman scattering measurements suggested a damage depth of 2-3 nm in the beginning of the etching which increased to 7-8 nm after etching for 4 min and more. However the results from Hall and Schottky diode measurements clearly indicated that the damage rate is less than 1 nm/min. On the other hand, the results from charaterization of MESFET performance again suggested that even with a very long overetching time (11 min), the devices still worked in the depletion mode, whereas there was a negligible degradation of the device characteristics even after 5 min of overetching which is about 1000% of overetching. Therefore the damage depth of 7-8 nm suggested by Raman scattering measurement seem to be unrealistic. The reasons why the results from Raman do not agree with the electrical characterisation results are not very clear. However one possible explanation is that Raman scattering is not very sensitive to very small changes in the surface depletion or the possibility of surface deposition may result in signal distortion and therefore the depletion depth deduced from Raman scattering may be under or over estimated. The damage assessment due to reactive ion etching in $SiCl_4/SiF_4$ plasma has been studied using Raman scattering and Hall measurements on HEMT layer structures with AlGaAs etch stop layers. The results presented in this chapter from Raman scattering experiments indicated that no damage occurs at all. Furthermore the actual surface depletion was seen to decrease on etching. The possibility that RIE in $SiCl_4/SiF_4$ plasma which uses very low dc bias ~ 20 V and high pressure of 150 mtorr, improves the surface states by the removal of contamination is not remote. The results from Hall measurements showed that no degradation of the sheet carrier concentration, mobility or sheet resistance occured even with prolonged overetching times. Therefore it seems that RIE in $SiCl_4/SiF_4$ plasma can really deliver "damage free" etching. The mechanisms by which damage free etching can be achieved is most likely to be related to the ion energies in the discharge; if the ion energies are less than the displacement threshold in semiconductors such as GaAs then no damage is expected to occur. Since the ion energies in $SiCl_4/SiF_4$ plasma have not been measured, one cannot be sure whether high energy ions exist in the plasma or not. However from the results presented in this chapter, it seems that ions with energy greater than 15-20 eV are not expected to be present in the $SiCl_4/SiF_4$ plasma and as a result there is no detectable damage effect.

6.6 References

6.1. S. Salimian, C. Yuen, C. Shih, C. Smith and C. B. Cooper, J. Vac. Sci. Technol., B **9**, 114, (1991).

6.2. W. H. Guggina, A. A. Ketterson, E. Andideh, I. Adesida, S. Caracci and J. Kolodzey, J. Vac. Sci. Technol., B **8**, 1956, (1990) .

6.3. T. Hara, H. Suzuki, and A. Suga, J. Appl. Phys., **62**, 4109, (1987).

6.4. S. W. Pang, G. A. Lincoln, R. W. McClelland, P. D. Degraff, M. W. and W. J. Piacentini, J. Vac. Sci. Technol., B **1**, 1334, (1983).

6.5. H. F. Wong, D. L. Green, T. Y. Liu, D. G. Lishan, and M. Bellies, J. Vac. Sci. Technol., B **6**, 1906, (1988).

6.6. S. W. Pang, W. D. Goodhue, T. M. Lyszczarz, D. J. Ehrlich, R. B. G. Man, and G. D. Johnson, J. Vac. Sci. Technol., B **6**, 1916, (1988).

6.7. C. M. Knoedler, L. Osterling, and H. Shtrikman, J. Vac. Sci. Technol. B **6**, 1573, (1988).

6.8. Yuhki Imai, and Kuniki Ohwada, J. Vac. Sci. Technol. B **5**, 889, (1987).

6.9. A. R. Long, M. Rahman, I. K. MacDonald, M. Kinsler, S. P. Beaumont, C. D. W. Wilkinson, and C. R. Stanley, Semicond. Sci. Technol., **8**, 39, (1993).

6.10. C. S. Wu, D. M. Scott, Wei-Xi Chen, and S. S. Lau, J. Electrochem. Soc., **132**, 921, (1985).

6.11. S. J. Pearton, W. C. Dautremont-Smith, J. Chevallier, C. W. Tau, and K. D. Cummings, J. Appl. Phys. **59**, 2821, (1986).

6.12. P. Collot, and C. Gaonach, Semicond. Sci. Technol. **5**, 237, (1990).

6.13. S. J. Fonash, J. Electrochem. Soc., **137**, 3885, (1990).

6.14. V. J. Law, S. J. Ingram, G. A. C. Jones, R. C. Grimwood, and H. Royal, Mat. Res. Soc. Symp. Proceed., **223**, 191, (1991).

6.15. J. Chevallier, W. C. Dautremont-Smith, C. W. Tau, and S. J. Pearton, Appl. Phys. Lett., **47**, 108, (1985).

6.16. S. W. Pang, J. Electrochem. Soc., **133**, 784, (1986).

6.17. C. M. Knoedler, L. Osterling, and M. Heibum, J. Appl. Phys. **65**, 1800, (1989).

6.18. P. Rabinzohn, G. Gautherin, B. Agius, and C. Cohen, J. Electrochem. Soc., **131**, 905, (1984).

6.19. E.M. Clausen, Jr., H. G. Craighead, J. P. Harbison, A. Scherer, L. M. Schiavone, B. Van der Gaag, and L. T. Florez, J. Vac. Sci. Technol. B **7**, 2011, (1989).

6.20. R. Cheung, S. Thoms, M. Watt, M. A. Foad, C. M. Sotomayor-Torres, C. D. W. Wilkinson, U. J. Cox, R. A. Cowley, C. Dunscombe, and R. H. Williams, Semicond. Sci. Technol., **7**, 1189, (1992).

6.21. M. A. Foad, S. Hefferman, J. Chapman, and C. D. W. Wilkinson, Proceedings of

the 17th Int. Symp. on GaAs and related compounds, pp. 293, (1990).

6.22. M. A. Foad, Ph D thesis , University of Glasgow, (1992).

6.23. S. Thoms, S. P. Beaumont, C. D. W. Wilkinson, J. Frost, C. R. Stanley, Microelectronic Engineering, **5**, 249, (1986).

6.24. M. Rahman, Ph D thesis, University of Glasgow, (1992).

6.25. S. K. Murad, C. D. W. Wilkinson, P. D. Wang, W. Parks, C. M. Sotomayor-Torres, and N. Cameron, J. Vac. Sci. Technol., B **11**, 2237, (1993).

6.26. E. H. Rhoderick, and R. H. Williams, Metal - Semiconductor contacts, Calrendon Press, Oxford, (1988).

6.27. P. D. Wang, M. A. Foad, C. M. Sotomayor-Torres, S. Thoms, M. Watt, R. Cheung, C. D. W. Wilkinson, and S. P. Beaumont, J. Appl. Phys. **71**, 3754, (1992).

6.28. M. A. Foad, S. Thoms, and C. D. W. Wilkinson, J. Vac. Sci. Technol., B **11**, 20, (1993).

6.29. N. P. Johnson, S. K. Murad, M. A. Foad, and C. D. W. Wilkinson, presented in the Material Reseasrch Society meeting Nov. (1993)

6.30. S. Sugata, and K. Asakawa, Jpn. J. Appl. Phys., **22**, L813, (1983).

6.31. M. Watt, C. M. Sotomayor-Torres, R. Cheung, C. D. W. Wilkinson, H. E. G. Arnot and S. P. Beaumont, J. Mod. Opt., **35**, 365, (1988).

6.32. D. G. Lishan, H. F. Wong, D. L. Green, E L. Hu, and J. L. Merz, J. Vac. Sci. Technol., B **7**, 553, (1988).

6.33. D. Kirillov, C. B. Cooper, III, and R. A. Powell, J. Vac. Sci. Technol., B **4**, 1316, (1986).

6.34. G. Abstreiter, E. Bauser, A. Fischer, and K. Ploog, Appl. Phys., 16, 345, (1978).

6.35. A. Mooradian, and G. Wright, Phys. Rev. Lett., **16**, 999, (1966).

6.36. A. Pinczuk, A. A. Ballman, R. E. Nahory, M. A. Pollak, and J. M. Worlock, J. Vac. Sci. Technol., **16**, 1168, (1979).

6.37. H. Richter, Z. P. Wang, and L. Ley, Solid state Commun., **39**, 625, (1987).

6.38. K. K. Tiong, P. M. Amirtharaj, F. H. Pollak, and D. E. Aspens, Appl. Phys. Lett., **44**, 122, (1983).

6.39. D. E. Aspnes, and A. A. Studna, Phys. Rev. B **27**, 985, (1983).

6.40. L. J. Van der Pauw, Philips Tech. Rev., **20**, 220, (1958).

6.41. Dieter K. Schroder, Semiconductor material and device characterization, John Wiley & sons (1990).

6.42. N. I. Cameron, S. P. Beaumont, C. D. W. Wilkinson, N. P. Johnson, A. H. Kean, and C. R. Stanley, J. Vac. Sci. Technol., B **8**, 1966, (1990).

6.43. D. G. Ballegeer, S. Agarwala, M. Tong, K. Nummila, A. A. Ketterson and I. Adesida, J. Vac. Sci. Tecnol., B **11**, 618, (1993).

6.44. N. I. Cameron, G. Hopkins, I. G. Thayne, S. P. Beaumont, C. D. W. Wilkinson,

M. Holland, A. H. Kean, and C. R. Stanley, J. Vac. Sci. Technol., B **9**, 3538, (1991).

6.45. A. A. Ketterson , E. Andideh, I. Adesida, T. L. Brock, J. Baillargeon, J. Laskar, K. Y. Cheng and J. Kolodzey, J. Vac. Sci. Technol., B **7**, 1493, (1989).

Chapter 7

Conclusions and future work

The work presented in this thesis has dealt with the development of Reactive Ion Etching processes for the GaAs/AlGaAs material system in Silicon Tetrachloride ($SiCl_4$) and a mixture of Silicon Tetrachloride and Silicon Tetrafluoride ($SiCl_4/SiF_4$) plasmas. Reactive Ion Etching processes that etch GaAs and not AlGaAs (selective) and ones that etch both (nonselective) have been developed. In developing these processes particular attention have been paid to achieving damage free etching. To acquire knowledge about the fundamental chemical and physical processes occurring in these plasmas during etching or without etching, Optical Emission Spectroscopy (OES) has been used as a tool for plasma diagnosis. OES has also been used for in situ etch initiation and end point determination.
In RIE processes the action of ions bombarding the surfaces to be etched leads to some of bombarding energy to be passed on to the crystal by some form of momentum transfer mechanism during collision of the bombarding ions with surface atoms. This energy transfer produces disordering in the crystal structure which leads to degradation (dry etch damage) in the optical and electronic properties of the materials. To reduce such damage the ion energies have to be reduced. In RIE processes the ion energies largely depend on the sheath potential with respect to the ground (the dc bias) which in turn depends on the applied rf power and to some extent on the pressure. Therefore to reduce the ion energies one has to reduce the rf power provided that the integrity of etching is maintained. However it is often difficult to reduce rf power while maintaining reasonable etch rates or anisotropy for various reasons such as deposition of nonvolatile species and presence of impurities and contaminants in the discharge which will have more prominent effect on the etching because of low density of etchants in the plasma at low levels of power.

In this thesis, a cleaning technique for cleaning the etching chamber in H_2 followed by O_2 plasmas was developed; this enabled the etching of GaAs/AlGaAs to be carried out in $SiCl_4$ or $SiCl_4/SiF_4$ plasma using rf powers as low as 10 W (0.05 W/cm^2) whilst maintaining the integrity of etching. The corresponding dc biases fell in the range of 20-60 V. Optical Emission Spectroscopic analysis presented in this thesis showed that the chamber treatment with H_2 plasma leads to formation of volatile species of hydrogenated chlorosilicon and HCl, hence cleaning the chamber from earlier chlorosilicon deposits. A further clean in O_2 plasma was required to remove the residual H_2 which was observed to affect the reproducibility of etching.

On the other hand Optical Emission spectroscopic analysis of $SiCl_4$ plasma showed that the chemistry and the etching mechanism are strongly dependent on the applied rf power. Two chemical regimes and hence two mechanisms of etching were identified including: "the low power regime" in the rf power range of 5-20 W and the high power regime in the power range of 25-150 W. In the low power regime, $SiCl_4$ molecules breakdown gradually by multiple electron impact excitations into $SiCl_2$ and SiCl radicals, Si and Cl atoms and molecular ions of Cl_2^+. In the high power regime, the breakdown of $SiCl_4$ molecules is mostly through one electron impact excitation into $SiCl_2$, SiCl radicals, Si and Cl atoms and atomic chlorine ion Cl^+. This gives rise to two etching mechanisms, the first is at low power regime where the etching depends on the concentration of mainly Cl_2^+ ions and chlorosilicon radicals. In this regime, as the applied rf power and hence the dc bias are very low 5-20 W and 20-60 V respectively, this mechanism of etching does not involve high energy electrons and thus does not involve ions with high energies. Therefore this mechanism of etching is expected to cause very little damage. The second etching mechanism is at high power regime where the etching depends on the concentration of atomic Cl ions Cl^+ and chlorosilicon species.

In the work reported in this thesis, a very low damage, anisotropic selective or nonselective RIE process was developed in $SiCl_4$ plasma for etching GaAs/AlGaAs which stops on an extremely thin AlGaAs layer (1.13 nm thick). Using a very low rf power of 10-15 W and a low dc bias $\leq$ 60 V (The low power regime), this process can be selective or nonselective over the AlGaAs depending on the $SiCl_4$ flow rate and the pressure. At low $SiCl_4$ flow rates of 4-6 sccm, using low pressures of $\leq$9 mtorr and under low power conditions, selectivities of the order of 10000:1 are readily obtainable whilst maintaining excellent verticality. Nanostructures 50-60 nm wide in GaAs have successfully been etched to a depth of 1.5 μm with excellent verticality and under low damage conditions. New mechanisms of selectivity for etching GaAs/AlGaAs were suggested here in which the selectivity depends on the formation of an etch stop layer, possibly Al_xO_y, Al_xN_y or both, from the residual O_2, air or water vapour in the chamber. It was postulated that because of low $SiCl_4$ flow rate, pressure and bias, the density of etching species is so low that low concentration or O_2 or air in the chamber may stop the surface reaction by oxidation or nitration and as the Al_xO_y and Al_xN_y are not volatile, the etching stops. Nonselective etching of GaAs/AlGaAs (ratio of 1.25:1) under low power conditions can still be obtained by using higher values of $SiCl_4$ flow rate (> 12 sccm) and higher pressures (>12 mtorr). In this case, the density of etching species outnumbers the residual O_2 or water vapour and thus nonselective etching can be obtained. However the AlGaAs profiles are undercut under these conditions. To improve the verticality of AlGaAs under low power conditions, it is suggested that the etching has to be carried out in an RIE system with a load lock under low pressure condition. The load lock will minimise the residual O_2 or water vapour, hence the AlGaAs can be etched under the same conditions as the GaAs, retaining vertically.

To identify the exact mechanism that causes selectivity and to simulate the effect of residual air and O_2 in the chamber, N_2 or O_2 was added to $SiCl_4$ at high pressure where the selectivity is low. The results presented in this work showed that the addition of O_2 did not improve the selectivity, whereas the addition of N_2 increased the selectivity from 1.25:1 to over 2000:1.

On the other hand, X-ray Photoelectron Spectroscopy (XPS) on samples selectively reactive ion etched in pure $SiCl_4$ plasma and on samples etched in a mixture of $SiCl_4/N_2$ plasma under high selectivity conditions showed that the formation of Al_2O_3 is most likely cause for the cessation of the etching in the case of $SiCl_4$ etching. In the case of $SiCl_4/N_2$ etching, the percentage of N_2 detected in the XPS spectra was found to be three times as high compared to $SiCl_4$. However because of the lack of high resolution XPS measurements, no conclusive evidence could be obtained as to which compound, N_2 is originating from (i.e. SiN_x or Al_xN_y). Therefore it is suggested that for a complete understanding of the nature of the etch stop layer, comprehensive and high resolution XPS measurements should be carried out.

The selective RIE in $SiCl_4$ plasma was applied for gate recessing of MESFETs. The results presented here showed that vertical gate profiles with very little gate off-set can be obtained. This kind of gate profile has the advantage of precise control of the effective gate length over the all known etching systems (i.e. fluorine based selective etching) because there is no lateral etching.

In this thesis, dry etching induced damage in $SiCl_4$ plasma has been measured using various techniques including: conductivity measurements of quantum like wires made in n^+-GaAs for the measurement of sidewall damage, Raman scattering on heavily doped GaAs for surface damage measurements, evaluation of MESFET performance whose gate recess etching was performed using the selective RIE in $SiCl_4$ plasma and also by Schottky diode characterisation which were fabricated on the same samples as the MESFETs.

Results of sidewall damage showed that etching in $SiCl_4$ plasma using the low power regime mentioned earlier is virtually damage free for the first two minute of etching. However, the results clearly showed that for a prolonged etching even at dc biases as low as 50 V, the damage on the sidewalls accumulate with time. Moreover the sidewall damage is undoubtedly greater when high dc biases are used compared to low dc bias. The results from sidewall damage measurements also indicate that plasma chemistry plays an important role (however not fully characterised) in determining the dominant type of ions in the discharge and in turn their contribution to damage. The results presented strongly indicate that the damage is very low in wires etched in a plasma chemistry dominated by molecular ions Cl_2^+, whereas the damage in wires etched in a plasma chemistry dominated by atomic ions of Cl^+ was considerably higher.

The surface damage measurements using Raman scattering showed that the thickness of the damaged layer after reactive ion etching in $SiCl_4$ plasma (under low power conditions)

increased very slowly at the beginning of the etching, then saturated at a damaged thickness of less than 7-8 nm after etching for ≥ 4 minutes. The saturation in the damaged region as the etching proceeds is due to the fact that a state of equilibrium has been reached in which the rate of damage is equal to the rate of the removal of the damaged material by etching. On the other hand, MESFET and Schottky diode characteristics clearly showed that no significant modification of carrier mobility or free carrier concentration in the channel occurs even after 3600% of overetching. Knowing that the actual conducting layer thickness of the MESFET channel was only 11 nm which was still working very well even after 11 min of continuous bombardment using the selective etching conditions. These results show that a damage depth of 7-8 nm suggested by Raman scattering on samples with no etch stop layers is not realistic as the damage does not accumulate unlike the samples with etch stop layers. It is obvious that in device applications one need not overetch more than say 2-3 min at worst. Therefore the selective RIE in $SiCl_4$ plasma at low power of 10-15 W should cause no damage to GaAs devices for appropriate overetching times. The reasons behind the discrepancies in the damage results obtained from Raman scattering and those obtained by electrical methods are still not very clear. However, it is suggested that Raman scattering may not be able to probe shallow damage or electronic traps, another possibility is the practical considerations, such the actual accuracy in the measurements may not be good enough to differentiate between samples with low damage.

In the work presented in this thesis, a "damage free" and selective RIE process for etching GaAs/AlGaAs has been developed in a mixture of $SiCl_4/SiF_4$ plasma using very low rf power of 10-12 W (0.055 W/cm^2), dc bias of 20-40 V and high pressure of ≥ 100 mtorr. The selectivity results showed that a very high selectivity of the order of 5000:1 can be obtained by the addition of large amounts (70-85 %) of SiF_4 to $SiCl_4$ at high pressures and reduced dc biases. Optical emission spectroscopic analysis showed the chemistry of $SiCl_4/SiF_4$ plasma is strongly dependent on the relative flow rates of both the $SiCl_4$ and SiF_4. Three chemical regimes have been identified in this etching system, the first regime is at "0-30%" of $SiCl_4$ where the plasma chemistry is dominated by fluorosilicon species and therefore very high selectivity for etching GaAs/AlGaAs is obtained. The second regime, is at "30-50 %" of $SiCl_4$, in this regime, the plasma chemistry is very complicated where there is a strong competition between the formation of silicon chlorides and silicon fluorides. OES analysis also indicates that in this regime there is some kind of preferential dissociation of $SiCl_4$ molecules and its constitute radicals over their SiF_4 counterparts. This may be due to the lower dissociation energies of $SiCl_4$ radicals compared to that of SiF_4. The selectivity in this regime is poor ≤ 100:1 because of inefficient formation of AlF_3 etch stop layer, since the plasma chemistry is no longer dominated by fluorine radicals. The third chemical regime is at "50-100 %" of $SiCl_4$, nonselective etching is obtained in this

regime, since the plasma chemistry is dominated by chlorosilicon species with little effect of fluorine species.

The damage assessment due to reactive ion etching in $SiCl_4/SiF_4$ plasma has been studied using Raman scattering and Hall measurements on HEMT layer structures with AlGaAs etch stop layers. The results presented in this thesis from Raman scattering experiments indicated that no damage occurs at all. Furthermore the actual surface depletion was seen to decrease on etching. The possibility that RIE in $SiCl_4/SiF_4$ plasma which uses very low dc bias ~ 20 V and high pressure of 150 mtorr, improves the surface states by the removal of contamination is not remote. The results from Hall measurements made on pseudomorphic High Electron Mobility Transistor (HEMT) structure which is highly sensitive to dry etch damage, showed that no degradation of the sheet carrier concentration, mobility or sheet resistance occur even with prolonged overetching times of 4000%. Therefore it seems that RIE in $SiCl_4/SiF_4$ plasma can really deliver a damage free etching.

The mechanisms by which damage free etching can be achieved is most likely be related to the ion energies in the discharge; if the ion energies are less than the displacement threshold in semiconductors such as GaAs then no damage is expected to occur. Since the ion energies in $SiCl_4/SiF_4$ plasma have not been measured, one cannot be sure whether high energy ions exist in the plasma or not. However from the results presented in this thesis it seems that ions with energy greater than 15-20 eV are not expected to be present in the $SiCl_4/SiF_4$ plasma and as a result there is no detectable damage effect. This SRIE process was applied to T-gate recess etching and the results showed a controllable gate off-set can be readily obtained.

The RIE process developed in this work can be regarded as the first to report achieving a highly selective RIE with no detectable damage "damage free". However it would be very desirable to apply these processes for gate recessing of high frequency MESFET and HEMTs to assess etching yield and uniformity.

Future work

The RIE processes developed in this thesis may be extended to other material systems such the InGaAs/AlInAs/InP where no RIE processes have yet been reported on which satisfy the damage free and high selectivity requirements.

Preliminary results obtained from etching InGaAs/AlInAs in $SiCl_4$ plasma and $SiCl_4/SiF_4$ plasma at high (120-180 °C) temperatures (not reported in this thesis) suggest that selectivity as high as 300:1 and low damage are likely to be obtained. These parameters are sufficient to be used in gates recessing of InP based HEMTs. However, there are some problems which need to be addressed concerning the application of gate recessing at high temperatures because the electron beam resists (the PMMAs) are not adequate for masking.

To solve the problem of masking in gate recessing at high temperatures, it is proposed that an alternative masking material should be sought such as SiO_2 or Si_3N_4 or a combination of both provided that a suitable etching process could be developed to etch or remove these masking materials to define the gate region which does not cause damage to the active layers of the devices.

Alternatively another gas chemistry should be considered such as HBr or HI. The role of hydrogen passivation on dopants in InGaAs/AlInAs should be clarified as a first step. Then similar analyses to the ones carried out in this work such as the use of OES, Secondary Ion Mass Spectrometry (SIMS) and other plasma diagnostic tools should be applied to study the chemistry of these plasmas to assess their adequacy for RIE of InGaAs/AlInAs at reduced power levels and hence reduced biases.

Appendix

Published papers

1. S. K. Murad, C. D. W. Wilkinson, P. D. Wang, W. Parks, C. M. Sotomayor-Torres, and N. Cameron, "Very low damage etching of GaAs" J. Vac. Sci. Technol., B **11**, 2237, (1993).
2. S. K. Murad, S. P. Beaumont and C. D. W. Wilkinson, "Selective and nonselective RIE of GaAs/AlGaAs in $SiCl_4$ plasma" Microelectronic Engineering, 23 , 357, (1994). This paper was awarded the best poster award in ME '93 conference held in Maastricht, Holland, Sept., (1993).
3. N. P. Johnson, S. K. Murad, M. A. Foad, and C. D. W. Wilkinson, DLTS study of traps in GaAs after RIE in $SiCl_4$ plasma" A paper presented in the Material Reseasrch Society meeting Nov. (1993).
4. S. K. Murad, N. I. Cameron, P. D. Wang, S. P. Beaumont and C. D. W Wilkinson, "Damage free and selective RIE of GaAs/AlGaAs for MESFET and pseudomorphic HEMT gate recess etching" Abstract submitted to MNE '94 conference to be held in Davos, Switzerland, Sept. (1994).
5. S. K. Murad, and C. D. W. Wilkinson, Optical Emission Observations in $SiCl_4$ and $SiCl_4/SiF_4$ plasma during selective and nonselective RIE of GaAs/AlGaAs. In preparation.